IMPLEMENTATION OF A BUBBLE MODEL IN *FLAC* AND ITS APPLICATION IN DYNAMIC ANALYSIS

Bing Ni

Supervised by
Professor M. J. Pender

A thesis submitted in partial fulfillment of the requirements for the Doctoral degree of Philosophy,
Department of Civil and Environmental Engineering
The University of Auckland, 2007

ABSTRACT

Methodologies of implementing nonlinear constitutive models of soil in *FLAC* are studied in order to reduce numerical distortion, which has been found to occur in nonlinear dynamic analysis when a nonlinear soil model is implemented using an 'apparent modulus' approach. Analyses undertaken using several simple nonlinear soil models indicate that use of 'plastic correction' approach can eliminate or minimize the problem. This approach is therefore adopted in the thesis to implement in *FLAC* a bounding surface bubble soil model, *i.e*. the Bubble model. Satisfactory performance of the Bubble model has been obtained in dynamic analysis without using any of the additional mechanical damping given in *FLAC*.

An analytical study on the Bubble model is carried out with *FLAC*. On the basis of the study, the hardening function is modified to better incorporate size ratio effects of the yield surface and is explored to eliminate abrupt transition in stiffness from elastic region to yielding. Pore water pressure is formulated with the assumption that the pore water pressure is generated as a response to the constant volume constraint which prevents the tendency for volume change when plastic volumetric strain takes place. The formulation is added to the Bubble model so that pore water pressure can be generated automatically by the model for fully saturated and undrained soil. *FLAC* analyses indicate that the Bubble model is generally in good agreement with published experimental data.

The parameters and initial conditions associated with the Bubble model are studied with *FLAC* analyses in triaxial stress space to investigate their influence on the model and to investigate their effective ranges. Both large and small strain behaviors of the model are explored in the parametric study.

Finally, the Bubble model is applied in the modeling of vertical vibration of rigid strip foundations. The influence of soil nonlinearity on vertical compliance of rigid foundations is investigated. Some major factors are considered, which include initial stress level in soil, level of excitation and mass ratio of foundation.

ACKNOWLEDGEMENTS

My sincere gratitude goes to Professor Michael J Pender for his guidance, inspiration and encouragement. His time spent on the initiation of the study, numerous discussions and review of the research proposal and the final thesis is gratefully acknowledged. I also feel very grateful to him for his help in providing many useful reference papers and books and for his kindness to offer opportunities for me to obtain financial support for my study (including attending one national and two international conferences).

I also wish to acknowledge the following individuals: Prof. Ian Collins, Dr Tam J Larkin, Prof. Bruce W Melville (University of Auckland) and Snr. Engineer Sergei Terzaghi (SKM NZ) for their involvement in reviewing the research proposal; Dr. Roger D Hart (Itasca USA) for his thoughts on numerical instability in non-linear dynamic analysis; Philip J Nel (UoA) for his computer support. The Auckland University Engineering Library is thanked for obtaining a key reference paper from overseas.

The University of Auckland Doctoral Scholarship, the financial support and work opportunities from Tonkin and Taylor Ltd are gratefully acknowledged.

Finally, my special thanks go to my wife, Xiao Wang, for her support throughout the study. Without her doing most of the housework, especially looking after our two daughters, the thesis would never have been completed as it was planned.

TABLE OF CONTENTS

LIST OF FIGURES

LIST OF TABLES

1 INTRODUCTION

1.1 General background

A study on numerical dynamic modeling with *FLAC* was carried out by the writer in 2001 for the purpose of investigating the influence of nonlinear behaviors of soil on the dynamic response of rigid shallow foundations. A simple nonlinear constitutive relationship for the cyclic response of lightly overconsolidated soil was implemented in *FLAC* for the study, which was simplified from the original Pender model (Pender, 1978) for a particular undrained case where effective mean principal pressure during triaxial compression is constant. Further study on the topic was undertaken by Pender and Ni in 2004.

The previous work had indicated that a numerical distortion (instability) problem occurs in nonlinear dynamic analysis when a nonlinear soil model is implemented in *FLAC* with 'apparent modulus' approach. Based on some initial study on Mohr-Coulomb model and the modified Cam-clay model, it was proposed that use of 'plastic correction' approach might be a solution to the problem. To verify this, further study needed to be carried out using more sophisticated nonlinear work-hardening soil models. This was the initial drive for the current study.

1.2 Objectives

The main objectives are:

- To explore methodologies of implementing nonlinear constitutive models of soil in *FLAC* to minimize numerical instability in dynamic analysis;
- To undertake a study on a bounding surface bubble soil model, *i.e*. the Bubble model, and implement the model in *FLAC*; and
- To investigate influence of nonlinearity of soil on dynamic response of rigid foundations using the Bubble model.

1.3 Scope of work

Methodologies of implementing nonlinear soil models in FLAC

A user can implement a constitutive model with the programming language *FISH* embedded in *FLAC*. A user-defined model (UDM) can be used in the same way as a built-in model. However, some aspects with regard to implementing a constitutive model are not explained explicitly in *FLAC* manuals. Much practice with simple models is required to thoroughly understand *FLAC*'s methodologies prior to implementing a sophisticated constitutive model.

On the other hand, numerical distortion is another issue to deal with in nonlinear dynamic analysis. Previous work has indicated that a special kind of numerical distortion can be introduced into a nonlinear dynamic analysis with *FLAC* (Ni, 2001). Although applying additional mechanical damping can minimize the problem, a better solution needs to be found so that results of nonlinear dynamic analysis can be more realistic.

The Bubble model

The Bubble model was first proposed by Al Tabbaa & Wood in 1989 as an extension to the modified Cam-clay model and was formulated within the kinematic hardening framework similar to the two-surface model proposed by Mróz et al. (1979). The model has been further developed for modeling of structured soils (Wood, 1995; Rouainia & Wood, 2000).

Although the framework of the model has been well established and the model can demonstrate essential phenomena of pre-failure behaviors of natural clays, the modulus functions of the model remain to be further studied.

Programming of the Bubble model

The 'plastic correction' approach is the recommended method for implementing the Bubble model. The key criterion is that satisfactory dynamic analysis should be achieved without using any additional damping.

Parametric study

The Bubble model has ten parameters. Some of them are non-standard parameters. The study is aimed to gain some general knowledge about the importance of each parameter, typical values of the non-standard parameters and qualitative inter-relationships between the parameters.

Vertical vibration of rigid foundations

As an application of the Bubble model, the study investigates the influence of nonlinearity of soil on dynamic response of rigid shallow foundations.

1.4 Layout of the thesis

Chapter 2 presents a literature review which covers 'Constitutive models of soil', 'Nonlinear dynamic analysis with *FLAC*' and 'Vertical vibration of rigid foundations'. The Bubble model and several other most relevant soil constitutive models are reviewed and the main differences between them are discussed.

In Chapter 3, some key fundamentals are discussed with regards to the incremental programming in *FLAC* as they are important to a successful implementation of a soil constitutive model.

In Chapter 4, strategies of implementing nonlinear constitutive models are explored in order to reduce numerical distortion. Two approaches, *i.e.* 'apparent modulus' approach and 'plastic correction' approach, are discussed. A hyperbolic model in *FLAC*, which is implemented with the 'apparent modulus' approach, is modified to demonstrate the phenomenon of numerical distortion in nonlinear dynamic analysis. A bilinear model is proposed and is implemented with the concept of the 'plastic correction' approach to show the capability of the method to cope with numerical instability in dynamic analysis.

Chapter 5 presents the Bubble model in detail. Modifications to the model are proposed and discussed. Some key aspects of the model are also discussed. The implementation of the Bubble model is explained and the *FISH* code is appended to the chapter.

In Chapter 6 analyses with *FLAC* are carried out to test the Bubble model and the implementation methodologies. The work includes illustration of the main features of the model (*e.g.* non-intersection translation of the yield surface and destructuration process of the structure surface), demonstration of its stress-strain behaviours, comparison with the modified Cam-clay model and published experimental data, and verification of numerical stability in dynamic analysis.

Chapter 7 presents a parametric study, which is carried out to investigate importance and the effective range of each parameter of the Bubble model. Stress-strain behaviours of the model with a maximum strain up to 10% are explored in the parametric study. G-γ behaviours over a small range of strain (less than 2%) are also analyzed and key parameters affecting G-γ curves are identified.

Chapter 8 is on the application of the Bubble model. *FLAC* analyses are undertaken to investigate effects of nonlinearity of soil on vertical dynamic compliance of rigid foundations. Factors studied include initial stress level in the soil, level of excitation and mass ratio of foundation.

Chapter 9 presents a summary of the main results of the study including conclusions and discussions.

1.5 General remarks

The study provides useful experience in implementation of soil constitutive models in *FLAC*. Particularly, it has been found that the methodology of 'plastic correction' approach should be adopted when a nonlinear soil model is implemented in order to eliminate or minimize numerical distortion in nonlinear dynamic analysis. In this method

dynamic damping can be purely hysteretic and no additional mechanical damping is required to obtain a satisfactory dynamic analysis. For static analysis or linear dynamic analysis, however, use of the method is not necessary.

The Bubble model was initially chosen for the study on numerical instability in nonlinear dynamic analysis. Apart from that, an extensive analytical study on the Bubble model has also been undertaken. Especially, the plastic modulus function and parameters of the model have been studied. A modified plastic modulus function has been proposed, which has been found to better incorporate the influence of the size ratio of the yield surface on behaviours of the model.

The Bubble model has been implemented in *FLAC* for 2D plane strain problems. For 2D plane stress or 3D problems, the *FISH* code of the model will need to be modified. Analyses have been carried out using the Bubble model to simulate laboratory triaxial tests and vertical vibration of rigid strip foundations. In general the results agree satisfactorily with published data.

2 LITERATURE REVIEW

This literature review covers three parts: 'Constitutive models', 'Nonlinear analysis with *FLAC*' and 'Vertical vibration of rigid foundations'.

A full description of a kinematic hardening model for structured soils (Rouainia & Wood, 2000) is given in Chapter 5. The review in the chapter has been focused on the most relevant background and development of the model. Recent development of other similar models has also been reviewed. The main relations and differences between those models are discussed. Attention has also been paid to application of those models in modeling behaviours of natural soils and parametric studies. An overall comment regarding the development of 2 or 3-surface models is given at the end of the chapter with areas identified for further research.

The review of 'nonlinear analysis with *FLAC*' has been focused on implementation of nonlinear constitutive models in *FLAC* and their application in dynamic modeling. The main problems in nonlinear modeling with *FLAC* are discussed in the chapter and will be addressed in Chapters 3 and 4.

2.1 Constitutive models of soil

2.1.1 Critical state soil mechanics and Cam-clay model

One of the main distinctive features of soil is its volumetric behaviour under shear. Prior to the critical state soil mechanics, soil mechanics was based on theories for solid engineering materials, *e.g.* metal. Those classical theories can not account for the volumetric behaviour of soil appropriately. Early constitutive models (*e.g.* elastic and perfectly plastic model) over-idealized the behaviours of soil. Although they are still widely used for engineering purposes, they are fundamentally inappropriate and are not representative of natural behaviours of soil. For the first time, critical state soil mechanics

proposed by Roscoe, Schofield and Wroth (1958) gave an appropriate description of volumetric response of soil under shear.

The critical state soil mechanics describes a state of soil in the '*p, q, e*' space. The critical state of soil is an ultimate state of shear failure which the soil will eventually reach regardless of its stress history and path. At the critical state, continuous shear strain develops without change in stress and volume of soil, *i.e.* $dq = dp = dv = 0$. The critical state line is shown in Figure 2.1. The projection of the critical state line in p, q plane is approximated by the relationship $q = Mp$. It is also assumed that soil behaviours under the surfaces are purely elastic. (Note: q is the deviator stress defined as the difference between the major principal stress and minor principal stress, *i.e.* $q = \sigma_1 - \sigma_3$. p is the effective mean stress, *i.e.* $p = (\sigma_1' + \sigma_2' + \sigma_3')/3$. e is void ratio of soil).

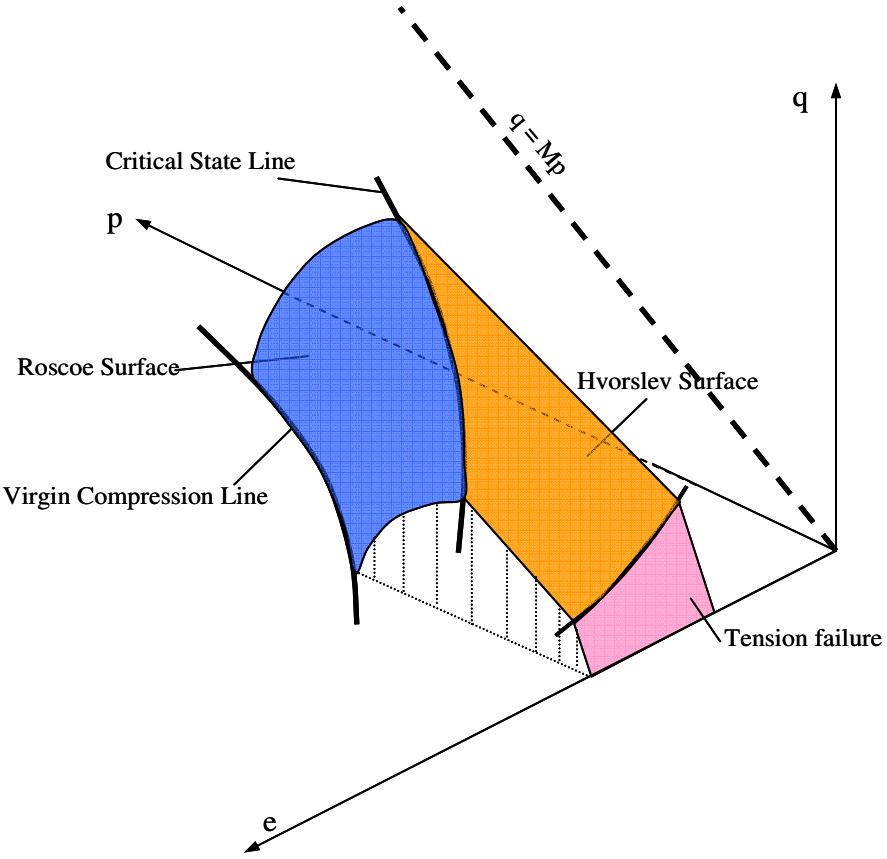

Figure 2.1 State boundary surfaces

The general concept of using the theory of work-hardening plasticity to describe soil stress-strain relationship was first proposed by Drucker *et al* (1957). They suggested using a spherical 'cap' on the 'Drucker-Prager cone'. The 'cap' can be expanded by hydrostatic loading of the soil. This 'cap' model was further developed by a group of researchers at Cambridge. With a small number of assumptions, a simple work-hardening model was proposed by Roscoe and Schofield (1963), *i.e*. the original Cam-clay model (See Figure 2.2). The use of simple formulations in p, e and p, q planes allows the model to predict more realistically many behaviours of soil under undrained and drained conditions.

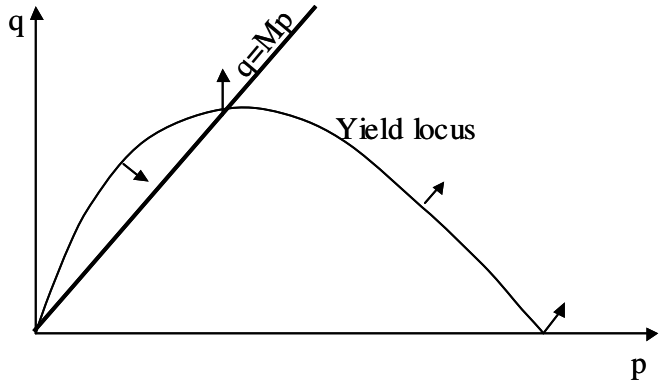

Figure 2.2 Yield locus of Original Cam-clay model

The Cam-clay model was soon further developed by Burland (1965) and Roscoe and Burland (1968) to improve its prediction of the behaviours of normally-consolidated soils. One of the main problems of the original Cam-clay model is the unrealistic prediction of strain at small stress ratios. Large shear strain is predicted even at an isotropic stress state. In the modified Cam-clay model (MCC), the yield and potential surfaces become elliptical due to choice of a new formulation of work dissipation (See Figure 2.3). The yield function in effective stress and isotropic hardening rule are given by

$$f = \frac{q^2}{M^2} + (p - p_0/2)^2 - (p_0/2)^2 = 0$$
$$dp_0 = \frac{p_0}{\lambda - \kappa} dv^p \tag{2.1}$$

Where p_0 denotes the size of the yield surface, dv^p is the change in specific volume, and λ, κ are the slope of virgin compression line and swelling line respectively on the v ~ $ln(p)$ plots (v is the specific volume of soil, *i.e.* $v = 1 + e$).

It is assumed that any change in mean pressure is accompanied by elastic change in volume and this suggests a formulation of the bulk modulus: $K = vp/\kappa$.

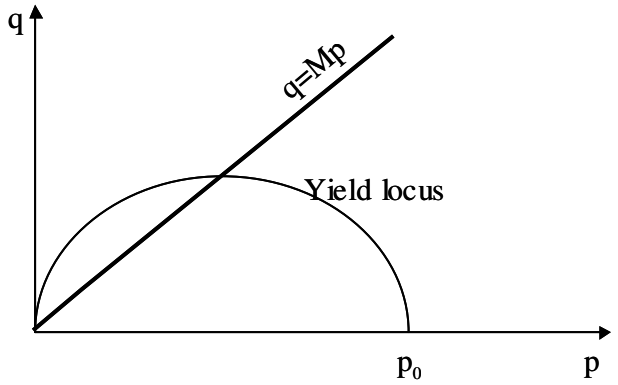

Figure 2.3 Yield locus of modified Cam-clay model

The flow rule associated with the yield surface gives the following incremental form of plastic strains.

$$\begin{bmatrix} d\varepsilon_v^p \\ d\varepsilon_q^p \end{bmatrix} = \frac{1}{H} \begin{bmatrix} (M^2 - \eta^2)p^2 & 2\eta(M^2 - \eta^2)q^2 \\ 2\eta(M^2 - \eta^2)p^2 & 4q^2 \end{bmatrix} \begin{bmatrix} dp \\ dq \end{bmatrix} \tag{2.2}$$

Where

$\eta = q/p$;

e is void ratio of soil; and

H is plastic modulus defined by a hardening function given by

$$H = \frac{(1+e)p^3(M^4 - \eta^4)}{\lambda - \kappa} \tag{2.3}$$

The Cam-clay model is a milestone in the development of non-linear constitutive laws. However the assumption of elasticity under the state boundary surface limits its application to monotonic loading because the model predicts a constant pore water pressure response after the first cycle of loading under cyclic loading. Cyclic accumulation of pore water pressure and cyclic degradation in stiffness can not be predicted by the model. To extend the Cam-clay model for use under cyclic loading, many constitutive models have been developed with different approaches. They include the two-surface model proposed by Mróz *et al* (1979), the vanishing yield surface model by Pender (1978) and the bounding surface model by Dafalias (1986). The following review of literature summarizes the main stream of two or three-surface models which are most relevant to the development of the Bubble model.

Note: The above literature review of the Cam-clay model is based on information from various sources including Wood (1990), Pender (1989), Brito & Gunn (1987) and Botts (1998).

2.1.2 Two - surface model (Mróz et al. 1979)

The concept of two-surface models is to reduce the elastic domain by introducing an inner surface (yield surface) inside an outer surface (bounding surface). These models involve an anisotropic (*i.e.* kinematic) hardening rule which allows the yield surface not only to expand but also to translate or even rotate inside the bounding surface. Mróz (1967) proposed a multi-surface kinematic hardening model for metal. The concept was used to develop two or multi-surface models for soil by Mróz, Norris and Zienkiewicz (1978a, 1978b and 1979).

A simple version of the two-surface model is illustrated in Figure 2.4. $F = 0$ is called the consolidation surface (*i.e.* bounding surface), which reflects isotropic properties of the material and depends on the density of soil. This surface is believed to represent the memory of peak stresses (phenomena of dependence of soil properties on the consolidation history). It may expand, contract and translate. Its function is given by

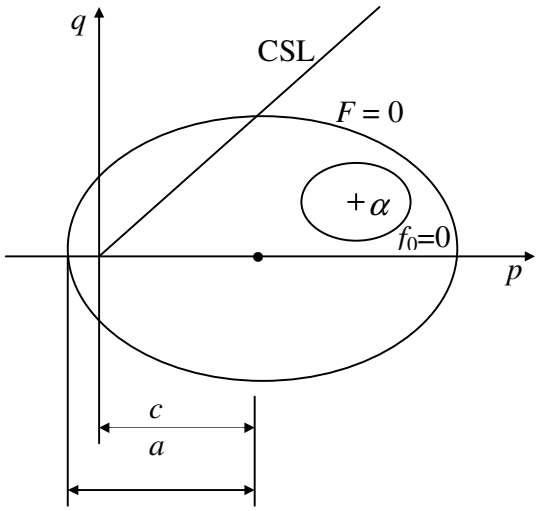

Figure 2.4 The two-surface model by Mróz

$$F = (p-c)^2 + \frac{q^2}{n^2} - a^2 = 0 \tag{2.4}$$

In equation 2.4, n is the ratio of minor and major axes of the elliptical consolidation surface; a is the major semi-diameter of ellipse; $c = a\frac{n}{m}$ is the distance from the origin to the centre of the consolidation surface on p axis; m is the slope of the critical state line. The consolidation surface is always centered on the p axis. When $c = a$, *i.e.* $n = m$, Eq. 2.4 is the same as the yield function of the modified Cam-clay model.

A smaller yield surface (inner surface) is introduced, which represents the anisotropic characteristics of plastic deformation. The yield function is given by

$$f_0 = (p-\alpha_p)^2 + \frac{(q-\alpha_q)^2}{n^2} - a_0^2 = 0 \tag{2.5}$$

Where a_0 is the semi-diameter of the ellipse; $\boldsymbol{\alpha} = (\alpha_p, \alpha_q)$ is the centre of the yield surface in p, q space. The yield surface has the same shape as the consolidation surface and the ratio of size between the yield and consolidation surfaces is a_0/a.

The flow rule is associated with the yield surface and is given by Equation 2.6.

$$\begin{bmatrix} d\varepsilon_v^p \\ d\varepsilon_q^p \end{bmatrix} = \frac{1}{K_p} \begin{bmatrix} \dfrac{p-\alpha_p}{G_f} \\ \dfrac{q-\alpha_q}{n^2 G_f} \end{bmatrix} d\sigma_n \tag{2.6}$$

$$d\sigma_n = \frac{(p-\alpha_p)dp + \dfrac{q-\alpha_q}{n^2}dq}{G_f}, \qquad G_f = \left[(p-\alpha_p)^2 + \frac{(q-\alpha_q)^2}{n^4} \right]^{0.5} \tag{2.7}$$

In Eq.2.6 Kp is plastic modulus defined by a general form of hardening function, which is given by

$$K_p = K_{PR} + (K_{P0} - K_{PR})(\frac{\delta}{\delta_0})^{\gamma} \tag{2.8}$$

Where δ is the transformed distance from the stress point P on the yield surface to its conjugate point R on the consolidation surface (see Figure 2.5), *i.e.* $\delta = [(q_R - q_P)^2 / n^2 + (p_R - p_P)^2]^{0.5}$. δ_0 is the maximum distance, *i.e.* $\delta_0 = 2(a - a_0)$. a_0 is the major semi-diameter of the yield surface. δ_0 plays a role in incorporating the

maximum preloading into the material memory. K_p varies continuously from its initial value K_{p0} on the yield surface when $\delta = \delta_0$ to the respective value K_{pR} on the consolidation surface for $\delta = 0$, that is, when the yield surface contacts the consolidation surface. γ is a parameter controlling the degradation rate of plastic modulus.

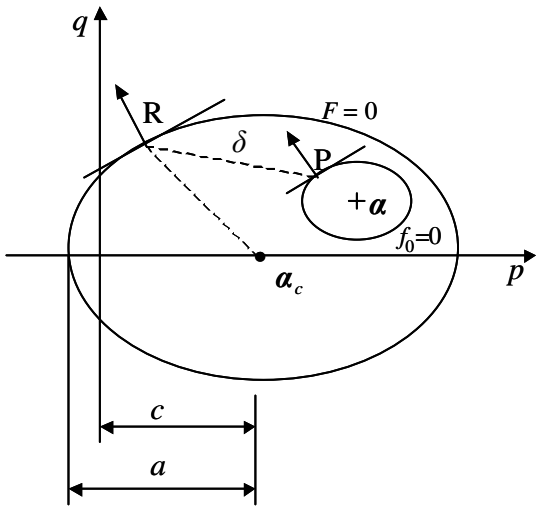

Figure 2.5 Illustration of kinematic hardening rule

The isotropic hardening rule is given by

$$a = a_i \exp[\frac{(1+e_0)d\varepsilon_v^p}{\lambda - \kappa}] \tag{2.9}$$

Kinematic hardening rule postulates that the surfaces f_0 and F do not intersect but engage each other along the common normal. This assumption can be expressed mathematically by associating each point P on the yield surface with a conjugate point R on the consolidation surface characterized by the same direction of normal (see Figure 2.5). Since the two surfaces have the same shape, the following scaling relationship is applicable for each stress state on the yield surface.

$$\frac{\boldsymbol{\sigma}_P - \boldsymbol{\alpha}}{a_0} = \frac{\boldsymbol{\sigma}_R - \boldsymbol{\alpha}_c}{a} \tag{2.10}$$

A descriptive form of the kinematic hardening rule is given by Eq.2.11. It has three terms. The first term denotes the change of centre of consolidation surface, the second term represents the size scaling and the third term denotes the translation along the line *PR* (*i.e.* β line).

$$\begin{aligned} d\boldsymbol{\alpha} &= d\boldsymbol{\alpha}_c + \frac{da - da_0}{a_0}(\boldsymbol{\sigma}_P - \boldsymbol{\alpha}) + \boldsymbol{\beta} d\mu \\ \boldsymbol{\beta} &= (\boldsymbol{\sigma}_R - \boldsymbol{\sigma}_P) \end{aligned} \tag{2.11}$$

Where $d\boldsymbol{\alpha}_c = [da\frac{n}{m}, 0]$, $d\mu$ is given by

$$d\mu = \frac{df_{0\sigma} - 2a_0 - [\frac{\partial f_0}{\partial p}(p_P - \alpha_P) + \frac{\partial f_0}{\partial q}(q_P - \alpha_q)](\frac{da - da_0}{a_0})}{\frac{\partial f_0}{\partial p}[c - p_P + \frac{a}{a_0}(p_P - \alpha_P)] + \frac{\partial f_0}{\partial q}[-q_P + \frac{a}{a_0}(q_P - \alpha_q)]} - \frac{\partial f_0}{\partial p}\frac{n}{m}da \tag{2.12}$$

The constitutive relation is given by.

$$\begin{aligned} dq &= 3G_s(d\boldsymbol{\varepsilon}_q - \frac{1}{K_p}\frac{q - \boldsymbol{\alpha}_q}{n^2 G_f} d\boldsymbol{\sigma}_n) \\ dp &= K_s(d\boldsymbol{\varepsilon}_v - \frac{1}{K_p}\frac{p - \boldsymbol{\alpha}_p}{G_f} d\boldsymbol{\sigma}_n) \end{aligned} \tag{2.13}$$

Where K_s is the bulk modulus formulated in the same way as in the modified Cam-clay model and G_s is the shear modulus.

For the undrained condition the following incremental formulation of pore water pressure is utilized, which is identical to the equation proposed by Skempton and Sowa (1963).

$$dp_w = dp^t + a_w dq \tag{2.14}$$

$$a_w = A_s - \frac{1}{3}$$

Where a_w is the incremental pore pressure coefficient, A_s denotes Skempton's pressure coefficient.

A vanishing elastic region (no yield surface) is considered by letting $a_0 = 0$, so there is no need to identify the start of yielding. The plastic flow is then associated with the consolidation surface. Similar equations to equations 2.6 can be obtained and apply from the beginning of loading as there is no elastic region. However, Hashiguchi (1985) reported that this vanishing model is not acceptable physically and mathematically.
Mróz, Norris and Zienkiewicz (1979) used the above two-surface model to study drained and undrained behaviours of kaolin and Weald clays after isotropic and anisotropic consolidation. The agreement between predicted and experimental stress paths were satisfactory, especially for lightly over-consolidated clay. Response under cyclic loading for a K_0 consolidation was also discussed for stress-controlled loading. The behaviours of progressive densification after 4 cycles was demonstrated. For an undrained case, a steady-state was reached after 50 cycles.

In summary, the kinematic hardening model proposed by Mróz *et al* in 1970s set up a general framework for other researchers to develop similar two or three-surface models. The model represented one branch of the efforts to extend the modified Cam-clay model for use in cyclic loading. The concepts used to formulate the kinematic rule and hardening function have been employed by many other workers to develop various models.

2.1.3 Kinematic hardening rule (Hashiguchi 1985)

Among many others, Hashiguchi (1981, 1983, 1985) formulated a two-surface model. The model is formulated for a generalized stress state. A distinct-yield surface (*i.e.* bounding surface) and a sub-yield surface are shown in Figure 2.6. A general form of the distinct-yield surface is described by the following equation.

$$\begin{aligned} &f(\hat{\boldsymbol{\sigma}}) - F(K) = 0 \\ &\hat{\boldsymbol{\sigma}} = \boldsymbol{\sigma} - \hat{\boldsymbol{\alpha}} \end{aligned} \tag{2.15}$$

Where $\boldsymbol{\sigma}$ is a second-order stress tensor. K is a scalar which describes the isotropic hardening/softening of surface, $\dot{K} = 0$ when $\dot{\boldsymbol{\varepsilon}}^{p} = 0$. $\hat{\boldsymbol{\alpha}}$ is the centre of the distinct-yield surface describing the translation of the surface according to a prescribed kinematic hardening rule. The degree of the function f is denoted by n.

The sub-yield surface has the same shape as the distinct-yield surface, which encloses the elastic region. The current stress stays either on or within the sub-yield surface. The equation of the sub-yield surface is given by

$$\begin{aligned} &f(\overline{\boldsymbol{\sigma}}) - \gamma^{n} F(K) = 0 \\ &\overline{\boldsymbol{\sigma}} = \boldsymbol{\sigma} - \overline{\boldsymbol{\alpha}} \end{aligned} \tag{2.16}$$

Where $\gamma\,(0 \le \gamma \le 1)$ is a material constant; $\overline{\boldsymbol{\alpha}}$ is the center of the sub-yield surface.

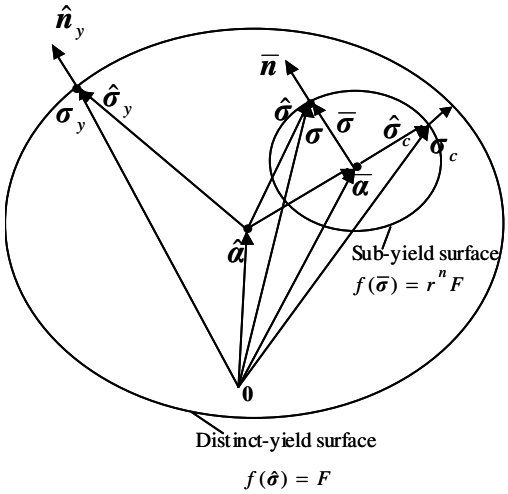

Figure 2.6 Two- surface model (Hashiguchi 1985)

A kinematic hardening rule was proposed by Hashiguchi (1985). It is formulated to avoid intersection of sub-yield surface with distinct-yield surface. The hardening rule of the distinct-yield surface is given as follows:

$$\dot{\hat{\boldsymbol{\alpha}}} = A\dot{\varepsilon}_v^p \mathbf{I} + B\mathrm{tr}(\dot{\boldsymbol{\varepsilon}}^p \frac{\bar{\boldsymbol{\sigma}}}{|\bar{\boldsymbol{\sigma}}|})\frac{\bar{\boldsymbol{\sigma}}}{|\bar{\boldsymbol{\sigma}}|} \tag{2.17}$$

In the above equation, the first term represents the contribution of isotropic hardening and $\mathbf{I}$ is the 2nd order identity tensor. The second term represents the anisotropic hardening. 'tr' is trace operator. A and B are two scalar functions of K ($A \geq 0, B \geq 0$). If B = 0, the hardening rule becomes isotropic.

Non-intersection condition of the surfaces is ensured by letting $f(\hat{\boldsymbol{\sigma}}_c) \leq F(K)$ and $\hat{\boldsymbol{\sigma}}_c = \boldsymbol{\sigma}_c - \hat{\boldsymbol{\alpha}}$. $\boldsymbol{\sigma}_c$ is the stress state at the intersecting point of the sub-yield surface and the line through the centres of the two surfaces. By satisfying the non-intersection condition and with a simple assumption, the kinematic hardening rule of the sub-yield surface is obtained as follows:

$$\dot{\bar{\boldsymbol{\alpha}}} = \dot{\hat{\boldsymbol{\alpha}}} + \frac{1}{n}\frac{\dot{F}}{F}(\bar{\boldsymbol{\alpha}} - \hat{\boldsymbol{\alpha}}) + \dot{\mu}\boldsymbol{\beta} \tag{2.18}$$

$$\boldsymbol{\beta} = \boldsymbol{\sigma}_y - \boldsymbol{\sigma}$$

$$\dot{\mu} = \frac{\mathrm{tr}\left\{\bar{\mathbf{n}}(\dot{\hat{\boldsymbol{\sigma}}} - \frac{1}{n}\frac{\dot{F}}{F}\hat{\boldsymbol{\sigma}})\right\}}{\mathrm{tr}(\bar{\mathbf{n}}\boldsymbol{\beta})}$$

Where $\boldsymbol{\sigma}_y$ is the conjugate stress on the distinct-yield surface. $\bar{\mathbf{n}}$ denotes the stress gradient on the sub-yield surface at the current stress state, which is normalized with respect to the center of the sub-yield surface.

Compared with the kinematic hardening rule (Eq. 2.11) proposed by Mróz *et al* (1979), the major change in Eq. 2.18 is the second term, which represents the translation along the line connecting the centers of the surfaces while in Eq.2.11 the second term is associated with the translation along the line connecting the current stress state and the center of the inner surface.

A three-surface model was also proposed by Hashiguchi (1985). Another surface, *i.e.* loading surface, is introduced inside the sub-yield surface. The purpose is to smoothen the transition of stiffness when stress path reaches on the sub-yield surface.

2.1.4 Recent development of two/three-surface models

Bubble model

The original Bubble model was proposed by Al Tabbaa & Wood (1989). It was formulated for triaxial stress state. The model is similar to the two-surface model proposed by Mróz *et a* (1979). The outer surface is the same as the modified Cam-clay surface, which is centered on the p axis and passes through the origin but does not intersect the q axis. The inner surface is called the 'bubble', which encloses the elastic region. The size of the Cam-clay surface is indicated by p_0. The bubble has the same shape as the Cam-clay surface. The ratio of size between the bubble and the Cam-clay

surface is a constant expressed by the parameter '*R*'. The two surfaces are illustrated in Figure 2.7. Their functions are given by

$$(p - p_0)^2 + \frac{q^2}{M^2} - p_0^2 = 0 \tag{2.19}$$

$$(p - p_\alpha)^2 + \frac{(q - q_\alpha)^2}{M^2} - R^2 p_0^2 = 0 \tag{2.20}$$

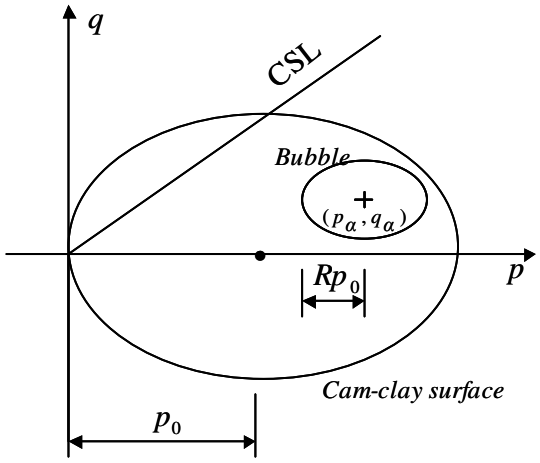

Figure 2.7 The original bubble model (Al Tabbaa & Wood, 1989)

The kinematic hardening rule of the bubble is given by

$$\begin{bmatrix} \delta p_\alpha \\ \delta q_\alpha \end{bmatrix} = \frac{\delta p_0}{p_0} \begin{bmatrix} p_\alpha \\ q_\alpha \end{bmatrix} + S \begin{bmatrix} \frac{p - p_\alpha}{R} - (p - p_0) \\ \frac{q - q_\alpha}{R} - q \end{bmatrix} \tag{2.21}$$

Where S is given by

$$S = \frac{(p - p_\alpha)(\delta p - \frac{\delta p_0}{p_0} p_0) + \frac{(q - q_\alpha)}{M^2}(\delta q - \frac{\delta p_0}{p_0} q)}{(p - p_\alpha)[\frac{p - p_\alpha}{R} - (p - p_0)] + \frac{q - q_\alpha}{M^2}(\frac{q - q_\alpha}{R} - q)} \tag{2.22}$$

The kinematic hardening rule is similar to the translation rule proposed by Hashiguchi (1985). The translation rule of the bubble has to guarantee that the bubble and the bounding surface can touch at a common normal, but must never intersect. A conjugate point on the bounding surface can be associated with the current stress point on the bubble in such a way that these two points have the same direction of outward normal. Translation of the bubble, which occurs when plastic strains are being generated, can be separated into two components. One part is associated with change in size of the surfaces (the first term in Eq.2.21), the other part is associated with translation of the bubble along the vector $\boldsymbol{\beta}$ (the second term of Eq.2.21).

The isotropic hardening rule is the same as that of the modified Cam-clay model but λ, κ are replaced by λ^*, κ^*.

$$\delta p_0 = \frac{p_0}{(\lambda^* - \kappa^*)} \delta \varepsilon_v^p \tag{2.23}$$

Where λ^* is the slope of normal compression lines in $lnv : lnp$ compression plane; κ^* is the initial slope of the unloading lines in the $lnv : lnp$ compression plane.

The hardening function is given by

$$h = h_0 + H \tag{2.24}$$

Where h_0 is the plastic modulus when the bubble and the bounding surface are in contact corresponding to the current stress point. H is a scalar quantity to ensure a smooth fall of

stiffness when the bubble approaches the bounding surface. h_0 and H are given by equations 2.25 and 2.26 respectively.

$$h_0 = \frac{(p - p_\alpha)}{(\lambda^* - \kappa^*)}\left[p(p - p_\alpha) + \frac{q(q - q_\alpha)}{M^2} \right] \tag{2.25}$$

$$H = \frac{p_0^3}{(\lambda^* - \kappa^*)}\left(\frac{b}{b_{\max}}\right)^{\psi} \tag{2.26}$$

Where b is the component of the vector $\boldsymbol{\beta}$ in the direction of the normal to the bubble at the current stress point. It is given by

$$b = \frac{1}{Rp_0}\left\{ (p - p_\alpha)\left[\frac{p - p_\alpha}{R} - (p - p_0)\right] + \frac{(q - q_\alpha)}{M^2}\left(\frac{q - q_\alpha}{R} - q\right)\right\} \tag{2.27}$$

For M<1, $b_{\max}$ is given by*

$$b_{\max} = 2p_0(1 - R) \tag{2.28}$$

It should be noted that in equation 2.28 $b_{\max}$ only depends on the size of the surfaces. Modification was made by Wood (1995) so that $b_{\max}$ also depends on the current stress state.

In fact many other functions of H can be chosen as long as they can ensure a smooth fall of stiffness. Choice of H may depend on the type of soil. Al Tabbaa & Wood (1989) reported that transition of stiffness as the effective stress path leaves the elastic region on reaching the edge of the bubble is too abrupt but this can be improved by altering the hardening function H.

In summary the Bubble model is a simplified version of the two-surface model proposed by Mróz *et a* (1979). The kinematic hardening rule is based on the non-intersection rule

* For $M \geq 1$, $b_{max} = 2p_0 M(1 - R)$

proposed by Hashiguchi (1985). A particular development of the Bubble model is the hardening function which has elements similar to those of the modified Cam-clay model. The model has been found to be quite successful in modeling some patterns of response observed in slow cyclic oedometer and triaxial tests of speswhite kaolin. It requires only two parameters in addition to the parameters of the Cam clay model.

Modified Bubble model (Wood, 1995)

The original Bubble model was extended by Wood (1995) for structured soil [Note: structured soil is defined for natural soil following Mitchell (1976) as having different mechanical behaviour after being remoulded due to damage to its initial structure, *i.e.* particle arrangement and bonding]. It is assumed that the initial structure of soil is progressively destroyed as plastic deformation occurs. The process of the destructuration is represented by the steady fall of the structure surface (bounding surface) towards the reference surface representing the intrinsic behaviours of remolded soil (Burland, 1990). The kinematic hardening rule proposed by Hashiguchi (1985) is utilized and the hardening function is similar to that proposed by Al Tabbaa & Wood (1989). The model is still formulated for the triaxial stress state and no anisotropy of the structure surface is considered. The structure and reference surfaces are centered on the p axis passing through the origin of coordinates. The bubble has the same elliptical shape as reference and structure surfaces. Their sizes are represented by Rp_0, p_0 and rp_0 respectively as shown in Figure 2.8. R is a constant (R = 0 ~1). r is between 1 and r_0 which represents the initial size of structure surface and is not less than 1. r = 1 indicates completion of destructuration when the structure surface coincides with the reference surface. r is determined by an exponential destructuration law (see Eq.2.29).

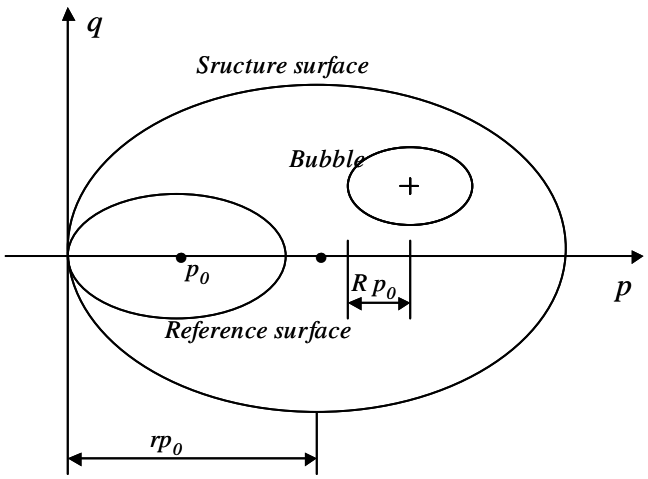

Figure 2.8 Bubble model for structured soil (Wood, 1995)

$$r = 1 + (r_0 - 1)\exp(\frac{-k\varepsilon_d}{\lambda - \kappa})$$
$$\delta r = \frac{-k}{(\lambda - \kappa)}(r-1)\delta\varepsilon_d \qquad (2.29)$$

Where k is a parameter controlling the rate of destructuration with strain; $\delta\varepsilon_d$ is the rate of destructuration strain (ε_d), which is given as follows.

$$\delta\varepsilon_d = \sqrt{(1-A)(\delta\varepsilon_p^p)^2 + A(\delta\varepsilon_q^p)^2} \qquad (2.30)$$

Where 'A' is a parameter ranging from 0 to 1, which reflects relative contribution of volumetric and distortional strains to destructuration. For A = 0, destructuration is purely volumetric and for A = 1, destructuration is entirely distortional.

The hardening function is similar to that proposed by Al Tabbaa & Wood (1989) but the definition of $b_{\max}$ is slightly different from eq.2.28 as it depends on both the size of surfaces and the current stress state. It is given by

$$b_{\max} = 2(\frac{r}{R} - 1)\overline{\boldsymbol{n}} \bullet \overline{\boldsymbol{\sigma}} \qquad (2.31)$$

Where $\overline{\boldsymbol{n}}$ is the unit normal to the bubble at the current stress point; $\overline{\boldsymbol{\sigma}}$ is the normalized stress state with respect to the center of the bubble.

The model was further generalized by Rouainia & Wood (1998) for general stress state with anisotropy of the structure surface and by Rouainia & Wood (2000) to incorporate the Lode angle θ into yield functions[†]. Details of the model are given in Chapter 5.

Comparison of the model with experimental data has shown that the Bubble model can demonstrate the essential phenomena of pre-failure behaviours of natural clays (Swedish clay): stiffness variation with strain, volumetric change accompanying distortion, peak strength at small strains.

In summary, the modified Bubble model is an extension to the modified Cam-clay model with kinematic hardening and bounding surface plasticity plus destructuration. Although the model has three surfaces, it is in fact a two-surface model as the reference surface is neither involved in the kinematic hardening rule nor the hardening function. It is used only as a reference to the intrinsic behaviours of remolded soil. The model can be regarded as a framework in the modeling of structured soil.

3-SKH model (Stallebrass)

An extension to the original Bubble model by Al Tabbaa & Wood (1989) was also proposed by Stallebrass (1990) and was further developed by Stallebrass & Taylor (1997). This is a three-surface model and is named '3-SKH'. Apart from the yield surface (*i.e.* the bubble), another kinematic yield surface (history surface) is introduced into the model to represent the influence of recent stress history on stiffness and shear-volumetric response of soil. An associated flow rule is utilized in the 3-SKH model. A simple non-

associated flow rule was used by McDowell (2002) and McDowell *et al* (2003) to improve the 3-SKH model in predicting the coefficient of earth pressure at rest (K_0) under one-dimensional normal compression. The Lode angle θ was incorporated into the critical state parameter M.

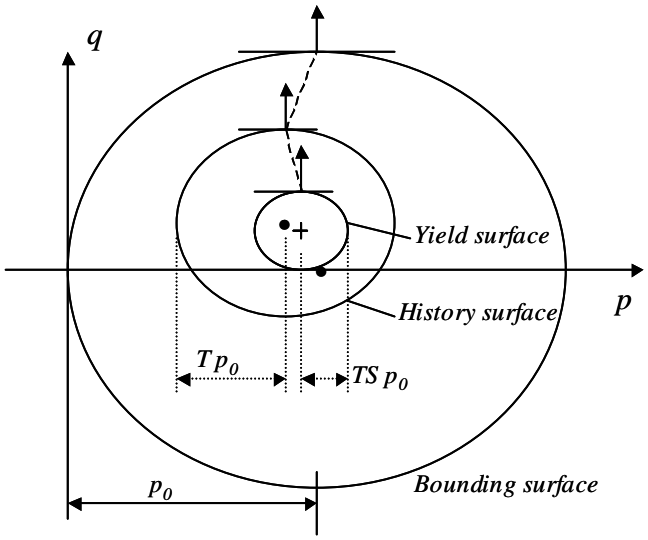

Figure 2.9 3-SKH model

The main change of the 3-SKH model to the original Bubble model is the involvement of a history surface in the translation rule and the hardening function (see Eq. 2.32). Compared to Eq. 2.23, the new hardening function has one more term which is associated with the history surface. This is believed to be able to ensure a smooth change in stiffness when the surfaces are in contact.

$$h = \frac{1}{\lambda^* - \kappa^*}\left\{(p - p_b)[p(p - p_b) + q\frac{(q - q_b)}{M^2}] + (\frac{b_1}{b_{1\max}})^{\psi} p_0{}^3 S^2 + (\frac{b_2}{b_{2\max}})^{\psi} p_o{}^3\right\} \quad (2.32)$$

It is understandable that the more surfaces are involved in the formulations of the kinematic hardening rule and the hardening function, the smoother the transition in stiffness. To introduce a precise memory of loading history within the bounding surface, a set of nesting surfaces were also introduced by Mróz (1967), Mróz, Norris &

† McDowell (2003) indicated that Lode angle has little effect under triaxial conditions.

Zienkiewicz (1978a) and Prevost (1977). Hashiguchi (1985) also proposed a 3-surface model for this purpose by introducing a loading surface inside rather than outside the yield surface.

S3-SKH model (Baudet and Stallebrass)

Baudet & Stallebrass (2004) extended the 3-SKH model for structured soil. In this model the degree of structure is entirely interpreted as and related to sensitivity of soil. The bounding surface is called sensitivity surface and its size is represented by a sensitivity parameter, *S*, which has a similar physical meaning as the parameter *r* of the modified Bubble model (Wood, 1995). However, the ultimate value of *S* is not necessarily unity and a value greater than unity can be used to simulate stable elements of structure such as in Sibari clay (Coop & Cotecchia, 1995). The same destructuration law as Equation 2.28 is used except for the slight difference in defining destructuration strain which is given by

$$\dot{\varepsilon}^d = \sqrt{(\dot{\varepsilon}_v^p)^2 + (\dot{\varepsilon}_s^p)^2} \tag{2.33}$$

Unlike Eq.2.30, the above equation gives a destructuration strain which comprises equally volumetric and distortional contributions (equivalent to $A = 0.5$ case in Eq.2.30). In this model the sensitivity surface is centered on the p axis and anisotropy is not included.

The model was used to simulate drained probing tests and undrained triaxial tests on natural specimens of Bothkennar clay. The sensitivity framework by Cotecchia & Chandler (2000) was the basis for choosing initial and ultimate values of the sensitivity parameter. Both sensitivity and destructuration parameters were derived from standard isotropic compression tests. A good agreement between computer simulation and experiments on the $G-\gamma$ curves was obtained by using an initial sensitivity of 13.5 and an ultimate sensitivity of 6. However, no data was shown for the small strain range less than 4×10^{-2} %.

Kavvadas and Amorosi (2000) proposed a two-surface constitutive model for structured soils. The model has two characteristic surfaces (see Figure 2.10): an internal plastic yield envelop (PYE) and an external bond strength envelop (BSE). The internal plastic surface (PYE) has the same role as the classical yield surface. The term 'plastic' was added to the 'yield surface' to point out the difference between plastic yielding and large-scale yielding , *i.e*. de-structuring (Jardine *et al*, 1991). The external surface corresponds to material states associated with appreciable rates of structure degradation.

In this model, the destructuration law and the isotropic hardening rule are combined into one function (Eq.2.34), which describes the change in size of BSE. Both volumetric and deviatoric contributions are equally included in the function.

$$\dot{\alpha} = \alpha\left[\left\{\left(\frac{1+e}{\lambda-\kappa}\right) - \xi_v \exp(-\eta_v, \varepsilon_v^p)\right\}\dot{\varepsilon}_v^p + \left\{\theta_q - \xi_q \exp(-\eta_q, \varepsilon_q^p)\right\}\dot{\varepsilon}_q^p\right] \qquad (2.34)$$

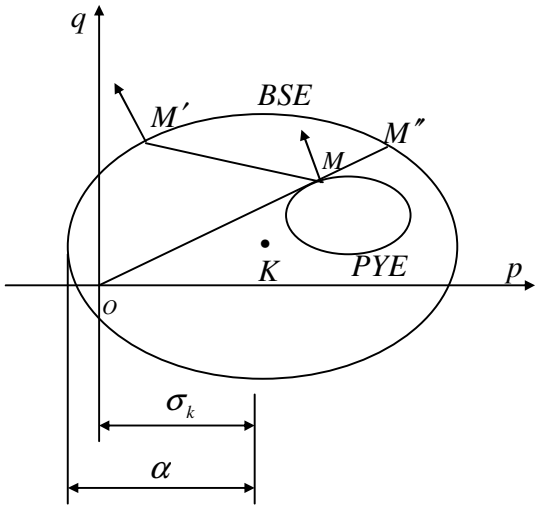

Figure 2.10 Two-surface by Kavvadas and Amorosi (2000)

The kinematic hardening rule of PYE is similar to that proposed by Al Tabbaa & Wood (1989) (Eq.2.21). The plastic modulus function is given by

$$H = H'' + H''[(1-\frac{\delta}{\delta_0})^{-\gamma} - 1] \qquad (2.35)$$

Where H'' is the plastic modulus at point M'' where vector $\overrightarrow{OM}$ intersect BSE; δ is the normalized length of MM'' (M is the current stress state); δ_0 is the value of δ upon initiation of yielding. Thus $\delta/\delta_0 = 1$ corresponds to initiation of yielding (*i.e.* $H = \infty$) and $\delta/\delta_0 = 0$ indicates that the material state lies on BSE (*i.e.* $H = H''$). The material constant γ (>0) determines the rate of degradation in plastic modulus H in the range (∞, H''). H'' is formulated in such a way that when the surfaces are in contact $H'' = 0$.

Unlike other hardening functions, H'' is associated with point M'' rather than M' and δ is associated with vector $\overrightarrow{MM''}$ rather than $\overrightarrow{MM'}$ (*i.e.* the so-called vector $\boldsymbol{\beta}$); the second term of the plastic modulus function is related to the first term while in other hardening functions these two terms are independent of each other.

In this model, δ_0 is associated with the stress state upon onset of yielding. Hence it depends on the position of the yield surface when yielding initiates. δ_0 becomes constant until it is reset when yielding re-initiates (in cyclic loading) while δ_0 in the model by Mróz's *et al* (1979) or b_{max} in the model by Al Tabbaa & Wood (1985) is a maximum quantity corresponding to the current yield surface. The formulations of δ and δ_0 ensures an automatic fall of H from infinity upon onset of yielding to zero when surfaces are in contact. The magnitude of H in other models such as the modified Bubble model is controlled by additional material parameters.

The model was calibrated against laboratory tests on the stiff overconsolidated Vallericca clay (isotropic and anisotropic consolidation tests, anisotropically consolidated triaxial shearing at both low and high pressures.). Very small yield surfaces were used. The ratio of *PYE* to *BSE* was between 0.005-0.05 while the ratio of size between bubble and structure surface was 0.048-0.145 in the paper by Rouainia & Wood (2000).

Although importance of the size of *PYS* was mentioned by Kavvadas and Amorosi (2000) no comment was made on how it affects the behaviours of soil.

All the kinematic hardening models discussed above are formulated in such a way that the yield surface can only expand (contract) and/or translate. A two-surface model, which allows the yield surface not only expand (contract) and translate but also rotate inside the bounding surface, was proposed by Gajo & Wood (2001) under the same framework of the modified Bubble model. Stresses are generalized with respect to size, location and the inclination of the bounding surface so that the bounding surface is fixed in a generalized stress space. In the model, the hardening function has a new form as follows:

$$H = \frac{b^2}{Bb_{\max}} \tag{2.36}$$

The model was calibrated against the modified Cam-clay model with the parameter B being varied between 10^{-3} and 10^{5}. Parametric study indicated that B has much more significant effects than bubble size R and *Poisson*'s ratio μ on the response of the model. A value of 10^{-3} for the parameter B was considered to be representative of many types of natural clay. Both R and μ were assumed to be 0.2 as they were found to have minor role in the model. This was consistent with Smith (1992). A similar exponential destructuration law was used as the modified Bubble model. A value of 0.5 was used for parameter A and it was suggested that A may be obtained by comparing triaxial test with one-dimensional compression test. It was also found that parameters k and ψ, which both control rate of destructuration, are interrelated.

2.2 Nonlinear dynamic analysis with *FLAC*

FLAC is a 2D finite difference programme and has become widely used for analysis and design in a variety of fields in civil and mechanical engineering. A fully dynamic analysis capability is offered in *FLAC*. However, only simple nonlinear soil models are available in *FLAC* and they are basically for quasi-static analyses.

Wang (1999) implemented a bounding surface hypoplasticity model for sands into *FLAC* to model the dynamic response of an embankment under cyclic loading. A sinusoidal velocity wave with an amplitude of 0.61m/s and a frequency of 1 Hz was applied as a horizontal input motion to the bottom and two vertical sides of the embankment. An analysis was conducted for five cycles of the input motion indicating satisfactory performance of the model. However, it is noticed that a 2% Rayleigh damping was applied to the model and there was no explanation of why this was necessary.

Pender (1999 and 2000) implemented a hyperbolic model in *FLAC* to analyze the propagation of shear wave and the dynamic response of a rigid foundation subjected to vertical vibration. The soil model is for undrained lightly over-consolidated soil (Pender, 1978). Rayleigh damping of up to 5% was used.

A systematic study on nonlinear dynamic modeling with *FLAC* was carried out by Ni (2001) to investigate dynamic response of rigid footings and a soil-footing-structure system. It has been shown that for a dynamic analysis in which a nonlinear soil model is implemented with 'apparent modulus' approach, a special kind of numerical distortion will occur. This is due to the changing of shear moduli, especially the sudden change of shear moduli when strain reversal takes place. Severe numerical distortion may occur in a nonlinear dynamic modeling even if the timestep and element size are very small. A typical phenomenon is a migrating stress-strain response (See Figure 2.11). The steady state response may be disturbed or may never be reached due to the numerical distortion. The higher the exciting frequency the more severe the problem is. In some cases, numerical distortion could result in collapsing of a numerical model.

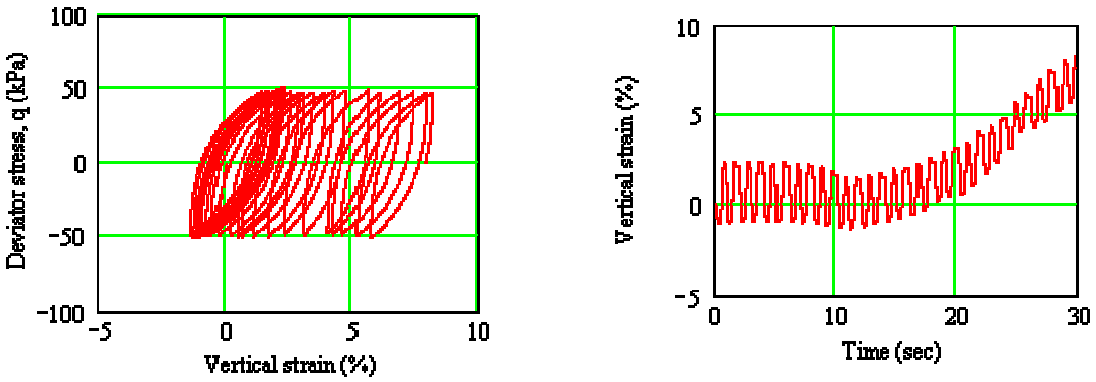

(a) Stress-strain response (b) Time history of vertical strain response

Figure.2.11. Cyclic response of a hyperbolic model in simulating a triaxial dynamic test

The specimen is 200 mm in diameter and 400 mm in height. Due to the symmetry of the specimen, only half of the specimen is modeled with a mesh of 32 elements. Soil properties of the Pender model: ρ = 1.8 t/m^3, p_{cs} = 100 kPa, M = 1.0, k = 0.05, e = 1.0, G = 20 MPa, K = 200 MPa. No additional damping is applied. The specimen is subjected to a 30-cycle sinusoidal stress loading with a frequency of 1 Hz and a stress amplitude of 50 kPa.

Since no cyclic degradation of shear modulus is considered in the above soil model, the dynamic response should settle down to a steady state and this steady state response should not change under a regular continuous excitation.

It was found that the problem of migrating response only occurs in a nonlinear model and reducing timestep or element size will not solve this problem. The problem was then addressed by introducing an additional damping.

Figure 2.12 shows the result of a dynamic analysis in modeling the same problem as in Figure 2.11. A 2% damping is applied. Compared to Figure 2.11a, Figure 2.12 gives a relatively stable response within 30 cycles of vibration.

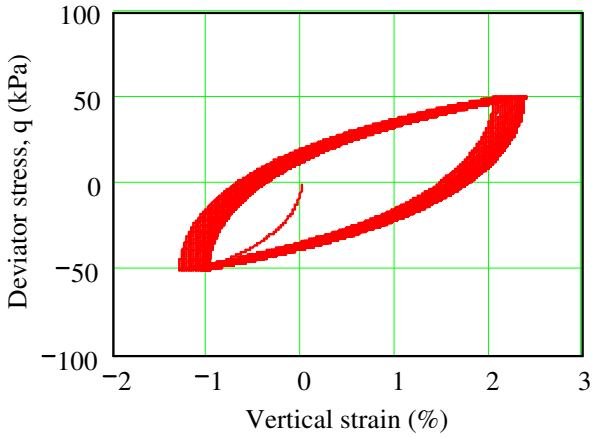

Figure 2.12 Stress-strain response with 2 % local damping.

The use of a small amount of additional damping is appropriate in a nonlinear dynamic analysis and is well established to cope with the 'shock' wave effect of the sudden change in shear modulus when the direction of loading is reversed. As the majority of the damping is from hysteresis, it is desirable from the theoretical point of view that a nonlinear soil model be implemented with 'plastic correction' approach so that the numerical distortion problem may be minimized. In *FLAC*, plasticity models, *e.g.* the modified Cam-clay model, are implemented with an approach that involves an elastic trial to estimate stress increments followed by a plastic correction for the stress increments at each timestep. Hereinafter, this approach is termed 'plastic correction' approach compared to the 'apparent modulus' approach. It is also called 'returning mapping' (Simo and Hughes 1998).

Further application of *FLAC* in modeling nonlinear dynamic response of rigid footings subject to vertical and rocking vibration was reported by Pender and Ni (2004).

2.3 Vertical vibration of rigid foundations

There are six possible degrees of freedom of vibration for a foundation due to unbalanced forces. They include vibrations in vertical, lateral and longitudinal directions and rotation about vertical, lateral and longitudinal axes. The work of the thesis is focused on the vertical vibration only.

The foundation design for vibrating equipment is based on displacement considerations. The medium on which a foundation is rested is soil or rock which exhibits significant nonlinear behaviours. The displacement of the foundation includes two parts: cyclic displacement due to elastic response of the soil-foundation system to the vibratory loading and permanent displacement due to compaction or lateral displacement of soil below the foundation.

Classical solutions to displacement of vertically-vibrating foundations are based on elastic theory and different compliance (stiffness) functions have been proposed by various workers. A brief description of the historical development is given below.

2.3.1 Classical work

Dynamic Boussinesq Problem

In 1904 Lamb studied the problem of vibration of a single vibrating force acting at a point on the surface of an elastic half-space. The study included cases in which the oscillating force R acts in the vertical direction. This is generally referred as the dynamic Boussinesq problem.

Reissner's solution

In 1936, Reissner proposed a solution to the problem of vibration of a uniformly loaded flexible circular foundation rested on an elastic half-space. The solution was obtained by integration of Lamb's solution for a point vibrating force. The vertical displacement at the center of the flexible loaded area can be given by

$$z = \frac{Q_0 e^{i\omega t}}{Gr_0}(f_1 + if_2) \tag{2.37}$$

Where

Q_0 = amplitude of the exciting force acting on the foundation

z = periodic displacement at the center of the loaded area

ω = circular frequency of the applied load

r_0 = radius of the loaded area

G = shear modulus of the soil

f_1, f_2 = Reissner's displacement (compliance) functions

The following relation was obtained for a flexible circular foundation:

$$A_z = \frac{Q_0}{Gr_0} Z \tag{2.38}$$

Where

A_z = the amplitude of the vibration

Z = dimensionless amplitude, $Z = \sqrt{\dfrac{f_1^2 + f_2^2}{(1 - ba_0^2 f_1)^2 + (ba_0^2 f_2)^2}}$

b = dimensionless mass ratio, $b = \dfrac{m}{\rho r_0^3} = (\dfrac{W}{g})\left[\dfrac{1}{(\gamma / g) r_0^3}\right] = \dfrac{W}{\gamma r_0^3}$

ρ = density of the elastic material

γ = unit weight of the elastic material

a_0 = dimensionless frequency, $a_0 = \omega r_0 \sqrt{\dfrac{\rho}{G}} = \dfrac{\omega r_0}{v_s}$

v_s = velocity of shear waves in the elastic material on which the foundation is resting

The classical work of Reissner was further extended by Quinlan (1953) and Sung (1953) to consider non-uniform distribution of the contact pressure. Three pressure distribution cases were considered, *i.e.* uniform, parabolic distribution and the distribution for a rigid foundation. Similar forms of solution can be obtained, but the displacement functions f_1, f_2 will depend on the distribution of contact pressure.

Richart and Whitman (1967) found that for a given a_0, the magnitude of the amplitude is highest for the case of parabolic pressure distribution and lowest for rigid bases. For a given type of pressure distribution and mass ratio, the magnitude of the amplitude also greatly depends on the assumption of Poisson's ratio. The larger the Poisson's ratio the smaller the amplitude.

Hsieh's analogy

Based on Reissner's displacement relation for flexible foundations, Hsieh (1962) developed an equation similar to that for damped vibrations of single-degree-of-freedom system. The soil is treated as a viscoelastic material (See Figure 2.13). The equation of motion is given by

$$m\ddot{z} + c_z \dot{z} + k_z z = Q_0 \sin(\omega t) \tag{2.39}$$

Where the spring constant and dashpot coefficient are frequency dependent,

$$k_z = Gr_0 \left(\frac{f_1}{f_1^2 + f_2^2}\right), \quad c_z = \frac{Gr_0}{\omega}\left(\frac{-f_2}{f_1^2 + f_2^2}\right)$$

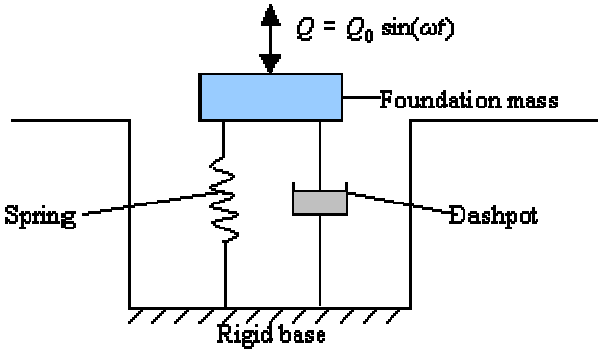

Figure 2.13 A lumped parameter vibrating system

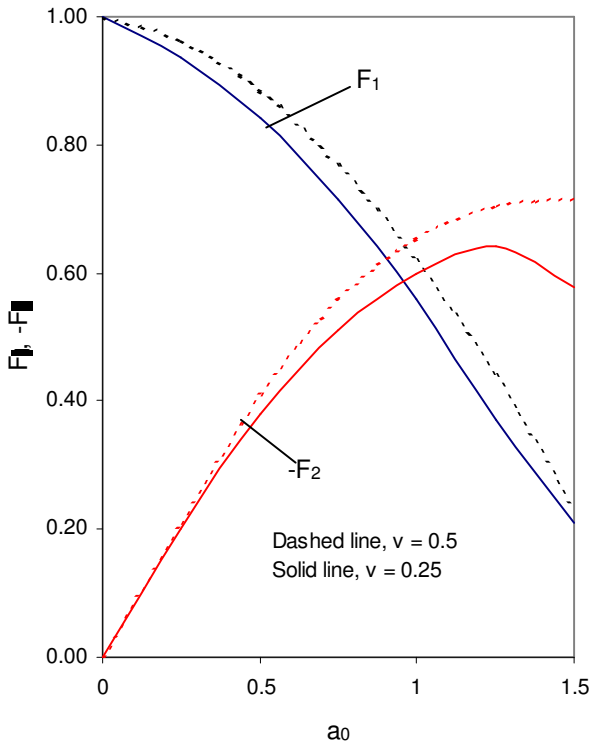

Figure 2.14 Vertical compliance functions for rigid circular foundations (redrawn after Lysmer and Richart, 1966)

Lysmer's Analogy

A simplified model was proposed by Lysmer and Richart (1966), in which k_z and c_z were frequency independent. The compliance functions were redefined in the following form:

$$F = \frac{f}{(\frac{1-v}{4})} = \frac{f_1 + if_2}{(\frac{1-v}{4})} = F_1 + iF_2 \qquad (2.40)$$

Where functions of F1 and F2 are practically independent of Poisson's ratio, shown as in the Figure 2.14. The mass ratio was also modified by multiplying the previous mass ratio with a factor of $(1-v)/4$.

Luco & Westmann's solution

Luco & Westmann (1968) proposed a set of compliance functions for strip rigid footings rested on elastic half space. Slight correction was made to the functions proposed by Gazetas and Roesset (1979) based on results for a linearly hysteretic soil (corresponding to 5% hysteretic damping).

The above compliance functions obtained from analytical calculations were found to be in good agreement with those obtained from numerical analysis using elastic soil model (See Figure 3.59, *FLAC 4.0 Optional Features* Manual). In the numerical model, a massless strip footing is modeled rigid by slaving structural nodes together. Viscous boundaries are used to model infinity. A sinusoidal vertical loading is applied to the footing directly with no prior stresses in the model. A 5% damping is applied to the model.

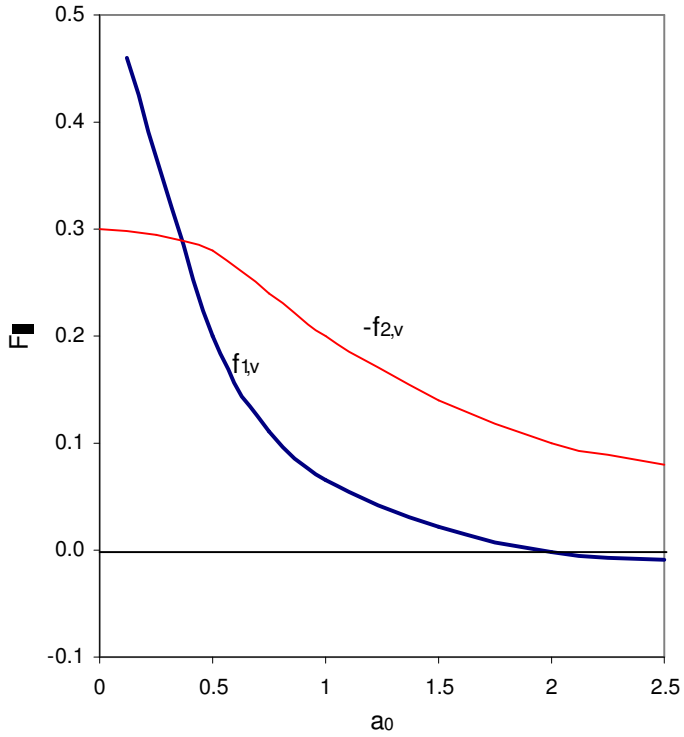

Figure 2.15 Vertical compliance functions for rigid strip foundations (redrawn after Gazetas and Roesset, 1979)

2.3.2 Nonlinear numerical modeling of vertical vibration of rigid foundations

In general behaviours of soil is nonlinear and only at low strain levels the elastic theory may be considered applicable to soil. Numerical methods provide an effective way to bridge elastic results and the realistic behaviours of soil.

Borja *et al* (1993) investigated the nonlinear dynamic response of vertically vibrating rigid foundations to harmonic loads. Both circular and square foundations rested on an elasto-viscoplastic half-space were modeled in the context of nonlinear finite element method. The elasto-viscoplastic theory of Duvaut and Lions (1976) was used to model the soil behaviours. It was shown that plastic deformation for vertically oscillating rigid foundations results in an overall increase in displacement amplitudes and creation of

resonance frequencies where motion is amplified above those at zero-frequency level (see Figure 2.16).

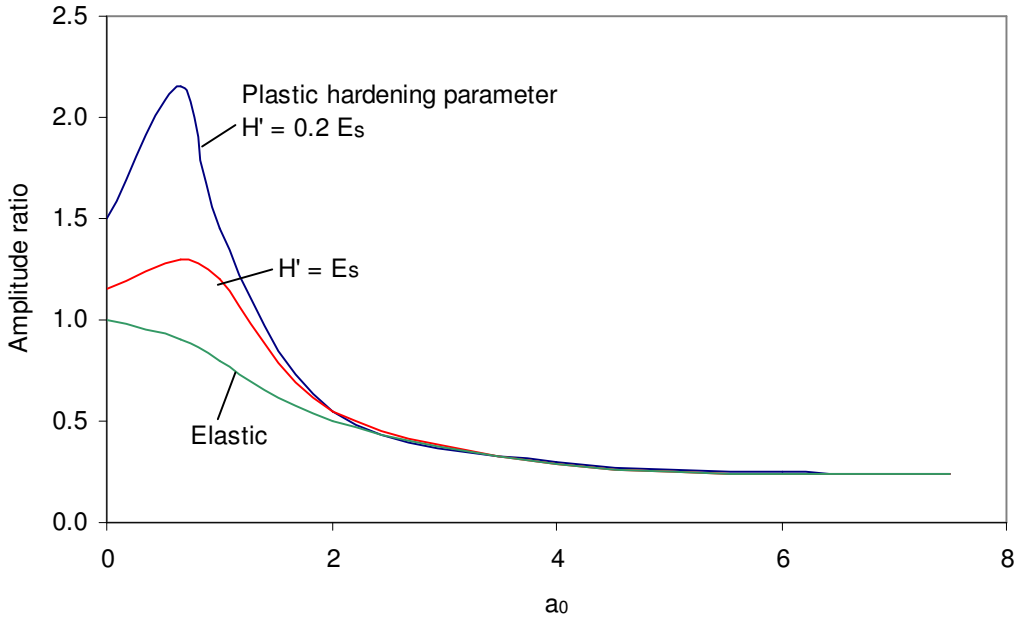

Figure 2.16 Vertically oscillating circular foundation on elastoplastic half space (redrawn after Borja et al, 1993)

Pender (2000) reported that there are two distinct aspects of shallow strip foundation response to loading: cyclic deformation and the accumulation of permanent settlement. It was noted that the dynamic compliance of a foundation on a nonlinear soil exhibits greater variation with cyclic loading frequency than the same foundation on an elastic soil. Recent applications of the Pender model in undrained lightly over-consolidated soil have been made by Pender (1999, 2000). The soil model was implemented in *FLAC* to analyze the propagation of the shear wave and the dynamic response of a rigid foundation subjected to vertical vibration. To simplify the calculation in *FLAC*, the nonlinear elastic approach was used with an equivalent tangent shear modulus introduced to incorporate elastic and plastic contributions. The nonlinear behaviours of soil is accounted for during unloading and reloading. The result is shown in Figure 2.17, which agrees well qualitatively with those by Borja *et al* (1993). However the resonance at low frequency

was not reported. The soil model was based on a work-hardening plasticity model by Pender (1978), which was implemented as a hyperbolic model in *FLAC* (Pender, 1999).

Using the same nonlinear model, the writer (Ni, 2001) further analyzed the problem with *FLAC* and the resonance at low frequency was found for both vertical and rocking vibrations of a rigid strip foundation. The foundation was modeled as massless and different loading levels were considered. Typical results are shown in Figures 2.18 and 2.19. A static pressure with a factor of safety of 4 was applied to the foundation prior to the dynamic loading.

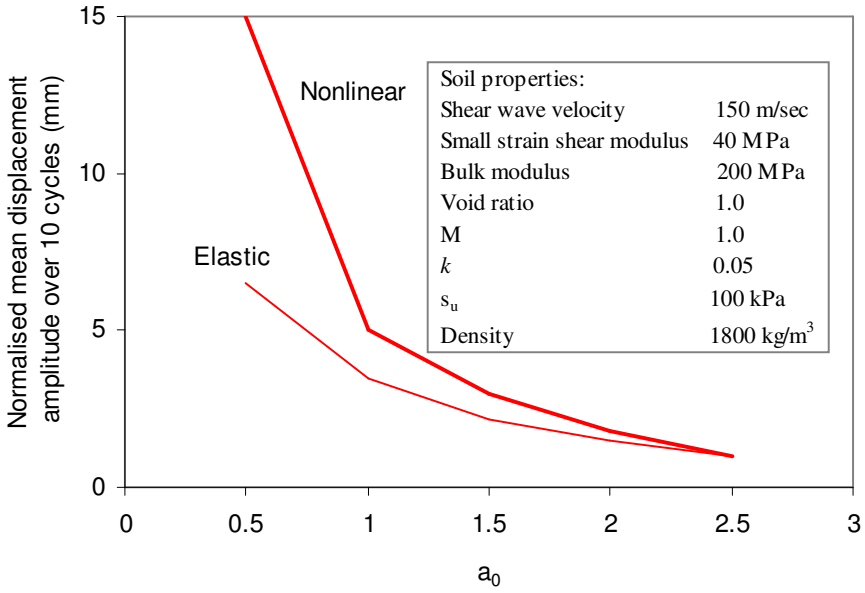

Figure 2.17 Cyclic displacement amplitude of a rigid foundation (redrawn after Pender, 2000)

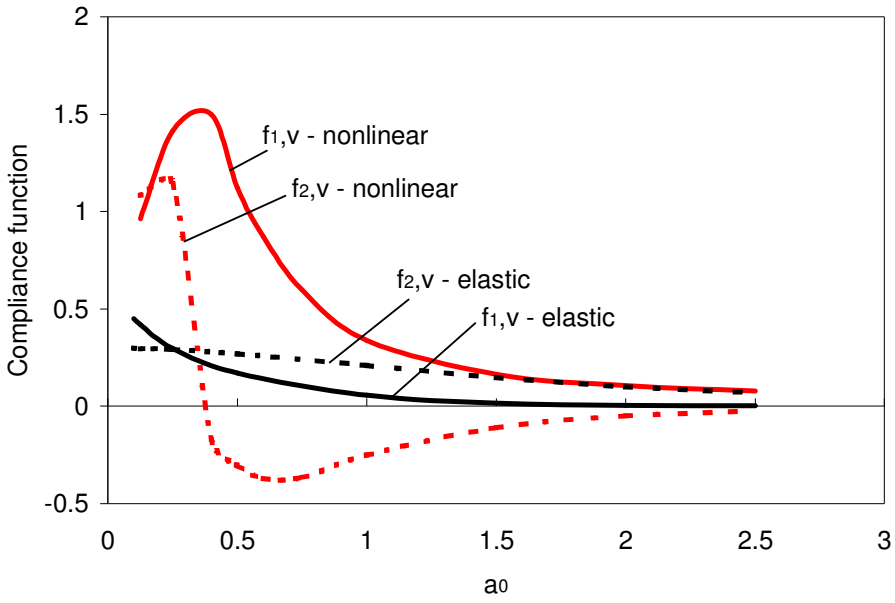

Figure 2.18 Compliance function of a rigid foundation subject to vertical vibration (stress amplitude =120 kPa)

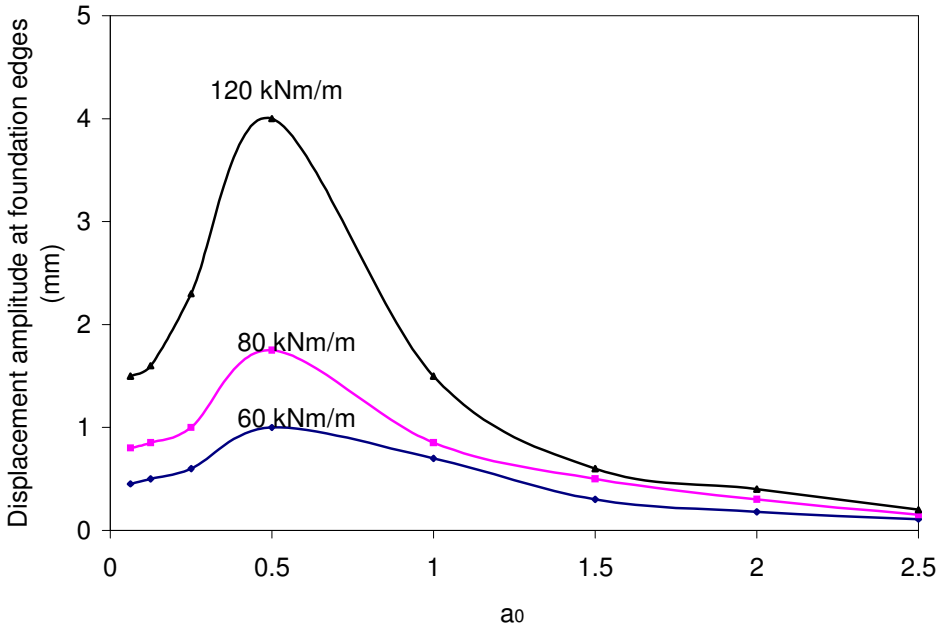

Figure 2.19 Vertical displacements a rigid strip foundation subject to rocking vibration

Pender and Ni (2004) investigated a rigid footing with mass subject to vertical harmonic vibration. Resonance at low frequency was complicated (see Figure 2.20). The displacement at very low frequency of a nonlinear soil can be much larger than that of an elastic soil when the stress level is high. However the influence of mass ratio needs to be further explored on nonlinear dynamic compliance. Two general conclusions were reached:

- The compliance function is found to be very close to that for the vibration of a rigid footing on an elastic layer when the cyclic loading amplitude is small.
- Under low frequency excitation nonlinear stress-strain behaviours of soil beneath the foundation has a significant effect on the dynamic response.

It was also noted that the static stress level prior to dynamic loading has a considerable influence on dynamic compliance at low frequencies (see Figure 2.21).

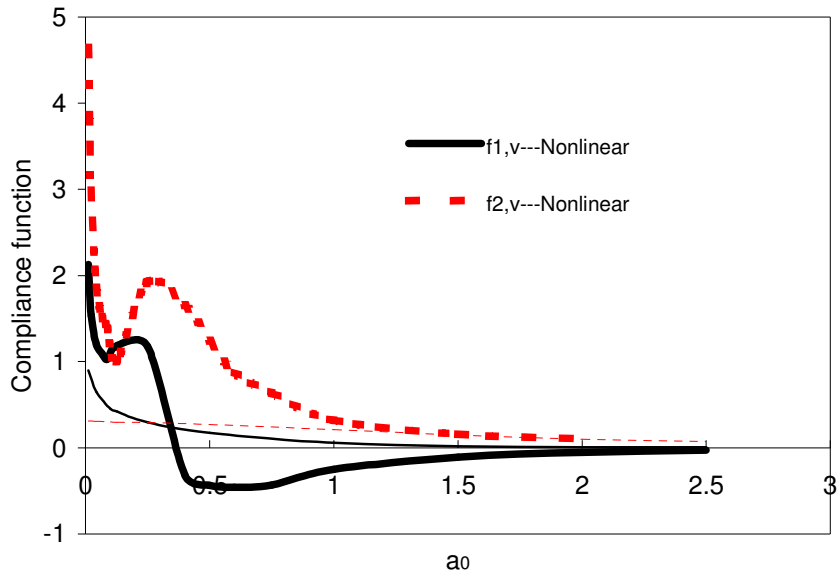

Figure 2.20 Vertical compliance function (cyclic pressure = 140 kPa)

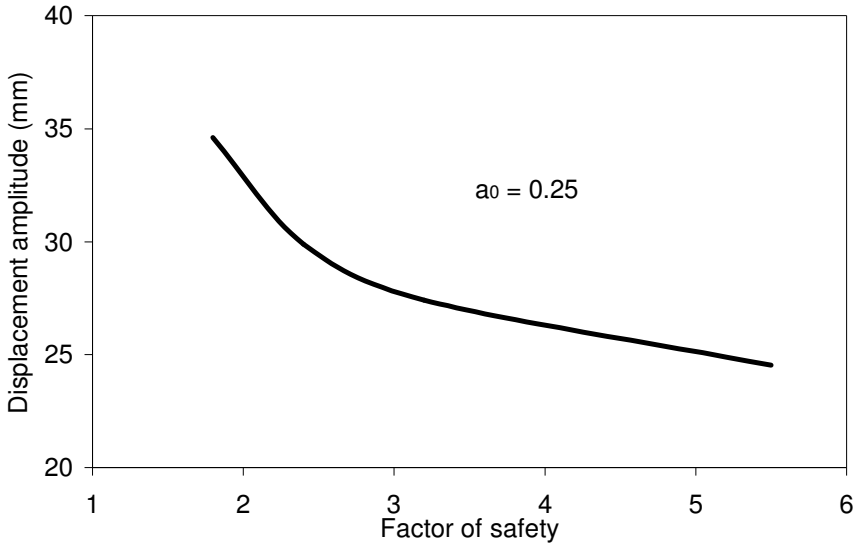

Figure 2.21 Influence of static factor of safety on displacement amplitude

2.4 Summary

Since the modified Cam-clay model was proposed in 1960s efforts have been made by many workers to extend its application to cyclic loading. Among other models, two or three-surface models, which introduce a small kinematically hardening yield surface inside the Cam-clay surface, represent one approach to that purpose. Recent development of two or three-surface models has been focused in simulating laboratory behaviours of structured soils.

The kinematic hardening model can be traced back to Mróz (1967). A general framework of two/three-surface models was established by Mróz, Norris and Zienkiewicz(1979) under the principles of the critical state soil mechanics. Many two/three-surface models have been developed under the framework mainly to improve the formulations of the kinematic hardening rule and hardening functions. The non-translation rule proposed by Hashiguchi (1985) and the hardening function by Al Tabbaa & Wood (1989) have been often used in various two/three-surface models. A unique hardening function proposed by Kavvadas and Amorosi (2000) seems to have some advantages in modeling a smooth transition in stiffness. Most of the two or three-surface models have been developed using the associated flow rule which tends to over-predict the coefficient of earth pressure at

rest (K_0). McDowell *et al* (2003) introduced a simple non-associated flow rule in the 3-SKH model (Stallebrass, 1990) to overcome the deficiency.

Wood (1995) extended the Bubble model (Al Tabbaa & Wood, 1989) for structured soils using an exponential destructuration law. A general framework of constitutive law for structured soils was outlined by Rouainia &Wood (2000) which incorporates the Lode angle in yield functions. A similar model for structured soils, based on the 3-SKH model, was proposed by Baudet & Stallebrass (2004). In this model parameters of structure and destructuration are related to some physical characteristics and efforts have been made to simulate behaviours of structured soils with those parameters derived from traditional laboratory tests.

In general, the research on determining parameters of constitutive models has lagged far behind the development of the models. Physical meanings of some parameters remain unclear or undefined not to mention the determination of these parameters in laboratory. More parametric study needs to be carried out to evaluate those models. By simulating experimental data a general knowledge about values of those non-standard parameters may be achieved for a particular type of soil.

The modified Bubble model (Rouainia & Wood, 2000) is selected for the research. It is believed that this model provides more flexibility in modeling different soil beahvours due to the following three facts: a general critical state stress ratio (M_θ) is utilized in the yield equations, which takes into account the unsymmetrical behaviors of soil under compression and extension; the model allows the consideration of initial anisotropy of the structure surface; contributions to destructuration of structured soil from plastic volumetric strain and distortional strain are not necessarily equal and their contribution percentages can be varied from 0 to 100%. Areas for further work may include improving formulation of the hardening function, establishing qualitative relationships between non-standard and standard parameters and determination of key parameters. Little reference can be found about application of the Bubble model in dynamic analysis. It is worthwhile to explore the dynamic performance of the model.

In terms of implementation of constitutive models in *FLAC*, numerical instability in dynamic analysis is to be addressed. The method of 'plastic correction' or 'return mapping' has been suggested to cope with the problem of numerical distortion.

The influence of nonlinearity of soil on dynamic compliance of rigid foundations needs to be further explored especially at low frequency range. Effects of mass ratio and bedrock also need to be explored.

3 SOME KEY ASPECTS OF PROGRAMMING WITH *FLAC*

FLAC has some basic soil constitutive models built in its source code. Any other soil models can be implemented into *FLAC* with *FISH* - the programming language utilised in *FLAC*. The *FISH* version of the modified Cam-clay model in *FLAC* provides an example for implementing nonlinear plasticity soil models in the thesis.

In this chapter, some aspects of implementation of soil models are discussed. They are important to a successful implementation of a soil constitutive model, but they are not explained explicitly in *FLAC* manuals.

3.1 Finite elements in *FLAC*

In a *FLAC* model, a finite difference mesh is divided by the user into quadrilateral elements. Internally, *FLAC* subdivides each quadrilateral element into two overlaid sets of triangular sub-elements shown as Figure 3.1. A user-defined model (UDM) is called four times per element (once for each sub-element) each time step. To get more accurate results, stress and strain may need to be averaged over the four sub-elements. If not specified, however, stress and strain of an element are only associated with the last-called sub-element.

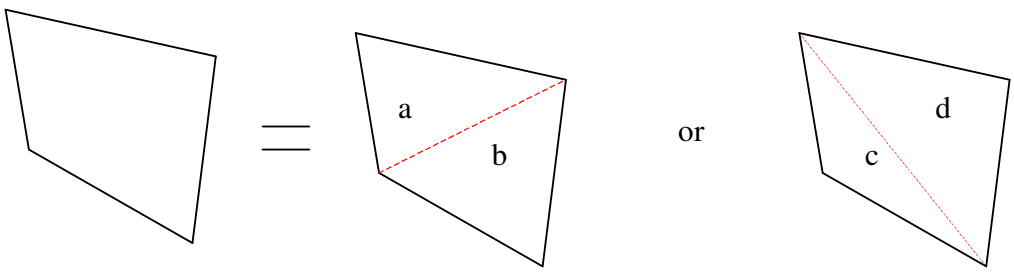

Figure 3.1 Sub-elements in a quadrilateral element

In *FLAC* strain is constant in each set of sub-elements. Whether strain or stress is constant or not between the two sets of sub-elements of an element depends on the shape and boundary condition of the element. The following is an example.

Figure 3.2 shows three single-element 2D models. A cyclic vertical stress loading is imposed on the top of each model. The amplitude of the stress is 50 kPa and the loading frequency is 1Hz. The soil is elastic with 5% local damping applied. Before cyclic loading is applied there is zero insitu stress. 'Models *a* and *b*' are the same in size and shape but slightly different in the boundary condition. For 'model *b*' the bottom is fixed at both *x* and *y* directions while for 'model *a*' only *y* direction is fixed. 'model *c*' has the same boundary condition as 'model *a*' but has a different geometric shape.

The linear elastic model in *FLAC* is utilised to demonstrate the influence of boundary condition and shape of an element on stress in sub-elements. Two local variables, 'vstress' and 'vstress_ave', are added to the *FISH* code of the linear elastic model to record respectively vertical stress of the last-called sub-element (*i.e* 'sub-element d') and the averaged vertical stress of the four sub-elements. Results are shown in Figure 3.3 and the code of the line elastic soil model is given at the end of this section.

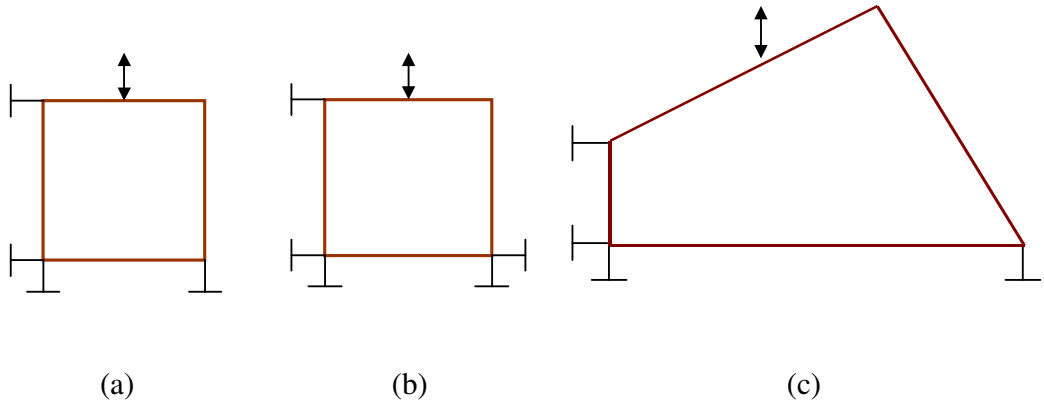

Figure 3.2 Three single-element 2D axisymmetric models

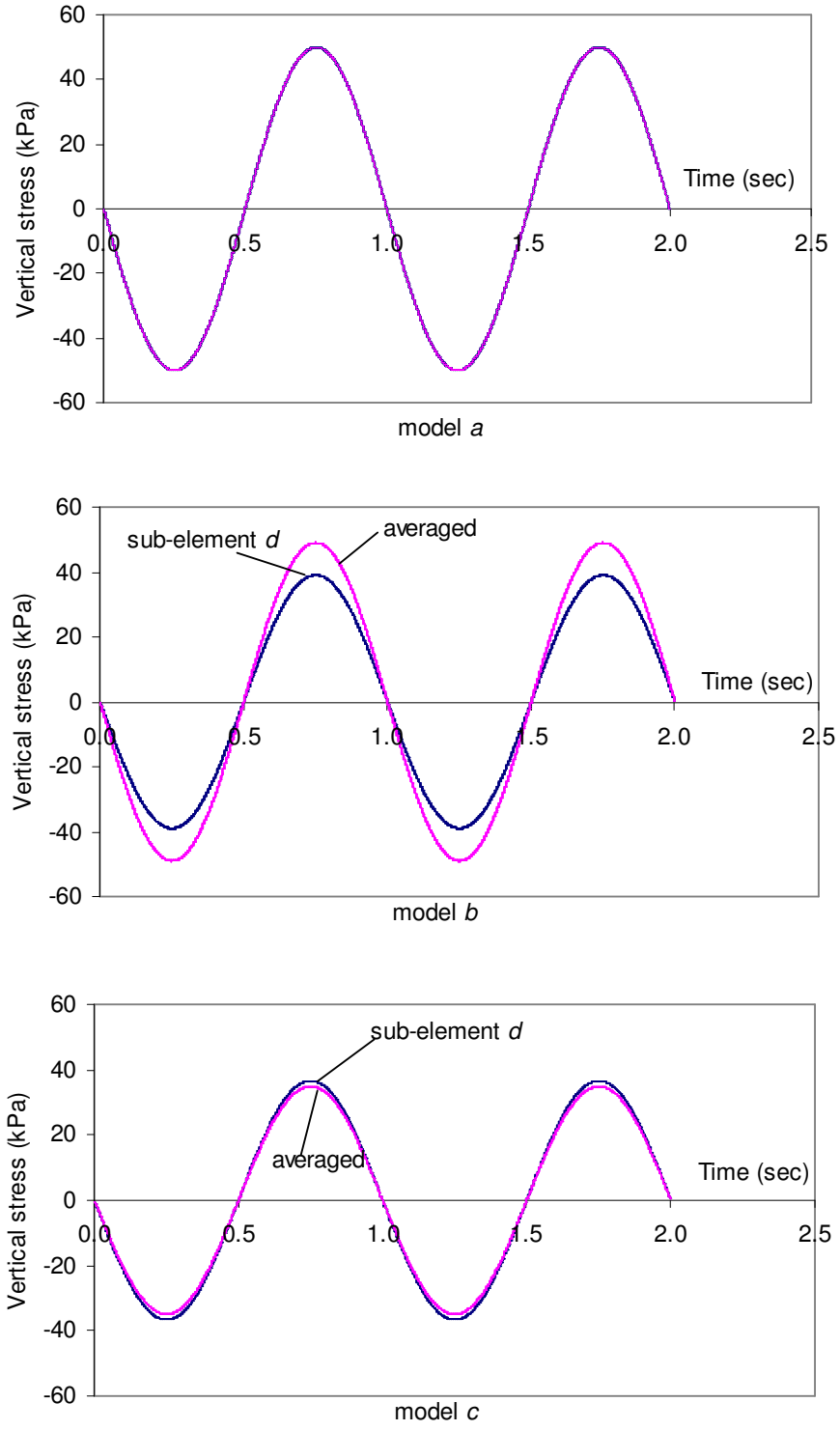

Figure 3.3 Influence of boundary condition and shape of element on stress

It can be seen from Figures 3.3a and 3.3b that boundary condition can have a significant influence on vertical stresses in the sub-elements. Figure 3.3a corresponding to Figure 3.2a indicates that due to symmetry of the boundary, vertical stress is uniform among the two sets of sub-elements. Therefore time histories of the two variables are identical. Figure 3.3b represents the result associated with Figure 3.2b. It shows that the averaged vertical stress is greater than 'sub-element *d*'. Figure 3.3c shows a slight difference in vertical stress between the sub-elements. This means that the shape of the element has less influence than the boundary condition on the uniformity of stress in sub-elements in this case.

```
;FISH version of the linear elastic soil model
def m_elas
  constitutive_model
  f_prop  m_g m_k m_e1 m_e2 m_g2
  f_prop  vstress vstress_ave
  float $sum1 $sum2

case_of  mode

  case 1 ; initialization
      m_e1 = m_k + 4.0 * m_g / 3.0
      m_e2 = m_k - 2.0 * m_g / 3.0
      m_g2 = 2.0 * m_g

  case 2 ; running section
      zs11  = zs11 + zde11 * m_e1 + (zde22+zde33) * m_e2
      zs22  = zs22 + zde22 * m_e1 + (zde11+zde33) * m_e2
      zs33  = zs33 + zde33 * m_e1 + (zde11+zde22) * m_e2
      zs12  = zs12 + zde12 * m_g2
      $sum1=$sum1+(zde11+zde33) * m_e2 + zde22 * m_e1
      vstress=zs22 ;vertical stress component

      if zsub > 0.0 then
        $sum1 = $sum1 / zsub
        vstress_ave=vstress_ave+$sum1;averaged vertical stress
        $sum1=0.0
      end_if

  case 3;  max modulus
      cm_max = m_k + 4.0 * m_g / 3.0
      sm_max = m_g
 end_case
end
```

3.2 Local and global variables

All variables, except property variables, are globally recognised for all the elements of a model. Values of global variables are not stored for each element. They are changed when the next element is processed. Hence, at the end of each time step, values of global variables are associated with the last-processed element.

Values of local variables are stored for each element and are retained unchanged until the next time step. To ensure this, all local variables must be put after the *FISH* statement **F_PROP** in a *FISH* code. All other statements such as **FLOAT** and **INT** are only for global variables. However, misplacing global variables after statement **F_PROP** will not cause any problems except increasing calculation burden and using more computer memory.

All global variables start with a dollar sign **$**. Although this is not compulsory, the use of symbol **$** makes it convenient to distinguish global variables from local variables. One advantage is that a list of all variables with names starting with sign **$** can be printed out using the command **PRINT $fish**.

3.3 Initialisation

In a typical UDM code, the first part following the statement '*case 1*' is normally for initilisation. Initialisation is not compulsory as in a simple model but it can be complicated in a sophisticated model.

It should be noted that 'initialisation' is executed only once per element per **STEP** command prior to stepping. If multiple **STEP** commands appear in a data file, *e.g* for a series of *FLAC* runs or quasi-static cyclic loading, initialisation will be repeated when each **STEP** command is executed. This will cause errors in most cases. Hence, 're-initialisation' should be avoided in a UDM if it is not required.

3.4 *FISH s*tate variables

Unlike user-defined state variables, all *FISH* state variables are manipulated internally by *FLAC*. Although these *FISH* state variables can be employed in a function or an equation in a UDM, they are either calculated internally by *FLAC* (*e.g* zde_{11}, zde_{22}, zde_{33} and zsub), or have to be calculated in a specific way (*e.g* zs_{11}, zs_{22}, zs_{33}, zs_{12}). All the *FISH* state variables can not be printed out directly by the command PRINT and their history in a run can not be recorded by the command HISTORY. The following will discuss some aspects in using *FISH* state variables since they are crucial to a successful coding of a soil constitutive relationship. These aspects are not explicitly discussed in the *FLAC* manuals.

3.4.1 Stress variables

In *FLAC*, zs_{11}, zs_{22}, zs_{33} and zs_{12} are *FISH* state variables associated with *FLAC* stresses, *i.e* s_{xx}, s_{yy}, s_{zz} and s_{xy}. They are not calculated according to the way in which they appear in a UDM code. They are recognized and processed in a special way which may confuse a user.

For example, to update stresses, the following incremental formulations are often used.

```
zs11  = zs11 + zde11 * m_e1 + (zde22+zde33) * m_e2
zs22  = zs22 + zde22 * m_e1 + (zde11+zde33) * m_e2        (3.1)
zs33  = zs33 + zde33 * m_e1 + (zde11+zde22) * m_e2
zs12  = zs12 + zde12 * m_g2
```

Where zde_{11}, zde_{22}, zde_{33} and zde_{12} are strain rates standing for $\dot{\varepsilon}_{xx}$, $\dot{\varepsilon}_{yy}$, $\dot{\varepsilon}_{zz}$ and $\dot{\varepsilon}_{xy}$ respectively; m_e_1, m_e_2 and m_g_2 are coefficients being function of elastic moduli.

As a UDM is called four times per element each timestep (once for each sub-element), it is apparent from the above equations that accumulation of stress increment is carried out four times for each stress component.

In fact, there is no accumulation of stress increments when these equations are called because they contain *FISH* state variables zs_{11}, zs_{22}, zs_{33} and zs_{12} and *FLAC* treats them

differently from user-defined variables. These equations are only executed once rather than four times per element each timestep although the UDM code is called four times. Only the stress increments associated with the last-called sub-element are added to current stresses.

FLAC can distinguish *FISH* state variables from user-defined variables. If the *FISH* state variables (zs_{11} …) are replaced by a set of user-defined variables (s_{11}…) in the above equations, four stress increments will be accumulated and added to each stress component. Therefore, 's_{11}…' are four times larger than (zs_{11}…). To demonstrate this, the model for Figure 3.2a is utilized. A vertical stress of 50 kPa is applied at the top of the model. The following equations are added to the *FISH* code of the previous linear elastic model.

```
      s11  = s11 + zde11 * m_e1 + (zde22+zde33) * m_e2
      s22  = s22 + zde22 * m_e1 + (zde11+zde33) * m_e2          (3.2)
      s33  = s33 + zde33 * m_e1 + (zde11+zde22) * m_e2
      s12  = s12 + zde12 * m_g2
```

```
;FISH version of the linear elastic model
def m_elas
  constitutive_model
  f_prop  m_g m_k m_e1 m_e2 m_g2 st22
  f_prop s11 s22 s33 s12

 case_of  mode
    case 1 ; initialization
      m_e1 = m_k + 4.0 * m_g / 3.0
      m_e2 = m_k - 2.0 * m_g / 3.0
      m_g2 = 2.0 * m_g
    case 2 ; running section
      zs11  = zs11 + zde11 * m_e1 + (zde22+zde33) * m_e2
      zs22  = zs22 + zde22 * m_e1 + (zde11+zde33) * m_e2
      zs33  = zs33 + zde33 * m_e1 + (zde11+zde22) * m_e2
      zs12  = zs12 + zde12 * m_g2
      st22=zs22

      s11  = s11 + zde11 * m_e1 + (zde22+zde33) * m_e2
      s22  = s22 + zde22 * m_e1 + (zde11+zde33) * m_e2
      s33  = s33 + zde33 * m_e1 + (zde11+zde22) * m_e2
      s12  = s12 + zde12 * m_g2

    case 3;  max modulus
      cm_max = m_k + 4.0 * m_g / 3.0
      sm_max = m_g
    end_case
end
```

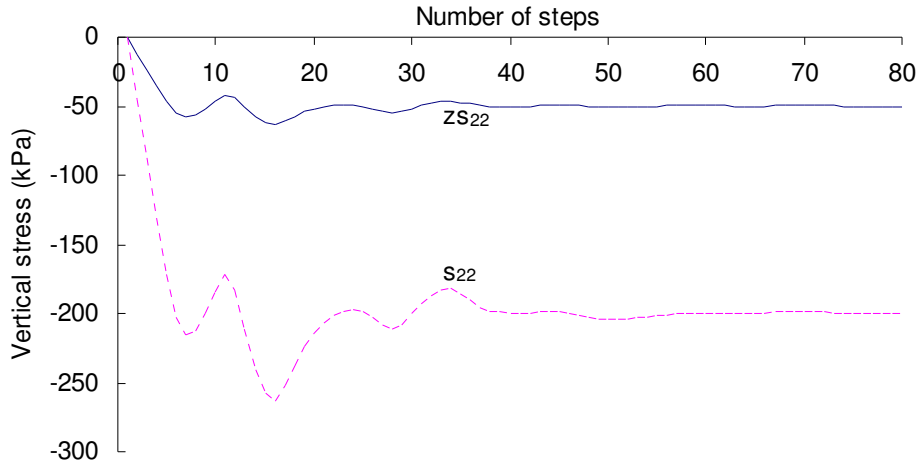

Figure 3.4 Comparison between FISH state variable and user-defined variable (zs_{22} is FISH state vertical stress; s_{22} is un-averaged user-defined vertical stress)

It can be seen from Figure 3.4 that the steady value of zs22 is 50 kPa while s22 is 200 kPa. This means that Eq.3.2 is executed four times each timestep while Eq.3.1 only once, hence, the user-defined stress variables need to be averaged, *i.e* to be divided by a factor of 4 (see Figure 3.5).

3.4.2 Sub-element averaging

Values of some variables, *e.g*. plastic strains, may need to be averaged over the four sub-elements. 'zsub' is an *FISH* state variable indicating when averaging can be processed. Initially "zsub" has a value of 0 and it becomes 2 or 4 when calculation of one element has been completed over its four sub-elements. Therefore when the statement "if zsub>0" is true averaging takes place.

"If zsub >0 then…end_if " is only used when a user-defined variable needs to be averaged over the four sub-elements. The previous *FISH* code of the linear elastic model is modified to get the correct values of user-defined stress variables (s_{11}, s_{22}, s_{33} and s_{12}) by averaging their stress increments.

```
;FISH version of the linear elastic model
def m_elas
  constitutive_model
  f_prop  m_g m_k m_e1 m_e2 m_g2
  f_prop s11 s22 s33 s12
  float $dzs11 $dzs22 $dzs33 $dzs12

 case_of  mode
    case 1 ; initialization
      m_e1 = m_k + 4.0 * m_g / 3.0
      m_e2 = m_k - 2.0 * m_g / 3.0
      m_g2 = 2.0 * m_g
    case 2 ; running section
      $dzs11=$dzs11 + zde11 * m_e1 + (zde22+zde33) * m_e2
      $dzs22=$dzs22 + zde22 * m_e1 + (zde11+zde33) * m_e2
      $dzs33=$dzs33 + zde33 * m_e1 + (zde11+zde22) * m_e2
      $dzs12=$dzs12 + zde12 * m_g2

      zs11=zs11 + zde11 * m_e1 + (zde22+zde33) * m_e2
      zs22=zs22 + zde22 * m_e1 + (zde11+zde33) * m_2
      zs33=zs33 + zde33 * m_e1 + (zde11+zde22) * m_2
      zs12=zs12 + zde12 * m_g2

    if zsub>0 then
      $dzs11=$dzs11/zsub
      $dzs22=$dzs22/zsub
      $dzs33=$dzs33/zsub
      $dzs12=$dzs12/zsub
      s11 = s11 + $dzs11
      s22 = s22 + $dzs22
      s33 = s33 + $dzs33
      s12 = s12 + $dzs12
      $dzs11=0.0
      $dzs22=0.0
      $dzs33=0.0
      $dzs12=0.0
    end_if
    case 3;  max modulus
      cm_max = m_k + 4.0 * m_g / 3.0
      sm_max = m_g
  end_case
end
```

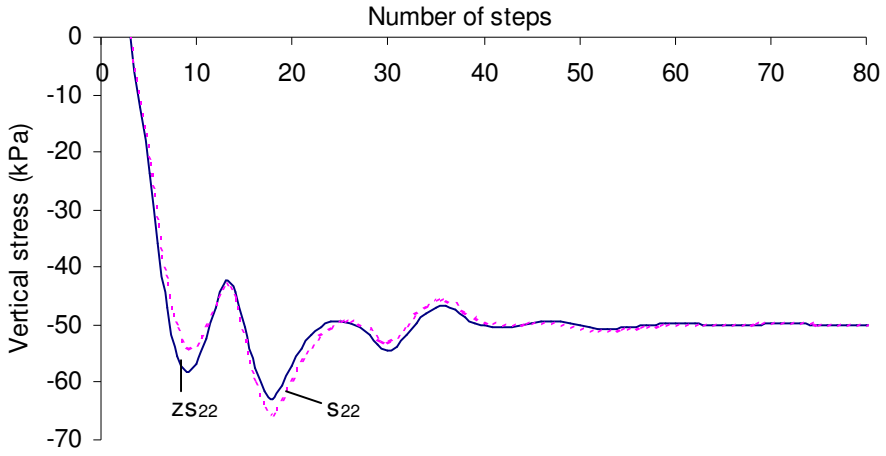

Figure 3.5 Comparison between FISH state variable and user-defined variable (zs_{22} is FISH state vertical stress; s_{22} is averaged user-defined vertical stress)

Figure 3.5 shows a comparison between the *FISH* state variable 'zs_{22}' and the user-defined variable 's_{22}'. Since 's_{22}' has been averaged, it gives the correct value of 50 kPa. As zs_{22} is associated with the last called sub-element while s_{22} is the averaged value of the four sub-elements, they are slightly different before the system reaches the equilibrium state.

Another important point is that if sub-element averaging is necessary in a UDM, *FISH* state variables (zs_{11}…) must be updated prior to the statement "if zsub>0…". Although they can appear in a function or equation, they should never be updated inside "if zsub>0 then…end_if" statements. This is different from user-defined variables. The following is a *FISH* code of the linear elastic model with *FISH* stress variables updated inside "if zsub>0 ...end_if" statements.

```
;FISH version of the linear elastic model
def m_elas
  constitutive_model
  f_prop  m_g m_k m_e1 m_e2 m_g2

 case_of  mode
    case 1 ; initialization
      m_e1 = m_k + 4.0 * m_g / 3.0
      m_e2 = m_k - 2.0 * m_g / 3.0
      m_g2 = 2.0 * m_g
    case 2 ; running section
    if zsub>0 then
      zs11  = zs11 + zde11 * m_e1 + (zde22+zde33) * m_e2
      zs22  = zs22 + zde22 * m_e1 + (zde11+zde33) * m_e2
      zs33  = zs33 + zde33 * m_e1 + (zde11+zde22) * m_e2
      zs12  = zs12 + zde12 * m_g2
    end_if
    case 3;  max modulus
      cm_max = m_k + 4.0 * m_g / 3.0
      sm_max = m_g
  end_case
end
```

Using the same problem as for Figure 3.3a, Figure 3.6 shows that if *FISH* stress variables (zs_{11}, zs_{22}, zs_{33} and zs_{12}) are updated inside "if zsub >0 … end_if" , they do not give the correct response. Stress amplitude of approximately 25 kPa is obtained (the thick line) while it should be about 50 kPa (*i.e.* the applied dynamic force) as inertia forces are negligible in this case.

An important task in a UDM is to update *FISH* stress variables, *i.e* zs_{11}, zs_{22}, zs_{33} and zs_{12}. No matter how simple or sophisticated a code is, there must be a section in a UDM updating the *FISH* stress variables and this section should not be put inside "if zsub>0 then … end_if" statements.

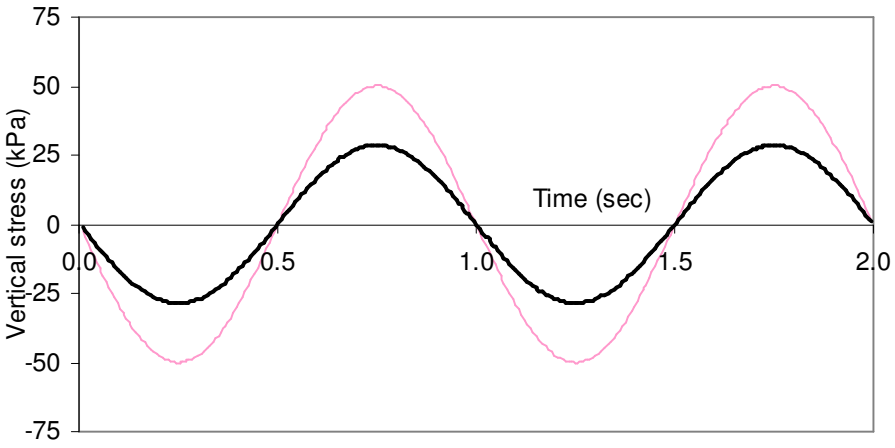

Figure 3.6 Influence of location where FISH stress variables are updated
(Thick line: inside "`if zsub>0…`"; thin line: prior to sub-element averaging)

3.4.3 Strain increments

zde_{11}, zde_{22}, zde_{33} and zde_{12} are strain increments. They are generated by *FLAC* internally according to boundary conditions and the current stress. They can appear in a function of a code but should not be updated by the user in a UDM.

3.4.4 Pore water pressure

In a *FLAC* calculation stresses stored at each timestep are normally total stresses (*e.g.* s_{xx}, s_{yy} and s_{zz}). When a soil constitutive law is called each time to calculate elastic moduli for the next timestep, effective stresses are always used, hence the following equation needs to be incorporated into the incremental formulations of a UDM:

$$\sigma' = \sigma - u \tag{3.3}$$

Where u is the pore water pressure generated by a soil model itself (see Chapter 5). σ is the total normal stress represented by zs_{11}, zs_{22} and zs_{33} in a *FISH* code.

For example, if the mean effective normal stress '*p*' is needed in a soil model, the following equation should appear in the *FISH* code:

$$p = (zs_{11} + zs_{22} + zs_{33})/3 - u \qquad (3.4)$$

However if the pore water pressure '*u*' is generated by means of the *ground water mode* approach in *FLAC* (*i.e* using '*gw*' configuration mode and '*set flow off*', see *FLAC*4.0 manual *Theory and Background*) rather than by the user-defined soil model, the effective stresses will be automatically calculated by *FLAC* and *FISH* state variables zs_{11}, zs_{22} and zs_{33} are always effective stresses. Therefore the above equation becomes as follows while the *FLAC* stresses, s_{xx}, s_{yy} and $s_{zz,}$ are still stored as total stresses:

$$p = (zs_{11} + zs_{22} + zs_{33})/3 \qquad (3.5)$$

This can be seen by the following example in which a conventional triaxial test of elastic soil is modeled (see the data file). The linear elastic soil model is used with modifications to the previous *FISH* code. *FLAC* stress (s_{yy}), pore water pressure (pp) and *FISH* state variable zs_{22} (represented by a user variable $\$zs_{22}$ as histories of *FISH* state variables can not be recorded directly by the command **HISTORY**). Pore water pressure is generated by *Ground water mode* approach in this example.

```
;data file for a triaxial test
config axi gw
grid 1,1
gen 0.0, 0.0 0.0,0.1 0.1,0.1 0.1,0.0
fix y j 1
fix x I 1
set flow off
water dens 1 bulk 2e6 tens 1e10
call elas.fis
model m_elas
prop m_g 4.0e3 m_k 2.0e4 den 1.7
his syy
His $zs22
his pp
his ydisp I 1 j 2
fix y j 2
ini yv -1.0e-6 j=2
step 2000
```

```
;FISH version of the linear elastic model
def m_elas
  constitutive_model
  f_prop  m_g m_k m_e1 m_e2 m_g2
  float $zs22

  case_of  mode
    case 1 ; initialization
      m_e1 = m_k + 4.0 * m_g / 3.0
      m_e2 = m_k - 2.0 * m_g / 3.0
      m_g2 = 2.0 * m_g
    case 2 ; running section
      zs11  = zs11 + zde11 * m_e1 + (zde22+zde33) * m_e2
      zs22  = zs22 + zde22 * m_e1 + (zde11+zde33) * m_e2
      zs33  = zs33 + zde33 * m_e1 + (zde11+zde22) * m_e2
      zs12  = zs12 + zde12 * m_g2
      $zs22=zs22
    case 3;  max modulus
      cm_max = m_k + 4.0 * m_g / 3.0
      sm_max = m_g
  end_case
end
```

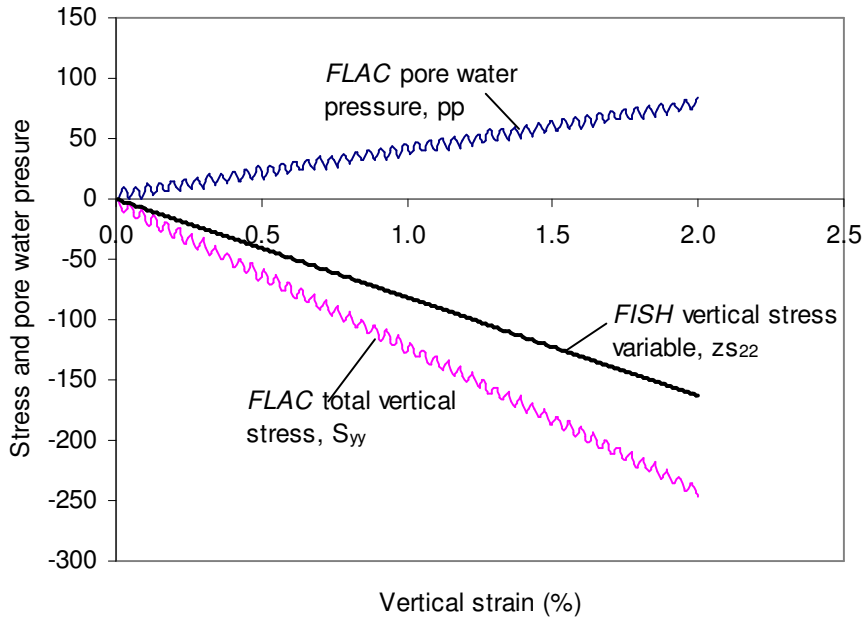

Figure 3.7 Effective and total stresses

It can be seen from Figure 3.7 that *FISH* variable zs_{22} is converted to effective stress automatically by *FLAC* although Eq.3.3 is not incorporated in the *FISH* code. If the pore water pressure is generated by the soil model itself, the user has to convert the *FISH* variables zs_{11}, zs_{22} and zs_{33} to effective stresses which are used to check yield and calculate elastic moduli in the *FISH* code of the soil constitutive model (see Chapter 5)

It is also noted that even if the *FISH* state variable zs_{22} is replaced with a user defined stress variables (here $\$zs_{22}$), the conversion from total stress to effective stress is still carried out by *FLAC* automatically. However the user's variable must be put after "zsub > 0 then" statement to avoid accumulation of stress over the four sub-element (see the following *FISH* code). Figure 3.8 shows that the user defined variable '$\$zs_{22}$' is effective stress.

```
;FISH version of Elastic model
def m_elas
  constitutive_model
  f_prop  m_g m_k m_e1 m_e2 m_g2
  float $zs22

  case_of  mode

   case 1 ; initialization
      m_e1 = m_k + 4.0 * m_g / 3.0
      m_e2 = m_k - 2.0 * m_g / 3.0
      m_g2 = 2.0 * m_g
    case 2 ; running section

      zs11  = zs11 + zde11 * m_e1 + (zde22+zde33) * m_e2
      zs22  = zs22 + zde22 * m_e1 + (zde11+zde33) * m_e2
      zs33  = zs33 + zde33 * m_e1 + (zde11+zde22) * m_e2
      zs12  = zs12 + zde12 * m_g2

      if zsub>0 then
       $zs22  = $zs22 + zde22 * m_e1 + (zde11+zde33) * m_e2
      end_if
    case 3;  max modulus
      cm_max = m_k + 4.0 * m_g / 3.0
      sm_max = m_g
  end_case
end
```

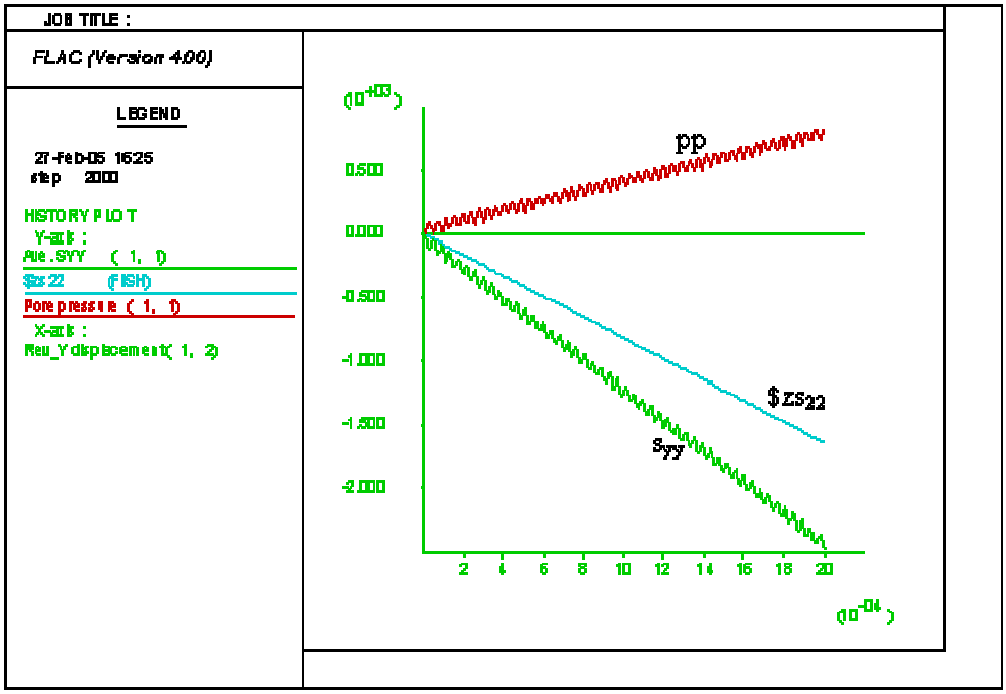

Figure 3.8 Effective stress using user defined variable

3.5 Summary

FLAC divides each quadrilateral element into two overlaid sets of triangular sub-elements. A user-defined model (UDM) is called four times per element (once for each sub-element) each timestep. Whether stress or strain is constant or not over the four sub-elements depends on boundary condition and shape of the element. To get more accurate results, stress and strain may need to be averaged over the four sub-elements although this may not always provide "the correct" solution if a specific boundary condition is involoved. If not specified, however, stress and strain of an element are only associated with the last-called sub-element.

All local variables (*e.g*. property variables) must be defined under statement **F_PROP** in a UDM code. Re-initialization should be avoided when multiple **STEP** commands occur in a data file.

FISH state variables are manipulated internally by *FLAC*. They are not treated according to the logic with which they appear in a code. They are not averaged over sub-elements and are only associated with the last-called sub-element. They should not be updated within 'if zsub>0 then… …end_if' statements.

If pore water pressure is generated by a user's soil model, stresses must be converted into effective stresses by the user before the yield function is called. If the pore water pressure is generated by *FLAC* as in '*gw*' model, stresses are automatically converted to effective stresses.

4 PLASTIC CORRECTION APPROACH

Previous study (Ni, 2001) has indicated that numerical distortion (instability) occurs in nonlinear dynamic analysis if a nonlinear constitutive law of soil is implemented using 'apparent modulus' approach. 'Plastic correction' approach is expected to be able to reduce the numerical distortion.

The above two implementation approaches are discussed in this chapter. The hyperbolic model in *FLAC*, which is implemented with 'apparent modulus' approach, has been modified for cyclic loading to demonstrate the phenomenon of numerical distortion in nonlinear dynamic modelling while a bilinear model has been implemented with the concept of 'plastic correction' approach. The bilinear model has been found to perform satisfactorily in dynamic analysis without using any additional damping to cope with the numerical distortion problem.

4.1 'Apparent modulus' approach

For a linear elastic model, there is no failure criterion. Only a set of constant deformational properties are required to perform a mechanical calculation. Either bulk modulus (K) and shear modulus (G) or Young's modulus (E) and Poisson's ratio (μ) can be used. A general form of stress-strain relationship is given as follows.

$$\dot{\boldsymbol{\sigma}} = D^e \cdot \dot{\boldsymbol{\varepsilon}} \qquad (4.1)$$

Where D^e is a 4 by 4 matrix of elastic deformational constants, *i.e.* K and G or E and μ (Note: *FLAC* prefers the use of K and G although any pair of the above four elastic parameters can be used for describing the deformational characteristics of an isotropic elastic material). $\dot{\boldsymbol{\sigma}}$ and $\dot{\boldsymbol{\varepsilon}}$ are stress and strain rate tensors respectively, each of which is

expressed by a 4 by 1 matrix. For the plane strain problem, the above equation can be expressed in the following form:

$$\begin{bmatrix} \Delta\sigma_{xx} \\ \Delta\sigma_{yy} \\ \Delta\sigma_{zz} \\ \Delta\sigma_{xy} \end{bmatrix} = \begin{bmatrix} e_1 & e_2 & e_2 & 0 \\ e_2 & e_1 & e_2 & 0 \\ e_2 & e_2 & e_1 & 0 \\ 0 & 0 & 0 & e_3 \end{bmatrix} \cdot \begin{bmatrix} \Delta\varepsilon_{xx} \\ \Delta\varepsilon_{yy} \\ \Delta\varepsilon_{zz} \\ \Delta\varepsilon_{xy} \end{bmatrix} \tag{4.1a}$$

Where $e_1 = K + \frac{4}{3}G$, $e_2 = K - \frac{2}{3}G$ and $e_3 = 2G$

Similarly, a nonlinear model may be expressed as follows:

$$\dot{\boldsymbol{\sigma}} = D^{ep} \cdot \dot{\boldsymbol{\varepsilon}} \tag{4.2}$$

Where D^{ep} is the matrix containing variable elements which depend on the current stress and strain. Equation 4.2 may be expressed in a similar form to Eq.(4.1a), except that the elements of the matrix are not constants.

In the 'apparent modulus' approach, at each timestep in an incremental calculation, D^{ep} needs to be computed according to a specific soil model. This may involve a series of complicated incremental computation as in a bounding surface model (See Eq.5.32 in Chapter 5) or a simple closed-form solution as in a hyperbolic model (*e.g.* Duncan and Chang, 1970, also see Eq. 4.6 in this chapter). The equivalent modulus (usually tangent modulus) is formulated in such a way that it varies from the small strain modulus (*i.e.* the elastic modulus) to a very small value close to zero. The 'apparent modulus' approach is conceptually illustrated in Figure 4.1, where G_{app} is the apparent shear modulus, G_e is the small strain shear modulus, q is the deviator stress and γ is the engineering shear strain.

At time t in a nonlinear incremental calculation, the equivalent modulus is calculated and is used to update the stress at time $t + \Delta t$ using Hooke's law, which is expressed herein as equations 4.1 and 4.2. At the first timestep of the entire calculation and the second

timestep after a strain reversal takes place (Note: it is the second timestep not the first timestep because there is a one-step delay in the calculation of modulus), the equivalent modulus is taken to be the small strain modulus (*i.e.* elastic modulus). At any other timesteps, the equivalent modulus is smaller than the small strain modulus and it decreases as plastic deformation increases. Therefore, a sudden change in the equivalent modulus occurs each time when a strain reversal takes place (See Figure 4.2). This is considered to be the cause of the numerical distortion in a nonlinear dynamic analysis. However, this is still an assumption (see Section 4.3.1 and Section 4.4). This assumption justifies the use of plastic correction approach to solve the distortion problem because this approach utilises elastic modulus which is constant or changes slightly.

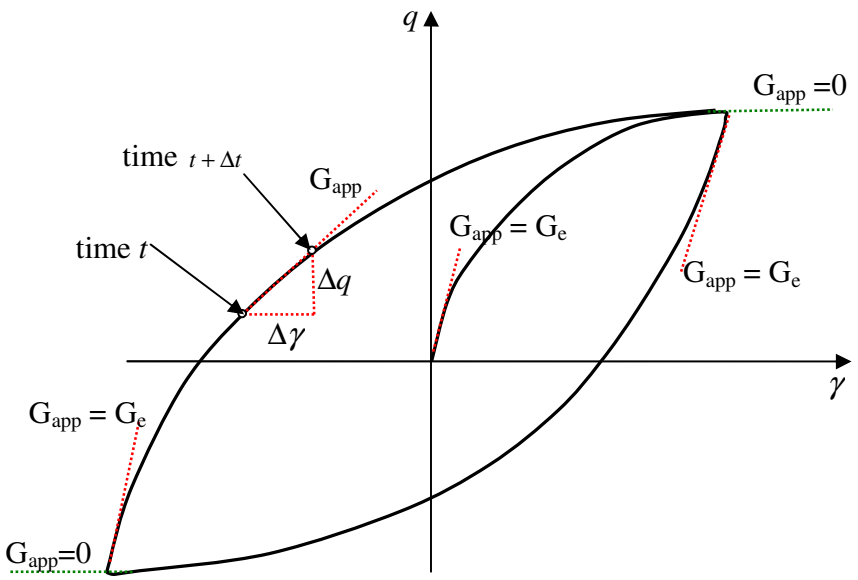

Figure 4.1 Illustration of 'apparent modulus' approach

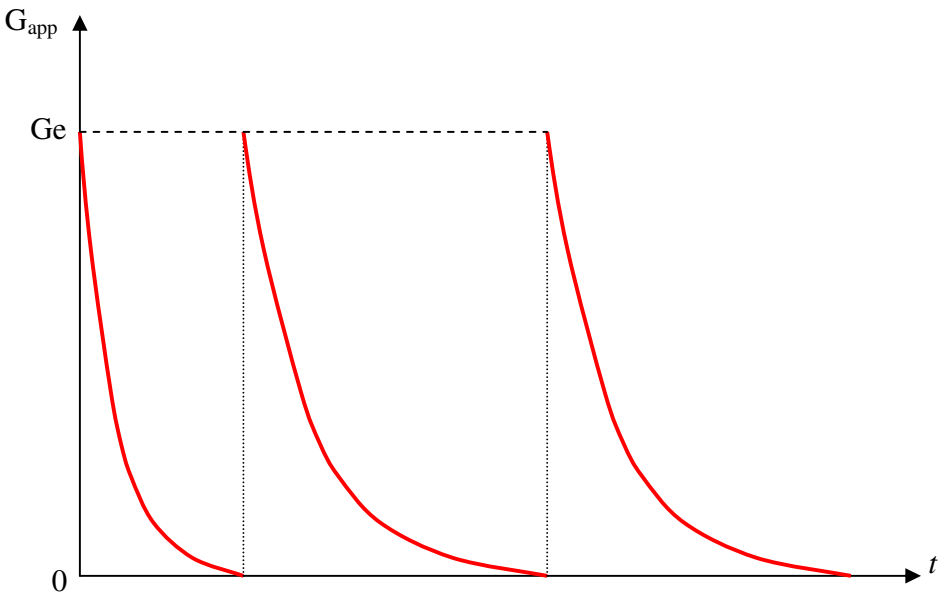

Figure 4.2 Sudden change in apparent modulus

It should be pointed out that in Eq. 4.2, $\dot{\varepsilon}$ is the total strain increment (or rate) rather than the elastic part of the strain increment as in 'plastic correction' approach. This is because that the nonlinear behaviour is taken into account by using the equivalent modulus which contains contributions form both elastic and plastic behaviours.

4.2 'Plastic correction' approach

4.2.1 Explicit and implicit integration

There are two ways to carry out the plastic correction, *i.e.* explicit and implicit (Dunne and Petrinic, 2005). The explicit integration method is normally employed in a finite difference program such as *FLAC* while the implicit method is often used in a finite element program. There is a good explanation in *FLAC* manual (Cundall, 2000) about the advantages and disadvantages between these two integration methods.

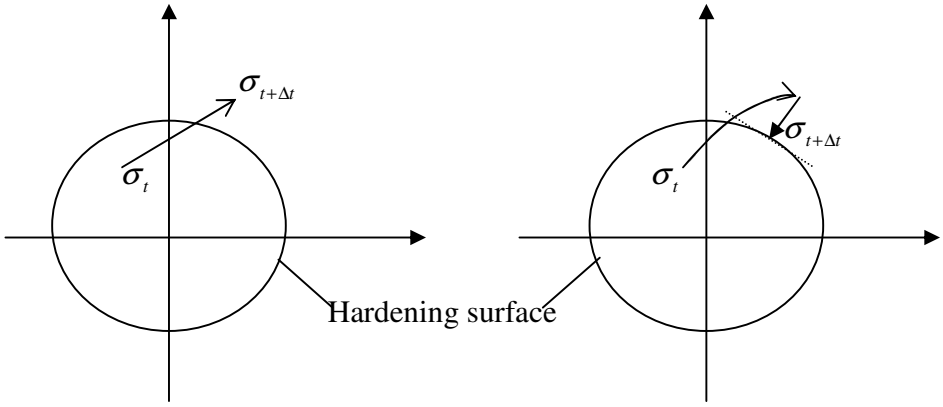

(a) Explicit integration (b) Implicit integration

Figure 4.3 Conceptual illustration in general stress space of plastic correction

The incremental form of Hooke's law same as Eq.4.2 is used in both explicit and implicit integration methods except that the total strain increment ($\dot{\boldsymbol{\varepsilon}}$) in Eq.4.2 needs to be replaced with the elastic part ($\dot{\boldsymbol{\varepsilon}}^e$) of the total strain increment and the equivalent elasto-plastic stiffness matrix D^{ep} needs to be replaced with the elastic stiffness matrix D^e (see Eq.4.3). The main difference between explicit and implicit methods is the way in which the plastic strain increment is obtained.

$$\dot{\boldsymbol{\sigma}} = D^e \cdot \dot{\boldsymbol{\varepsilon}}^e \tag{4.3}$$

In the explicit method (shown as Figure 4.3a), a very small timestep is required to ensure that stress after the plastic correction stays on the hardening surface. The use of a large timestep may result in the stress drifting from the surface after many timesteps. Therefore the solution of the explicit method is conditionally stable. After the stress increment is obtained through the above equation, it is added directly to the stress at time t to get the new stress at the end of time $t + \Delta t$. Whether the new stress remains on the hardening

surface or not depends on how small the timestep is. An error is inevitable after many timesteps of calculation and satisfactory results can only be achieved by using very small timesteps.

In the implicit method (shown as Figure 4.3b), plastic strain increment is obtained through an iteration process (using Newton's method to solve the yield function), which ensures that the stress at $t + \Delta t$ satisfies the yield condition, *i.e*. falls onto the hardening surface. Therefore, the solution of the implicit integration is unconditionally stable and a large timestep may be used in a calculation.

4.2.2 Procedures of plastic correction

In 'plastic correction' approach, D^e rather than D^{ep} is computed each timestep and only the elastic part of a strain rate contributes to change in the stress rate. However components of D^e may not be necessarily constant.

The incremental algorithm used in *FLAC* involves computation of the elastic modulus at time t, which is used to obtain a trial stress at time $t + \Delta t$ with the Hooke's law corresponding to the total strain increment ($\dot{\boldsymbol{\varepsilon}}$). If no yielding occurs, the trial stress is taken to be the real stress. Otherwise, the real stress is obtained by replacing the total strain increment with the elastic part ($\dot{\boldsymbol{\varepsilon}}^e$) of the total strain increment in the Hookes' law while the modulus remains to be the elastic modulus computed at time t. As the elastic modulus is much less variable than the equivalent modulus, there is no abrupt change in the modulus during the incremental calculation. Therefore, the numerical distortion encountered in the 'apparent modulus' approach is expected to be reduced or eliminated.

Figure 4.4 shows the flow chart utilised to programme the 'plastic correction' approach in *FLAC*. The 'plastic correction' approach is illustrated in Figures 4.5 (a) and (b).

Given a total strain rate ($\dot{\boldsymbol{\varepsilon}}$), a trial stress rate ($\dot{\boldsymbol{\sigma}}^{trial}$) is first obtained from an elastic trial using the following relation.

$$\dot{\boldsymbol{\sigma}}^{trial} = D^e \cdot \dot{\boldsymbol{\varepsilon}} \tag{4.4}$$

This trial stress rate ($\dot{\boldsymbol{\sigma}}^{trial}$) is then used to check plastic yielding and the plastic part ($\dot{\boldsymbol{\varepsilon}}^{p}$) of the strain rate ($\dot{\boldsymbol{\varepsilon}}$) is calculated if yielding occurs. The actual stress rate ($\dot{\boldsymbol{\sigma}}$) is obtained through a correction of the strain rate in Eq.4.4 so that only the elastic part of the strain rate contributes to the change in the stress rate, *i.e.*

$$\dot{\boldsymbol{\sigma}} = D^e \cdot (\dot{\boldsymbol{\varepsilon}} - \dot{\boldsymbol{\varepsilon}}^{p}) = D^e \cdot \dot{\boldsymbol{\varepsilon}}^{e} \tag{4.5}$$

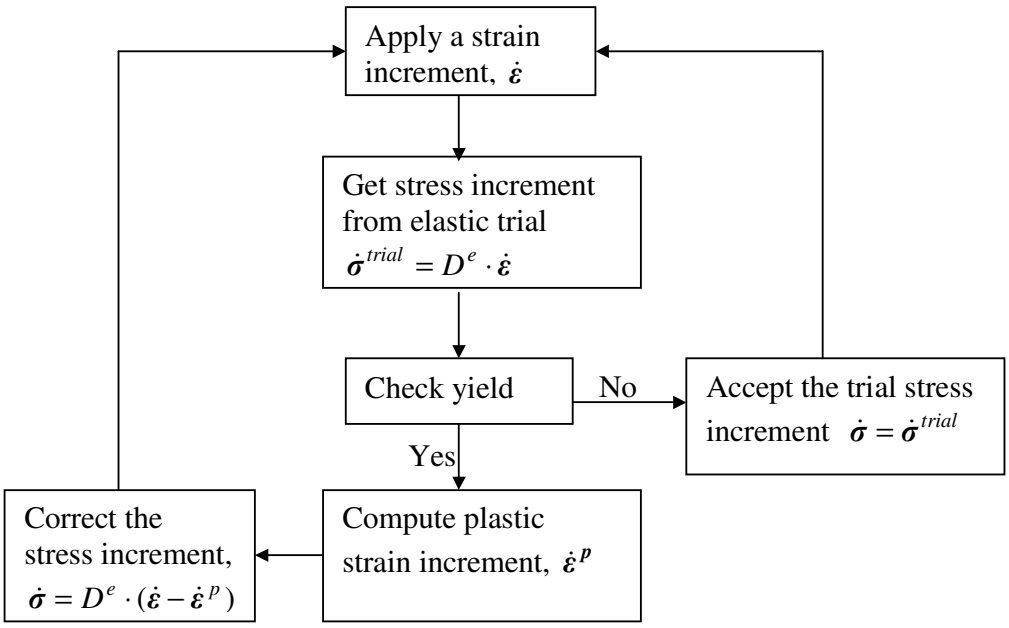

Figure 4.4 Flow chart of 'plastic correction' approach

(D^e is the matrix of elastic moduli)

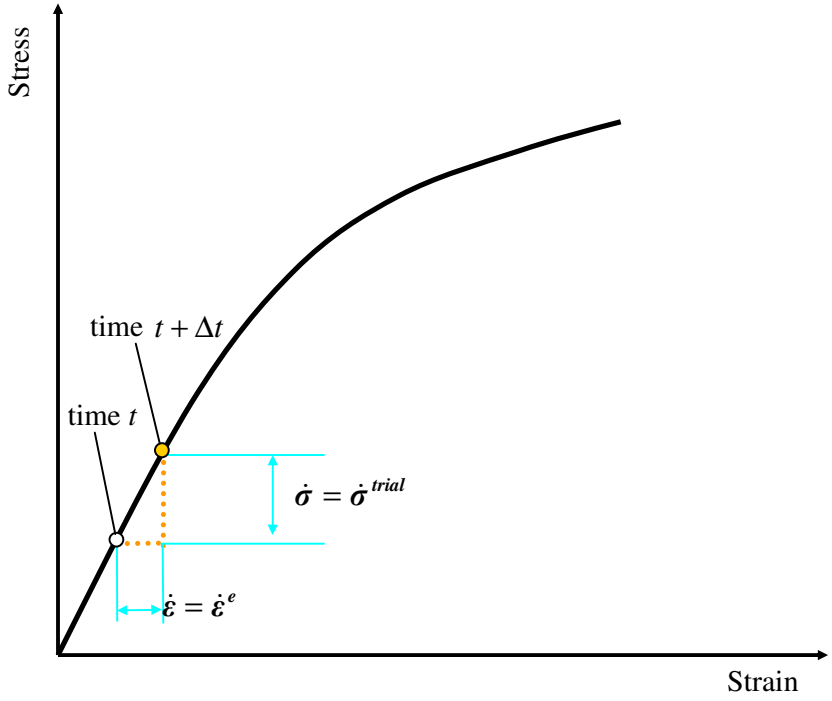

(a) No Yielding

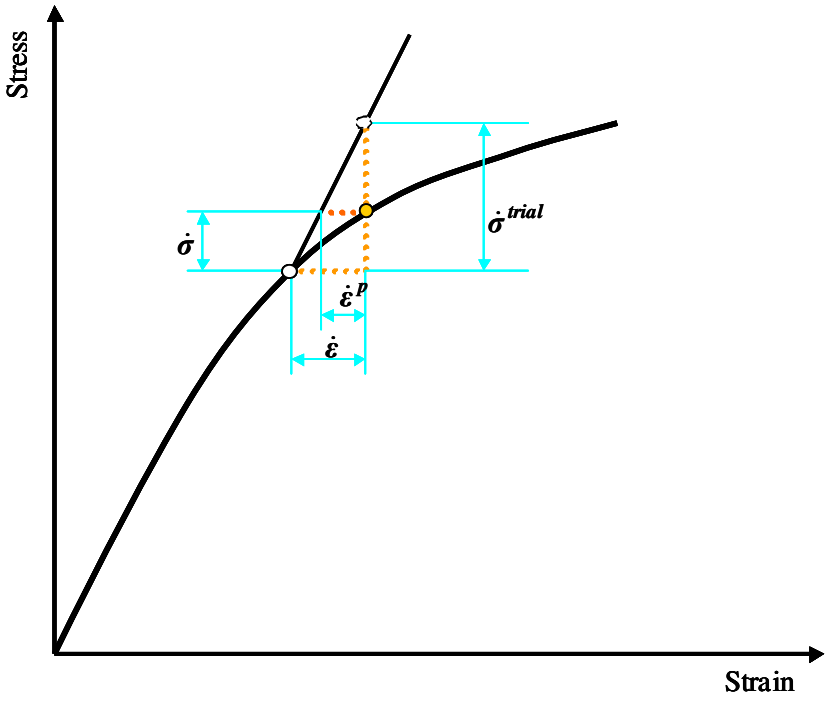

(b) Yielding

Figure 4.5 Conceptual illustration of 'plastic correction' approach

4.3 Implementation of two nonlinear models

4.3.1 A hyperbolic model

The hyperbolic soil model developed by Duncan and Chang (1970) is implemented in *FLAC* with 'apparent modulus' approach. In the model, the apparent tangent Young's modulus, E_t, is defined by the following relation.

$$E_t = (1 - R_f .SL)^2 .E_i \text{ and } E_i = KP_a(\sigma_3 / P_a)^n \quad (4.6)$$

Where

$SL = (\sigma_1 - \sigma_3)/(\sigma_1 - \sigma_3)_f$ is stress level;

$(\sigma_1 - \sigma_3)_f = (2c\cos\varphi + 2\sigma_3 \sin\varphi)/(1 - \sin\varphi)$ is the deviatoric stress at failure as determined by the Mohr-Coulomb criterion;

E_i is the initial Young's modulus;

K, n are model parameters; P_a is atmospheric pressure;

$R_f = (\sigma_1 - \sigma_3)_f / (\sigma_1 - \sigma_3)_{ult}$ is a model parameter used to describe the curvature of the hyperbolic function; $(\sigma_1 - \sigma_3)_{ult}$ is the theoretical asymptote of the hyperbolic function.

The model was developed for use in static loading condition. Hereinafter the model is extended for cyclic loading purely for the purpose to explore the problem of numerical distortion. It is assumed that the stress-strain relation in unloading follows the same relation as Eq.4.6 but the stress level (SL) is modified as follows:

$$SL = [(\sigma_1 - \sigma_3) - (\sigma_1 - \sigma_3)_0]/(\sigma_1 - \sigma_3)_f \quad (4.7)$$

where

$(\sigma_1 - \sigma_3)_0$ is the deviator stress, *i.e.* q_0 at the last turning point.

The above modification has been incorporated in the *FISH* code of the hyperbolic model appended to this section, in which R_f is assumed to be 1.0 and for convenience the initial

Yong's modulus E_i and strength $(\sigma_1 - \sigma_3)_f$ are given as inputs. Figure 4.6 shows the flow chart used in coding of the model.

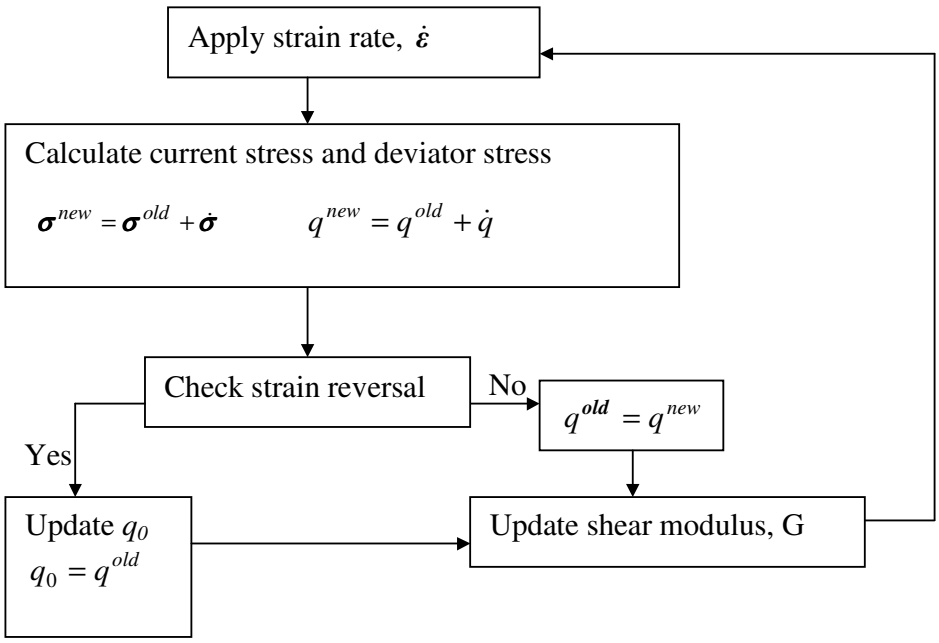

Figure 4.6 Flow chart of a hyperbolic model modified for cyclic loading

Figure 4.7 shows the response of an axisymmetrical single-zone model simulating a conventional triaxial specimen subject to a 100-cycle vertical sinusoidal loading. The frequency is 1Hz and axial strain amplitude is 1%. E_i =112.5 MPa, $(\sigma_1 - \sigma_3)_f$ = 400 kPa, bulk modulus = 200 MPa, σ_3=100 kPa, ρ = 18 kN/m^3. 1% Rayleigh damping is applied. The response is stable within 100 cycles.

Numerical distortion occurs if there is no additional damping applied to the model (See discussions in Section 4.4). Figure 4.8 shows that an unstable response occurs within 12 cycles. This is due to the sudden change in modulus at turning points. A non-physical vibration is caused when strain reversal takes place. Hence extra unbalanced forces are introduced into the grid nodes. These unbalanced forces are accumulated cyclically and may lead to collapsing of the model.

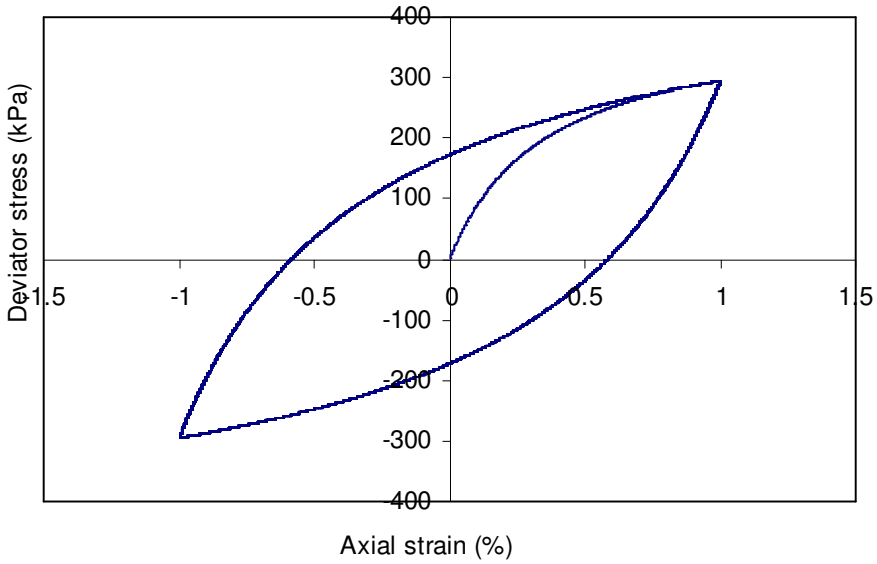

Figure 4.7 Dynamic response of the hyperbolic model (100-cycle vertical sinusoidal loading, frequency =1 Hz with 1% Rayleigh damping, timestep = 1×10^{-4} second)

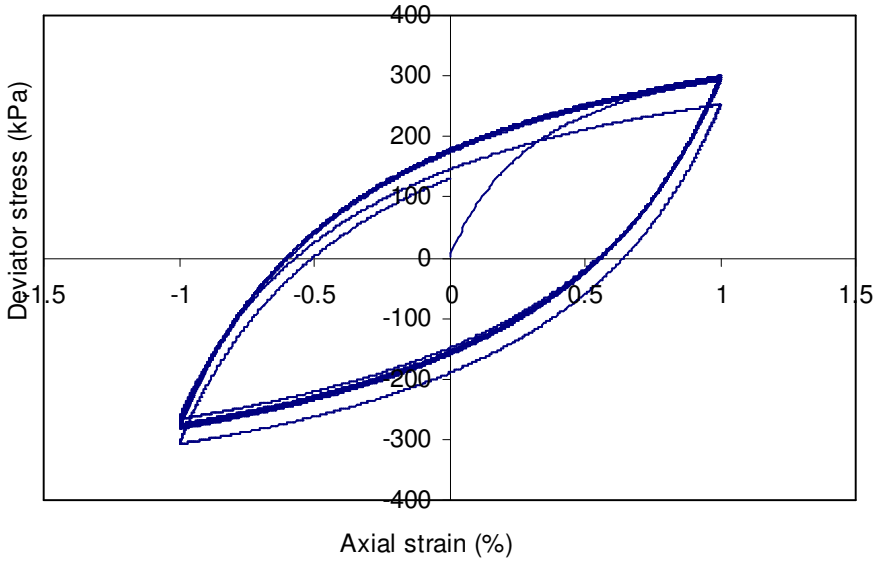

Figure 4.8 Dynamic response of the hyperbolic model without additional damping (12- cycle vertical sinusoidal loading, frequency =1 Hz, timestep=1.0×10^{-5} second)

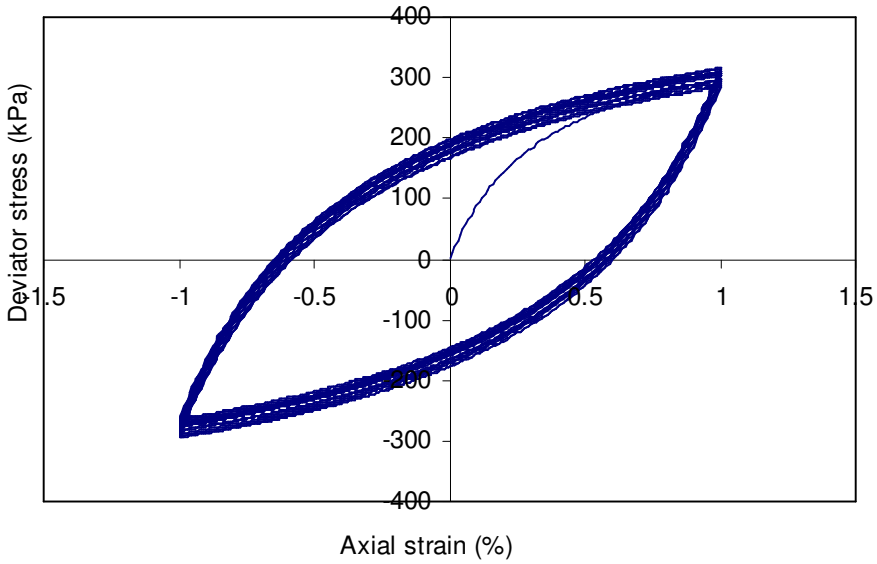

Figure 4.9 Static response of the hyperbolic model
(20 cycles, maximum strain = 1%, strain increment = 0.001% per step)

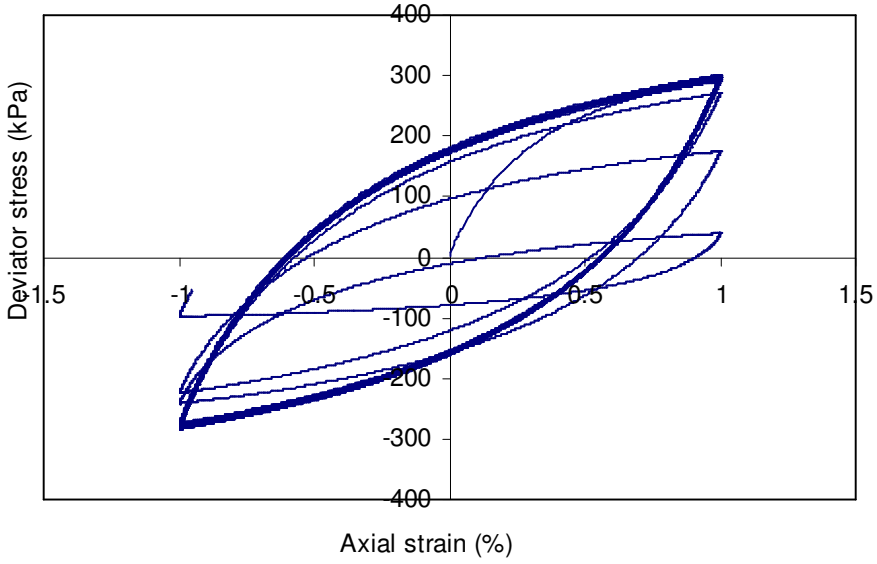

Figure 4.10 Dynamic response with a timestep of 1.0×10^{-6} second
(15- cycle vertical sinusoidal loading, frequency =1 Hz, no damping)

It has been found that the model works well in a static analysis (see Figure 4.9) and a satisfactory performance of the model can be obtained using an appropriate strain increment. In a dynamic analysis, however, reducing timestep (similar to reducing the strain increment in static analysis) does not help solve the problem of numerical distortion. In Figure 4.10, the timestep is 10 times smaller than that in Figure 4.8. The performance of the model is stable within the first 12 cycles, but it gets worse and worse afterwards. Therefore it is essential to apply an additional damping, as in Figure 4.7, to obtain a satisfactory performance of a nonlinear soil model if it is implemented with the 'apparent modulus' approach.

```
;FISH code of the Duncan elastic-hyperbolic model
;based on FLAC's hyp.fis and modified for cyclic loading
;update young's modulus each timestep while bulk modulus is constant
set echo off
def hyper_bn
  constitutive_model
;--- model variables ---
  f_prop y_mod b_mod yield y_initial
  ;soil property variables, yield=2*Su
  ;y_initial=initial Young's modulus
  f_prop h_e1  h_e2  h_g2  y_squared
  f_prop q0 q sign_old q_old G0
  float $dq $sign $shear $q_ult
  float $dzs11 $dzs22 $dzs33 $dzs12
  float $ds1 $ds2 $ds3 $dif $sum1 $sum2
  f_prop stepCommand
  case_of  mode
;--- initialization ---
    case 1
     if StepCommand=0 then
      if y_mod = 0.0 then
         y_mod = y_initial
      end_if
      $shear    = 3.0 * y_mod * b_mod / (9.0*b_mod-y_mod)
      h_e1      = b_mod + 1.333333  * $shear
      h_e2      = b_mod - 0.6666667 * $shear
      h_g2      = 2.0 * $shear
      yield_1 =2.0*yield
      G0=$shear
      StepCommand=1.0
    Endif
;--- running section ---
    case 2
      zvisc = 0.0
      ;calculate stress increments
      $dzs11    = (zde22+zde33) * h_e2 + zde11 * h_e1
      $dzs22    = (zde11+zde33) * h_e2 + zde22 * h_e1
```

```
      $dzs33    = (zde11+zde22) * h_e2 + zde33 * h_e1
      $dzs12    = zde12 * h_g2
      ;calculate deviator stress increment
      $ds1      = $dzs11 - $dzs22
      $ds2      = $dzs22 - $dzs33
      $ds3      = $dzs33 - $dzs11
      $dq       = $ds1*$ds1 + $ds2*$ds2 + $ds3*$ds3
      $dq       = 0.7071*sqrt($dq + 6.0*$dzs12*$dzs12)
      ;Calculate stresses
      zs11      = zs11 + $dzs11
      zs22      = zs22 + $dzs22
      zs33      = zs33 + $dzs33
      zs12      = zs12 + $dzs12
      ;accumulate deviator stress increment among sub-zones
      $sum1    = $sum1 + $dq
      ;accumulate strain increment among sub-zones
      $sum2=$sum2+zde22

      ;Average user's variables over sub-zones

      if zsub > 0.0 then
        $dq=$sum1/zsub
        $sum1=0.0
        $sign=sgn($sum2/zsub)
        $sum2=0.0
        q=q+$dq*$sign ;current deviator stress
        ;check strain reversal
        if $sign*sign_old<0.0 then
          q0=q_old
           yield=yield_1
        end_if
        ;update Young's modulus
        $dif   = max(0.0,yield-abs(q-q0))
        y_mod  = y_initial * $dif^2/ yield^2
        ;convet Young's modulus to shear modulus
        $shear = 3.0 * y_mod * b_mod / (9.0*b_mod-y_mod)
        ;calculate the three modulus variables for next step
        h_e1   = b_mod + 1.333333  * $shear
        h_e2   = b_mod - 0.6666667 * $shear
        h_g2   = 2.0 * $shear
        ;store variables
        q_old=q
        sign_old=$sign
     end_if
    case 3
;--- max modulus ---
      $shear = 3.0 * y_mod * b_mod / (9.0*b_mod-y_mod)
      cm_max = b_mod + 1.333333 * $shear
    sm_max=G0
    cm_max=b_mod + 1.333333 * G0
  end_case
end
;opt hyper_bn
set echo on
```

4.3.2 A bilinear model

It has been found in previous study (Ni, 2001) that an unstable response will occur in a dynamic analysis if a bilinear model is implemented with the 'apparent modulus' approach. The larger the difference between yield and elastic modulus of soil, the more severe the problem.

Herein the bilinear model is implemented using the concept of 'plastic correction' approach. A constant modulus is used and when yielding occurs a stress correction is carried out instead of using a yield modulus.

The bilinear model is formulated in a triaxial stress space. It is assumed that the same stress-strain relation applies to both compression and extension and there is no tension failure. The yield function is defined as follows:

$$f = |q| - \left| A \cdot \frac{q}{|q|} + B \cdot \varepsilon_a \right| \tag{4.8}$$

Where ε_a is the axial strain; q is the deviator stress; A and B are two constants with the same unit as q, which determines two yield lines as shown in Figure 4.11.

An elastic trial calculation is carried out each timestep to get a trial stress and if yielding occurs, *i.e.* $f>0$, the trial stress point is corrected back onto the yield lines. As there is no formulation in calculating plastic strain in this case, the plastic correction is performed with a correction ratio defined as follows:

$$ratio = \left| \frac{A \cdot \frac{q}{|q|} + B \cdot \varepsilon_a}{q} \right| = \left| \frac{A}{|q|} + B \cdot \frac{\varepsilon_a}{q} \right| \tag{4.9}$$

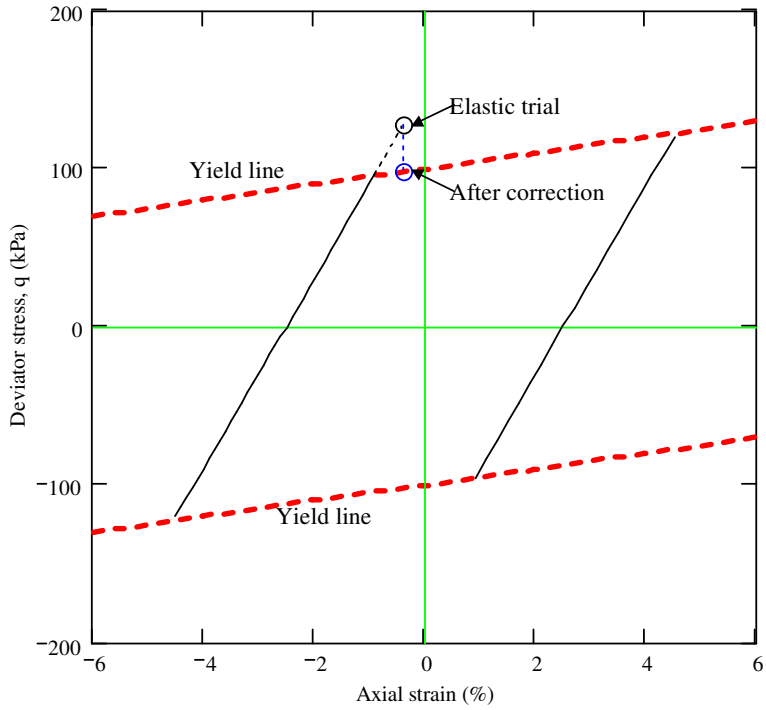

Figure 4.11 A bilinear model using 'plastic correction' approach

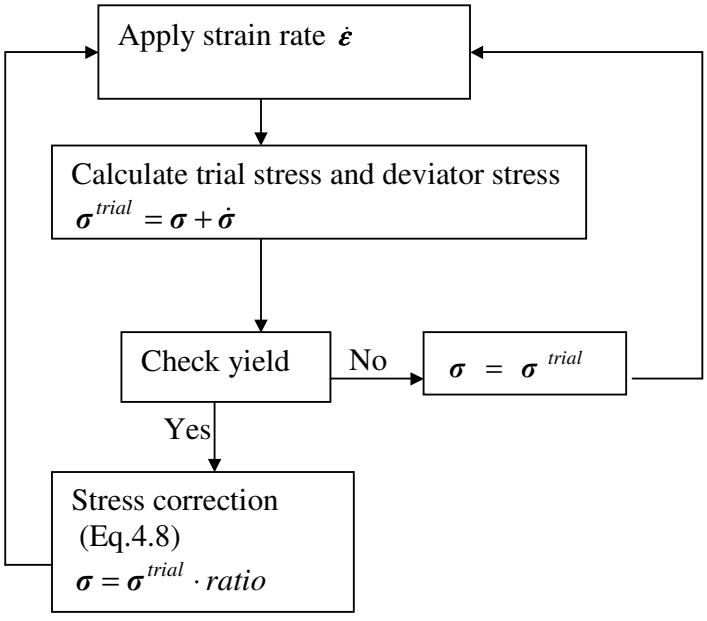

Figure 4.12 Flow chart of implementation of a bilinear model

$$\boldsymbol{\sigma} = \boldsymbol{\sigma}^{trial} \cdot ratio \tag{4.10}$$

Figure 4.12 shows the flow chart for implementation of the bilinear model and the *FISH* code is also given at the end of this section. The bilinear model has been found to perform well in dynamic analysis without any additional damping. Figure 4.13 shows that a 16-zone model (simulating a triaxial specimen 0.4 m in height and 0.2 m in diameter) undergoes a dynamic loading for 1000 cycles without any sign of numerical distortion. No additional damping is applied. A high frequency of 20 Hz is chosen to test the performance of the bilinear model as numerical distortion is frequency dependent and the higher the frequency, the more severe the distortion.

The bilinear model is identical to the Mohr-Coulomb model when B = 0. A comparison in dynamic analysis between these two models is shown in Figure 4.14. There is virtually no difference in the dynamic response.

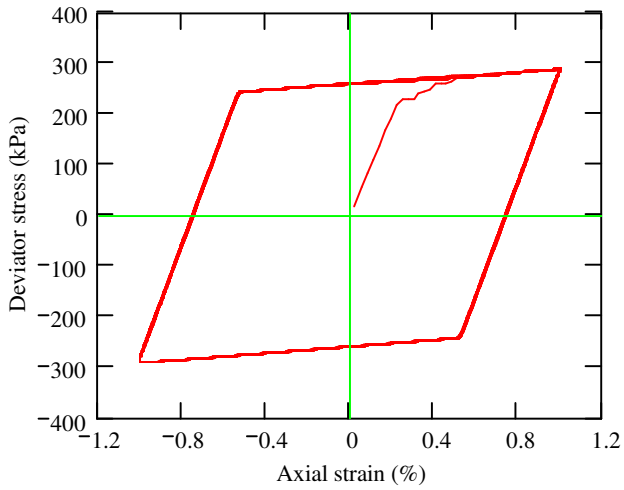

Figure 4.13 Dynamic response of a multi-zone bilinear model

(triaxial specimen 0.2 m by 0.4 m, 16 elements, sinusoidal loading, 1000 cycles, 20 Hz; G=40 MPa, K = 200 MPa, A=260 kPa, B = 800 kPa.)

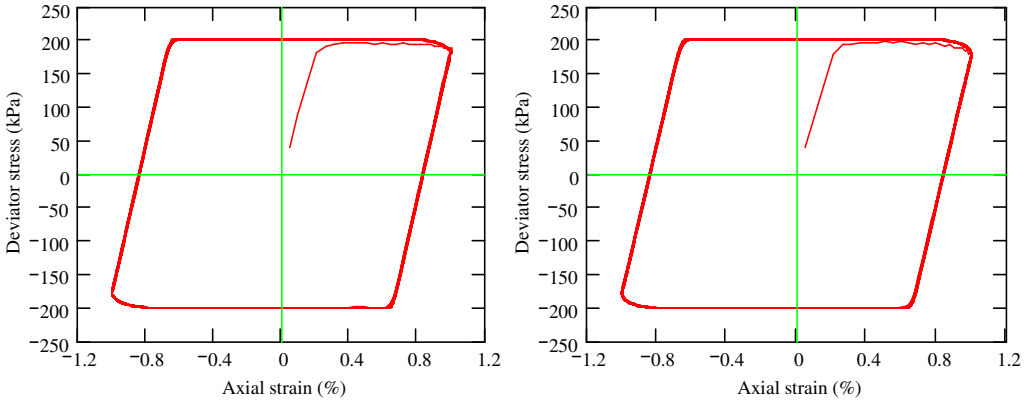

Figure 4.14 Comparison of the bilinear model with Mohr-Coulomb model

(triaxial specimen 0.2 m by 0.4 m, 16 elements, sinusoidal loading, 200 cycles, 20 Hz; G=40 MPa, K = 200 MPa; left – Bilinear model, A=200 kPa, B = 0 kP; right – Mohr-Coulomb model, q_u=200 kPa)

```
;FISH version of the bilinear model
;imlemented with 'Plastic correction approach'
;this version is for triaxial stress condition
set echo off
def m_bilinear
  constitutive_model
 f_prop b_g b_k A B
 f_prop b_e1 b_e2 b_sh2
 f_prop strain
 float $ratio $zde22 $q $q_max

 case_of  mode
; --- initialization ---
    case 1
      b_e1    = b_k + 4.0 * b_g / 3.0
      b_e2    = b_k - 2.0 * b_g / 3.0
      b_sh2   = 2.0 * b_g

; --- running section ---
    case 2
     zvisc = 0.0
; --- get new stresses from old
      zs11= zs11 + (zde22 + zde33) * b_e2 + zde11 * b_e1
      zs22= zs22 + (zde11 + zde33) * b_e2 + zde22 * b_e1
      zs33= zs33 + (zde11 + zde22) * b_e2 + zde33 * b_e1
      zs12 =zs12 + zde12 * b_sh2
      $zde22=$zde22+zde22
      $q=(zs22-zs11)
      strain=strain+zde22
      $q_max=sgn($q)*A+ B*strain
      if abs($q)>abs($q_max) then
       $ratio=abs($q_max/$q)
       zs11=zs11*$ratio
       zs22=zs22*$ratio
       zs33=zs33*$ratio
       zs12=zs12*$ratio
     end_if

; --- max modulus ---
    case 3
      cm_max = b_k + 4.0 * b_g / 3.0
      sm_max = b_g
  end_case
end
opt m_bilinear
set echo on
```

4.4 Discussion on numerical distortion

The numerical distortion (instability) encountered in 'apparent modulus' approach is considered to have nothing to do with the effects of timestep or zone size. As shown in Section 4.3.1, reducing timestep does not help to solve the problem. Previous study has also indicated that reducing zone size does not help either.

The problem may be partly due to the formulation of a soil model. For example, in a nonlinear model, an equivalent apparent tangent shear modulus may be formulated as follows:

$$G_{app} = \frac{G^e G^p}{G^e + G^p} \tag{4.11}$$

Where G_{app} is the apparent tangent shear modulus, G^e is the small strain shear modulus and G^p is the plastic shear modulus.

G^p may be formulated in such a way that it varies from infinity (∞) to zero so that G_{app} has a range of value between the small shear modulus and zero. Therefore, around the strain reversal points, G^p may well exceed the precision limits of a computer, which can cause computational error. One can solve the problem by specifying values of shear modulus when G^p exceed the precision limits (*i.e.* using 'if … then' statements in a *FLAC* program to avoid execution of the above equation). However, this will normally result in non-smooth transition in calculated stiffness.

The above computational error may also be introduced into a nonlinear model implemented using 'plastic correction' approach as a large plastic modulus is also required at the onset of yielding in order to obtain a smooth transition from elastic region to elasto-plastic region.

However there may be other reasons causing the problem, which can be more dominating than the precision limits of numbers. From analyses using the Duncan and Chang model (Section 4.3.1), it has been found that even though values of variables do not exceed the precision limits, severe distortion still occurs. It is suspected that the sudden change in apparent modulus appears to be one of the main reasons. Due to the repetitive sudden change in stiffness, some non-physical vibrations may be generated in the system.

In 'apparent modulus' approach, both of the above two factors contribute to the problem. It is expected that the distortion problem can be reduced in 'plastic correction' approach (as shown in Section 4.3.2) because there is no sudden change in modulus. However, computational errors may still be generated if the value of a variable exceeds the precision limits of a computer during the calculation.

4.5 Summary

Two approaches for implementing nonlinear soil models in *FLAC*, *i.e.* 'apparent modulus' and 'plastic correction', have been discussed.

The hyperbolic model provided in *FLAC* has been modified for cyclic loading to explore the problem of numerical distortion. It has been found that numerical distortion occurs in dynamic analysis if a nonlinear model is implemented with 'apparent modulus' approach.

This kind of numerical distortion is considered to be associated with strain reversals. Computational errors are introduced into the calculation around the turning points. The reasons for the errors may include: computed values of some variables exceed the precision limits of a computer; non-physical vibration is caused by the sudden change in stiffness of the model.

No matter what reason it is, it has been found that the problem has nothing to do with the size of timestep. Hence, reducing timestep does not help to reduce the problem. However, it can be minimised by applying an additional damping, which damps out to some extent the extra unbalanced forces caused by the errors. The numerical distortion does not occur in a static situation because a large default damping ratio (80%) is applied in *FLAC*. In a dynamic analysis, the numerical distortion becomes more severe as the errors can accumulate cyclically. An additional damping (say 5%) may not be sufficient to eliminate the problem. On the other hand, this additional damping may well affect the results of the analysis. Therefore, for dynamic analysis, 'plastic correction' approach has to be used to obtain a satisfactory result.

A bilinear model has been implemented in *FLAC* using the principle of 'plastic correction' approach. Satisfactory dynamic performance has been obtained from the bilinear model without using any additional damping. This has formed the basis for the work of implementing a more advanced plasticity model, *i.e.* the Bubble model in Chapter 5.

5 THE BUBBLE MODEL AND ITS IMPLEMENTATION IN *FLAC*

The Bubble model was first proposed by Tabbaa & Wood (1989). It was extended by Wood (1995) for structured soils, *i.e.* most natural soils, which have different stress-strain behaviours after being remoulded. More general formulations were given by Rouania & Wood (1998, 2000) in general stress space and Lode's angle was introduced into the yield functions. Further work was undertaken by Gajo & Wood (2001) to include rotational hardening in the model.

A full description of the model proposed by Rouania & Wood (2000) is presented in Section 5.1. For consistency, it is still called 'Bubble model'. An alternative form to the plastic modulus function of the model is proposed and discussed in Section 5.2, which has been found to better incorporate the influence of bubble's size on response of the model. The elastic bulk modulus function has also been extended for over-consolidated soils. The modified model has been implemented in *FLAC* with the 'Plastic correction' approach as described in Chapter 4. Main aspects of the implementation are discussed in Section 5.4. A complete *FISH* code of the model is attached to the chapter with detailed notations.

5.1 Description of the model (Rouania & Wood, 2000)

The Bubble model is an extension to the modified Cam-clay model and is formulated within the kinematic hardening framework similar to the two-surface model proposed by Mróz et al. (1979). The non-intersection translation rule proposed by Hashiguchi (1985) is utilised in the model. The model can be used for both structured and non-structured soils. It can also be reduced to the modified Cam-clay model.

Basic elasto-plastic assumption

The Bubble model, like other elasto-plastic models, has been developed on the basic assumption that strain rate consists of two parts, *i.e*. elastic and plastic strain rates.

$$\dot{\boldsymbol{\varepsilon}} = \dot{\boldsymbol{\varepsilon}}^{e} + \dot{\boldsymbol{\varepsilon}}^{p} \tag{5.1}$$

The constitutive relation presented in this section is formulated in general stress space. All the tensor quantities are denoted by bold characters. The superimposed dot stands for time differentiation. Further details of all the tensor quantities and tensor products are given in Appendix B attached to this chapter.

The elastic constitutive relation is given by the following equation.

$$\dot{\boldsymbol{\sigma}} = D^{e} \cdot \dot{\boldsymbol{\varepsilon}}^{e} \tag{5.2}$$

Where D^{e} is a matrix of isotropic elastic properties presented by the bulk and shear moduli, K and G. The bulk modulus, K, is defined as follows:

$$K = \frac{p}{\kappa^{*}} \tag{5.3}$$

Where p is the mean effective principal stress, κ^{*} is the slope of the swelling line in a logarithmic specific volume-logarithmic mean stress compression plane (*i.e*. $lnv \sim lnp$ plane) rather than in a specific volume-logarithmic mean stress compression plane (Butterfield, 1979).

Yield surfaces

The Bubble model has three surfaces, *i.e.* reference surface, bubble and structure surface. The three surfaces have the same elliptical shape and their size and location change when plastic strain occurs. The analytical equations are expressed in 'p, $\boldsymbol{s}$' space. p is mean principal stress and $\boldsymbol{s}$ is deviatoric stress tensor.

$$p = \frac{1}{3} tr[\boldsymbol{\sigma}] \qquad \boldsymbol{s} = \boldsymbol{\sigma} - p\boldsymbol{I} \tag{5.4}$$

Where $\boldsymbol{\sigma}$ is the stress tensor, $\boldsymbol{I}$ is the second-rank identity tensor and tr[.] is the trace operator of [.].

The reference surface is utilised to model intrinsic behaviour of reconstituted soils. It passes through the stress origin and is always centered on the p axis in the p, q space. Its size changes when plastic volumetric strain occurs according to an isotropic hardening rule (See Eq.5.19). The analytical equation is defined as follows:

$$f = \frac{3}{2M_\theta^2}(\boldsymbol{s}) : (\boldsymbol{s}) + (p - p_c)^2 - (p_c)^2 = 0 \tag{5.5}$$

Where p_c is a scalar variable defining the size of the reference surface (See Figure 5.1); M_θ is a dimensionless scaling function of Lode's angle θ, which affects the shape of the surfaces in deviatoric space. It is given by

$$M_\theta = \frac{2mM}{(1+m) - (1-m)\sin(3\theta)} \tag{5.6}$$

Where m is the ratio between radii of the sections through the surface for axisymmetrical extension and compression in deviatoric plane. It should be between 0.7 and 1.0 to ensure convexity. M is the critical state stress ratio for axisymmetrical compression. Lode's angle θ is related to the second and third deviatoric invariants, *i.e*. *J2* and *J3*:

$$\frac{-\pi}{6} \le \theta = \frac{1}{3}\sin^{-1}\left[\frac{-3\sqrt{3}J_3}{2J_2^{3/2}}\right] \le \frac{\pi}{6} \tag{5.7}$$

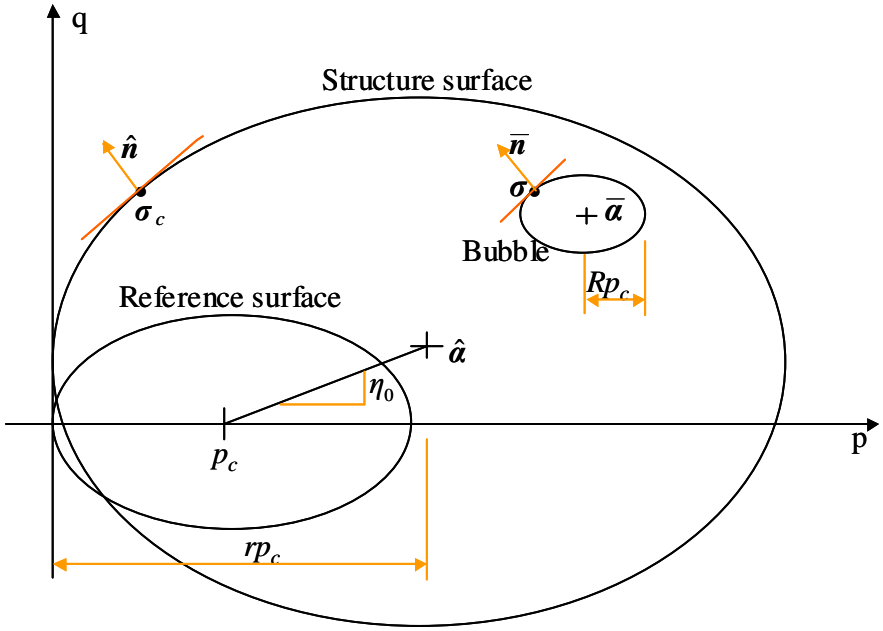

Figure 5.1 Three surfaces of the Bubble model

The bubble is the boundary of elastic behaviour. When stress path engages the bubble plastic deformation occurs and the size of the bubble changes according to the isotropic hardening rule, and, at the same time, it translates inside the structure surface according to a kinematic hardening rule. Its analytical equation, *i.e.* the yield function, is defined as follows:

$$f_b = \frac{3}{2M_\theta^2}(\boldsymbol{s}-\boldsymbol{s}_{\bar{\alpha}}):(\boldsymbol{s}-\boldsymbol{s}_{\bar{\alpha}})+(p-p_{\bar{\alpha}})^2-(Rp_c)^2=0 \qquad (5.8)$$

In the above equation, $\{p_{\bar{\alpha}}, \boldsymbol{s}_{\bar{\alpha}}\}^T = \bar{\boldsymbol{\alpha}}$ denotes the location of the centre of the bubble. R is a constant parameter representing the ratio of size between the bubble and reference surface.

The structure surface acts as a bounding surface. It collapses towards the reference surface as plastic strain develops. Both volumetric and shear strain contribute to the destructuration. After completion of the destructuration, the size of structure surface is

only controlled by the isotropic hardening rule. The analytical equation of the structure surface is given by

$$F = \frac{3}{2M_\theta^2}[\boldsymbol{s} - (r-1)\boldsymbol{\eta}_0 p_c] : [\boldsymbol{s} - (r-1)\boldsymbol{\eta}_0 p_c] + (p - rp_c)^2 - (rp_c)^2 = 0 \qquad (5.9)$$

Where $\boldsymbol{\eta}_0$ is a dimensionless deviatoric tensor controlling the structure surface, $\{rp_c, (r-1)\boldsymbol{\eta}_0 p_c\}^T = \hat{\boldsymbol{\alpha}}$ denotes the centre of the structure surface. The scalar variable *r,* which represents the process of the progressive destructuration of a structured soil, is the ratio of the sizes between the structure surface and the reference surface and it is assumed to be a monotonically decreasing function of the plastic strain.

$$r = 1 + (r_0 - 1)\exp\left[\frac{-k\varepsilon_d}{(\lambda^* - \kappa^*)}\right] \qquad (5.10)$$

Where λ^* is the slope of the normal compression line expressed in a logarithmic specific volume-logarithmic mean stress compression plane (*i.e. lnv ~ lnp* plane); r_0 is the initial size of the structure surface and *k* is a parameter controlling the rate of destructuration with strain. The incremental form of equation (5.10) is given as follows:

$$\dot{r} = -\frac{k}{(\lambda^* - \kappa^*)}(r-1)\dot{\varepsilon}_d \qquad (5.11)$$

In this equation $\dot{\varepsilon}_d$ is an assumed destructuration strain rate having the following form:

$$\dot{\varepsilon}_d = [(1-A)(\dot{\varepsilon}_v^p)^2 + A(\dot{\varepsilon}_q^p)^2]^{1/2} \qquad (5.12)$$

Where $\dot{\varepsilon}_{\mathrm{q}}^{\mathrm{p}} = [\frac{2}{3}(\dot{\boldsymbol{\varepsilon}}^{\mathrm{p}} : \dot{\boldsymbol{\varepsilon}}^{\mathrm{p}})]^{1/2}$ is the equivalent plastic shear strain rate, $\dot{\varepsilon}_v^p = tr[\dot{\boldsymbol{\varepsilon}}^p]$ is the plastic volumetric strain rate. '*A*' is a scaling parameter ranging between 0 and 1. For *A* =

0 the destructuration is entirely volumetric, while for $A = 1$ the destructuration is entirely distortional.

Flow rule

The flow rule is associated with the bubble. When the yield function $f_b = 0$ (*i.e.* in numerical analysis, $f_b \geq 0$) is satisfied, plastic strain occurs, which is given by

$$\dot{\boldsymbol{\varepsilon}}^p = \frac{1}{H}(\overline{\boldsymbol{n}} : \dot{\boldsymbol{\sigma}})\overline{\boldsymbol{n}} \tag{5.13}$$

Where $\dot{\boldsymbol{\sigma}}$ is the stress rate and $\overline{\boldsymbol{n}}$ denotes a unit vector representing the normalised stress gradient on the bubble at the current stress state and $\|\overline{\boldsymbol{n}}\| = |\overline{\boldsymbol{n}} : \overline{\boldsymbol{n}}|^{1/2} = 1$. The computation of $\overline{\boldsymbol{n}}$ involves the derivatives of Lode's angle with respect to stress (see Appendix 5.3). H is the scalar plastic modulus expressed as follows:

$$H = H_{\mathrm{c}} + \frac{1}{\|\boldsymbol{n}\|^2}\frac{Bp_{\mathrm{c}}^3}{(\lambda^* - \kappa^*)R}\left(\frac{b}{b_{\max}}\right)^{\psi} \tag{5.14}$$

Where $\boldsymbol{n}$ is the stress gradient on the bubble at the current stress state. $\|\boldsymbol{n}\| = [\boldsymbol{n} : \boldsymbol{n}]^{1/2}$. B, ψ are two material parameters controlling the rate of decay of stiffness with strain. H_c is the plastic modulus associated with the conjugate stress state $\boldsymbol{\sigma}_c$ on the structure surface. It is given by

$$H_c = \frac{rp_c\left\langle T\left[(p - p_{\bar{\alpha}}) + \frac{3}{2M_\theta^2}(\boldsymbol{s} - \boldsymbol{s}_{\bar{\alpha}}) : \boldsymbol{\eta}_0 + Rp_c\right] - \frac{3}{2M_\theta^2}(p - p_{\bar{\alpha}})(\boldsymbol{s} - \boldsymbol{s}_{\bar{\alpha}}) : \frac{\boldsymbol{\eta}_0}{r}\right\rangle}{(\lambda^* - \kappa^*)\left[(p - p_{\bar{\alpha}})^2 + \frac{3}{2M_\theta^4}(\boldsymbol{s} - \boldsymbol{s}_{\bar{\alpha}}) : (\boldsymbol{s} - \boldsymbol{s}_{\bar{\alpha}})\right]} \tag{5.15}$$

Where the quantity T is given by

$$T = (p - p_{\bar{\alpha}}) - k(\frac{r-1}{r})\left[(1-A)(p-p_{\bar{\alpha}})^2 + \frac{3A}{2M_\theta^2}(\boldsymbol{s}-\boldsymbol{s}_{\bar{\alpha}}):(\boldsymbol{s}-\boldsymbol{s}_{\bar{\alpha}})\right]^{1/2} \tag{5.16}$$

In Eq.5.14, b is a normalised distance between current stress point $\boldsymbol{\sigma}$ on the bubble and the conjugate stress point $\boldsymbol{\sigma}_c$ on the structure surface, and $b_{\max}$ is obtained when the bubble is touching the structure surface at a point diametrically opposite to the conjugate stress point (see Figure 5.10 in Section 5.3). b and $b_{\max}$ are expressed as follows:

$$b = \bar{\boldsymbol{n}} : (\boldsymbol{\sigma}_c - \boldsymbol{\sigma}) \tag{5.17}$$

$$b_{\max} = 2(\frac{r}{R} - 1)\bar{\boldsymbol{n}} : \bar{\boldsymbol{\sigma}} \tag{5.18}$$

Where $\bar{\boldsymbol{\sigma}} = \boldsymbol{\sigma} - \bar{\boldsymbol{\alpha}}$ is the normalised stress with respect to the centre of the bubble.

Isotropic hardening rule

In line with the Cam-clay model, a volumetric hardening rule is adopted in the Bubble model, *i.e.* all the three surfaces change in size only when plastic volumetric strain occurs. It is given by

$$\frac{\dot{p}_c}{p_c} = \frac{\dot{\varepsilon}_v^p}{(\lambda^* - \kappa^*)} \tag{5.19}$$

Kinematic hardening rule

When plastic strain occurs the bubble translates inside the structure surface according to the kinematic hardening rule given by

$$\dot{\bar{\boldsymbol{\alpha}}} = \dot{\hat{\boldsymbol{\alpha}}} + (\bar{\boldsymbol{\alpha}} - \hat{\boldsymbol{\alpha}})(\frac{\dot{r}}{r} + \frac{\dot{p}_c}{p_c}) + \frac{\bar{\boldsymbol{n}} : \left\{\dot{\hat{\boldsymbol{\sigma}}} - \hat{\boldsymbol{\sigma}}[(\dot{r}/r) + (\dot{p}_c/p_c)] + \bar{\boldsymbol{\sigma}}(\dot{r}/r)\right\}}{\bar{\boldsymbol{n}} : (\boldsymbol{\sigma}_c - \boldsymbol{\sigma})}(\boldsymbol{\sigma}_c - \boldsymbol{\sigma}) \tag{5.20}$$

Where $\hat{\boldsymbol{\sigma}} = \boldsymbol{\sigma} - \hat{\boldsymbol{\alpha}}$ is the normalised stress with respect to the centre of the structure surface. Discussions about the kinematic hardening rule are given in the next section.

5.2 Modifications of the Bubble model

5.2.1 Plastic modulus function

In the hardening modulus function, *i.e.* $H = H_c + \frac{1}{\|\boldsymbol{n}\|^2} \frac{Bp_c^3}{(\lambda^* - \kappa^*)R} (\frac{b}{b_{max}})^{\psi}$, the second term is an interpolation function which affects the behaviour of the model significantly. The interpolation function is not unique. Any other form can be adopted as long as a steady fall of stiffness with strain towards Cam-clay value can be achieved as the bubble approaches the structure surface. This will not change the fundamental framework of the constitutive model in Section 5.1.

It has been found that for a given set of parameters, in order to obtain a realistic response of the model, the value of parameter *B* has to be varied in a large range if the bubble size parameter *R* changes.

Figure 5.2 shows the initial state of a non-structured soil in triaxial stress space. To show the influence of bubble size on the response of the model, three bubble sizes (*R* = 0.1, 0.2 and 0.3) are considered while other parameters are the same, which are given as follows:

$\lambda^* = 0.3$ $\kappa^* = 0.02$ $\mu = 0.25$ $M = 1.0$ $m = 1.0$ $B = 4$ $\psi = 1.0$

$\eta_0 = 0$ $r_0 = 1.0$ $A = 0.5$ $k = 8$ $\sigma_3' = p_{c0} = 100\ kPa$

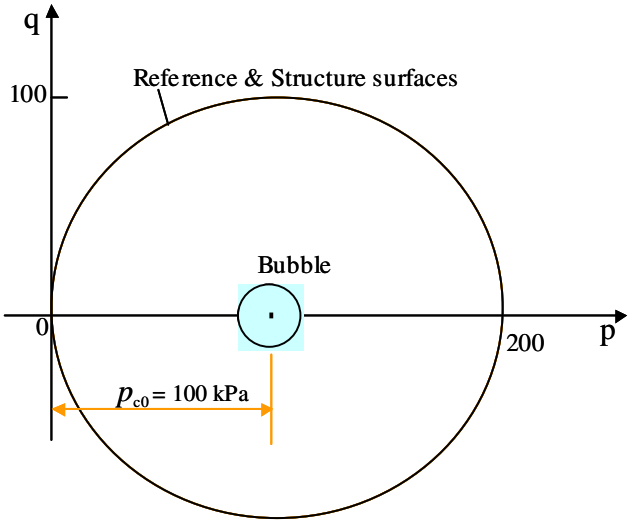

Figure 5.2 Initial state of a non-structured soil

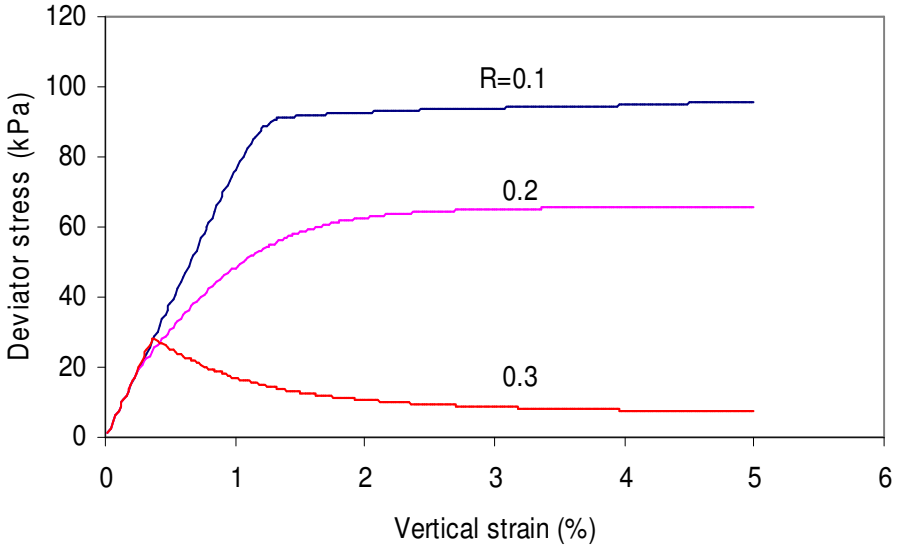

Figure 5.3 Stress-strain behaviour with variable bubble size (B = 4)

Figure 5.3 shows the undrained stress-strain curves of the model corresponding to the three bubble sizes. As $\sigma_3' = p_{c0}$=100 kPa and M = 1, a realistic response of the model should correspond to an ultimate deviator stress of about 100 kPa. Therefore the curve for R = 0.1 represents the realistic response. It is expected that the ultimate stress for the

other two bubble sizes should be similar as the initial conditions are the same. To achieve similar results for different bubble sizes, the value of parameter *B* has to be varied. It has been found that *B* has to be varied from 0.5 to 50 if bubble size *R* changes from 0.05 to 0.3 in order to get consistent realistic results (see Figures 5.4 and 5.5).

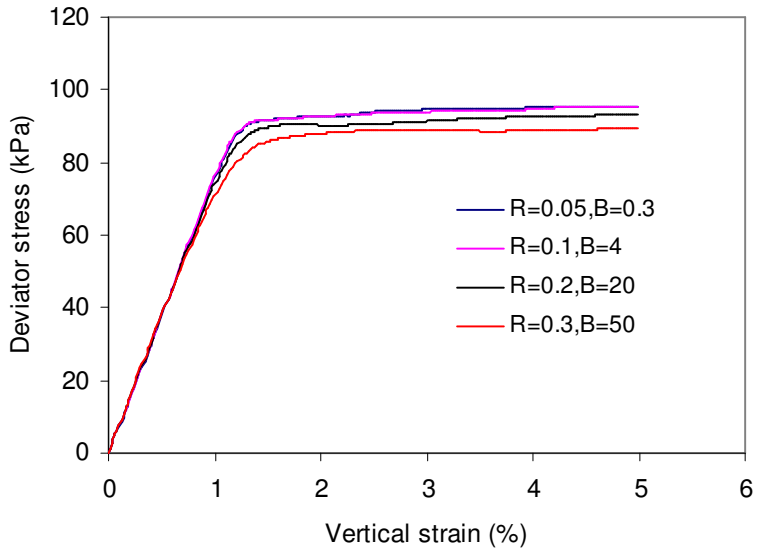

Figure 5.4 Response of the bubble model to different combinations of B and R

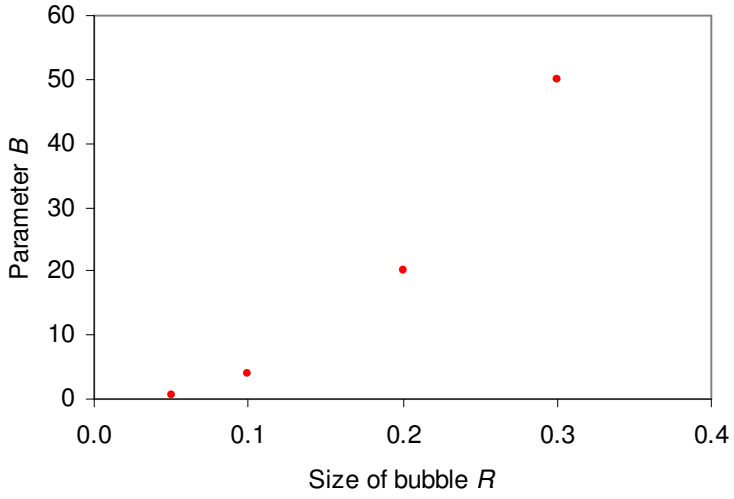

Figure 5.5 Relationship between B and R

Although it is not difficult to find a value of B to suit a particular bubble size, it is more desirable that B should be less sensitive to the bubble size. To better incorporate the influence of bubble size into the interpolation function, a temporary parameter, C, is introduced into the function (Note: The bubble size R is also hidden in b, b_{max}, H_c and $\boldsymbol{n}$). C is a function of bubble size R. The hardening function is now given by

$$H = H_c + \frac{1}{\|\boldsymbol{n}\|^2} \frac{C p_c^3}{(\lambda^* - \kappa^*)} \left(\frac{b}{b_{\max}}\right)^{\psi}$$

Using the same parameters and varying ψ between 0.5 and 1.5, a relationship of parameters C and R is found by trial and error to achieve realistic responses of the model. Results are shown in Figure 5.6. It can be seen that the relation of C and R in the original interpolation function is opposite to the best fit curve. This explains why B has to be varied in a large range.

The best fit relation of C and R, *i.e.* $C = 580.0\, R^{1.8}$, suggests a new form of the hardening modulus function as follows:

$$H = H_c + \frac{1}{\|\boldsymbol{n}\|^2} \frac{B R^2 p_c^3}{(\lambda^* - \kappa^*)} \left(\frac{b}{b_{\max}}\right)^{\psi} \tag{5.21}$$

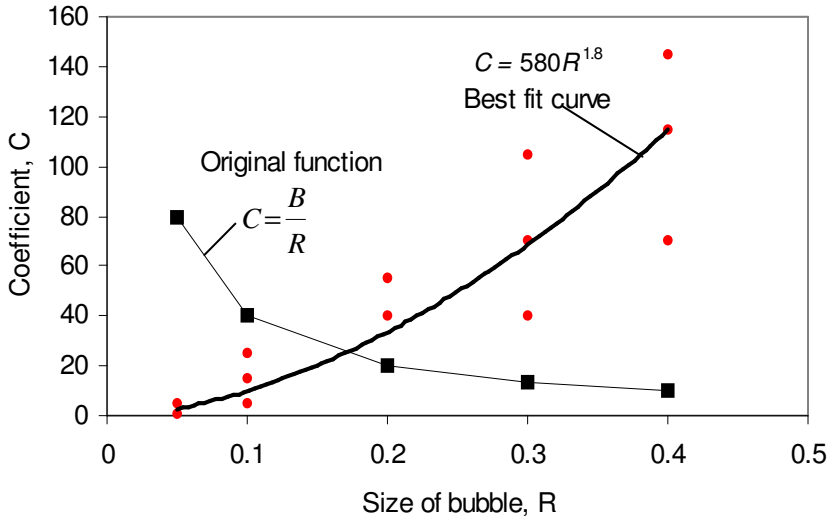

Figure.5.6 Relationship of C and R

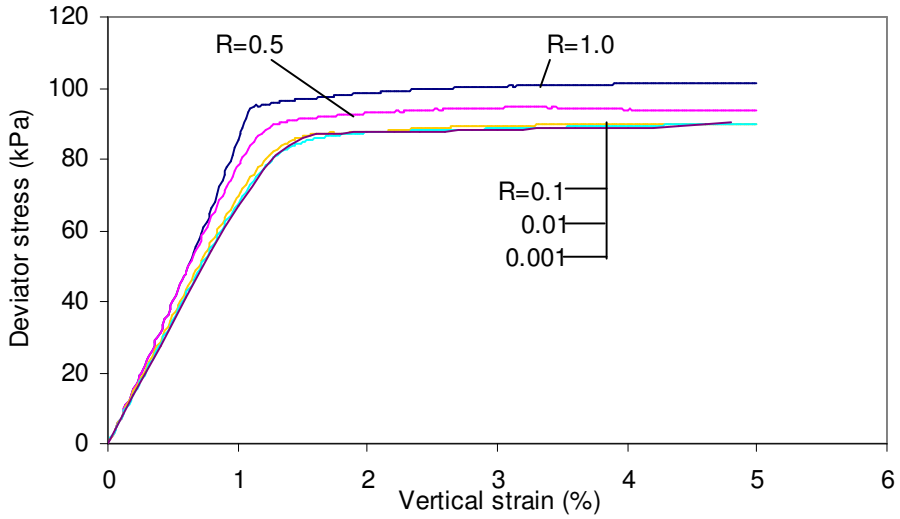

Figure 5.7 Response of the model with new hardening function and constant B (R = 0.001 ~1.0, B = 2000)

Figure 5.7 presents responses of the model using the new hardening modulus function for the same problem. The bubble size is varied between 0.001 and 1.0 while all other parameters are the same for each bubble size. All the responses are similar and realistic using a constant value of *B*.

5.2.2 Elastic bulk modulus

In the Bubble model elastic bulk modulus is defined as Eq.5.3, *i.e.* $K = \frac{p}{\kappa^*}$. It is obvious that if the confining pressure is zero the bulk modulus would be zero. This is true for normally consolidated soil but not for over-consolidated soil. For natural soil, use of the equation tends to result in over estimation of deformation. Therefore, for over-consolidated soil the bulk modulus is modified as follows.

$$K = \frac{p}{\kappa^*} + K_0 \tag{5.22}$$

Where K_0 is the bulk modulus when the confining pressure is zero.

5.3 Discussions

Comparison of parameters between Bubble model and the modified Cam-clay model

When R = 1.0, r_0 = 1.0 and $\eta_0 = 0$, the Bubble model is reduced to the modified Cam-clay model. Parameters k and A have no influence as no initial structure of soil is involved. Parameter m is ranged between 0.7 and 1.0 and has no influence in axisymmetrical compression. Therefore parameters of the Bubble model are reduced to $\lambda^*, \kappa^*, M, p_c, B, \psi, \mu$.

Parameters of the modified Cam-clay model include: $\lambda, \kappa, M, p_{cm}, \mu$. A reference point $(v_{\lambda 0}, p_0)$ on the normal consolidation line must be specified to use the model.

p_{cm} and p_c represent the size of yield surface. In the Bubble model p_c corresponds to the centre of the yield surface while p_{cm} in the modified Cam-clay model is associated with the intersection point of the yield surface and the p axis, *i.e* $p_{cm} = 2p_c$ (see Figure 5.8).

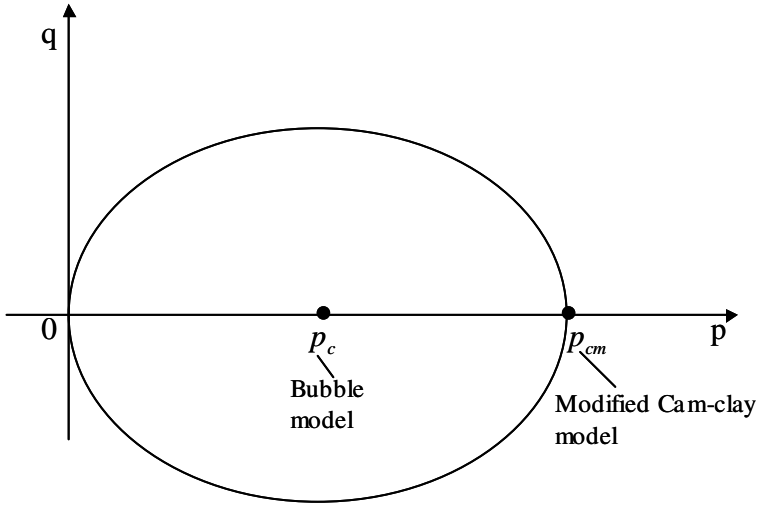

Figure 5.8 Yield surface

Butterfield (1979) suggested using a logarithmic specific volume-logarithmic mean stress compression plane rather than a specific volume-logarithmic mean stress compression plane. Typical values for the two parameters λ^*, κ^* from Butterfiled are given in Table 1.

Table 5.1 Typical values of parameters λ^* and κ^*
(Butterfield, 1979)

Soil	λ^*	κ^*
Mexico City Clay	0.498	0.025
London Clay	0.083	0.037
Newfoundland peat	0.214	0.117
Newfoundland silt	0.103	0.016
Chicago Clay	0.154	0.045
Boston blue Clay	0.122	0.024
Drammen Clay, plastic	0.140	0.016
Drammen Clay, lean	0.104	0.018

Stallebrass and Taylor (1997) used $\lambda^* = 0.073$ and $\kappa^* = 0.005$ in the *3-SKH* model for Speswhite kaolin while Morrison (1994) used $\lambda = 0.18$ and $\kappa = 0.035$ in the modified Cam-clay model for the same soil.

Rouainia and Wood (2000) used $\lambda^* = 0.252$ and $\kappa^* = 0.0297$ in the Bubble model for Norrköping clay.

In fact, λ^*, κ^* vary with mean principal stress. For small strain problems λ^*, κ^* can be related to λ, κ by

$$\lambda^* \approx \frac{\lambda}{v_0} \text{ and } \kappa^* \approx \frac{\kappa}{v_0} \tag{5.23}$$

Where v_0 is the initial specific volume corresponding to the initial mean effective principal stress p_0. Further explanation about the above relationships is given as follows.

In the logarithmic specific volume-logarithmic mean stress compression plane shown as Figure 5.9, the compression line is defined by

$$ln(\frac{v}{v_{\lambda 0}}) = -\lambda^* ln(\frac{p}{p_0}) \tag{5.24}$$

Differentiation of Eq.5.24 gives

$$\frac{dv}{v} = -\lambda^* \frac{dp}{p} \tag{5.25}$$

On the other hand, in the specific volume-logarithmic mean stress compression plane, the compression line is defined by

$$v = v_{\lambda 0} - \lambda ln(\frac{p}{p_0}) \tag{5.26}$$

Differentiation of Eq.5.26 gives

$$dv = -\lambda \frac{dp}{p} \tag{5.27}$$

Substitution of Eq.5.25 gives

$$\lambda^* = \frac{\lambda}{v} \tag{5.28}$$

Similarly, the following relationship can be obtained

$$\kappa^* = \frac{\kappa}{v} \tag{5.29}$$

For small strain problems, $v \approx v_0$, hence $\lambda^* \approx \frac{\lambda}{v_0}$ and $\kappa^* \approx \frac{\kappa}{v_0}$

The above relationships will be used in Section 6.3 when the Bubble model is compared with the modified Cam-clay model.

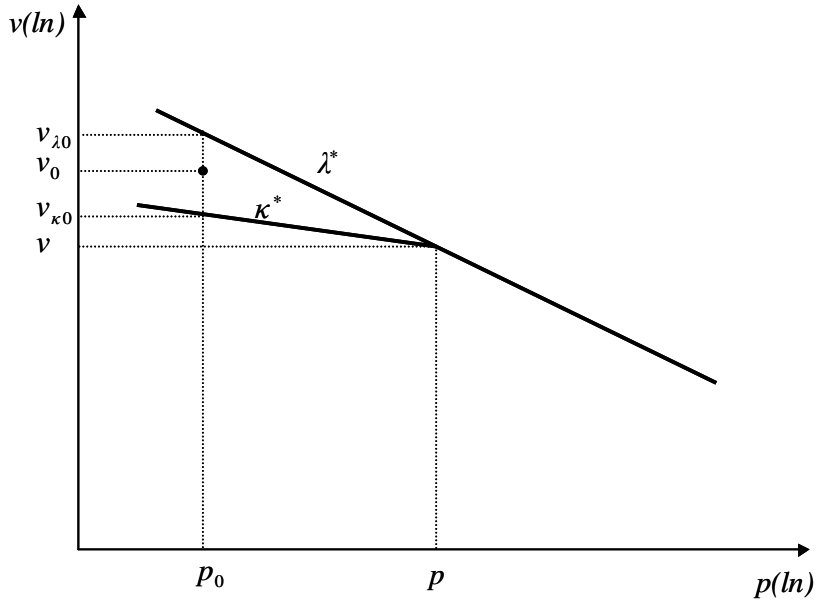

Figure 5.9 Normal consolidation line and swelling line

Stress gradient and normalized stress gradient

The hardening modulus, $H = H_c + \frac{1}{\|\boldsymbol{n}\|^2}\frac{BR^2 p_c^3}{(\lambda^* - \kappa^*)}(\frac{b}{b_{\max}})^{\psi}$, involves the magnitude of stress gradient $\boldsymbol{n}$ at the current stress state on the bubble. In all other formulations of the model, normalised stress gradient $\overline{\boldsymbol{n}}$ has to be used, which is the stress gradient normalised with respect to its magnitude, i.e. $\|\overline{\boldsymbol{n}}\| = [\overline{\boldsymbol{n}} : \overline{\boldsymbol{n}}]^{1/2} = 1$.

Distance of current stress state to structure surface

The hardening modulus depends on the location of current stress state, which is measured as a normalised distance between the current and conjugate stress points with respect to the direction of stress gradient, *i.e.* $b = \overline{\boldsymbol{n}} : (\boldsymbol{\sigma}_c - \boldsymbol{\sigma})$. $b_{\max}$ is obtained when the bubble is touching the structure surface at a point diametrically opposite to the conjugate stress point, i.e. $b_{\max} = 2(\frac{r}{R} - 1)\overline{\boldsymbol{n}} : \overline{\boldsymbol{\sigma}}$.

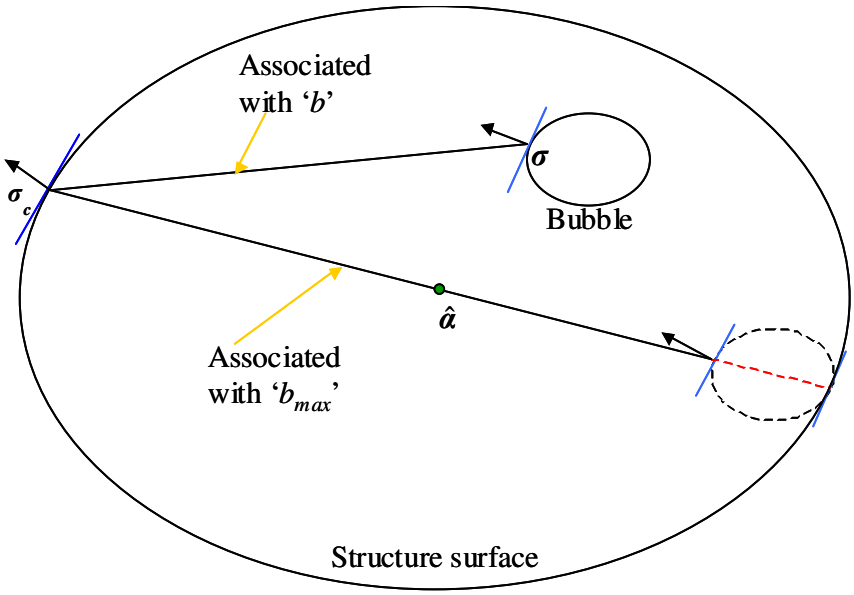

Figure 5.10 Normalised distance of bubble to structure surface

Non-intersection translation rule

In the Bubble model, the non-intersection translation rule proposed by Hashiguchi (1985) is employed to describe the kinematic hardening of the bubble, *i.e*,

$$\dot{\bar{\boldsymbol{\alpha}}} = \dot{\hat{\boldsymbol{\alpha}}} + (\bar{\boldsymbol{\alpha}} - \hat{\boldsymbol{\alpha}})(\frac{\dot{r}}{r} + \frac{\dot{p}_c}{p_c}) + \frac{\bar{\boldsymbol{n}} : \left\{\dot{\hat{\boldsymbol{\sigma}}} - \hat{\boldsymbol{\sigma}}[(\dot{r}/r) + (\dot{p}_c / p_c)] + \bar{\boldsymbol{\sigma}}(\dot{r}/r)\right\}}{\bar{\boldsymbol{n}} : (\boldsymbol{\sigma}_c - \boldsymbol{\sigma})}(\boldsymbol{\sigma}_c - \boldsymbol{\sigma})$$

The bubble translates along the line connecting the current and conjugate stress points and eventually comes into contact with the structure surface as shown in Figure 5.11. However this hardening process is significantly influenced by hardening modulus. As the interpolation function of the hardening modulus is arbitrarily defined and is not interrelated to the translation rule, the bubble may never reach the structure surface if an inappropriate value of parameter B is selected, *i.e.* the critical state of soil can be reached before the bounding surface is engaged by the current stress state (See Figures 6.15 and 6.17 in Section 6.1).

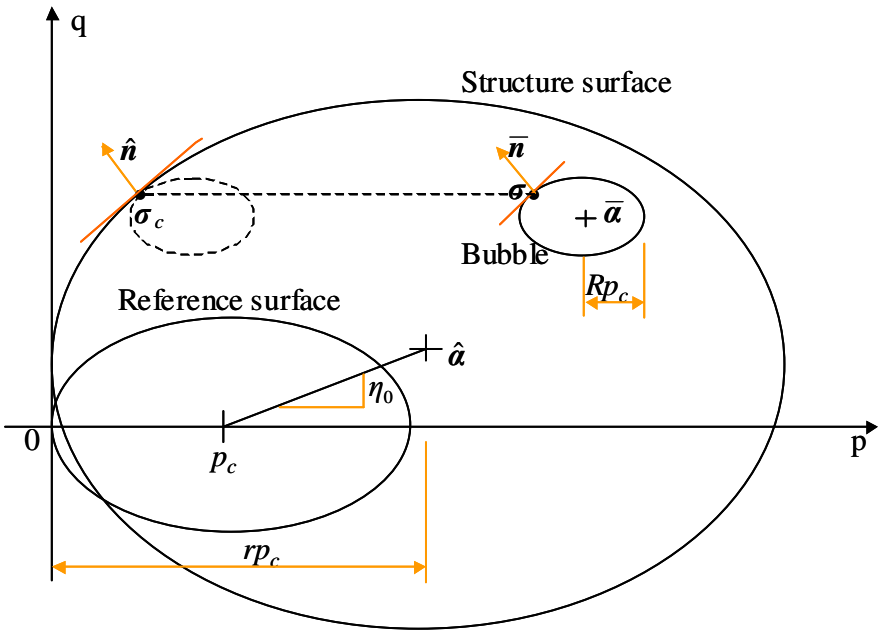

Figure 5.11 Kinematic hardening of bubble

Volumetric hardening

Although the Bubble model is formulated in kinematic hardening framework, volumetric hardening has a major influence on the response of the model. When $r_0 = 1$ translation of the centre of the structure surface is given by

$$\dot{\hat{\boldsymbol{\alpha}}} = [\, \dot{p}_c, \;\; 0 \,]^T \tag{5.30}$$

While translation of the centre of the bubble is given by

$$\dot{\bar{\boldsymbol{\alpha}}} = \dot{\hat{\boldsymbol{\alpha}}} + (\bar{\boldsymbol{\alpha}} - \hat{\boldsymbol{\alpha}})(\frac{\dot{p}_c}{p_c}) + \frac{\bar{\boldsymbol{n}} : \{\dot{\hat{\boldsymbol{\sigma}}} - \hat{\boldsymbol{\sigma}}(\dot{p}_c / p_c)\}}{\bar{\boldsymbol{n}} : (\boldsymbol{\sigma}_c - \boldsymbol{\sigma})}(\boldsymbol{\sigma}_c - \boldsymbol{\sigma}) \tag{5.31}$$

As p_c is only controlled by plastic volumetric strain hence hardening of the yield surface is purely volumetric when $r_0 = 1$.

Reference surface

The Bubble model is actually a two-surface model. The reference surface represents the intrinsic behaviour of a remoulded soil. It is not directly involved in the hardening rule or hardening function. However the use of a reference surface makes it possible to illustrate the destructuration process of a structured soil.

Incremental stress-strain relation

The incremental stress-strain relation is given by

$$\boldsymbol{D}^{ep} = \boldsymbol{D}^{e} - \frac{(\boldsymbol{D}^{e} : \overline{\boldsymbol{n}}) \otimes (\overline{\boldsymbol{n}} : \boldsymbol{D}^{e})}{H + \overline{\boldsymbol{n}} : \boldsymbol{D}^{e} : \overline{\boldsymbol{n}}} \tag{5.32}$$

Where the symbol $\otimes$ denotes a tensor product in the sense that $(a \otimes b)_{ijkl} = a_{ij} b_{kl}$. This relation is only necessary when the 'apparent modulus' approach is utilised. In the thesis, Eq.5.32 is not involved in the formulations of the Bubble model as the 'plastic correction' approach is adopted.

Determination of parameters

Parameters λ^*, κ^*, M and m have clear physical meanings and can be readily obtained from conventional laboratory tests. λ^* and κ^* represent the compressibility of soil and can be obtained from oedometer tests. M represents the slope of the critical state line in p, q space can be obtained from triaxial tests. m can be expressed as the ratio of deviator stresses between triaxial extension and triaxial compression tests.

The parameter R reflects the size elastic region. It is believed that R depends on several factors including overconsolidation ratio, initial effective confining stress and initial density of soil. However, no reference has been found as to how to determine the value of R experimentally. For this reason, the influence of R has been investigated in the parametric study in Section 7.2 to assess its effective ranges. For a particular type of soil, R can be obtained by comparison between numerical analyses and triaxial compression tests.

r_0 represents the sensitivity of a structured soil and can be related to the sensitivity index. As the sensitivity index can be easily obtained from triaxial tests, the relationship between r_0 and the sensitivity index can be established for a particular type of soil by matching numerical modelling results with triaxial testing data. A preliminary study is given in Section 7.6 (see Figure 7.36).

p_{c0} is the initial value of p_c and is related to the preconsolidation pressure. It is believed that it is adequate for a numerical modelling to assume: p_{c0} = preconsolidation pressure/(2 r_0). More discussion on determination of p_{c0} is given in Section 7.6.

Parameters η_0, B, A, ψ and k can not be related directly to physical characteristics of soil. However, for a specific soil, these parameters can be quantified by fitting numerical modelling results with experimental curves (e.g. triaxial stress-strain curves). A preliminary study on these parameters is also carried out in Chapter 7.

5.4 Pore water pressure

Water and soil particles are assumed to be incompressible, hence, under undrained condition when the soil is fully saturated, the following equation is assumed to be applicable:

$$\dot{\varepsilon}_v^p + \dot{\varepsilon}_v^e = 0 \tag{5.33}$$

Where $\dot{\varepsilon}_v^p, \dot{\varepsilon}_v^e$ are plastic and elastic volumetric strain rate respectively due to relative movement between soil particles.

If plastic deformation takes place, *i.e.* $\dot{\varepsilon}_v^p \neq 0$, to maintain the constant volume of soil, pore water pressure is generated to compensate the plastic volumetric change (Schofield and Wroth, 1968), *i.e.* $\dot{\varepsilon}_v^e = -\dot{\varepsilon}_v^p$. The pore water pressure is given by

$$u = K\dot{\varepsilon}_v^e = -K\dot{\varepsilon}_v^p \tag{5.34}$$

Where K is the drained bulk modulus of the soil.

If the current stress is inside the bubble, there is no plastic deformation, *i.e.* $\dot{\varepsilon}_v^p = \dot{\varepsilon}_v^e = 0$. Therefore zero pore water pressure will be generated.

5.5 Implementation

The Bubble model is implemented in *FLAC* using the computer language *FISH* embedded in *FLAC*. Some key aspects in implementing a constitutive model with *FISH* are discussed in the Chapter 3. The 'plastic correction' approach described in the Chapter 4 is utilised for the implementation of the Bubble model. A general flow chart of the programme for the Bubble model is shown in Figure 5.12. The complete programme with detailed notations is appended to this chapter.

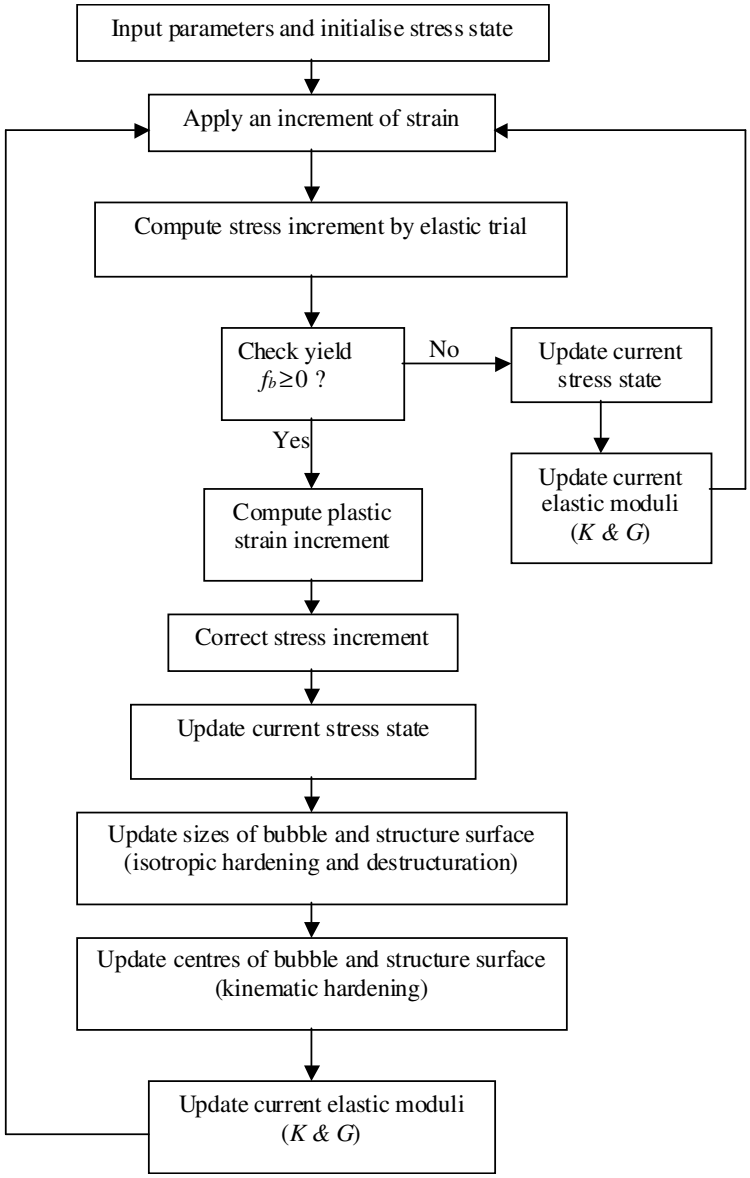

Figure 5.12 Flow chart for implementation of the Bubble model

Appendix 5.1 Notation

A	A scaling factor ranged between 0 and 1 controlling the ratio of contribution to destructuration between equivalent plastic shear strain and plastic volumetric strain
B	A material parameter controlling the magnitude of plastic modulus
b	A normalised distance between current stress point ($\boldsymbol{\sigma}$)on the bubble and the conjugate stress point ($\boldsymbol{\sigma}_c$) on the structure surface (*i.e.* normalised with respect to $\overline{\boldsymbol{n}}$)
$b_{\max}$	The maximum value of b and it is obtained when the bubble is touching the structure surface at a point diametrically opposite to the conjugate stress point
D^e	Matrix of isotropic elastic properties
H	Plastic modulus at the current stress state
H_c	Plastic modulus at the conjugate stress state $\boldsymbol{\sigma}_c$ on the structure corresponding to the current stress state
$\boldsymbol{I}$	Second-rank identity tensor (bold characters denote tensors)
$J2$	Second deviatoric stress invariant
$J3$	Third deviatoric stress invariant
K	Bulk modulus
K_0	Bulk modulus when the effective confining pressure is zero
k	A scalar controlling the rate of destructuration with strain
m	Ratio between radii of sections through the structure surface for axisymmetrical extension and compression in deviatoric plane
M	Critical state stress ratio for axisymmetrical compression (*i.e.* q/p)
M_θ	A dimensionless scaling function of Lode angle θ, m and M
$\overline{\boldsymbol{n}}$	A unit vector representing the normalised stress gradient on the bubble at the current stress state($\boldsymbol{\sigma}$)
$\hat{\boldsymbol{n}}$	A unit vector representing the normalised stress gradient on the structure surface at the conjugate stress state ($\boldsymbol{\sigma}_c$)

p Current mean effective stress

p_0 Initial mean effective stress

p_c Distance from the origin of the p, q coordinate system to the centre of the reference surface on the p axis

p_{c0} Initial value of p_c

$p_{\bar{\alpha}}$ A scalar variable defining the distance from the origin of the p, q coordinate system to the projection of the bubble centre on the p axis

r A scalar defining the relative size of the structure surface with respect to the reference surface (*i.e.* ratio of the major or minor radii between the structure surface and the reference surface)

$\dot{r}$ Rate of r (the superimposed dot denotes rate or increment)

r_0 Initial value of r (≥ 1)

R A scalar defining the relative size of the bubble with respect to the reference

$\boldsymbol{s}$ Deviatoric stress tensor

$\boldsymbol{s}_{\bar{\alpha}}$ A tensor defining the location of the bubble centre in deviatoric stress space

$\dot{\boldsymbol{\varepsilon}}$ Total strain rate tensor

$\dot{\boldsymbol{\varepsilon}}^e$ Elastic strain rate tensor

$\dot{\boldsymbol{\varepsilon}}^p$ Plastic strain rate tensor

$\dot{\varepsilon}_d$ An assumed destructuration strain rate

$\dot{\varepsilon}_v^p$ Plastic volumetric strain rate

$\dot{\varepsilon}_q^p$ Equivalent plastic shear strain rate

$\dot{\boldsymbol{\sigma}}$ Current stress rate tensor

$\boldsymbol{\sigma}$ Current stress tensor

$\bar{\boldsymbol{\sigma}}$ Current stress tensor normalised with respect to the bubble centre

$\hat{\boldsymbol{\sigma}}$ Current stress tensor normalised with respect to the centre of the structure surface

$\boldsymbol{\sigma}_c$ Conjugate stress tensor on the structure surface at a point where the normal of the structure surface is the same as that of the bubble at the current stress point if it engages the bubble

θ Lode's angle

$\bar{\boldsymbol{\alpha}}$ A tensor defining the location of the bubble centre in normal stress space

$\dot{\bar{\boldsymbol{\alpha}}}$ Rate of $\bar{\boldsymbol{\alpha}}$ controlled by the kinematic hardening rule

$\boldsymbol{\eta}_0$ A dimensionless tensor denoting the initial anisotropy of the structure surface

$\hat{\boldsymbol{\alpha}}$ A tensor defining the centre of the structure surface in normal stress space

$\dot{\hat{\boldsymbol{\alpha}}}$ Rate of $\hat{\boldsymbol{\alpha}}$

surface (*i.e.* ratio of the major or minor radii between the bubble and the reference surface)

κ^* The slope of the swelling line in a logarithmic specific volume-logarithmic mean stress compression plane (*i.e.* $lnv \sim lnp$ plane)

λ^* The slope of the compression line in a logarithmic specific volume-logarithmic mean stress compression plane

ψ A material parameter controlling the rate of decay of plastic modulus

μ Poisson's ratio

v_0 Initial specific volume corresponding to the initial mean effective stress

$v_{\lambda 0}$ Specific volume on the normal consolidation line corresponding to the initial mean effective stress

v Specific volume on the normal consolidation line corresponding to the current mean effective stress

Appendix 5.2 Expanded equations

The following equations are given in the order they appear in Section 5.1.

(1) Equation 5.1

$$\dot{\boldsymbol{\varepsilon}} = \dot{\boldsymbol{\varepsilon}}^{\boldsymbol{e}} + \dot{\boldsymbol{\varepsilon}}^{\boldsymbol{p}}$$

Where,

Total strain increment $$\dot{\boldsymbol{\varepsilon}} = \begin{bmatrix} \Delta\varepsilon_{11} & \Delta\varepsilon_{12} & 0 \\ \Delta\varepsilon_{21} & \Delta\varepsilon_{22} & 0 \\ 0 & 0 & \Delta\varepsilon_{33} \end{bmatrix} \text{ or } \begin{bmatrix} \Delta\varepsilon_{xx} & \Delta\varepsilon_{xy} & 0 \\ \Delta\varepsilon_{yx} & \Delta\varepsilon_{yy} & 0 \\ 0 & 0 & \Delta\varepsilon_{zz} \end{bmatrix}$$

Elastic strain increment $$\dot{\boldsymbol{\varepsilon}}^{e} = \begin{bmatrix} \Delta\varepsilon^{e}_{11} & \Delta\varepsilon^{e}_{12} & 0 \\ \Delta\varepsilon^{e}_{21} & \Delta\varepsilon^{e}_{22} & 0 \\ 0 & 0 & \Delta\varepsilon^{e}_{33} \end{bmatrix} \text{ or } \begin{bmatrix} \Delta\varepsilon^{e}_{xx} & \Delta\varepsilon^{e}_{xy} & 0 \\ \Delta\varepsilon^{e}_{yx} & \Delta\varepsilon^{e}_{yy} & 0 \\ 0 & 0 & \Delta\varepsilon^{e}_{zz} \end{bmatrix}$$

Plastic strain increment $$\dot{\boldsymbol{\varepsilon}}^{p} = \begin{bmatrix} \Delta\varepsilon^{p}_{11} & \Delta\varepsilon^{p}_{12} & 0 \\ \Delta\varepsilon^{p}_{21} & \Delta\varepsilon^{p}_{22} & 0 \\ 0 & 0 & \Delta\varepsilon^{p}_{33} \end{bmatrix} \text{ or } \begin{bmatrix} \Delta\varepsilon^{p}_{xx} & \Delta\varepsilon^{p}_{xy} & 0 \\ \Delta\varepsilon^{p}_{yx} & \Delta\varepsilon^{p}_{yy} & 0 \\ 0 & 0 & \Delta\varepsilon^{p}_{zz} \end{bmatrix}$$

Note: in all the codes provided in the thesis, the subscripts x, y and z correspond to 1, 2 and 3 respectively, which are consistent with *FLAC*. Hence, the following equations are expressed using subscripts 1, 2 and 3.

The equation may be rewritten as follows:

$$\begin{bmatrix} \Delta\varepsilon_{11} & \Delta\varepsilon_{12} & 0 \\ \Delta\varepsilon_{21} & \Delta\varepsilon_{22} & 0 \\ 0 & 0 & \Delta\varepsilon_{33} \end{bmatrix} = \begin{bmatrix} \Delta\varepsilon_{11}^{e} & \Delta\varepsilon_{12}^{e} & 0 \\ \Delta\varepsilon_{21}^{e} & \Delta\varepsilon_{22}^{e} & 0 \\ 0 & 0 & \Delta\varepsilon_{33}^{e} \end{bmatrix} + \begin{bmatrix} \Delta\varepsilon_{11}^{p} & \Delta\varepsilon_{12}^{p} & 0 \\ \Delta\varepsilon_{21}^{p} & \Delta\varepsilon_{22}^{p} & 0 \\ 0 & 0 & \Delta\varepsilon_{33}^{p} \end{bmatrix}$$

$$= \begin{bmatrix} (\Delta\varepsilon_{11}^{e} + \Delta\varepsilon_{11}^{p}) & (\Delta\varepsilon_{12}^{e} + \Delta\varepsilon_{12}^{p}) & 0 \\ (\Delta\varepsilon_{21}^{e} + \Delta\varepsilon_{21}^{p}) & (\Delta\varepsilon_{22}^{e} + \Delta\varepsilon_{22}^{p}) & 0 \\ 0 & 0 & (\Delta\varepsilon_{33}^{e} + \Delta\varepsilon_{33}^{p}) \end{bmatrix}$$

(2) Equation 5.2

$$\dot{\boldsymbol{\sigma}} = D^{e} \cdot \dot{\boldsymbol{\varepsilon}}^{e}$$

The equation can be rewritten as follows:

$$\begin{bmatrix} \Delta\sigma_{11} \\ \Delta\sigma_{22} \\ \Delta\sigma_{33} \\ \Delta\sigma_{12} \end{bmatrix} = \begin{bmatrix} e_1 & e_2 & e_2 & 0 \\ e_2 & e_1 & e_2 & 0 \\ e_2 & e_2 & e_1 & 0 \\ 0 & 0 & 0 & e_3 \end{bmatrix} \cdot \begin{bmatrix} \Delta\varepsilon_{11} \\ \Delta\varepsilon_{22} \\ \Delta\varepsilon_{33} \\ \Delta\varepsilon_{12} \end{bmatrix} \text{ or } \begin{aligned} \Delta\sigma_{11} &= e_1\Delta\varepsilon_{11} + e_2\Delta\varepsilon_{22} + e_2\Delta\varepsilon_{33} \\ \Delta\sigma_{22} &= e_2\Delta\varepsilon_{11} + e_1\Delta\varepsilon_{22} + e_2\Delta\varepsilon_{33} \\ \Delta\sigma_{33} &= e_2\Delta\varepsilon_{11} + e_2\Delta\varepsilon_{22} + e_1\Delta\varepsilon_{33} \\ \Delta\sigma_{12} &= e_3\Delta\varepsilon_{12} \end{aligned}$$

Where $e_1 = K + \frac{4}{3}G$, $e_2 = K - \frac{2}{3}G$ and $e_3 = 2G$

(3) Equation 5.4

$$p = \frac{1}{3} tr[\boldsymbol{\sigma}] \;=\; p = \frac{1}{3}(\sigma_{11} + \sigma_{22} + \sigma_{33})$$

The equation, $\boldsymbol{s} = \boldsymbol{\sigma} - p\boldsymbol{I}$, can be rewritten as follows:

$$\boldsymbol{s} = \begin{bmatrix} s_{11} & s_{12} & 0 \\ s_{21} & s_{22} & 0 \\ 0 & 0 & s_{33} \end{bmatrix} = \begin{bmatrix} \sigma_{11} - p & \sigma_{12} & 0 \\ \sigma_{12} & \sigma_{22} - p & 0 \\ 0 & 0 & \sigma_{33} - p \end{bmatrix} \text{ or } \begin{aligned} s_{11} &= \sigma_{11} - p \\ s_{22} &= \sigma_{22} - p \\ s_{33} &= \sigma_{33} - p \\ s_{12} &= s_{21} = \sigma_{12} \end{aligned}$$

(4) Equation 5.5

$$f = \frac{3}{2M_\theta^2}(\boldsymbol{s}) : (\boldsymbol{s}) + (p - p_c)^2 - (p_c)^2 = 0$$

i.e.

$$f = \frac{3}{2M_\theta^2}\begin{bmatrix} s_{11} & s_{12} & 0 \\ s_{21} & s_{22} & 0 \\ 0 & 0 & s_{33} \end{bmatrix} : \begin{bmatrix} s_{11} & s_{12} & 0 \\ s_{21} & s_{22} & 0 \\ 0 & 0 & s_{33} \end{bmatrix} + (p - p_c)^2 - (p_c)^2$$

$$= \frac{3}{2M_\theta^2}\left\{s_{11}s_{11} + s_{22}s_{22} + s_{33}s_{33} + 2s_{12}s_{12}\right\} + (p - p_c)^2 - (p_c)^2$$

$$= \frac{3}{2M_\theta^2}\left\{s_{11}^2 + s_{22}^2 + s_{33}^2 + 2s_{12}^2\right\} + (p - p_c)^2 - (p_c)^2 = 0$$

(5) Equation 5.7

$$\frac{-\pi}{6} \le \theta = \frac{1}{3}\sin^{-1}\left[\frac{-3\sqrt{3}J_3}{2J_2^{3/2}}\right] \le \frac{\pi}{6}$$

Where,

$$J_2 = \frac{1}{2}(\boldsymbol{s} : \boldsymbol{s}) = \frac{1}{2}(s_{11}^2 + s_{22}^2 + s_{33}^2 + 2s_{12}^2)$$

$$J_3 = s_{11}s_{22}s_{33} - s_{33}s_{12}^2$$

(6) Equation 5.8

$$f_b = \frac{3}{2M_\theta^2}(\boldsymbol{s} - \boldsymbol{s}_{\bar{\alpha}}) : (\boldsymbol{s} - \boldsymbol{s}_{\bar{\alpha}}) + (p - p_{\bar{\alpha}})^2 - (Rp_c)^2 = 0$$

Where,

$\boldsymbol{s}_{\bar{\boldsymbol{\alpha}}} = \begin{bmatrix} s_{11bc} & s_{12bc} & 0 \\ s_{12bc} & s_{22bc} & 0 \\ 0 & 0 & s_{33bc} \end{bmatrix}$ is the bubble centre in deviatoric space, and

$p_{\bar{\alpha}} = \frac{1}{3}(\sigma_{11bc} + \sigma_{22bc} + \sigma_{33bc})$, the subscript '*bc*' stands for bubble centre.

Hence,

$$(\boldsymbol{s}-\boldsymbol{s}_{\bar{\alpha}})=\begin{bmatrix} s_{11} & s_{12} & 0 \\ s_{21} & s_{22} & 0 \\ 0 & 0 & s_{33} \end{bmatrix}-\begin{bmatrix} s_{11bc} & s_{12bc} & 0 \\ s_{12bc} & s_{22bc} & 0 \\ 0 & 0 & s_{33bc} \end{bmatrix}$$

$$=\begin{bmatrix} \sigma_{11}-p & \sigma_{12} & 0 \\ \sigma_{12} & \sigma_{22}-p & 0 \\ 0 & 0 & \sigma_{33}-p \end{bmatrix}-\begin{bmatrix} \sigma_{11bc}-p_{\bar{\alpha}} & \sigma_{12bc} & 0 \\ \sigma_{12bc} & \sigma_{22bc}-p_{\bar{\alpha}} & 0 \\ 0 & 0 & \sigma_{33bc}-p_{\bar{\alpha}} \end{bmatrix}$$

$$=\begin{bmatrix} (\sigma_{11}-p)-(\sigma_{11bc}-p_{\bar{\alpha}}) & \sigma_{12}-\sigma_{12bc} & 0 \\ \sigma_{12}-\sigma_{12bc} & (\sigma_{22}-p)-(\sigma_{22bc}-p_{\bar{\alpha}}) & 0 \\ 0 & 0 & (\sigma_{33}-p)-(\sigma_{33bc}-p_{\bar{\alpha}}) \end{bmatrix}$$

$$=\begin{bmatrix} (\sigma_{11}-\sigma_{11bc}-p+p_{\bar{\alpha}}) & \sigma_{12}-\sigma_{12bc} & 0 \\ \sigma_{12}-\sigma_{12bc} & (\sigma_{22}-\sigma_{22bc}-p+p_{\bar{\alpha}}) & 0 \\ 0 & 0 & (\sigma_{33}-\sigma_{33bc}-p+p_{\bar{\alpha}}) \end{bmatrix}$$

$$(\boldsymbol{s}-\boldsymbol{s}_{\bar{\alpha}}):(\boldsymbol{s}-\boldsymbol{s}_{\bar{\alpha}})=(\sigma_{11}-\sigma_{11bc}-p+p_{\bar{\alpha}})^2+(\sigma_{22}-\sigma_{22bc}-p+p_{\bar{\alpha}})^2+(\sigma_{33}-\sigma_{33bc}-p+p_{\bar{\alpha}})^2 + 2(\sigma_{12}-\sigma_{12bc})^2$$

$$f_b=\frac{3}{2M_\theta^2}(\boldsymbol{s}-\boldsymbol{s}_{\bar{\alpha}}):(\boldsymbol{s}-\boldsymbol{s}_{\bar{\alpha}})+(p-p_{\bar{\alpha}})^2-(Rp_c)^2$$

$$=\frac{3}{2M_\theta^2}\left\{(\sigma_{11}-\sigma_{11bc}-p+p_{\bar{\alpha}})^2+(\sigma_{22}-\sigma_{22bc}-p+p_{\bar{\alpha}})^2+(\sigma_{33}-\sigma_{33bc}-p+p_{\bar{\alpha}})^2+2(\sigma_{12}-\sigma_{12bc})^2\right\}$$

$$+(p-p_{\bar{\alpha}})^2-(Rp_c)^2=0$$

(7) Equation 5.9

$$F = \frac{3}{2M_\theta^2}[\boldsymbol{s} - (r-1)\boldsymbol{\eta}_0 p_c] : [\boldsymbol{s} - (r-1)\boldsymbol{\eta}_0 p_c] + (p - rp_c)^2 - (rp_c)^2 = 0$$

Where, $\boldsymbol{s}$ is the deviatoric stress tensor as shown in Eq.5.4, and

$$\boldsymbol{\eta}_0 = \begin{bmatrix} 0 & \frac{\eta_0}{\sqrt{3}} & 0 \\ \frac{\eta_0}{\sqrt{3}} & 0 & 0 \\ 0 & 0 & 0 \end{bmatrix}$$ is tensor coefficient controlling anisotropy of the structure surface

in deviatoric stress space. η_0 is shown as in Figure 5.1 and is defined in *p-q* plane.

The reference (Rouania & Wood, 2000) does not give a description of the contents in the tensor coefficient $\boldsymbol{\eta}_0$. The above expression has been obtained from information in Figure 5.1 and the following assumption made by the writer: the anisotropy of the structure surface in deviatoric stress space is only caused by the shear stress components. In other words, all the normal stresses of the centre of the structure surface are taken to be the same. This assumption is only made to approximate the anisotropy and the actual centre of the structure surface is not affected.

The stress and deviatoric tensors at the centre are given by the following expressions:

$$\hat{\boldsymbol{\alpha}} = \begin{bmatrix} r & \eta_0'(r-1) & 0 \\ \eta_0'(r-1) & r & 0 \\ 0 & 0 & r \end{bmatrix} p_c \text{ and } \boldsymbol{s}_{\hat{\alpha}} = \begin{bmatrix} 0 & \eta_0' & 0 \\ \eta_0' & 0 & 0 \\ 0 & 0 & 0 \end{bmatrix} (r-1)p_c = \boldsymbol{\eta}_0 (r-1)p_c = (r-1)\boldsymbol{\eta}_0 p_c$$

From the above deviatoric stress, the deviatoric stress measure is obtained:

$$q_{\hat{\alpha}} = \sqrt{\frac{3}{2}(\boldsymbol{s}_{\hat{\alpha}} : \boldsymbol{s}_{\hat{\alpha}})} = \sqrt{3}\eta_0'(r-1)p_c$$

From *p-q* plane given in Figure 5.1, the deviatoric stress measure is obtained as follows:

$$q_{\bar{\alpha}} = \eta_0 (r - 1) p_c$$

By comparing the above two expressions of the deviatoric stress measure, we get

$$\eta_o' = \frac{\eta_0}{\sqrt{3}}$$

Hence, $\boldsymbol{\eta}_0 = \begin{bmatrix} 0 & \frac{\eta_0}{\sqrt{3}} & 0 \\ \frac{\eta_0}{\sqrt{3}} & 0 & 0 \\ 0 & 0 & 0 \end{bmatrix}$

$$[\boldsymbol{s} - (r-1)\boldsymbol{\eta}_0 p_c] = \begin{bmatrix} s_{11} & s_{12} & 0 \\ s_{21} & s_{22} & 0 \\ 0 & 0 & s_{33} \end{bmatrix} - (r-1) \begin{bmatrix} 0 & \frac{\eta_0}{\sqrt{3}} & 0 \\ \frac{\eta_0}{\sqrt{3}} & 0 & 0 \\ 0 & 0 & 0 \end{bmatrix} p_c$$

$$= \begin{bmatrix} s_{11} & [s_{12} - \frac{\eta_0}{\sqrt{3}}(r-1)p_c] & 0 \\ [s_{12} - \frac{\eta_0}{\sqrt{3}}(r-1)p_c] & s_{22} & 0 \\ 0 & 0 & s_{33} \end{bmatrix}$$

$$[\boldsymbol{s} - (r-1)\boldsymbol{\eta}_0 p_c] : [\boldsymbol{s} - (r-1)\boldsymbol{\eta}_0 p_c] = s_{11}^2 + s_{22}^2 + s_{33}^2 + 2[s_{12} - \frac{\eta_0}{\sqrt{3}}(r-1)p_c]^2$$

$$F = \frac{3}{2M_\theta^2}[\boldsymbol{s} - (r-1)\boldsymbol{\eta}_0 p_c] : [\boldsymbol{s} - (r-1)\boldsymbol{\eta}_0 p_c] + (p - rp_c)^2 - (rp_c)^2$$

$$= \frac{3}{2M_\theta^2}\left\{ s_{11}^2 + s_{22}^2 + s_{33}^2 + 2[s_{12} - \frac{\eta_0}{\sqrt{3}}(r-1)p_c]^2 \right\} + (p - rp_c)^2 - (rp_c)^2$$

(7) Equation 5.12

$$\dot{\varepsilon}_d = [(1-A)(\dot{\varepsilon}_v^p)^2 + A(\dot{\varepsilon}_q^p)^2]^{1/2}$$

Where $\dot{\varepsilon}_{\mathrm{q}}^{\mathrm{p}}$ is the equivalent plastic shear strain increment given by as follows,

$$\dot{\varepsilon}_{\mathrm{q}}^{\mathrm{p}} = [\frac{2}{3}(\dot{\boldsymbol{\varepsilon}}^{\mathrm{p}} : \dot{\boldsymbol{\varepsilon}}^{\mathrm{p}})]^{1/2} = \sqrt{\frac{2}{3}}\left\{\begin{bmatrix} \Delta\varepsilon_{11}^p & \Delta\varepsilon_{12}^p & 0 \\ \Delta\varepsilon_{21}^p & \Delta\varepsilon_{22}^p & 0 \\ 0 & 0 & \Delta\varepsilon_{33}^p \end{bmatrix} : \begin{bmatrix} \Delta\varepsilon_{11}^p & \Delta\varepsilon_{12}^p & 0 \\ \Delta\varepsilon_{21}^p & \Delta\varepsilon_{22}^p & 0 \\ 0 & 0 & \Delta\varepsilon_{33}^p \end{bmatrix}\right\}^{1/2}$$

$$= \sqrt{\frac{2}{3}\left[(\Delta\varepsilon_{11}^p)^2 + (\Delta\varepsilon_{22}^p)^2 + (\Delta\varepsilon_{33}^p)^2 + 2(\Delta\varepsilon_{12}^p)^2\right]}$$

$\dot{\varepsilon}_v^p$ is the plastic volumetric strain increment given as follows,

$$\dot{\varepsilon}_v^p = tr[\dot{\boldsymbol{\varepsilon}}^p] = \Delta\varepsilon_{11}^p + \Delta\varepsilon_{22}^p + \Delta\varepsilon_{33}^p$$

(8) Equation 5.13

$$\dot{\boldsymbol{\varepsilon}}^p = \frac{1}{H}(\overline{\boldsymbol{n}} : \dot{\boldsymbol{\sigma}})\overline{\boldsymbol{n}}$$

Where $\dot{\boldsymbol{\sigma}}$ is the stress increment same as in Eq.5.2 except it is expressed in second rank tensor,

$$i.e.\ \dot{\boldsymbol{\sigma}} = \begin{bmatrix} \Delta\sigma_{11} & \Delta\sigma_{12} & 0 \\ \Delta\sigma_{21} & \Delta\sigma_{22} & 0 \\ 0 & 0 & \Delta\sigma_{33} \end{bmatrix}, \text{ and}$$

$\overline{\boldsymbol{n}}$ denotes a unit vector representing the normalised stress gradient on the bubble at the current stress. It is given by

$$\overline{\boldsymbol{n}} = \frac{1}{\|\boldsymbol{n}\|}\boldsymbol{n} = \frac{1}{\|\boldsymbol{n}\|}\begin{bmatrix} n_{11} & n_{12} & 0 \\ n_{21} & n_{22} & 0 \\ 0 & 0 & n_{33} \end{bmatrix} = \frac{1}{\sqrt{(n_{11}^2 + n_{22}^2 + n_{33}^2 + 2n_{12}^2)}}\begin{bmatrix} n_{11} & n_{12} & 0 \\ n_{21} & n_{22} & 0 \\ 0 & 0 & n_{33} \end{bmatrix}$$

Hence,

$$\dot{\boldsymbol{\varepsilon}}^p = \frac{1}{H}(\overline{\boldsymbol{n}} : \dot{\boldsymbol{\sigma}})\overline{\boldsymbol{n}}$$

$$= \frac{1}{H(n_{11}^2 + n_{22}^2 + n_{33}^2 + 2n_{12}^2)}\begin{bmatrix} n_{11} & n_{12} & 0 \\ n_{21} & n_{22} & 0 \\ 0 & 0 & n_{33} \end{bmatrix} : \begin{bmatrix} \Delta\sigma_{11} & \Delta\sigma_{12} & 0 \\ \Delta\sigma_{21} & \Delta\sigma_{22} & 0 \\ 0 & 0 & \Delta\sigma_{33} \end{bmatrix} . \begin{bmatrix} n_{11} & n_{12} & 0 \\ n_{21} & n_{22} & 0 \\ 0 & 0 & n_{33} \end{bmatrix}$$

$$= \frac{1}{H(n_{11}^2 + n_{22}^2 + n_{33}^2 + 2n_{12}^2)}\{n_{11}\Delta\sigma_{11} + n_{22}\Delta\sigma_{22} + n_{33}\Delta\sigma_{33} + 2n_{12}\Delta\sigma_{12}\} . \begin{bmatrix} n_{11} & n_{12} & 0 \\ n_{21} & n_{22} & 0 \\ 0 & 0 & n_{33} \end{bmatrix}$$

n_{11}, n_{22}, n_{33} and n_{12} are derived and given in Appendix C.

(9) Equations 5.15 and 5.16

$$H_c = \frac{rp_c\left\langle T\left[(p - p_{\bar{\alpha}}) + \frac{3}{2M_\theta^2}(\boldsymbol{s} - \boldsymbol{s}_{\bar{\alpha}}) : \boldsymbol{\eta}_0 + Rp_c\right] - \frac{3}{2M_\theta^2}(p - p_{\bar{\alpha}})(\boldsymbol{s} - \boldsymbol{s}_{\bar{\alpha}}) : \frac{\boldsymbol{\eta}_0}{r}\right\rangle}{(\lambda^* - \kappa^*)[(p - p_{\bar{\alpha}})^2 + \frac{3}{2M_\theta^4}(\boldsymbol{s} - \boldsymbol{s}_{\bar{\alpha}}) : (\boldsymbol{s} - \boldsymbol{s}_{\bar{\alpha}})]}$$

Where the quantity T is given by

$$T = (p - p_{\bar{\alpha}}) - k(\frac{r-1}{r})\left[(1-A)(p - p_{\bar{\alpha}})^2 + \frac{3A}{2M_\theta^2}(\boldsymbol{s} - \boldsymbol{s}_{\bar{\alpha}}) : (\boldsymbol{s} - \boldsymbol{s}_{\bar{\alpha}})\right]^{1/2}$$

$p_{\bar{\alpha}}$ is a scalar quantity given in Eq.8. Deviatoric stress tensor $\boldsymbol{s}$ is given in Eq.4.

$(\boldsymbol{s}-\boldsymbol{s}_{\bar{\alpha}}):(\boldsymbol{s}-\boldsymbol{s}_{\bar{\alpha}})$ is also the same as in Eq.5.8. All other terms in Eq.5.15 are scalar quantities except the following tensor inner product:

$$(\boldsymbol{s}-\boldsymbol{s}_{\bar{\alpha}}):\boldsymbol{\eta}_0$$

$$=\begin{bmatrix}(\sigma_{11}-p)-(\sigma_{11bc}-p_{\bar{\alpha}}) & \sigma_{12}-\sigma_{12bc} & 0\\ \sigma_{12}-\sigma_{12bc} & (\sigma_{22}-p)-(\sigma_{22bc}-p_{\bar{\alpha}}) & 0\\ 0 & 0 & (\sigma_{33}-p)-(\sigma_{33bc}-p_{\bar{\alpha}})\end{bmatrix}:\begin{bmatrix}0 & \frac{\eta_0}{\sqrt{3}} & 0\\ \frac{\eta_0}{\sqrt{3}} & 0 & 0\\ 0 & 0 & 0\end{bmatrix}$$

$$=2(\sigma_{12}-\sigma_{12bc})\frac{\eta_0}{\sqrt{3}}$$

(10) Equation 5.17

$$b=\overline{\boldsymbol{n}}:(\boldsymbol{\sigma}_c-\boldsymbol{\sigma})$$

$$=\frac{1}{\sqrt{(n_{11}^2+n_{22}^2+n_{33}^2+2n_{12}^2)}}\begin{bmatrix}n_{11} & n_{12} & 0\\ n_{21} & n_{22} & 0\\ 0 & 0 & n_{33}\end{bmatrix}:\left\{\begin{bmatrix}\sigma_{11cj} & \sigma_{12cj} & 0\\ \sigma_{21cj} & \sigma_{22cj} & 0\\ 0 & 0 & \sigma_{33cj}\end{bmatrix}-\begin{bmatrix}\sigma_{11} & \sigma_{12} & 0\\ \sigma_{21} & \sigma_{22} & 0\\ 0 & 0 & \sigma_{33}\end{bmatrix}\right\}$$

$$=\frac{1}{\sqrt{(n_{11}^2+n_{22}^2+n_{33}^2+2n_{12}^2)}}\left\{n_{11}(\sigma_{11cj}-\sigma_{11})+n_{22}(\sigma_{22cj}-\sigma_{22})+n_{33}(\sigma_{33cj}-\sigma_{33})+2n_{12}(\sigma_{12cj}-\sigma_{12})\right\}$$

The subscript '*cj*' stands for conjugate.

(10) Equation 5.18

$$b_{\max} = 2(\frac{r}{R} - 1)\overline{\boldsymbol{n}} : \overline{\boldsymbol{\sigma}}$$

Where $\overline{\boldsymbol{\sigma}} = \boldsymbol{\sigma} - \overline{\boldsymbol{\alpha}}$ is the normalised stress with respect to the centre of bubble. $\overline{\boldsymbol{\alpha}}$ is the stress tensor of the bubble center and is given by,

$$\overline{\boldsymbol{\alpha}} = \begin{bmatrix} \sigma_{11bc} & \sigma_{12bc} & 0 \\ \sigma_{21bc} & \sigma_{22bc} & 0 \\ 0 & 0 & \sigma_{33bc} \end{bmatrix}$$

Hence,

$$\overline{\boldsymbol{\sigma}} = \boldsymbol{\sigma} - \overline{\boldsymbol{\alpha}} = \begin{bmatrix} \sigma_{11} & \sigma_{12} & 0 \\ \sigma_{21} & \sigma_{22} & 0 \\ 0 & 0 & \sigma_{22} \end{bmatrix} - \begin{bmatrix} \sigma_{11bc} & \sigma_{12bc} & 0 \\ \sigma_{21bc} & \sigma_{22bc} & 0 \\ 0 & 0 & \sigma_{33bc} \end{bmatrix} = \begin{bmatrix} \sigma_{11} - \sigma_{11bc} & \sigma_{12} - \sigma_{12bc} & 0 \\ \sigma_{21} - \sigma_{21bc} & \sigma_{22} - \sigma_{22bc} & 0 \\ 0 & 0 & \sigma_{33} - \sigma_{33bc} \end{bmatrix}$$

$$b_{\max} = 2(\frac{r}{R} - 1)\overline{\boldsymbol{n}} : \overline{\boldsymbol{\sigma}}$$

$$= \frac{2(\frac{r}{R} - 1)}{\sqrt{(n_{11}^2 + n_{22}^2 + n_{33}^2 + 2n_{12}^2)}} \begin{bmatrix} n_{11} & n_{12} & 0 \\ n_{21} & n_{22} & 0 \\ 0 & 0 & n_{33} \end{bmatrix} : \begin{bmatrix} \sigma_{11} - \sigma_{11bc} & \sigma_{12} - \sigma_{12bc} & 0 \\ \sigma_{21} - \sigma_{21bc} & \sigma_{22} - \sigma_{22bc} & 0 \\ 0 & 0 & \sigma_{33} - \sigma_{33bc} \end{bmatrix}$$

$$= \frac{2(\frac{r}{R} - 1)}{\sqrt{(n_{11}^2 + n_{22}^2 + n_{33}^2 + 2n_{12}^2)}} \{n_{11}(\sigma_{11} - \sigma_{11bc}) + n_{22}(\sigma_{22} - \sigma_{22bc}) + n_{33}(\sigma_{33} - \sigma_{33bc}) + 2n_{12}(\sigma_{12} - \sigma_{12bc})\}$$

(10) Equation 5.20

$$\dot{\overline{\boldsymbol{\alpha}}} = \dot{\hat{\boldsymbol{\alpha}}} + (\overline{\boldsymbol{\alpha}} - \hat{\boldsymbol{\alpha}})(\frac{\dot{r}}{r} + \frac{\dot{p}_c}{p_c}) + \frac{\overline{\boldsymbol{n}} : \left\{\dot{\hat{\boldsymbol{\sigma}}} - \hat{\boldsymbol{\sigma}}[(\dot{r}/r) + (\dot{p}_c / p_c)] + \overline{\boldsymbol{\sigma}}(\dot{r}/r)\right\}}{\overline{\boldsymbol{n}} : (\boldsymbol{\sigma}_c - \boldsymbol{\sigma})}(\boldsymbol{\sigma}_c - \boldsymbol{\sigma})$$

Where r and p_c are two scalar quantities (all the dots denote increment *i.e.* rate). $\hat{\boldsymbol{\alpha}}$ is the stress tensor at the centre of the structure surface. Its general expression is given as follows (Note: an assumption is made in Eq. 5.9 for approximation to account for anisotropy of the structure surface):

$\hat{\boldsymbol{\alpha}} = \begin{bmatrix} \sigma_{11sc} & \sigma_{12sc} & 0 \\ \sigma_{21sc} & \sigma_{22sc} & 0 \\ 0 & 0 & \sigma_{33sc} \end{bmatrix}$, and the increment of the structure surface center is

$$\dot{\hat{\boldsymbol{\alpha}}} = \begin{bmatrix} \Delta\sigma_{11sc} & \Delta\sigma_{12sc} & 0 \\ \Delta\sigma_{21sc} & \Delta\sigma_{22sc} & 0 \\ 0 & 0 & \Delta\sigma_{33sc} \end{bmatrix}$$

The subscript '*sc*' stands for structure surface center.

$\hat{\boldsymbol{\sigma}} = \boldsymbol{\sigma} - \hat{\boldsymbol{\alpha}}$ is the normalised stress with respect to the centre of the structure surface, which is given by,

$$\hat{\boldsymbol{\sigma}} = \boldsymbol{\sigma} - \hat{\boldsymbol{\alpha}} = \begin{bmatrix} \sigma_{11} & \sigma_{12} & 0 \\ \sigma_{21} & \sigma_{22} & 0 \\ 0 & 0 & \sigma_{33} \end{bmatrix} - \begin{bmatrix} \sigma_{11sc} & \sigma_{12sc} & 0 \\ \sigma_{21sc} & \sigma_{22sc} & 0 \\ 0 & 0 & \sigma_{33sc} \end{bmatrix} = \begin{bmatrix} \sigma_{11} - \sigma_{11sc} & \sigma_{12} - \sigma_{12sc} & 0 \\ \sigma_{21} - \sigma_{21sc} & \sigma_{22} - \sigma_{22sc} & 0 \\ 0 & 0 & \sigma_{33} - \sigma_{33sc} \end{bmatrix}$$

Hence,

$$\dot{\hat{\boldsymbol{\sigma}}} = \begin{bmatrix} \Delta\sigma_{11} - \Delta\sigma_{11sc} & \Delta\sigma_{12} - \Delta\sigma_{12sc} & 0 \\ \Delta\sigma_{21} - \Delta\sigma_{21sc} & \Delta\sigma_{22} - \Delta\sigma_{22sc} & 0 \\ 0 & 0 & \Delta\sigma_{33} - \Delta\sigma_{33sc} \end{bmatrix}$$

$\bar{\boldsymbol{n}} : (\boldsymbol{\sigma}_{\mathrm{c}} - \boldsymbol{\sigma})$ is given by Eq.5.17.

For clarity three scalar quantities, they are given by,

$$c_1 = (\frac{\dot{r}}{r} + \frac{\dot{p}_c}{p_c}) \text{ and } c_2 = \frac{\dot{p}_c}{p_c}$$

$$c_3 = \frac{\bar{\boldsymbol{n}} : \left\{\dot{\hat{\boldsymbol{\sigma}}} - \hat{\boldsymbol{\sigma}}[(\dot{r}/r) + (\dot{p}_c / p_c)] + \bar{\boldsymbol{\sigma}}(\dot{r}/r)\right\}}{\bar{\boldsymbol{n}} : (\boldsymbol{\sigma}_{\mathrm{c}} - \boldsymbol{\sigma})} = \frac{\bar{\boldsymbol{n}} : \left\{\dot{\hat{\boldsymbol{\sigma}}} - c_1\hat{\boldsymbol{\sigma}} + c_2\bar{\boldsymbol{\sigma}}\right\}}{\bar{\boldsymbol{n}} : (\boldsymbol{\sigma}_{\mathrm{c}} - \boldsymbol{\sigma})}$$

Each tensor term in the above function has been given previously, therefore, for clarity c_3 is not expanded. As the result of c_3 is a scalar quantity, Eq.5.20 becomes as follows,

$$\dot{\bar{\boldsymbol{\alpha}}} = \dot{\hat{\boldsymbol{\alpha}}} + (\bar{\boldsymbol{\alpha}} - \hat{\boldsymbol{\alpha}})c_1 + c_3(\boldsymbol{\sigma}_c - \boldsymbol{\sigma})$$

$$\dot{\bar{\boldsymbol{\alpha}}} = \begin{bmatrix} \Delta\sigma_{11bc} & \Delta\sigma_{12bc} & 0 \\ \Delta\sigma_{21bc} & \Delta\sigma_{22bc} & 0 \\ 0 & 0 & \Delta\sigma_{33bc} \end{bmatrix}$$

$$= \begin{bmatrix} \Delta\sigma_{11sc} & \Delta\sigma_{12sc} & 0 \\ \Delta\sigma_{21sc} & \Delta\sigma_{22sc} & 0 \\ 0 & 0 & \Delta\sigma_{33sc} \end{bmatrix} + \left\{ \begin{bmatrix} \sigma_{11bc} & \sigma_{12bc} & 0 \\ \sigma_{21bc} & \sigma_{22bc} & 0 \\ 0 & 0 & \sigma_{33bc} \end{bmatrix} - \begin{bmatrix} \sigma_{11sc} & \sigma_{12sc} & 0 \\ \sigma_{21sc} & \sigma_{22sc} & 0 \\ 0 & 0 & \sigma_{33sc} \end{bmatrix} \right\} c_1$$

$$+ c_3 \left\{ \begin{bmatrix} \sigma_{11cj} & \sigma_{12cj} & 0 \\ \sigma_{21cj} & \sigma_{22cj} & 0 \\ 0 & 0 & \sigma_{33cj} \end{bmatrix} - \begin{bmatrix} \sigma_{11} & \sigma_{12} & 0 \\ \sigma_{21} & \sigma_{22} & 0 \\ 0 & 0 & \sigma_{33} \end{bmatrix} \right\}$$

Each element of the above stress tensor $\dot{\boldsymbol{\alpha}}$ can be obtained as follows:

$$\Delta\sigma_{11bc} = \Delta\sigma_{11sc} + (\sigma_{11bc} - \sigma_{11sc})c_1 + c_3(\sigma_{11cj} - \sigma_{11})$$

$$\Delta\sigma_{22bc} = \Delta\sigma_{22sc} + (\sigma_{22bc} - \sigma_{22sc})c_1 + c_3(\sigma_{22cj} - \sigma_{22})$$

$$\Delta\sigma_{33bc} = \Delta\sigma_{33sc} + (\sigma_{33bc} - \sigma_{33sc})c_1 + c_3(\sigma_{33cj} - \sigma_{33})$$

$$\Delta\sigma_{12bc} = \Delta\sigma_{12sc} + (\sigma_{12bc} - \sigma_{12sc})c_1 + c_3(\sigma_{12cj} - \sigma_{12})$$

$$\Delta\sigma_{12bc} = \Delta\sigma_{21bc}$$

Appendix 5.3 Derivation of stress gradient

$$n_{ij} = \frac{\partial f_b}{\partial \sigma_{ij}} \ (i, j = 1\text{-}3)$$

Stress tensor, $\boldsymbol{\sigma} = \begin{bmatrix} \sigma_{11} & \sigma_{12} & 0 \\ \sigma_{12} & \sigma_{22} & 0 \\ 0 & 0 & \sigma_{33} \end{bmatrix}$

Mean principal stress, $p = \frac{1}{3}\mathrm{tr}[\boldsymbol{\sigma}]$

Deviator stress tensor, $\boldsymbol{s} = \boldsymbol{\sigma} - p\boldsymbol{I}$, $\boldsymbol{I} = \begin{bmatrix} 1 & 0 & 0 \\ 0 & 1 & 0 \\ 0 & 0 & 1 \end{bmatrix}$

$$i.e.\ \boldsymbol{s} = \begin{bmatrix} (\sigma_{11} - p) & \sigma_{12} & 0 \\ \sigma_{12} & (\sigma_{22} - p) & 0 \\ 0 & 0 & (\sigma_{33} - p) \end{bmatrix} = \begin{bmatrix} s_{11} & s_{12} & 0 \\ s_{12} & s_{22} & 0 \\ 0 & 0 & s_{33} \end{bmatrix}$$

Centre of the bubble in deviator stress space,

$$\boldsymbol{s}_{\bar{\boldsymbol{\alpha}}} = \begin{bmatrix} s_{11bc} & s_{12bc} & 0 \\ s_{12bc} & s_{22bc} & 0 \\ 0 & 0 & s_{33bc} \end{bmatrix}$$

Deviator stress normalised with respect to the centre of bubble,

$$\bar{\boldsymbol{s}} = \boldsymbol{s} - \boldsymbol{s}_{\bar{\boldsymbol{\alpha}}} = \begin{bmatrix} s_{11} - s_{11bc} & s_{12} - s_{12bc} & 0 \\ s_{12} - s_{12bc} & s_{22} - s_{22bc} & 0 \\ 0 & 0 & s_{33} - s_{33bc} \end{bmatrix}$$

$$or\ \bar{s}_{ii} = \boldsymbol{\sigma}_{ii} - \frac{1}{3}\sum_{j=1}^{3}\boldsymbol{\sigma}_{jj} - s_{iibc} \qquad i = 1-3 \text{ and } \bar{s}_{12} = s_{12} - s_{12bc} = \boldsymbol{\sigma}_{12} - s_{12bc}$$

The yield function of the bubble is given by

$$f_b = \frac{3}{2M_\theta^2}(\boldsymbol{s}-\boldsymbol{s}_{\bar{\alpha}}):(\boldsymbol{s}-\boldsymbol{s}_{\bar{\alpha}}) + (p-p_{\bar{\alpha}})^2 - (Rp_c)^2 = 0$$

or $f_b = \frac{3}{M_\theta^{\,2}}\bar{J}_2 + (p-p_{\bar{\alpha}})^2 - (Rp_c)^2 = 0$

Where $\bar{J}_2 = \frac{1}{2}(\boldsymbol{s}-\boldsymbol{s}_{\bar{\alpha}}):(\boldsymbol{s}-\boldsymbol{s}_{\bar{\alpha}}) = \frac{1}{2}\bar{\boldsymbol{s}}:\bar{\boldsymbol{s}} = \frac{1}{2}(\bar{s}_{11}^2 + \bar{s}_{22}^2 + \bar{s}_{33}^2 + 2\bar{s}_{12}^2)$

Components of the stress gradient are given by

$$n_{ij} = \frac{\partial f_b}{\partial \sigma_{ij}} = \frac{-6}{M_\theta^{\,3}}\bar{J}_2\frac{\partial M_\theta}{\partial \sigma_{ij}} + \frac{3}{M_\theta^2}\frac{\partial \bar{J}_2}{\partial \sigma_{ij}} + 2(p-p_{\bar{\alpha}})\frac{\partial p}{\partial \sigma_{ij}}$$

Where:

$$\frac{\partial p}{\partial \sigma_{ij}} = \frac{1}{3}(i=j)\ or = 0(i \neq j)$$

$$M_\theta = \frac{2mM}{(1+m)-(1-m)\sin(3\theta)} = \frac{4mM}{2(1+m)+3\sqrt{3}(1-m)\frac{J_3}{J_2^{3/2}}}$$

$$\frac{\partial M_\theta}{\partial \sigma_{ij}} = \frac{-12\sqrt{3}m(1-m)M}{\left[2(1+m)+3\sqrt{3}(1-m)\frac{J_3}{J_2^{3/2}}\right]^2}\cdot\frac{\partial\left[\frac{J_3}{J_2^{3/2}}\right]}{\partial \sigma_{ij}}$$

$$J_2 = \frac{1}{2}(\boldsymbol{s}:\boldsymbol{s}) = \frac{1}{2}(s_{11}^2 + s_{22}^2 + s_{33}^2 + 2s_{12}^2)$$

$$\frac{\partial J_2}{\partial \sigma_{ii}} = \frac{1}{3}(3s_{ii} - \sum_{j=1}^{3} s_{jj}) = s_{ii} \quad i = 1-3$$

$$\frac{\partial J_2}{\partial \sigma_{12}} = 2s_{12}$$

$$\frac{\partial \bar{J}_2}{\partial \sigma_{ii}} = \frac{1}{3}(3\bar{s}_{ii} - \sum_{j=1}^{3} \bar{s}_{jj}) = \bar{s}_{ii} \quad i = 1-3 \qquad \frac{\partial \bar{J}_2}{\partial \sigma_{12}} = 2\bar{s}_{12}$$

$$J_3 = s_{11}s_{22}s_{33} - s_{33}s_{12}^2$$

$$\frac{\partial\left[\frac{J_3}{J_2^{3/2}}\right]}{\partial \sigma_{ij}} = \frac{J_2^{3/2}\frac{\partial J_3}{\partial \sigma_{ij}} - \frac{3}{2}J_2^{1/2}J_3\frac{\partial J_2}{\partial \sigma_{ij}}}{J_2^3}$$

$$\frac{\partial J_3}{\partial \sigma_{11}} = \frac{1}{3}[3s_{22}s_{33} - (s_{11}s_{22} + s_{11}s_{33} + s_{22}s_{33}) + s_{12}^2]$$

$$\frac{\partial J_3}{\partial \sigma_{22}} = \frac{1}{3}[3s_{11}s_{33} - (s_{11}s_{22} + s_{11}s_{33} + s_{22}s_{33}) + s_{12}^2]$$

$$\frac{\partial J_3}{\partial \sigma_{33}} = \frac{1}{3}[3s_{22}s_{11} - (s_{11}s_{22} + s_{11}s_{33} + s_{22}s_{33}) - 2s_{12}^2]$$

$$\frac{\partial J_3}{\partial \sigma_{12}} = -2s_{33}s_{12}$$

Appendix 5.4 *FISH* code of the Bubble model

```
; Implemented for axisymmetric or 2D plane strain problems

set echo off
def bubble
  constitutive_model
;
;- Model variables
f_prop b_kmax b_poss
; b_poss is Poisson's ratio, μ, assumed to be constant
; b_kmax is the maximum bulk modulus, K, chosen to ensure numerical
; stability.

f_prop b_lambda b_kappa b_M b_mm b_bod0
; λ*,κ*,M,m, K0
; K0 is initial bulk modulus corresponding to zero confining pressure

f_prop r_bub AA BB k psigh nambda0 r_str0 pc0
; R, A, B, k, ψ, η0, r0, pc0

f_prop r_str pc s_mod b_mod b_g0 e1 e2 e3
f_prop s_zs11c s_zs22c s_zs33c s_zs12c
; center of structure surface in general stress space, α̂
f_prop b_zs11c b_zs22c b_zs33c b_zs12c
; center of bubble in general stress space, ᾱ
f_prop s_ds11c s_ds22c s_ds33c s_ds12c
; center of structure surface in deviator stress space, s_α̂
f_prop b_ds11c b_ds22c b_ds33c b_ds12c
; center of bubble in terms of deviator stress, s_ᾱ

f_prop b_p b_q s_p s_q
; center of bubble and structure surface in p,q space, p_ᾱ, q_ᾱ
; and p_α̂, q_α̂

float $dzs11 $dzs22 $dzs33 $dzs12
; stress rate, σ̇
float $zs11 $zs22 $zs33 $zs12
; Stress from elastic trial, σ^trial
float $s_dzs11c $s_dzs22c $s_dzs33c $s_dzs12c
; translation rate of structure surface center, α̂̇
float $b_dzs11c $b_dzs22c $b_dzs33c $b_dzs12c
; translation rate of bubble center, ᾱ̇
float $ds11 $ds22 $ds33 $ds12
; deviator stress, s
float $J2 $J3 $J_2
; the 2nd and 3rd deviatoric invariants
; $J_2 is the 2nd deviatoric invariant w.r.t bubble centre
float $p $q
; current stress in p, q space
float $fb $M $Hc $H
```

```
; f_b, M_θ, H_c, H
float $s $s_dp $ds
float $b $bmax $dgamma $dpc $dr_str
;$dpc is rate of p_c, ṗ_c
;$dr_str is rate of structure surface size, ṙ
float $b_zs11 $b_zs22 $b_zs33 $b_zs12
;stress w.r.t bubble centre, σ̄
float $s_zs11 $s_zs22 $s_zs33 $s_zs12
;stress w.r.t center of structure surface, σ̂
float $zs11cj $zs22cj $zs33cj $zs12cj
;conjugate stresses on the structure surface, σ_c
float $s_zs11cj $s_zs22cj $s_zs33cj $s_zs12cj
;conjugate stress w.r.t center of structure surface, σ̂_c
float $b_ds11 $b_ds22 $b_ds33 $b_ds12
; deviator stress w.r.t center of bubble, s̄
float $s_ds11 $s_ds22 $s_ds33 $s_ds12
; deviator stress w.r.t centre of structure surface, ŝ
float $s_dzs11 $s_dzs22 $s_dzs33 $s_dzs12
; stress rate w.r.t center of structure surface, σ̂̇
float $pzde11 $pzde22 $pzde33 $pzde12
; plastic strain rate, ε̇^p
float $pv_zde $pq_zde
; $pv_zde is plastic volumetric strain ε̇_v^p
; $pq_zde is equivalent plastic shear strain rate ε̇_q^p
float $dq_trial $dq $ds1 $ds2 $ds3 $q_zde
; $q_zde is equivalent total shear strain rate ε̇_q
f_prop pv volumetric_strain vertical_strain q_strain qt_strain
; pv is the accumulated plasic volumeric strain Σ ε̇_v^p
; q_strain is the accumulated equivalent plastic shear strain Σ ε̇_q^p
; qt_strain is accumulated equivalent total shear strain Σ ε̇_q
float $n11 $n22 $n33 $n12 $n
; $n11 $n22 $n33 $n12 are components of stress gradient on the bubble
; $n is the inner product of the stress gradient tensor, $n=($n11)^2+
; ($n22)^2+($n33)^2+2($n12)^2.
float $sp $T $theta
; $sp is inner product of deviator stress w.r.t bubble centre,
; $sp=s̄ : s̄ = (s - s_ᾱ) : (s - s_ᾱ)
; $theta is Lode angle, θ.
float $c1 $c2 $c3 $c4 $c5 $c6 $c7 $c8 $c9 $c10 $c11 $c12 $c13
float $M11 $M22 $M33 $M12 $J11 $J22 $J33 $J12
float $sum_fb $sum_pzde11 $sum_pzde22 $sum_pzde33 $sum_pzde12
float $sum_zde11 $sum_zde22 $sum_zde33 $sum_zde12
float $zde11 $zde22 $zde33 $zde12
float $sum_P $sum_pvStrain $sum_pqStrain
f_prop stepCommand bulk_max shear_max
f_prop app_g ; apparent shear modulus
;the following are for undrained
```

```
float $dpwp $dv $sum_pwp $app_g
f_prop pwp

case_of  mode
;- Initialization ---
case 1
if stepCommand=0 then
 ; this "if" statement is necessary due to the multiple
 ; "step" commands
 pc=-pc0
 ; centre of reference surface is always on p axis
 ; pco given by user is positive if it is compressive
 ; pc must be compressive in the bubble model
 ; according to FLAC's sign convention, compressive pressure
 ; is negative
 r_str=r_str0
 nambda0=nambda0/1.732
 ;η0 is defined in p, q space (see Figure 2 on page 156),
 ;i.e. at the centre of the structure surface, q=(r0-1)pcη0
 ; but from page 155, the centre of the structure surface in deviator
```

; stress space, $\boldsymbol{s}_c = (r_0 - 1)\boldsymbol{\eta}_0 p_c$, $\boldsymbol{\eta}_0 = \begin{bmatrix} 0 & \eta_0 & 0 \\ \eta_0 & 0 & 0 \\ 0 & 0 & 0 \end{bmatrix}$

```
 ; hence if nambda0 (η0) is specified from the definition in Figure 2,
 ; it should be divided by a factor of 1.732 for being consistent with
```

; elements of tensor $\boldsymbol{\eta}_0$, i.e $\boldsymbol{\eta}_0 = \begin{bmatrix} 0 & \frac{\eta_0}{\sqrt{3}} & 0 \\ \frac{\eta_0}{\sqrt{3}} & 0 & 0 \\ 0 & 0 & 0 \end{bmatrix}$ (see explanation in Appendix B)

```
 ; initial stress in p, q space
 $p=(zs11+zs22+zs33)/3.0
 if $p=0 then;for analysis starting from zero insitu stress
    $p=-0.001
 end_if
 $q=zs22-zs11;only for triaxial stress condition

 ;====initial center of structure surface and bubble====

 ;<structure surface>
```

; center of structure surface, $\hat{\boldsymbol{\alpha}} = \{rp_c, (r-1)\boldsymbol{\eta}_0 p_c\}^T$

```
 $s=nambda0*(r_str-1)*pc
```

s_p=r_str*pc ; $\boldsymbol{p}_c$

```
 ; center of structure surface in deviator stress space
```

; $\boldsymbol{s}_{\hat{\alpha}} = \begin{bmatrix} 0 & \$s & 0 \\ \$s & 0 & 0 \\ 0 & 0 & 0 \end{bmatrix}$

```
s_ds11c=0.0
s_ds22c=0.0
s_ds33c=0.0
s_ds12c=$s
```

; centre of structure surface, $\boldsymbol{\sigma}_{\hat{\alpha}} = \begin{bmatrix} s\_p & \$s & 0 \\ \$s & s\_p & 0 \\ 0 & 0 & s\_p \end{bmatrix}$

```
s_zs11c=s_p
s_zs22c=s_p
s_zs33c=s_p
s_zs12c=$s
s_q=s_zs12c*1.732

;<bubble>
; center of bubble, α̅
; initial bubble centre is assumed to be at the initial stress point
; check if bubble model is reduced to MCC model
if r_bub>0.95 then
; Bubble model is reduced to Cam-clay model and reset bubble's
; centre, i.e. coincide with the centre of reference surface
; Bubble model becomes MCC model when R=1.0 for non-structured soil.
; In data file, less than 1.0 (e.g. 0.998)should be used rather than
; 1.0 for R, otherwise b_max = 0 → eq.26 unexecutable
  b_zs11c=pc
  b_zs22c=pc
  b_zs33c=pc
  b_zs12c=0
end_if
; center of bubble in p axis, p_ᾱ
b_p=(b_zs11c+b_zs22c+b_zs33c)/3.0
; check if bubble interescts structure surface
; the following two "if" statements are only valid for isotropic
; initial stress condition,i.e both structure surface and bubble are
; initially centered on p axis. In the case of anisotrpic condition,
; checking must be conducted manually to enure a non-intersection
; initial condition.

if abs(b_p)<abs(r_bub*pc) then
  ;initial bubble centre is at the far left side
  ; reset it to the 'minimum' point i.e (Rp_c,0) in p,q space
  b_zs11c=r_bub*pc
  b_zs22c=b_zs11c
  b_zs33c=b_zs11c
  $p=(zs11+zs22+zs33)/3.0
end_if
if abs(b_p)>abs(2*r_str0*pc-r_bub*pc) then
  ;initial bubble centre is at the far right side
  ; reset it to the 'maximum' point i.e (2r_0p_c-Rp_c,0) in p,q space
```

```
    b_zs11c=2*r_str0*pc-r_bub*pc
    b_zs22c=b_zs11c
    b_zs33c=b_zs11c
    $p=(zs11+zs22+zs33)/3.0
  end_if
```

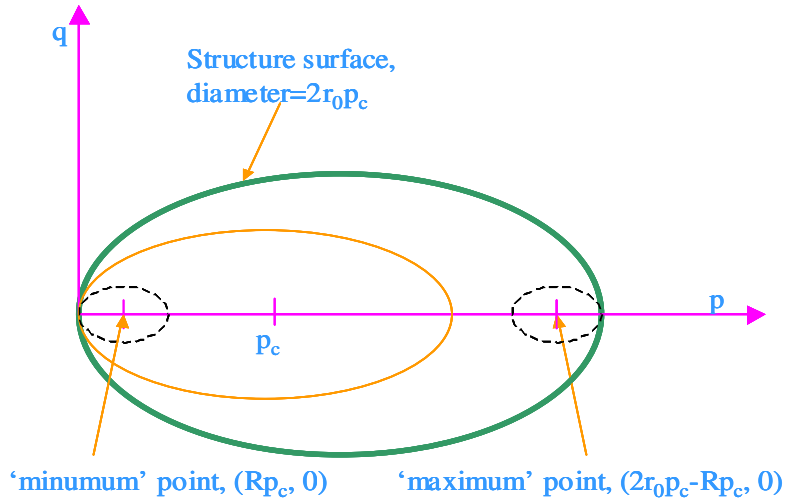


```
  ;
```

```
  ; center of bubble in deviator stress space, s_α
  b_ds11c=b_zs11c-b_p
  b_ds22c=b_zs22c-b_p
  b_ds33c=b_zs33c-b_p
  b_ds12c=b_zs12c
  b_q=b_zs22c-b_zs11c;only for triaxial stress condition

  ; initial shear modulus, maximum value chosen for controlling
  ; numerical stability
  b_g0=3.0*b_kmax*(1.0-2.0*b_poss)/(2.0*(1.0+b_poss))
  ;initial buck modulus calculated from the initial stress
  b_mod=abs($p)/b_kappa+b_mod0
  ;initial shear modulus
  s_mod=3.0*b_mod*(1.0-2.0*b_poss)/(2.0*(1.0+b_poss))
  stepCommand=1.0
end_if ; "if stepCommand =0 then"

;--- Running section ---
case 2
zvisc = 1.0  ;set to 1.0 for stiffness proportional damping
;<elastic coefficients>
e1      = b_mod + 4.0  * s_mod/3.0
e2      = b_mod - 2.0 * s_mod/3.0
e3      = 2.0 * s_mod

;========= apply strain rate =======
;<stress rate (σ̇)from elatic trial>
$dzs11=e1*zde11+e2*zde22+e2*zde33
```

```
$dzs22=e2*zde11+e1*zde22+e2*zde33
$dzs33=e2*zde11+e2*zde22+e1*zde33
$dzs12=e3*zde12
; calculating apparent shear modulus s_m
if apparent=1 then
  $ds1       = $dzs11 - $dzs22
  $ds2       = $dzs22 - $dzs33
  $ds3       = $dzs33 - $dzs11
  $dq_trial  = $ds1*$ds1 + $ds2*$ds2 + $ds3*$ds3
  $dq_trial  = 0.7071*sqrt($dq_trial + 6.0*$dzs12*$dzs12)
end_if
```

;<trial stresses, $\boldsymbol{\sigma}^{trial}$>

```
$zs11=zs11+$dzs11+pwp
$zs22=zs22+$dzs22+pwp
$zs33=zs33+$dzs33+pwp
$zs12=zs12+$dzs12
$p=($zs11+$zs22+$zs33)/3.0;mean effective stress
```

; deviator stress, $\boldsymbol{s}$

```
$ds11=$zs11-$p
$ds22=$zs22-$p
$ds33=$zs33-$p
$ds12=$zs12
```

; deviator stress w.r.t bubble center, $\bar{\boldsymbol{s}} = \boldsymbol{s} - \boldsymbol{s}_{\bar{\boldsymbol{\alpha}}}$

```
$b_ds11=$ds11-b_ds11c
$b_ds22=$ds22-b_ds22c
$b_ds33=$ds33-b_ds33c
$b_ds12=$ds12-b_ds12c
; invariants J2, J3
```

; $J_2 = \frac{1}{2}\boldsymbol{s} : \boldsymbol{s}, \quad J_3 = \det|\boldsymbol{s}|$

```
$J2=($ds11*$ds11+$ds22*$ds22+$ds33*$ds33+2*$ds12*$ds12)/2.0

$J3=$ds11*$ds22*$ds33-$ds33*$ds12*$ds12
$J_2=($b_ds11^2+$b_ds22^2+$b_ds33^2+2*$b_ds12^2)/2.0
; Lode's angle
if $J2=0.0 then
    $M=2*b_mm/(1+b_mm)*b_M
  else
```

$\$c1=-2.59807*\$J3/(\$J2)^{1.5}$; $\sin(3\theta) = \frac{-3\sqrt{3}J_3}{2J_2^{3/2}}$

```
    if abs($c1)=1.0 then
        if $c1=1.0 then
         $M=b_M
        end_if
        if $c1=-1.0 then
          $M=b_m*b_mm
        end_if
      else
        $c1=sgn($c1)*min(abs($c1),0.99999)
        $theta=atan($c1/sqrt(1-$c1^2))/3.0
        ; FLAC has no asin function
        $M=2*b_mm*b_M/((1+b_mm)-(1-b_mm)*sin(3*$theta))
```

; $M_\theta = \dfrac{2mM}{(1+m)-(1-m)\sin 3\theta}$

```
    end_if
end_if
; Inner product of deviator stress w.r.t bubble centre
```

; $\bar{\boldsymbol{s}} : \bar{\boldsymbol{s}} = (\boldsymbol{s} - \boldsymbol{s}_{\bar{\alpha}}) : (\boldsymbol{s} - \boldsymbol{s}_{\bar{\alpha}})$

```
$sp=2*$J_2
;<Bubble yield function>
```

; $f_b = \dfrac{3}{2M_\theta^2}\bar{\boldsymbol{s}} : \bar{\boldsymbol{s}} + (p - p_{\bar{\alpha}})^2 - (Rp_c)^2$

```
$fb=$sp*3.0/$M^2/2.0+($p-b_p)^2-r_bub^2*pc^2

$sum_zde11=$sum_zde11+zde11
$sum_zde22=$sum_zde22+zde22
$sum_zde33=$sum_zde33+zde33
$sum_zde12=$sum_zde12+zde12

if $fb >0.0 then
 ;yield (plastic deformation) takes place
 ;use trial stress σ^trial to calculate plastic strain rate
 ;<computation of normalised stress gradient on bubble>
```

; $\boldsymbol{n}_{ij} = \dfrac{\partial f_b}{\partial \boldsymbol{\sigma}_{ij}}$

```
 $c1=-12*1.732*b_mm*(1-b_mm)*b_M
 $c2=2*(1+b_mm)
 $c3=3*1.732*(1-b_mm)
 $c4=sqrt($J2)
 $c5=1/($c2+$c3*$J3/$J2/$c4)
 $c5=$c1*$c5^2
 $c6=$ds12^2
 $c7=$ds11*$ds22+$ds11*$ds33+$ds22*$ds33

 $M11=(3*$ds22*$ds33-$c7+$c6)/3.0
 $M11=1/$c4^3*$M11
 $M11=$M11-3.0/2.0/$c4^5*$J3*$ds11
 $M11=$c5*$M11

 $M22=(3*$ds11*$ds33-$c7+$c6)/3.0
 $M22=1/$c4^3*$M22
 $M22=$M22-3.0/2.0/$c4^5*$J3*$ds22
 $M22=$c5*$M22

 $M33=(3*$ds22*$ds11-$c7-2*$c6)/3.0
 $M33=1/$c4^3*$M33
 $M33=$M33-3.0/2.0/$c4^5*$J3*$ds33
 $M33=$c5*$M33

 $M12=-2/$c4^3*$ds12*$ds33
 $M12=$M12-3/$c4^5*$J3*$ds12
 $M12=$c5*$M12

 $J11=$b_ds11
```

```
$J22=$b_ds22
$J33=$b_ds33
$J12=2*$b_ds12

$n11=-6/$M^3*$J_2*$M11
$n11=$n11+3.0/$M^2*$J11+2.0/3.0*($p-b_p)

$n22=-6/$M^3*$J_2*$M22
$n22=$n22+3.0/$M^2*$J22+2.0/3.0*($p-b_p)

$n33=-6/$M^3*$J_2*$M33
$n33=$n33+3.0/$M^2*$J33+2.0/3.0*($p-b_p)

$n12=-6/$M^3*$J_2*$M12
$n12=$n12+3.0/$M^2*$J12
```

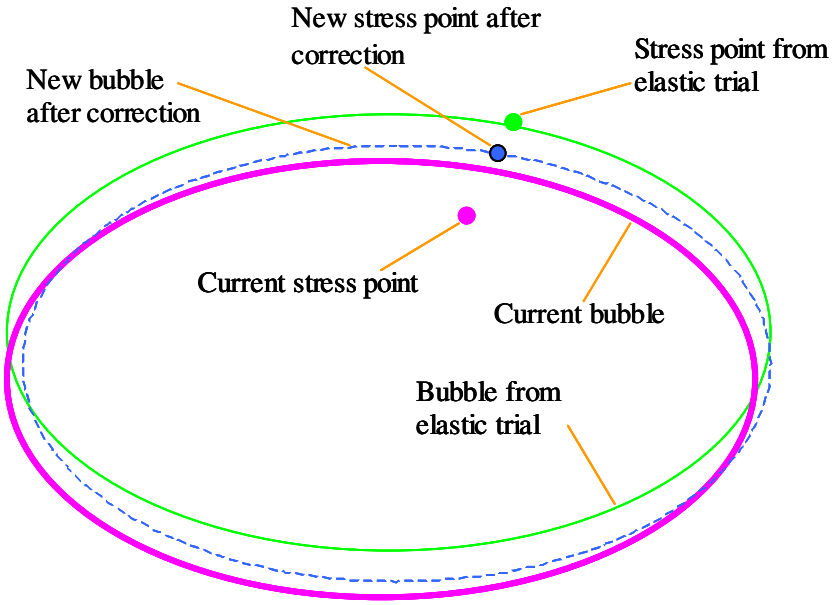

; normalise stress gradient, $\bar{n}$

```
$n=sqrt($n11^2+$n22^2+$n33^2+2*$n12^2);
```
$\|n\| = (n:n)^{0.5}$

```
$n11=$n11/$n;
```
$\bar{n}_{ij} = \dfrac{n_{ij}}{\|n\|}$

```
$n22=$n22/$n
$n33=$n33/$n
$n12=$n12/$n
$n=$n*$n ;
```
$\|n\|^2$

;<stress w.r.t the bubble center $\bar{\sigma}$>

```
$b_zs11=$zs11-b_zs11c
```

```
$b_zs22=$zs22-b_zs22c
$b_zs33=$zs33-b_zs33c
$b_zs12=$zs12-b_zs12c

;<stresses w.r.t structure surface centre $\hat{\boldsymbol{\sigma}}$>
$s_zs11=$zs11-s_zs11c
$s_zs22=$zs22-s_zs22c
$s_zs33=$zs33-s_zs33c
$s_zs12=$zs12-s_zs12c

;<conjugate stress w.r.t structure surface centre $\hat{\boldsymbol{\sigma}}_c$>
; $\frac{\hat{\boldsymbol{\sigma}}_c}{r}=\frac{\overline{\boldsymbol{\sigma}}}{R}$
$s_zs11cj=r_str/r_bub*$b_zs11
$s_zs22cj=r_str/r_bub*$b_zs22
$s_zs33cj=r_str/r_bub*$b_zs33
$s_zs12cj=r_str/r_bub*$b_zs12

; conjugate stress point on structure surface
; $\boldsymbol{\sigma}_c=\hat{\boldsymbol{\sigma}}_c+\hat{\boldsymbol{\alpha}}$
$zs11cj=$s_zs11cj+s_zs11c
$zs22cj=$s_zs22cj+s_zs22c
$zs33cj=$s_zs33cj+s_zs33c
$zs12cj=$s_zs12cj+s_zs12c
; <plastic variables at current point>
; $b=\overline{\boldsymbol{n}}:(\boldsymbol{\sigma}_c-\boldsymbol{\sigma})$
$b=$n11*($zs11cj-$zs11)
$b=$b+$n22*($zs22cj-$zs22)
$b=$b+$n33*($zs33cj-$zs33)
$b=$b+2*$n12*($zs12cj-$zs12)

; $b_{max}=2(\frac{r}{R}-1)\overline{\boldsymbol{n}}:\overline{\boldsymbol{\sigma}}$
$bmax=$n11*$b_zs11
$bmax=$bmax+$n22*$b_zs22
$bmax=$bmax+$n33*$b_zs33
$bmax=$bmax+2*$n12*$b_zs12
$bmax=2.0*(r_str/r_bub-1)*$bmax
$c11=abs($b/$bmax)

; $T=(p-p_{\bar{\alpha}})-k(\frac{r-1}{r})\left[(1-A)(p-p_{\bar{\alpha}})^2+\frac{3A}{2M_\theta^4}(\boldsymbol{s}-\boldsymbol{s}_{\bar{\alpha}}):(\boldsymbol{s}-\boldsymbol{s}_{\bar{\alpha}})\right]^{1/2}$
$c1=3.0/(2.0*$M^2)
$c2=$c1/$M^2
$c3=$p-b_p
$T=sqrt(((1-AA)*$c3^2+AA*$c2*$sp))
$T=$c3-k*(r_str-1)/r_str*$T
```

; $H_c = \dfrac{rp_c\left\langle T\left[(p-p_{\bar{\alpha}})+\dfrac{3}{2M_\theta^2}(\boldsymbol{s}-\boldsymbol{s}_{\bar{\alpha}}):\boldsymbol{\eta}_0+Rp_c\right]-\dfrac{3}{2M_\theta^2}(p-p_{\bar{\alpha}})(\boldsymbol{s}-\boldsymbol{s}_{\bar{\alpha}}):\dfrac{\boldsymbol{\eta}_0}{r}\right\rangle}{(\lambda^*-\kappa^*)[(p-p_{\bar{\alpha}})^2+\dfrac{3}{2M_\theta^4}(\boldsymbol{s}-\boldsymbol{s}_{\bar{\alpha}}):(\boldsymbol{s}-\boldsymbol{s}_{\bar{\alpha}})]}$

```
$c4=nambda0/r_str
$c5=2*$b_ds12*nambda0
$c6=$c5/r_str
$Hc=$T*($c3+$c1*$c5+r_bub*pc)
$Hc=$Hc-$c3*$c1*$c6
$Hc=r_str*pc*$Hc
$Hc=$Hc/(b_lambda-b_kappa)
$Hc=abs($Hc)/($c3^2+$c2*$sp)
```

;original $H = H_c + \dfrac{1}{\|\boldsymbol{n}\|^2}\dfrac{Bp_c^3}{(\lambda^*-\kappa^*)R}(\dfrac{b}{b_{\max}})^{\psi}$

```
;$H=$Hc+BB*(abs(pc))^3*$c11^psigh/r_bub/(b_lambda-b_kappa)/$n
```

;modified equation, $H = H_c + \dfrac{1}{\|\boldsymbol{n}\|^2}\dfrac{Bp_c^3R^2}{(\lambda^*-\kappa^*)}(\dfrac{b}{b_{\max}})^{\psi}$

```
$H=$Hc+BB*(abs(pc))^3*r_bub^2.0*$c11^psigh/(b_lambda-b_kappa)/$n
```

;calculate plastic multiplier, $\dot{\gamma} = \dfrac{1}{H}(\overline{\boldsymbol{n}} : \dot{\boldsymbol{\sigma}})$

```
$dgamma=($n11*$dzs11+$n22*$dzs22+$n33*$dzs33+2*$n12*$dzs12)/$H
```

;plastic strain rate, $\dot{\boldsymbol{\varepsilon}}^p = \dot{\gamma}\overline{\boldsymbol{n}}$

```
$pzde11=$dgamma*$n11
$pzde22=$dgamma*$n22
$pzde33=$dgamma*$n33
$pzde12=$dgamma*$n12
;plastic volumetric strain rate
$dv=$pzde11+$pzde22+$pzde33
;pwp rate
if Dranage=0 then
   $dpwp=-b_mod*$dv;undrained
   $sum_pwp=$sum_pwp+$dpwp
  else
   $dpwp=0;drained
end_if
```

; corrected stress rate, $\dot{\boldsymbol{\sigma}} = \boldsymbol{D}^e \cdot (\dot{\boldsymbol{\varepsilon}} - \dot{\boldsymbol{\varepsilon}}^p)$

```
$zde11=zde11-$pzde11
$zde22=zde22-$pzde22
$zde33=zde33-$pzde33
$zde12=zde12-$pzde12

$dzs11=e1*$zde11+e2*$zde22+e2*$zde33
$dzs22=e2*$zde11+e1*$zde22+e2*$zde33
$dzs33=e2*$zde11+e2*$zde22+e1*$zde33
```

```
 $dzs12=e3*$zde12
 ; calculate apparent shear modulus, app_g
 if apparent = 1 then
  $ds1 = $dzs11 - $dzs22
  $ds2 = $dzs22 - $dzs33
  $ds3 = $dzs33 - $dzs11
  $dq  = $ds1*$ds1 + $ds2*$ds2 + $ds3*$ds3
  $dq  = 0.7071*sqrt($dq + 6.0*$dzs12*$dzs12)
  app_g=s_mod*$dq/$dq_trial;apparent tangent shear modulus
 end_if
 $sum_pzde11=$sum_pzde11+$pzde11
 $sum_pzde22=$sum_pzde22+$pzde22
 $sum_pzde33=$sum_pzde33+$pzde33
 $sum_pzde12=$sum_pzde12+$pzde12
 zvisc=0.0
end_if; if $fb>0.0
;update stress, σ = σ + σ̇
zs11=zs11+$dzs11
zs22=zs22+$dzs22
zs33=zs33+$dzs33
zs12=zs12+$dzs12

if zsub>0.0 then
 if $p>=0 then
   ;$p=-0.01
   nerr=168
   error=1
 end_if
 pwp=pwp+$sum_pwp/zsub
 $sum_pwp=0
 $p=(zs11+zs22+zs33)/3.0+pwp
 $q=zs22-zs11;only for triaxial stress condition
 ; total strain rate ε̇
 $zde11=$sum_zde11/zsub
 $sum_zde11=0.0
 $zde22=$sum_zde22/zsub
 $sum_zde22=0.0
 $zde33=$sum_zde33/zsub
 $sum_zde33=0.0
 $zde12=$sum_zde12/zsub
 $sum_zde12=0.0
 vertical_strain=vertical_strain+$zde22*100
 volumetric_strain=volumetric_strain+($zde11+$zde22+$zde33)*100
 $q_zde=$zde11^2+$zde22^2+$zde33^2+2*$zde12^2
 $q_zde=sqrt(2.0/3.0*$q_zde);toal equivalent shear strain rate ε̇q
 qt_strain=qt_strain+$q_zde*100 ;total equivalent shear strain εq

 if $fb>0.0 then
  ; update str surface & bubble centers and size
  ; plastic strain rate ε̇p
  $pzde11=$sum_pzde11/zsub
  $sum_pzde11=0.0
  $pzde22=$sum_pzde22/zsub
  $sum_pzde22=0.0
```

```
$pzde33=$sum_pzde33/zsub
$sum_pzde33=0.0
$pzde12=$sum_pzde12/zsub
$sum_pzde12=0.0

;---- isotropic and kinematic hardening ---
$pv_zde=$pzde11+$pzde22+$pzde33 ; plastic volumetric strain rate
pv=$pv_zde*100+pv ;plastic volumetric strain
; equivalent plastic shear stain

$pq_zde=$pzde11^2+$pzde22^2+$pzde33^2+$pzde12^2
$pq_zde=sqrt(2.0/3.0*$pq_zde) ;
q_strain=q_strain+$pq_zde*100 ;

$dpc=$pv_zde/(b_lambda-b_kappa)*abs(pc) ;
; destruction strain rate,
$pq_zde=sqrt((1-AA)*$pv_zde*$pv_zde+AA*$pq_zde*$pq_zde)
; destruction strain rate,
$dr_str=-k/(b_lambda-b_kappa)*(r_str-1)*$pq_zde
; kinematic hardening (update centers of bubble and str surface)
; translation rate of str surface centre
; change of str surface centre in deviator space,
;
$ds=nambda0*((r_str-1)*$dpc+pc*$dr_str)
; change of str surface centre in p axis,
$s_dp=r_str*$dpc+pc*$dr_str
pc=pc+$dpc ;isotropic hardening
r_str=r_str+$dr_str ;update size of str surface
; change of str surface centre in general stress space,
$s_dzs11c=$s_dp
$s_dzs22c=$s_dp
$s_dzs33c=$s_dp
$s_dzs12c=$ds
; stress rate w.r.t str surface centre
$s_dzs11=$dzs11-$s_dzs11c
$s_dzs22=$dzs22-$s_dzs22c
$s_dzs33=$dzs33-$s_dzs33c
$s_dzs12=$dzs12-$s_dzs12c

; use corrected stress to calculate new bubble centre
; recalculate deviator stresses
$ds11=zs11+pwp-$p
$ds22=zs22+pwp-$p
$ds33=zs33+pwp-$p
$ds12=zs12
; recalculate deviator stress w.r.t bubble centre
```

```
$b_ds11=$ds11-b_ds11c
$b_ds22=$ds22-b_ds22c
$b_ds33=$ds33-b_ds33c
$b_ds12=$ds12-b_ds12c
; recalculate stress w.r.t bubble centre  σ̄
$b_zs11=zs11+pwp-b_zs11c
$b_zs22=zs22+pwp-b_zs22c
$b_zs33=zs33+pwp-b_zs33c
$b_zs12=zs12-b_zs12c
; recalculate stress w.r.t str surface centre  σ̂
$s_zs11=zs11+pwp-s_zs11c
$s_zs22=zs22+pwp-s_zs22c
$s_zs33=zs33+pwp-s_zs33c
$s_zs12=zs12-s_zs12c
; recalculate conjugate stress w.r. str surface centre  σ̂_c
$s_zs11cj=r_str/r_bub*$b_zs11
$s_zs22cj=r_str/r_bub*$b_zs22
$s_zs33cj=r_str/r_bub*$b_zs33
$s_zs12cj=r_str/r_bub*$b_zs12
; recalculate conjugate stress on str surface  σ_c
$zs11cj=$s_zs11cj+s_zs11c
$zs22cj=$s_zs22cj+s_zs22c
$zs33cj=$s_zs33cj+s_zs33c
$zs12cj=$s_zs12cj+s_zs12c
; translation rate of bubble centre  α̇
$c7=$dr_str/r_str
$c8=$dpc/pc+$c7
$b_dzs11c=($dzs11-$s_dzs11c)-$s_zs11*$c8+$b_zs11*$c7
$b_dzs22c=($dzs22-$s_dzs22c)-$s_zs22*$c8+$b_zs22*$c7
$b_dzs33c=($dzs33-$s_dzs33c)-$s_zs33*$c8+$b_zs33*$c7
$b_dzs12c=($dzs12-$s_dzs12c)-$s_zs12*$c8+$b_zs12*$c7

$c9=$n11*$b_dzs11c+$n22*$b_dzs22c+$n33*$b_dzs33c
$c9=$c9+2.0*$n12*$b_dzs12c
$c10=$n11*($zs11cj-zs11-pwp)+$n22*($zs22cj-zs22-pwp)
$c10=$c10+$n33*($zs33cj-zs33-pwp)+2*$n12*($zs12cj-zs12)

$b_dzs11c=$c9/$c10*($zs11cj-zs11-pwp)
$b_dzs22c=$c9/$c10*($zs22cj-zs22-pwp)
$b_dzs33c=$c9/$c10*($zs33cj-zs33-pwp)
$b_dzs12c=$c9/$c10*($zs12cj-zs12)

$b_dzs11c=$s_dzs11c+(b_zs11c-s_zs11c)*$c8+$b_dzs11c
$b_dzs22c=$s_dzs22c+(b_zs22c-s_zs22c)*$c8+$b_dzs22c
$b_dzs33c=$s_dzs33c+(b_zs33c-s_zs33c)*$c8+$b_dzs33c
$b_dzs12c=$s_dzs12c+(b_zs12c-s_zs12c)*$c8+$b_dzs12c
; new bubble centre  ᾱ = ᾱ + α̇
b_zs11c=b_zs11c+$b_dzs11c
b_zs22c=b_zs22c+$b_dzs22c
b_zs33c=b_zs33c+$b_dzs33c
b_zs12c=b_zs12c+$b_dzs12c
; new bubble centre on p axis  p_ᾱ
b_p=(b_zs11c+b_zs22c+b_zs33c)/3.0
```

```
  ; new bubble centre in deviator stress space, s_ᾱ
  b_ds11c=b_zs11c-b_p
  b_ds22c=b_zs22c-b_p
  b_ds33c=b_zs33c-b_p
  b_ds12c=b_zs12c
  b_q=b_zs22c-b_zs11c
  ; new center of structure surface α̂ = α̂ + α̇̂
  s_zs11c=s_zs11c+$s_dzs11c
  s_zs22c=s_zs22c+$s_dzs22c
  s_zs33c=s_zs33c+$s_dzs33c
  s_zs12c=s_zs12c+$s_dzs12c

  ; new center of str surface on p axis
  s_p=r_str*pc ; or s_p=(s_zs11c+s_zs22c+s_zs33c)/3.0
  s_q=s_zs12c*1.732
  ; new center of str surface in deviator stress space s_α̂
  s_ds11c=s_zs11c-s_p
  s_ds22c=s_zs22c-s_p
  s_ds33c=s_zs33c-s_p
  s_ds12c=s_zs12c
 end_if ;if $fb>0
 ; calculate elastic moduli
 b_mod=abs($p)/b_kappa+b_mod0
 s_mod=3.0*b_mod*(1.0-2.0*b_poss)/(2.0*(1.0+b_poss))
end_if ;zsub>0.0
case 3
; calculate apparent shear modulus
if apparent =1 then
  if $fb>0 then
     $app_g=s_mod*$dq/$dq_trial
    else
     $app_g=s_mod
  end_if
end_if
;- Max modulus ---
bulk_max=b_kmax
shear_max=b_g0
sm_max    = shear_max
cm_max    = bulk_max + 1.333333 * shear_max
end_case
end
;opt bubble
set echo on
```

6 VERIFICATION OF THE BUBBLE MODEL

The Bubble model described in Chapter 5 is implemented in *FLAC* using the methodologies explained in Chapters 3 and 4. This chapter presents some typical results of numerical modelling with *FLAC* to verify the implementation. The non-intersection condition and destructuration process are verified. Typical responses of the model are demonstrated. The model is also verified against the modified Cam-clay model and published experimental data.

Dynamic analyses are carried out to verify the plastic correction approach in coping with numerical distortion (instability) in dynamic analysis.

6.1 Modelling of non-structured soil

6.1.1 Example 1

To demonstrate basic features of the Bubble model, non-structured soil is considered herein (*i.e.* r_0=1.0). A set of parameters are chosen to simulate behaviours of normally consolidated to overconsolidated stiff clay. Figure 6.1 shows initial surfaces of the model for three cases, which are assumed to be associated with three remoulded triaxial specimens. The three specimens are compacted to have a same initial void ratio, *i.e.* they have a same initial structure (bounding) surface corresponding to a same pre-consolidation pressure of 400 kPa. The specimens then undergo triaxial compression under different effective confining pressures (*i.e.* 50 kPa, 200 kPa and 350 kPa). Therefore, the three specimens correspond to an overconsolidation ratio of 4, 2 and 1.14 respectively.

It is assumed that the initial bubble size is the same for the three specimens as they have the same preconsoildation pressure. A single zone axisymmetrical *FLAC* model is utilised

to simulate the conventional triaxial test. The following parameters are used for the Bubble model:

$\lambda^* = 0.3$ $\kappa^* = 0.02$ $\mu = 0.25$ $M = 1$ $m = 1$ $B = 600$ $\psi = 0.5$ $R = 0.1$

As non-structured soil is considered, the parameters A and k are not required. Elastic bulk modulus is determined by Equation 5.3. Apart from the above parameters initial conditions are specified as follows: $\eta_0 = 0$ $p_{c0} = 200\ kPa$

An isotropic confining stress σ_3' is applied, *i.e.* 50 kPa, 200 kPa and 350 kPa for Case 1, Case 2 and Case 3 respectively. Hereinafter, the initial centre of the bubble is always assumed to be at the initial stress point.

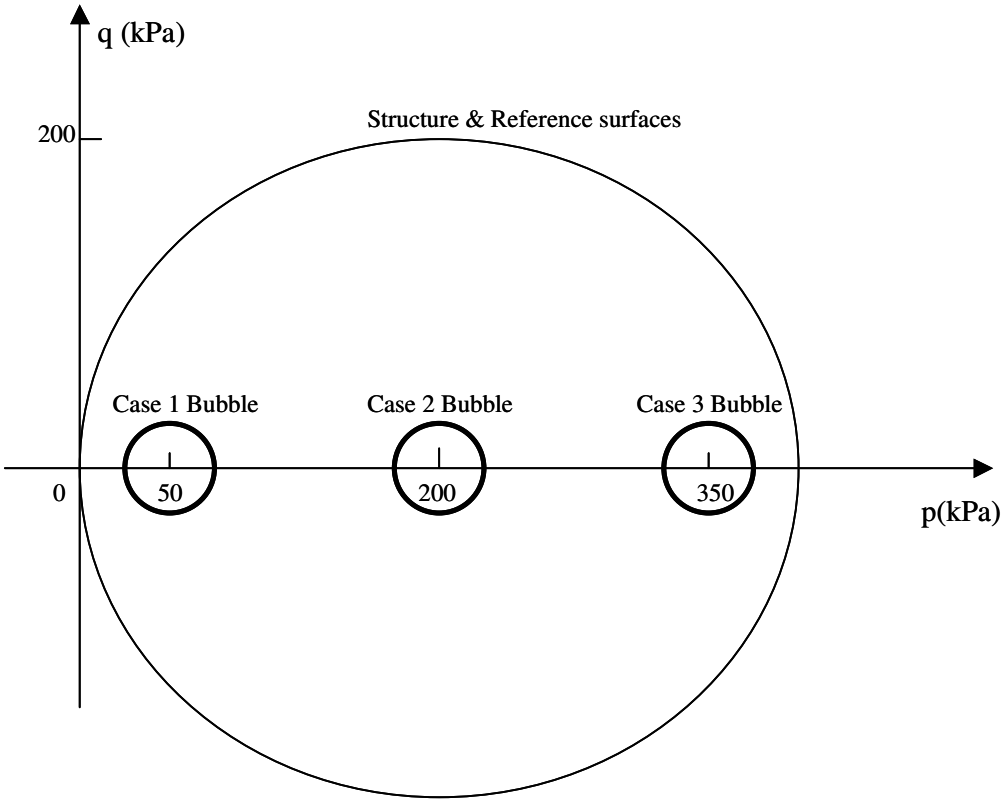

Figure 6.1 Initial stress conditions of three cases (same structure surface)

6.1.1.1 Drained behaviour

The non-intersection translation rule proposed by Hashiguchi (1985) is employed in the Bubble model to ensure a smooth transition of the bubble without intersecting the structure surface. A typical stress-strain behaviour of the model for Case 2 is shown in Figure 6.2. To verify the non-intersection condition, locations and sizes of the bubble and structure surface at 5%, 10% and 20% vertical strain are illustrated respectively in Figures 6.3, 6.4 and 6.5. Stress path and trace of the bubble centre are also shown in the figures. Figure 6.3 shows that the bubble is very close to the structure surface at 5% strain but they are not in contact. They are in contact from a strain between 5% and 10%. Figures 6.4 and 6.5 shows the bubble and structure surface are in touch while their sizes are only slightly larger than at 5% strain. The bubble is contained inside the structure surface during the whole loading process. This verifies that the non-intersection condition is satisfied.

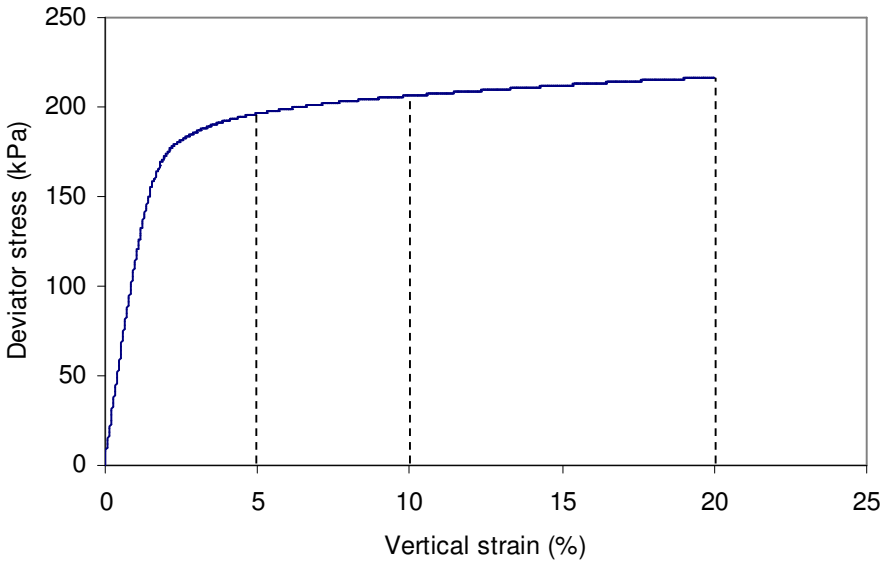

Figure 6.2 Drained stress-strain behaviour for Case 2

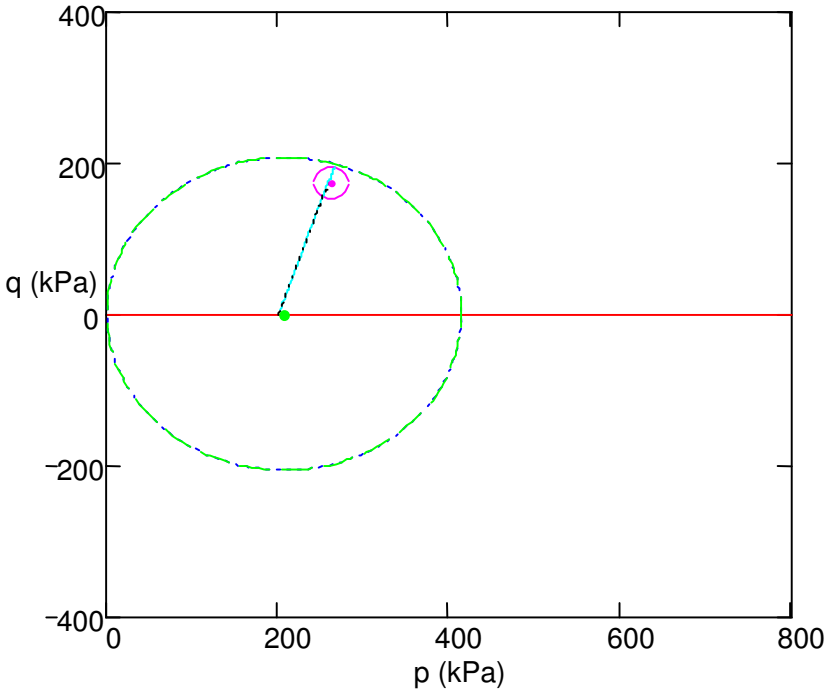

Figure 6.3 Location of surfaces at 5% vertical strain

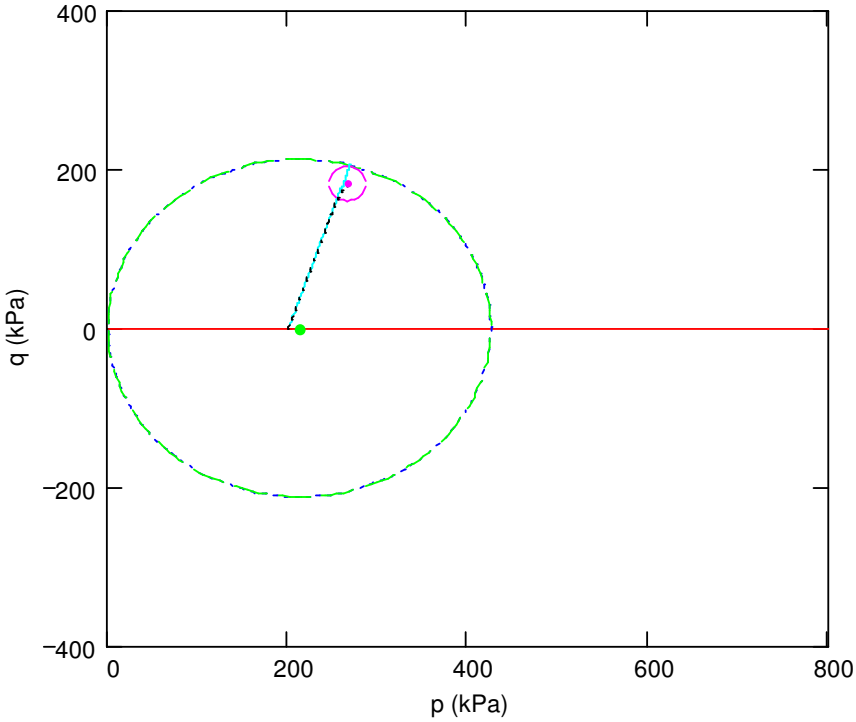

Figure 6.4 Location of surfaces at 10% vertical strain

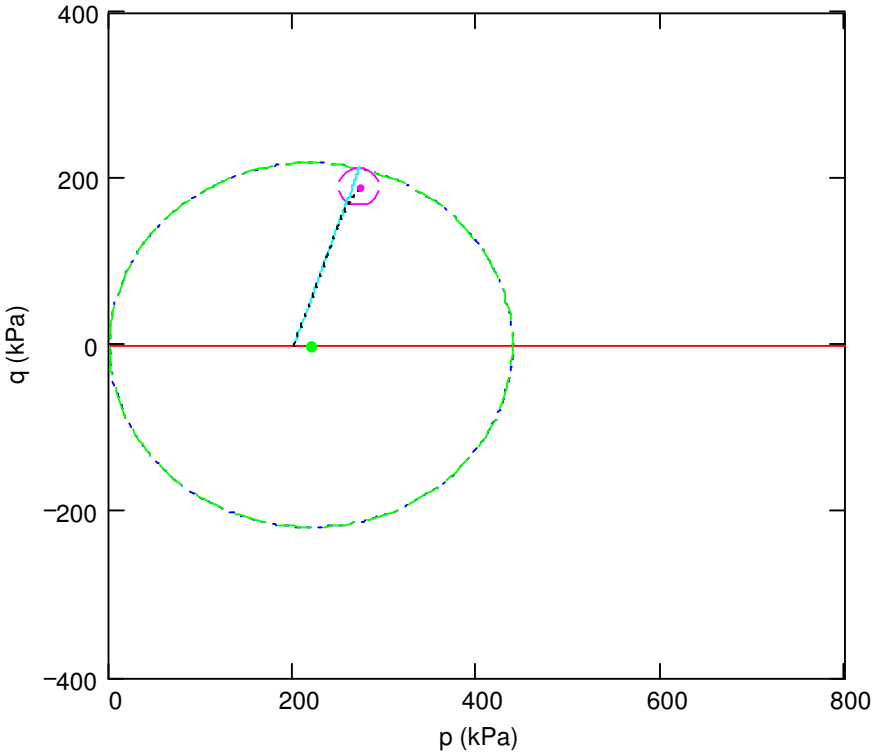

Figure 6.5 Location of surfaces at 20% vertical strain

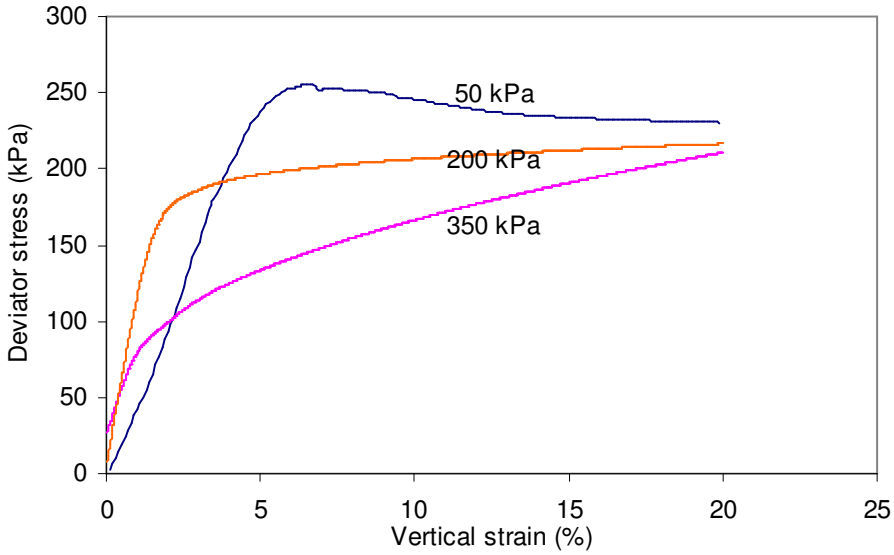

Figure 6.6 Drained stress-strain behaviour (same initial structure surface)

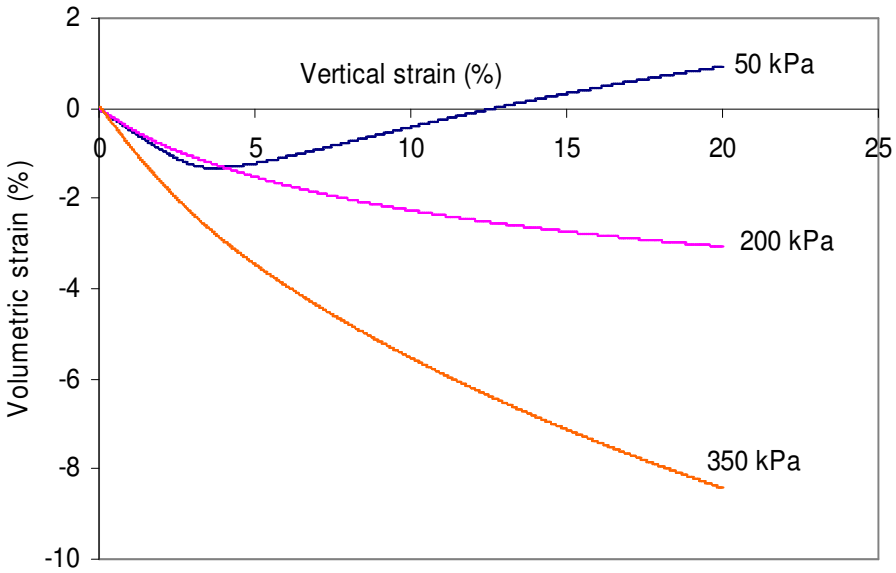

Figure 6.7 Volumetric strain (same initial structure surface)

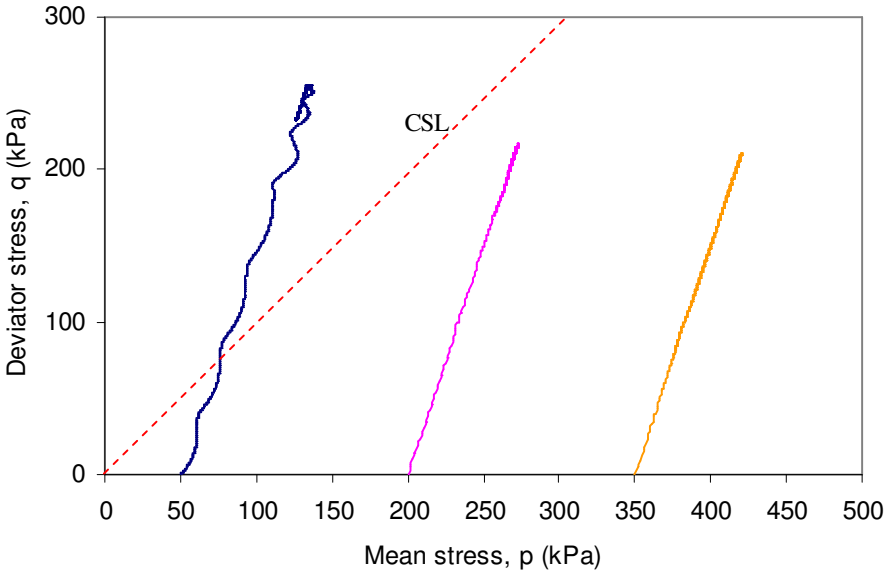

Figure 6.8 Drained stress path (same initial structure surface)

Figure 6.6 shows drained stress-strain curves for the three cases. It can be seen that higher confining pressure corresponds to larger small strain stiffness but the deviator stress is similar at 20% strain regardless of the confining pressure.

Figure 6.7 shows the volumetric strain behaviour of the model. A dilative behaviour can be seen for Case 1, which starts from a vertical strain of approximately 3%. At a higher confining pressure, *e.g.* for Case 2 (200 kPa) and Case 3 (350 kPa), the model shows contractive behaviour. Therefore the model qualitatively agrees with normally observed laboratory behaviours of soil. Figure 6.8 shows stress paths of the three cases. The gradient of the stress path is the same for the three cases as expected, *i.e.* $\Delta q / \Delta p = 3$. However, at the vertical strain of 20%, the stress paths have not reached the critical state line (CSL). This suggests that the soil parameters need to be further optimised in order to obtain better quantitative agreement with experimental results. The set of selected parameters appear to be more satisfactory to Case 2. For the other two cases, some parameters (*e.g.* B and ψ) need to be adjusted individually in order to achieve better results.

6.1.1.2 Undrained behaviour

Undrained stress-strain curves for the above three cases are presented in Figure 6.9. The ultimate stress is virtually the same, which is smaller than the drained strength and is reached at smaller strains compared to the drained cases. This is due to the undrained condition under which the isotropic hardening is insignificant so that the size of the structure surface (p_c) changes in much smaller scales than under the drained condition. This can be seen form Figure 6.10.

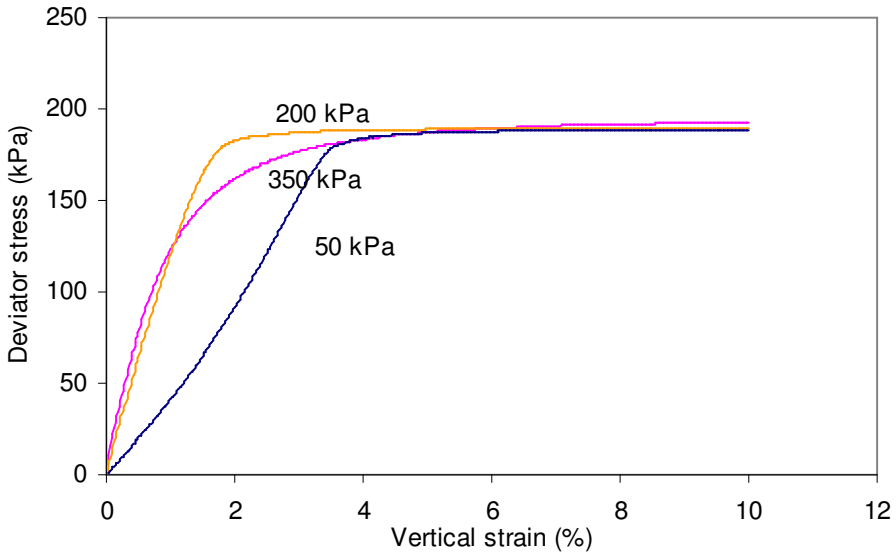

Figure 6.9 Undrained stress-strain behaviour (same initial structure surface)

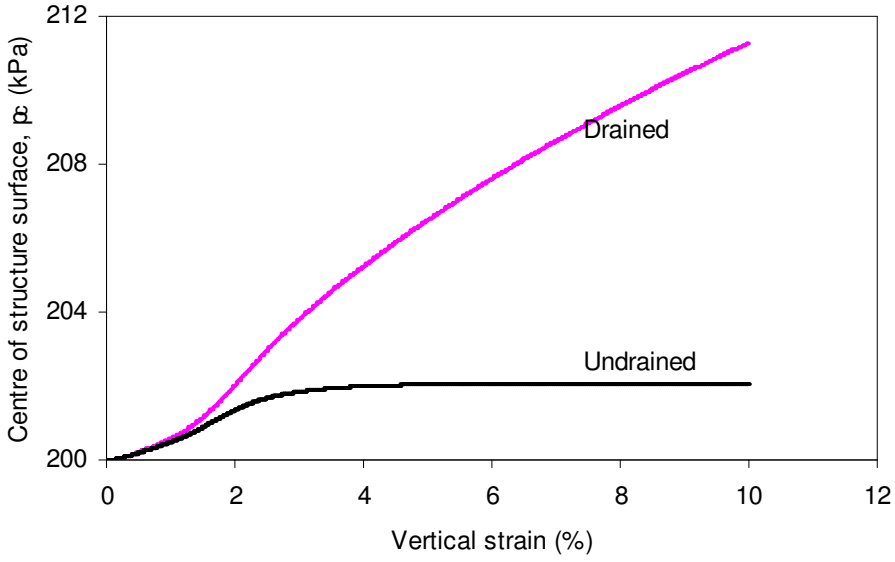

Figure 6.10 Isotropic hardening of the structure surface

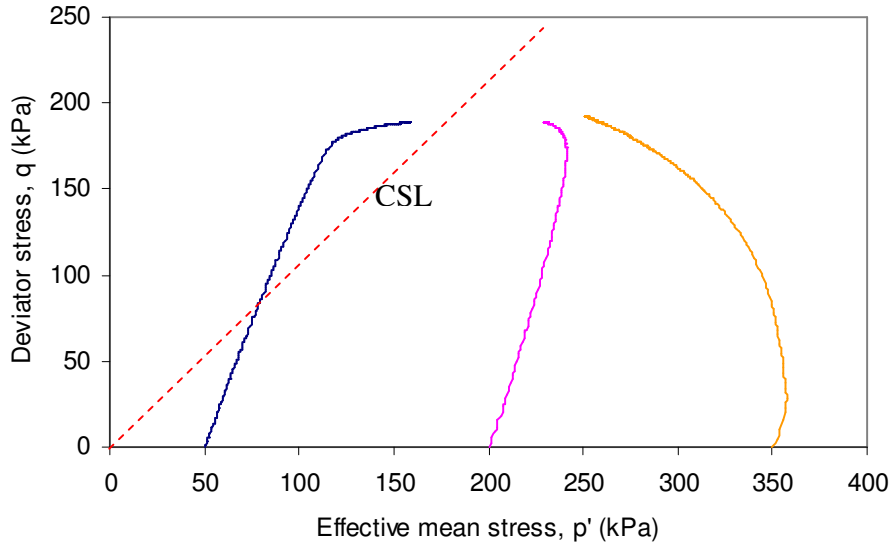

Figure 6.11 Undrained effective stress path (same initial structure surface)

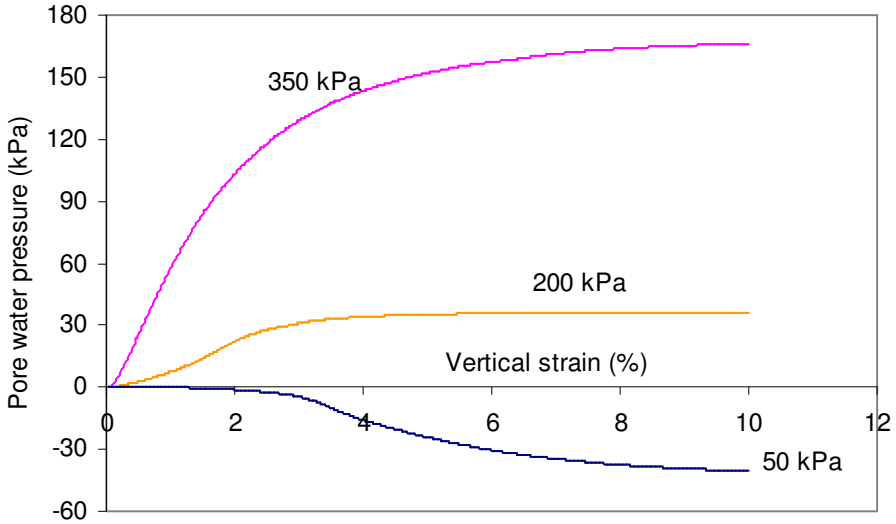

(a) Comparison between the three cases

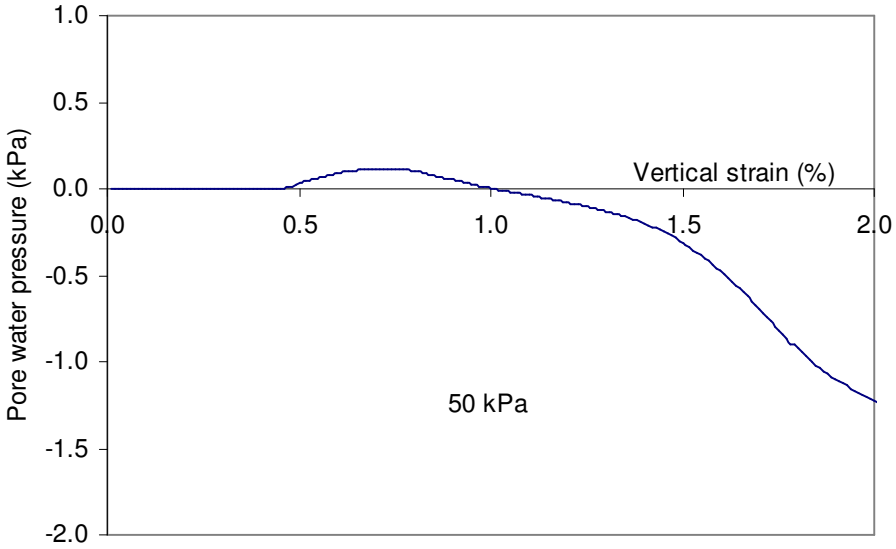

(b) Enlarged at small strain range for 50 kPa confining pressure

Figure 6.12 Pore water pressure (same initial structure surface)

Figure 6.11 shows effective stress paths under the undrained condition and Figure 6.12a shows pore water pressure response for the three cases up to 10% strain. For Case 1, negative pore water pressure is generated from about 1% strain and this corresponds to its effective stress path curving towards the right hand side to meet the critical state line (CSL). Prior to 1% strain, pore water pressure is positive but is too small to be shown in the figure. An enlargement of the pore water pressure at small strains is shown in Figure 6.12b.

6.1.2 Example 2

Figure 6.13 shows initial surfaces for another set of three different cases. Each case is assumed to be associated with a different initial structure surface. The actual bubble size varies for each case accordingly. Only the undrained condition is considered herein.

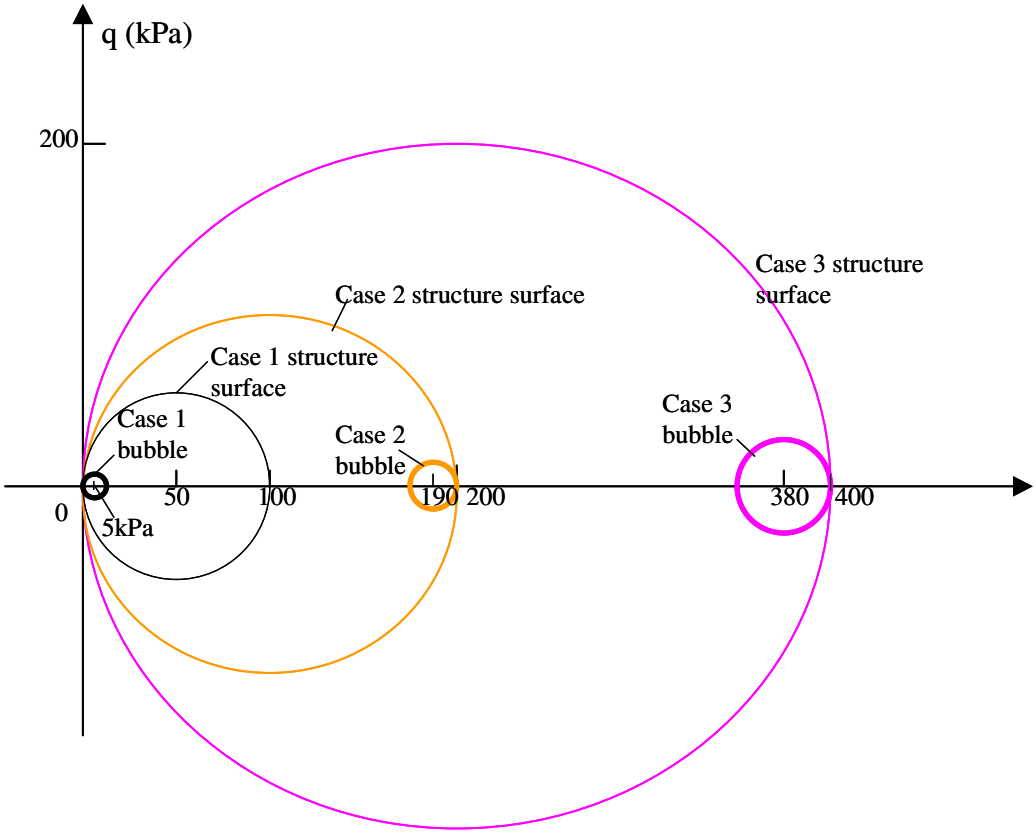

Figure 6.13 Initial stress states of three cases (variable initial structure surface)

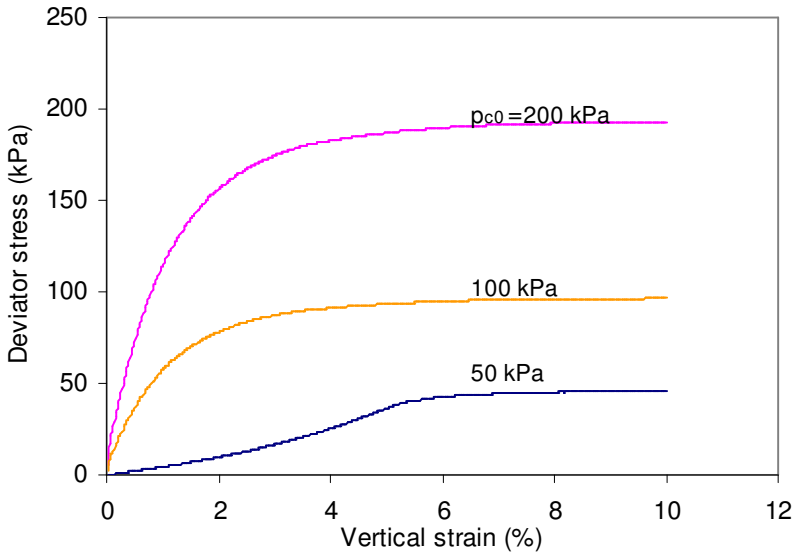

Figure 6.14 Undrained stress-strain behaviour (variable initial structure surface)

Cases 2 and 3 correspond to normally-consolidated stiff clay while Case 1 represents over-consolidated clay in a firm state. The bubble is initially in contact with structure surface for each case. All other parameters are the same as those given in previous example in Section 6.1.1. Results are shown in Figures 6.14 to 6.16.

As expected, the ultimate stress linearly increases with initial size of structure surface as shown in Figure 6.14. Effective stress paths are shown in Figure 6.15. It can be seen that all the three curves tend to approach the theoretical critical state line (CSL) regardless of initial stress state but stay slightly short of the CSL at 10% vertical strain. Figure 6.15 shows pore water response, which also suggests that the critical state has not been reached at 10% strain as pore water pressure is not stable. In fact when the bubble is close to the structure surface, plastic modulus falls quickly so a large strain is needed for the stress path to reach the critical state line. On the other hand, it is possible that in a numerical modelling a steady flow occurs while the stress path may never reach the theoretical CSL. The stress path is mainly affected by the parameter B. Figure 6.17 shows the influence of B on stress path. It can be seen from Figure 6.17a that stress paths at 10% strain are closer to the CSL for B = 1000 than for B = 600. When B is increased to 2000, the CSL is reached at 20% strain (see Figure 6.17b)

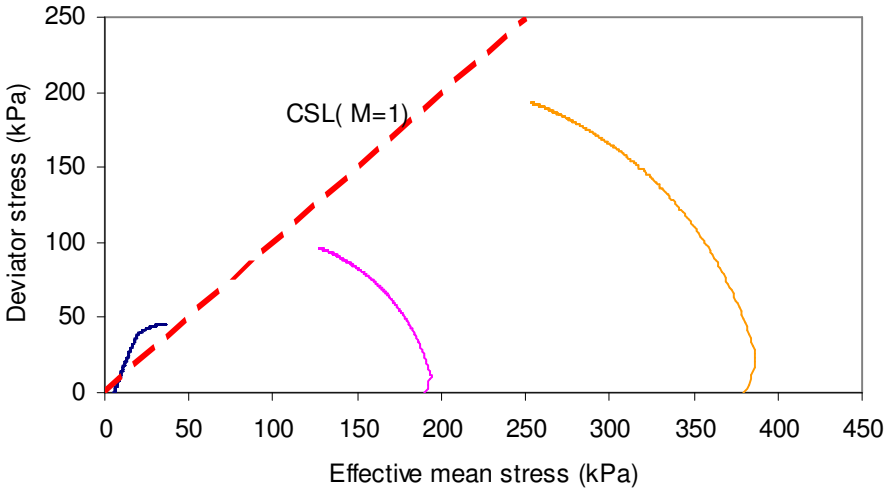

Figure 6.15 Effective stress path (variable initial structure surface)

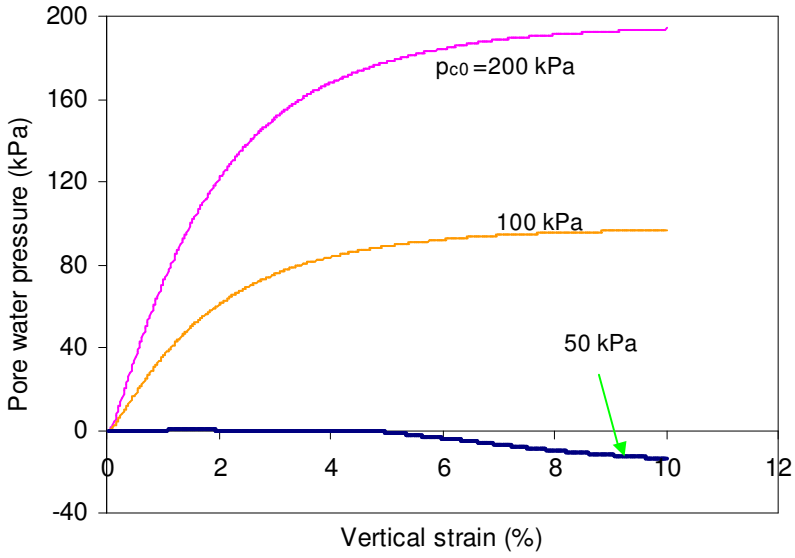

Figure 6.16 Pore water pressure (variable structure surface)

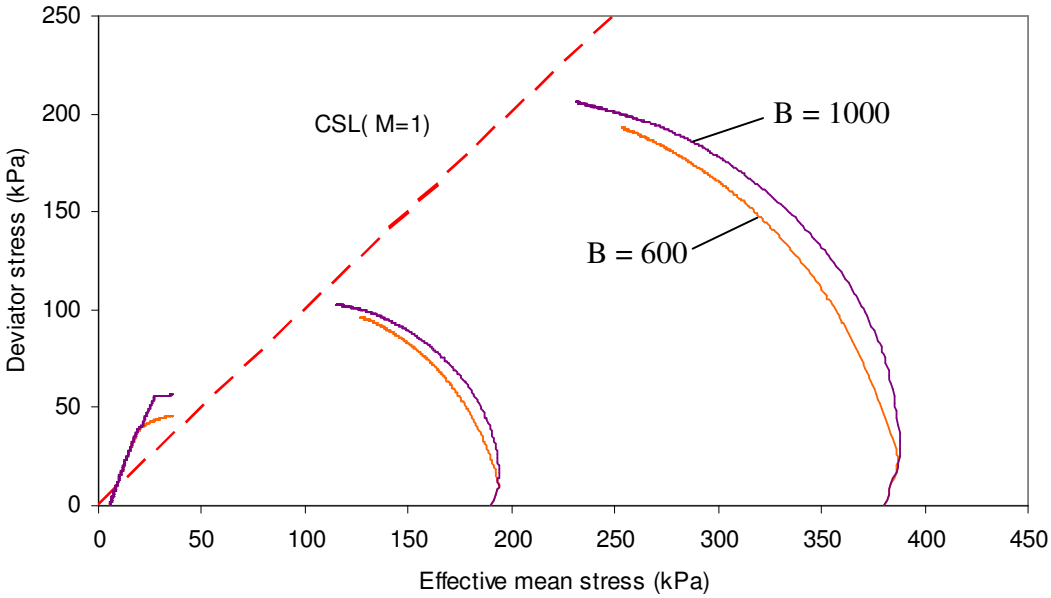

(a) Maximum strain = 10%

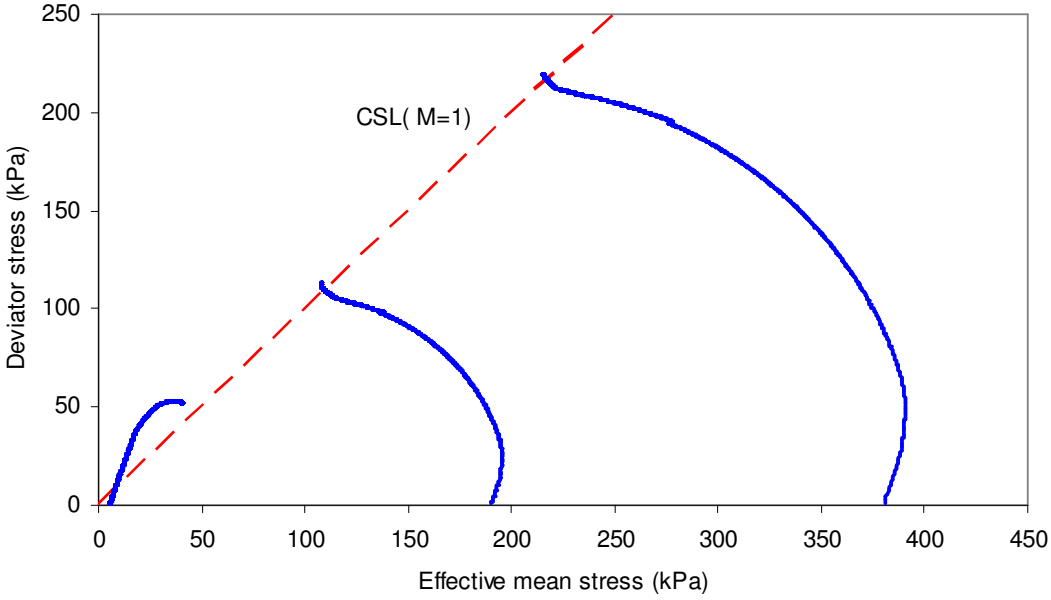

(b) Maximum strain = 20 %, B = 2000

Figure 6.17 Influence of 'B' on effective stress path

6.2 Modelling of structured soil

6.2.1 Example 1

In this section the purpose is to verify the capability of the Bubble model in modelling general behaviours of structured soil. The parameters selected herein are typically for very stiff over-consolidated cohesive soil, whihc are given as follows:

Standard parameters	$\lambda^* = 0.3$ $\kappa^* = 0.02$ $M = 1.0$ $\mu = 0.25$ $m = 1.0$
Destructuration parameters	$A = 0.5$ $k = 8$
Bubble size	$R = 0.2$
Hardening modulus parameters	$B = 600$ $\psi = 0.5$
Initial conditions	$\eta_0 = 0$ $r_0 = 2$ $p_{c0} = 200\ kPa$ $\sigma'_3 = 350\ kPa$

Where $r_0 = 2$ means initial size of the structure surface is twice that of the reference surface as shown in Figure 6.18.

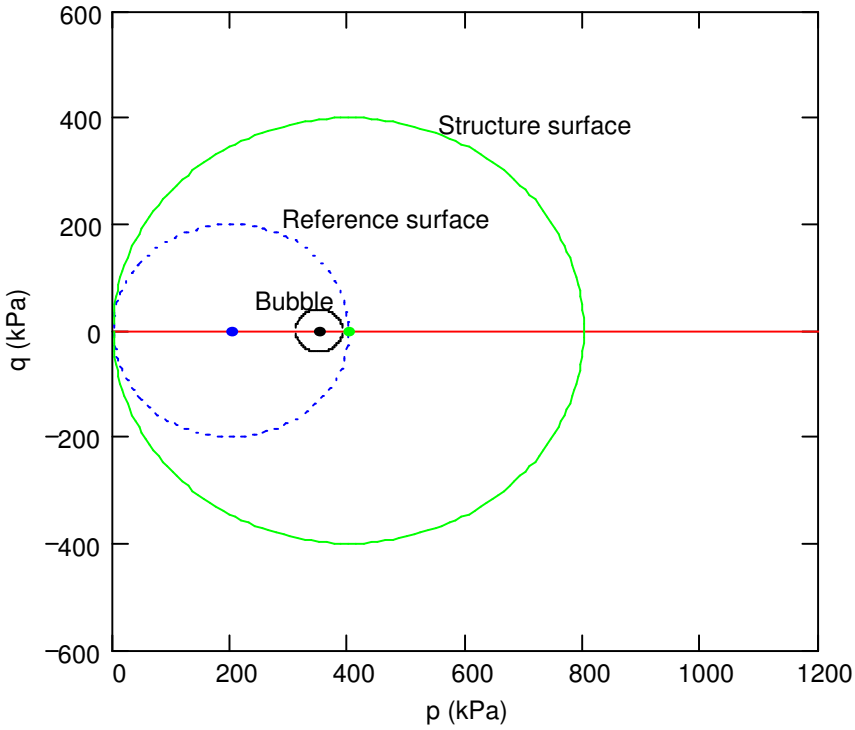

Figure 6.18 Initial stress conditions of structured soil

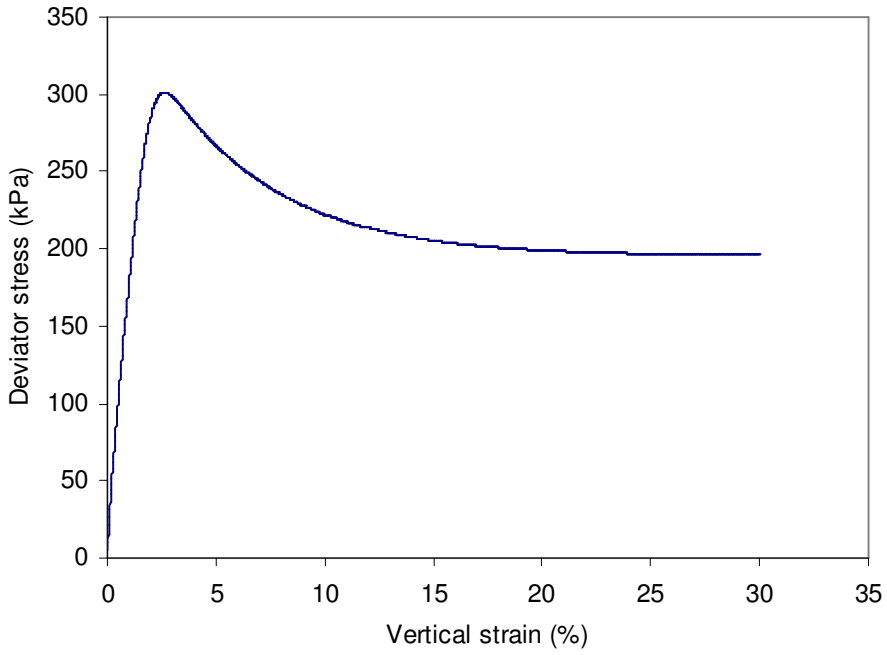

Figure 6.19 Undrained stress-strain behaviour of structured soil

Undrained stress-strain behaviour of the structured soil is shown in Figure 6.19. Compared to the previous non-structured soil, it can be seen that a peak stress of 300 kPa is reached at a vertical strain of about 3% due to the initial structure of soil (*i.e.* $r_0 = 2$). However, the residual stress is similar in magnitude to the ultimate stress for the non-structured soil shown in Figure 6.9 as the reference surface has the same size for the two cases.

In this case isotropic hardening is insignificant due to the undrained condition, hence there is little change in p_c, *i.e* $p_c \approx p_{c0} = 200\ kPa$. This means the reference surface and the bubble are almost constant in size.

The structure surface always decreases in size upon occurrence of plastic deformation and collapses towards the reference surface no matter the plastic deformation is contractive or dilative. When the initial structure is totally removed, *i.e.* r is reduced from r_0 to 1.0 the two surfaces are in contact. Under undrained condition the destructuration is mainly controlled by distortional plastic strain. The destructuration process is expressed

by reduction of the size ratio r. Figure 6.20 shows that r is initially 2.0 and decreases to 1.0 when the vertical strain is about 30%. The rate of destructuration is controlled by the parameter k which is 8 in this example. Influence of k on destructuration will be discussed in Chapter 7.

The destructuration process is illustrated more directly in Figures 6.21 to 6.23. The reference surface and the bubble virtually do not change in size. The bubble is brought upwards after being engaged by the current stress then pushed downwards again due to destructuration which results in collapsing of the structure surface. Destructuration is completed at about 30% strain, at which the structure surface coincides with the reference surface as shown in Figure 6.23. It can be seen that the bubble is always contained under the structure surface. This again verifies the non-intersection condition of the model.

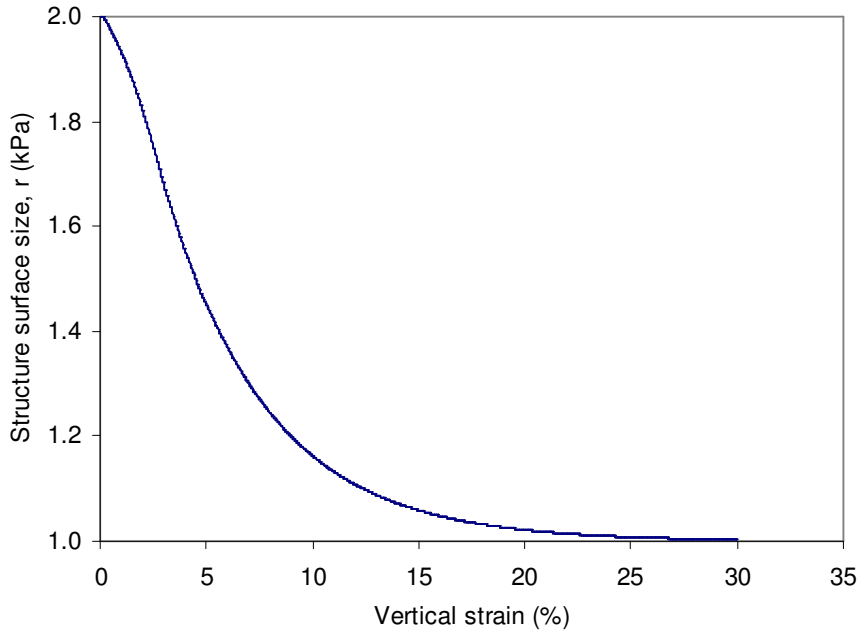

Figure 6.20 Destructuration of structured soil

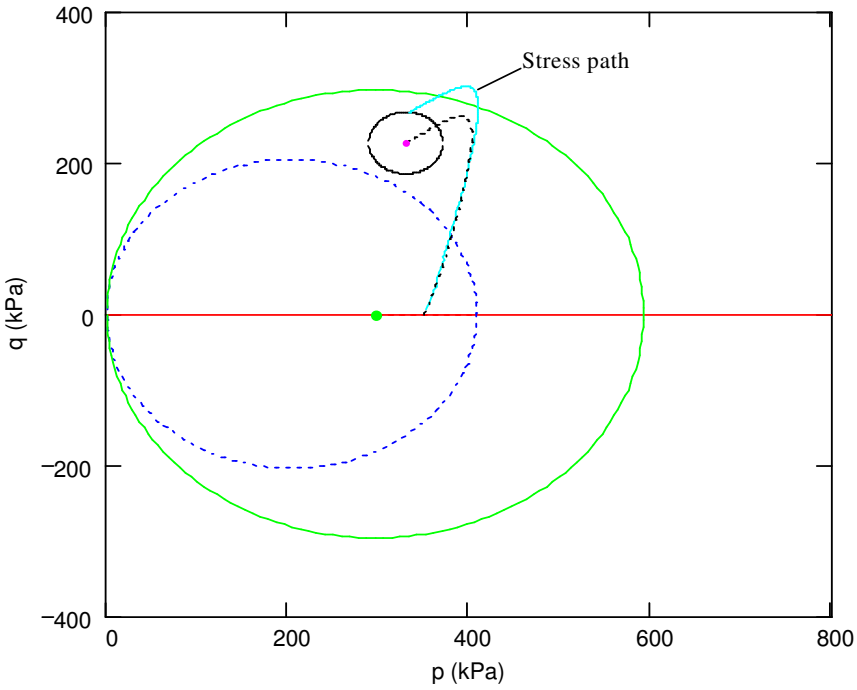

Figure 6.21 Surfaces at 5% strain

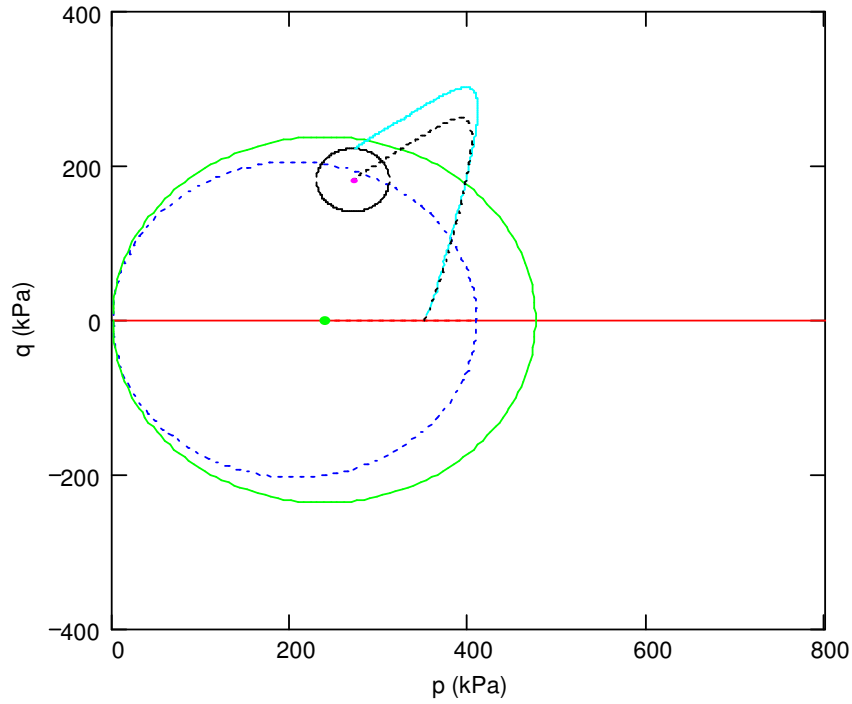

Figure 6.22 Surfaces at 10% strain

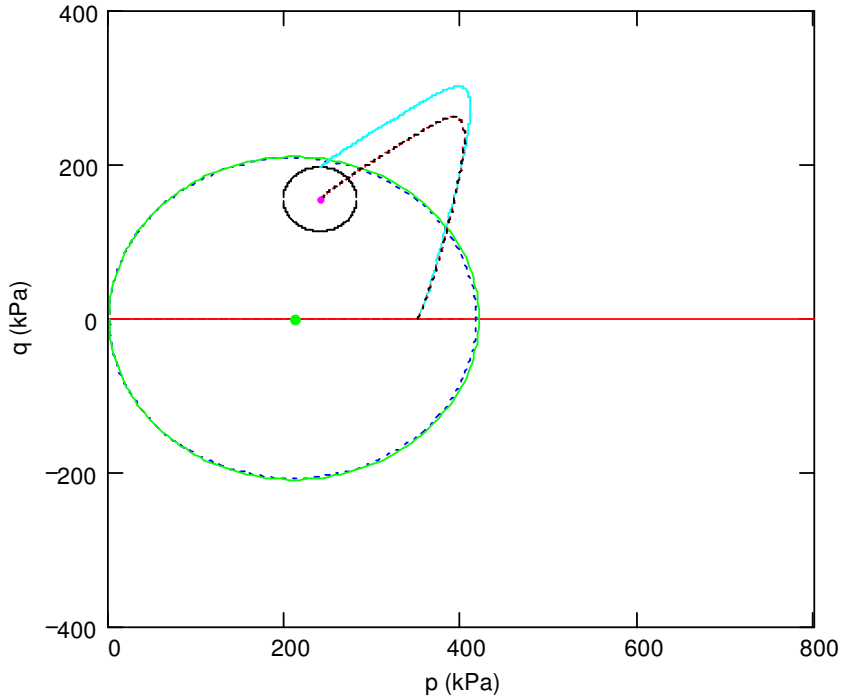

Figure 6.23 Surfaces at 30% strain

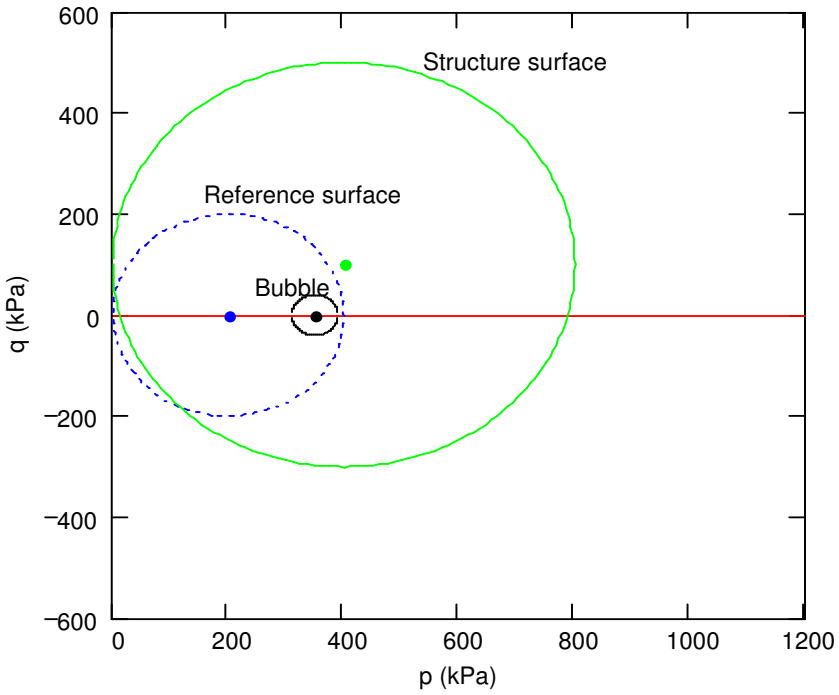

Figure 6.24 Initial stress conditions of structured soil with anisotropy

The soil described in Figure 6.18 has an isotropic initial structure surface, *i.e.* $\eta_0 = 0$. Figure 6.24 shows the initial stress state of the structured soil which has an anisotropic structure surface ($\eta_0 = 0.5$). In p, q pace, the centre of the structure surface is at (400, 100). All other parameters are the same as those for Figure 6.18.

Figure 6.25 indicates that the anisotropy results in a smaller peak stress but no difference in residual stress. Figure 6.26 shows the surfaces when the vertical strain is 30%. Comparison of Figure 6.26 with Figure 6.23 indicates that the anisotropy affects the stress path and translation path of the bubble but does not affect the final sizes and locations of the surfaces as they are only controlled by the intrinsic behaviour of soil.

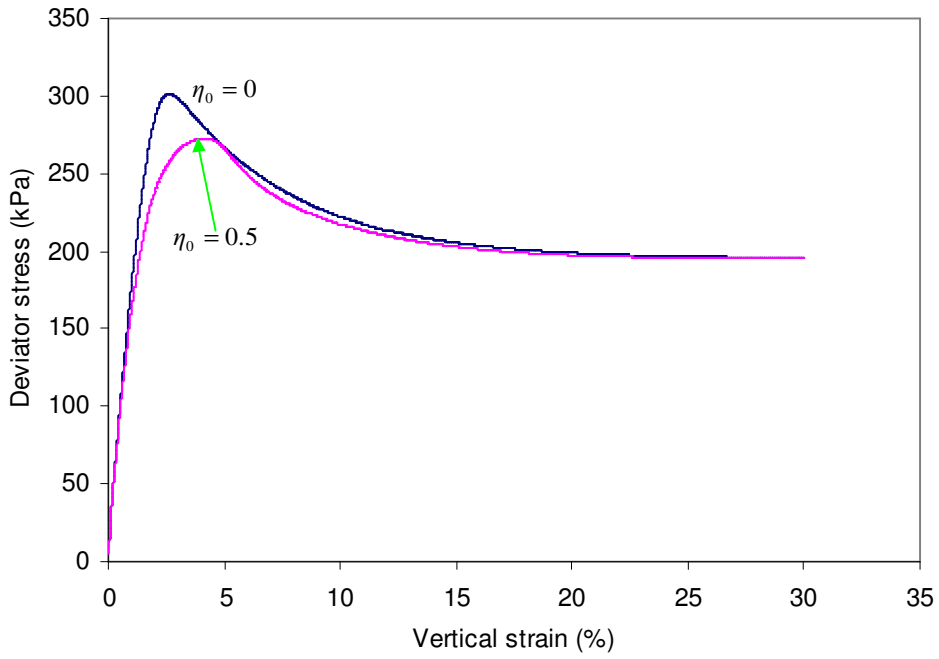

Figure 6.25 Influence of anisotropy on stress-strain behaviour

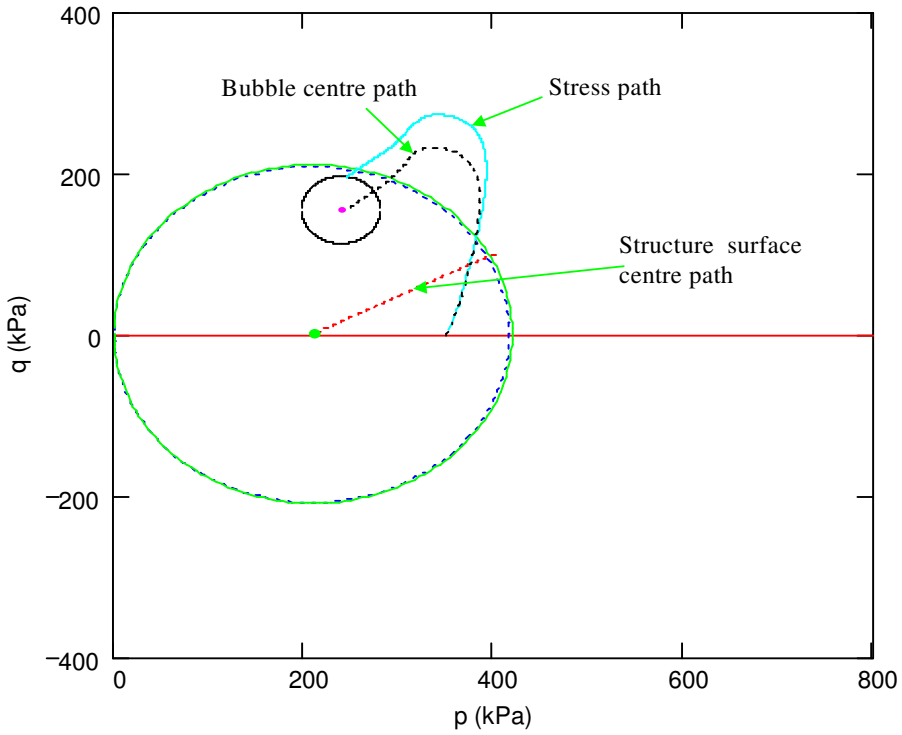

Figure 6.26 Surfaces after destructuration at 30% strain ($\eta_0 = 0.5$)

6.2.2 Example 2

Figure 6.27 shows three different initial stress conditions of the same structured soil as showed in Figure 6.18. Each case corresponds to a different location of the initial bubble but the structure and reference surfaces remain the same as before. The centre of bubble is at current stress point for each case. $\sigma_3^{'}$ is 100 kPa, 350 kPa and 600 kPa for Case 1, Case 2 and Case 3 respectively. The three cases correspond to cohesive soil which is in a very stiff state. The over-consolidation ratio is approximately 8 for case 1, 2.3 for Case 2 and 1.3 fro case 3. All other parameters are the same as those for the previous structured soil.

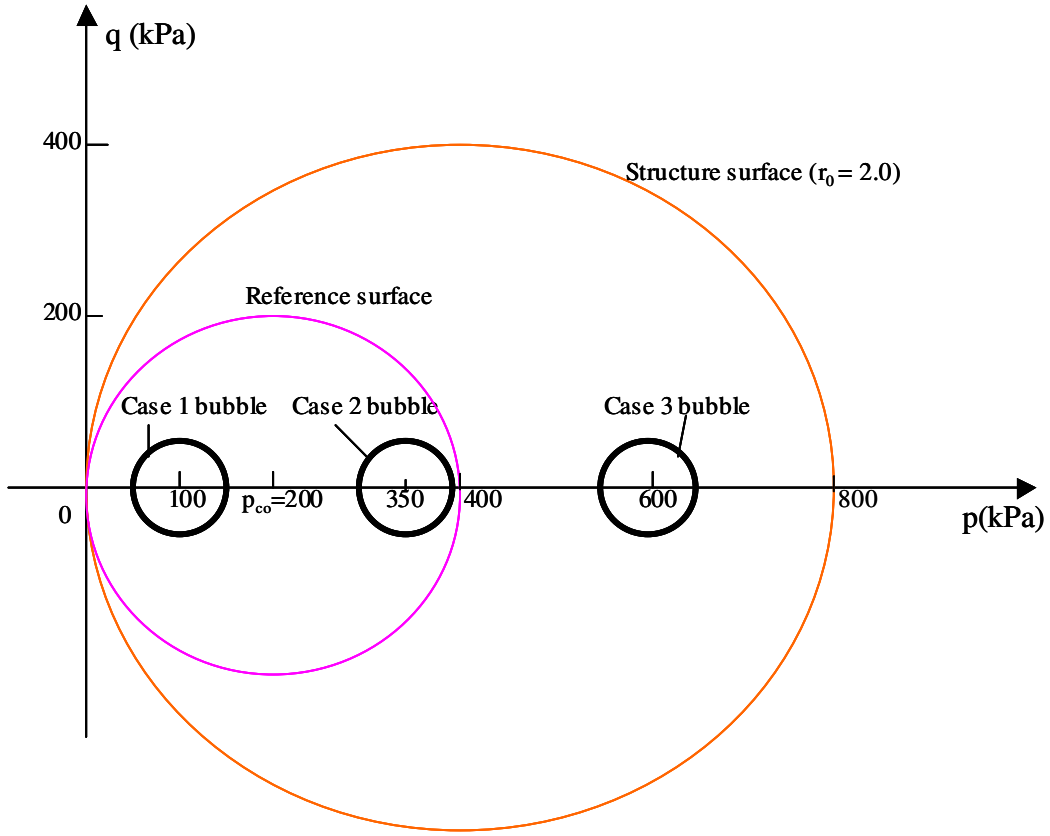

Figure 6.27 Initial stress conditions for three cases of a structured soil

The results are presented in Figures 6.28 to 6.30. It can be seen that small strain response including peak stress varies between the three cases due to variable initial stress states while there is no significant difference in residual stress. However, Figure 6.29 shows that the effective stress path for case 1 deviates from the CSL unlike the other two cases. This indicates that one single set of parameters can not satisfy all the three cases. Although their structure and reference surfaces are the same, some parameters may need to be adjusted individually to suit the different initial location of the bubble.

Figure 6.30(a) show pore water pressure for the three cases. Figure 30(b) shows the pore water pressure at small strain range for Case 1 only.

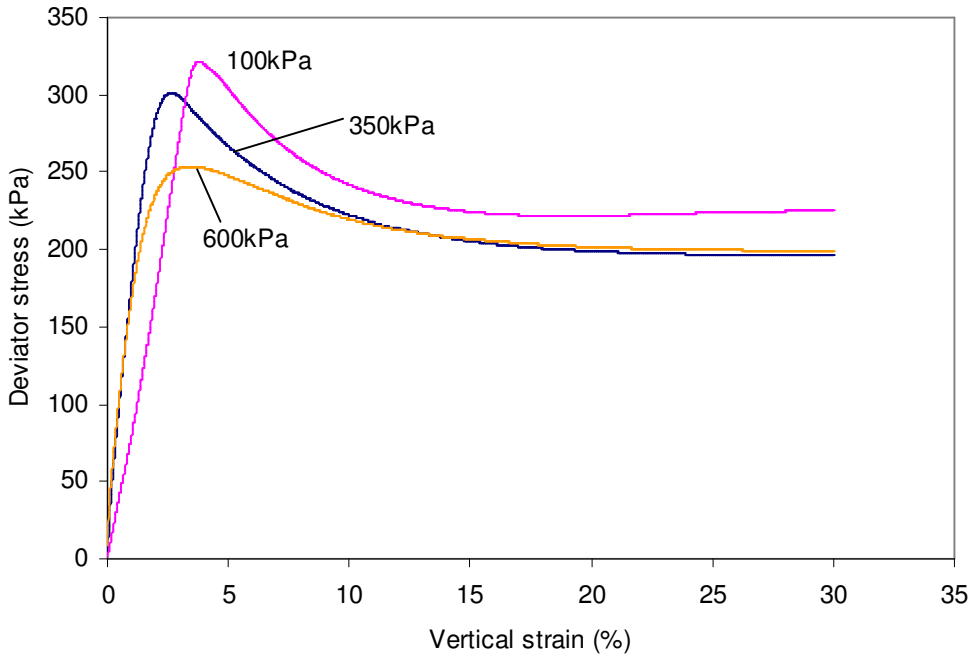

Figure 6.28 Undrained stress-strain behaviour of structured soil

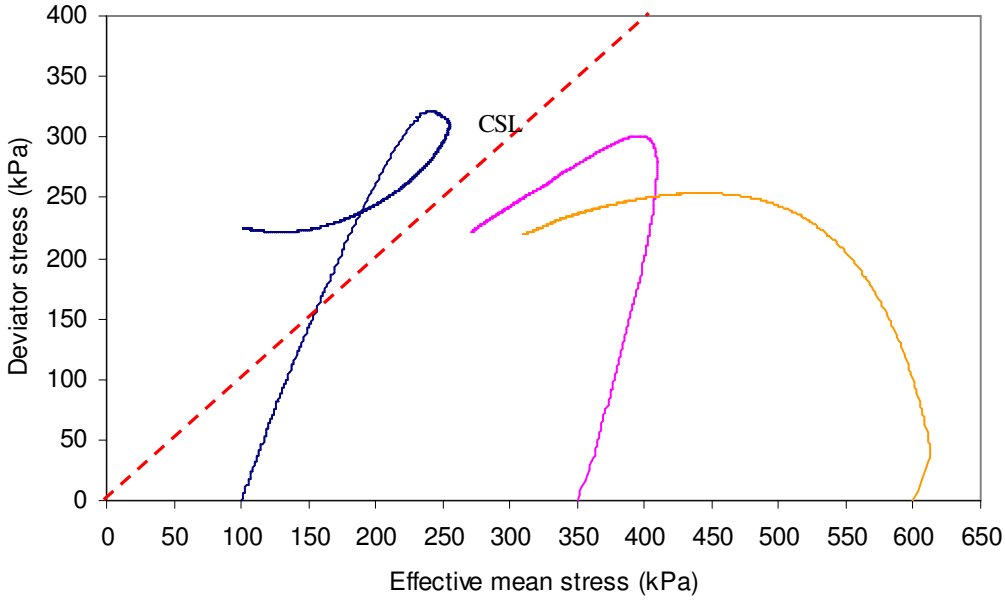

Figure 6.29 Effective stress path of structured soil

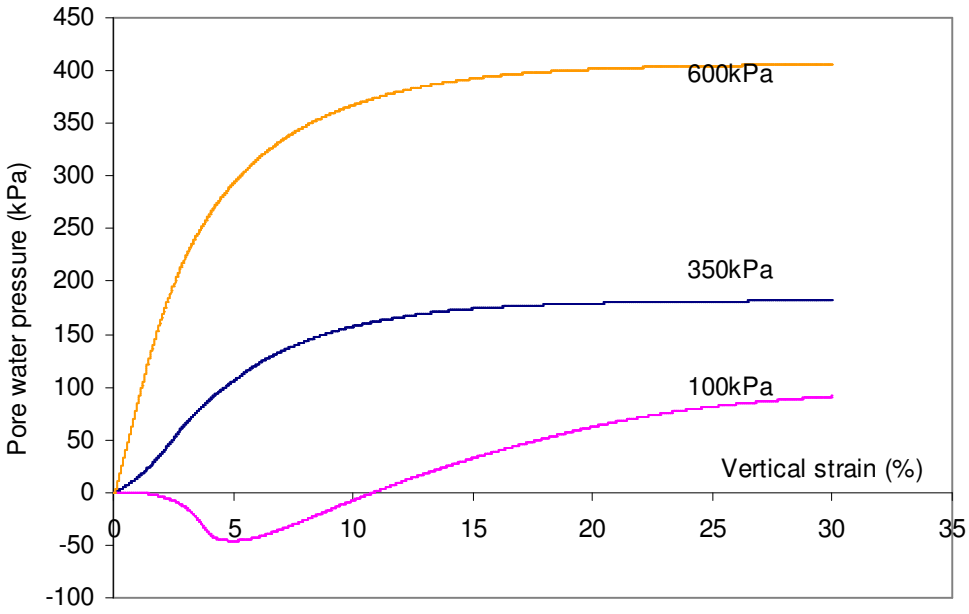

(a) Large strain for the three cases

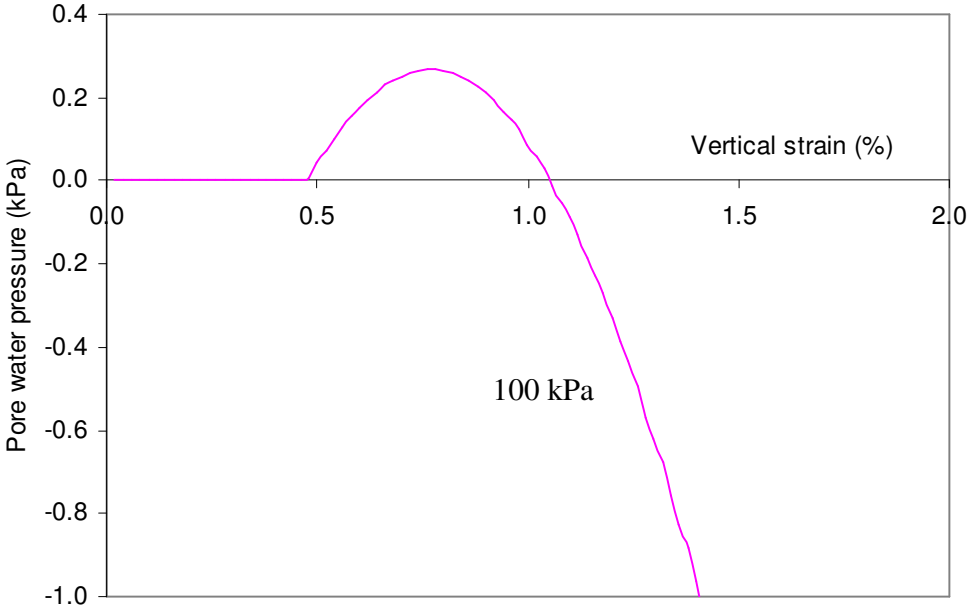

(b) Small strain for Case 1

Figure 6.30 Pore water pressure response of the structured soil

6.3 Comparison with the modified Cam-clay model

The bubble model can be reduced to the modified Cam-clay model when $R = 1$, $r_0 = 1$ and $\eta_0 = 0$. A *FISH* version of the modified Cam-clay model is available in *FLAC*. The Bubble model is compared with the modified Cam-clay model. Correlations between parameters of the two soil models have been discussed in Section 5.3. Two compatible sets of parameters and initial conditions for stiff cohesive soil are given as follows:

The Bubble model	The Modified Cam-clay model
$\lambda^* = 0.3$ $\kappa^* = 0.02$ $M = 1$ $m = 1$ $\mu = 0.25$	$\lambda = 0.426$ $\kappa = 0.0284$ $M = 1$ $\mu = 0.25$
$B = 400$ $\psi = 0.5$	$p_1 = 50\ kPa$ $v_1 = 2.0$ (reference point)
$p_{c0} = 200\ kPa$ $\sigma_3' = 200\ kPa$	$p_{c0} = 400\ kPa$ $\sigma_3' = 200\ kPa$

Figure 6.31 shows a good agreement in stress-strain behaviour between the two models. A value of 0.998 is used for parameter R instead of 1.0 to avoid execution of a quantity being divided by zero in computing hardening modulus (see Equations 5.14 and 5.18 in Chapter 5).

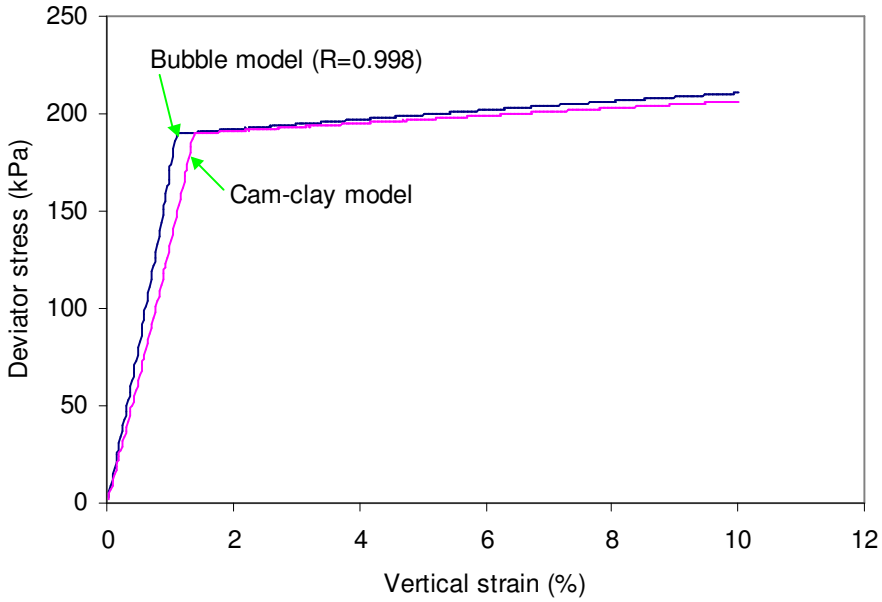

Figure 6.31 Comparison with modified Cam-clay model (Drained)

6.4 Comparison with experiment

Experimental data used herein for comparison was published by Lee and Seed (1967). The soil used in their experiment was fine uniform sand which was dredged from Sacramento River about 30 miles upstream from San Francisco Bay. The specific gravity and limiting void ratio were $G_s = 2.68$, $e_{min} = 0.61$ and $e_{max} = 1.03$. Tests were performed on samples prepared to four initial densities. The loose sample had an initial void ratio of 0.87, a relative density of 38% and a frictional angle of 34˚. Three drained triaxial test results of the loose sample are used here for comparison. The confining pressure is 100 kPa, 450 kPa and 2000 kPa respectively.

It is appropriate to assume that the sand was non-structured as it was reconstituted, i.e. $r_0 = 1$. The parameter R can be assumed to be the same for the three tests. Key parameters to be selected are initial size of the structure surface (p_{c0}) and hardening modulus parameters (B and ψ). Parameter ψ controls curvature of a stress-strain curve. For a qualitative comparison, it is reasonable to assume ψ to be the same for the three tests and only to vary parameter B for each test. It was reported that the sand was relatively incompressible at low pressures and at high pressures there was considerable volume change due to crushing of grains (See Figure 6.32). To simulate the three tests, parameters of the Bubble model are given as follows and initial stress conditions of the three samples are shown in Figure 6.33.

$\lambda^* = 0.3$ $\kappa^* = 0.02$ $M = 1$ $m = 1$ $\mu = 0.3$

$R = 0.15$ $\eta_0 = 0$ $\psi = 1$

σ_3 (kPa)	B	p_{c0} (kPa)
100	600	300
450	1800	900
2000	25000	1200

Note: For non-structured soils A *and* k *are not used.*

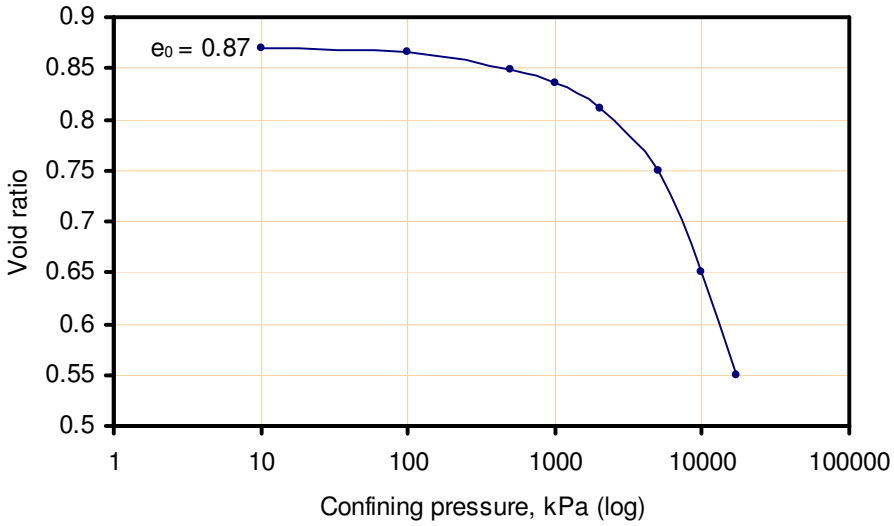

Figure 6.32 Pressure-void ratio curve for loose sands.
(redrawn after Lee and Seed, 1967)

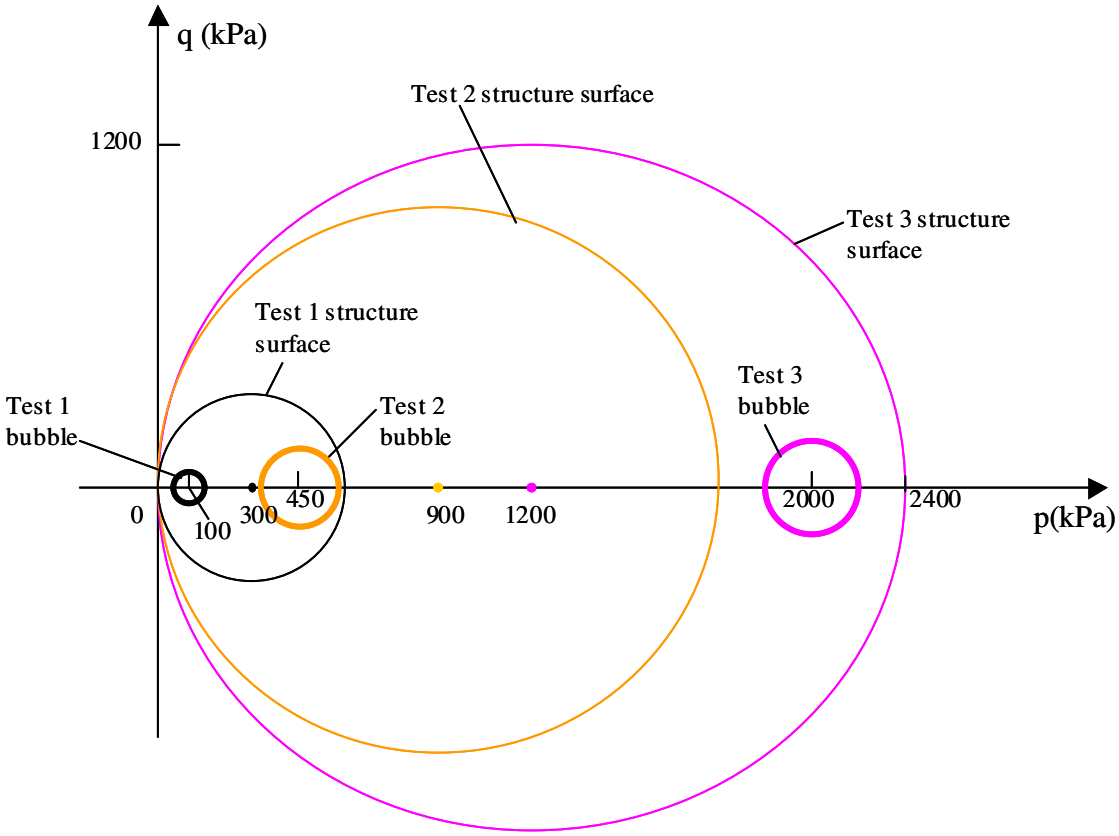

Figure 6.33 Initial stress conditions of three tests

A general agreement in stress-strain-volume behaviour between the modeling and test results can be seen from Figures 6.34 (a) and (b), where solid curves present results of the modeling. The difference is generally smaller at high confining pressures than at low confining pressures. However variation in small-strain behaviour is not insignificant, especially for low confining pressures. The Bubble model with the selected parameters predicts smaller moduli and less dilative behaviour than the experiment. Therefore, for further research, more comparisons with laboratory testing results are required to identify the capabilities and limitations of the Bubble model. Stress-strain behaviour at small strain of the model will be studied in Chapter 7.

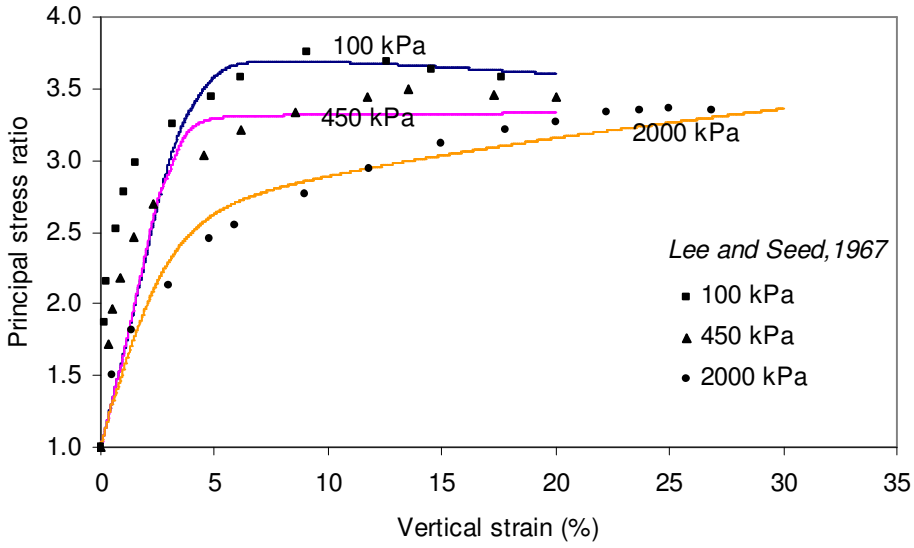

(a) Stress-strain behaviour of loose sand

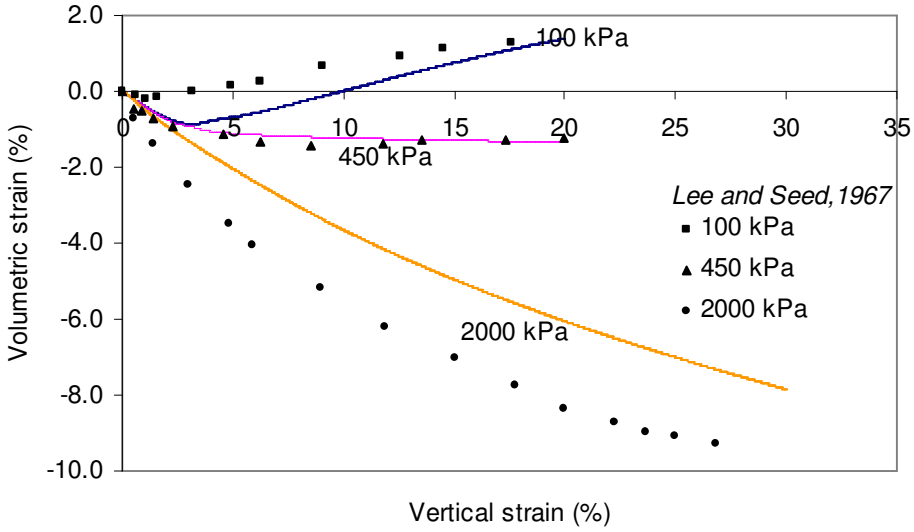

(b) Volumetric behaviour of loose sand

Figure 6.34 Comparison of Bubble model with published experiment data

6.5 Dynamic behaviour of the Bubble model

The main purpose to employ the 'plastic correction' approach in implementing the Bubble model in *FLAC* is to minimise numerical distortion (non-physical instability) without applying any additional damping. To verify whether or not this has been achieved, dynamic performance of the Bubble model is investigated under both drained and undrained conditions. For drained condition, a steady state response should be reached after an initial vibration and should stay reasonably stable. For undrained condition, whether or not a steady state response can be reached and can stay stable depends on generation of pore water pressure. If cyclic change in pore water pressure is small, the steady state response should also stay stable (*i.e.* non-liquefiable).

6.5.1 A single-zone *FLAC* triaxial model

A single zone axisymmetrical model is utilised to represent a dynamic triaxial test (see Figure 6.35). The zone is a 0.1 m by 0.1 m square. The only reason to use a square zone is to avoid another type of numerical distortion which may occur in dynamic analysis if non-squared zones are used. The zone size is chosen to be much smaller than 10% of the shear wave wavelength of soil so that no size effects will be introduced into the modelling.

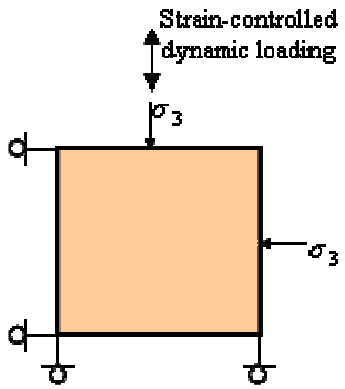

Figure 6.35 A single zone triaxial model

Non-structured loose sand is considered for the analysis herein with the parameters given as follows:

$\lambda^* = 0.3$ $\kappa^* = 0.02$ $M = 1$ $m = 1$ $\mu = 0.25$ $R = 0.2$ $B = 400$ $\psi = 1.0$ $p_{c0} = 100\ kPa$

Two initial stress conditions are considered. σ_3' is 50 kPa for Case1and 150 kPa for Case 2. The single zone model is subjected to a strain-controlled sinusoidal loading with a magnitude of maximum vertical strain of 2.5% and a frequency of 1Hz.

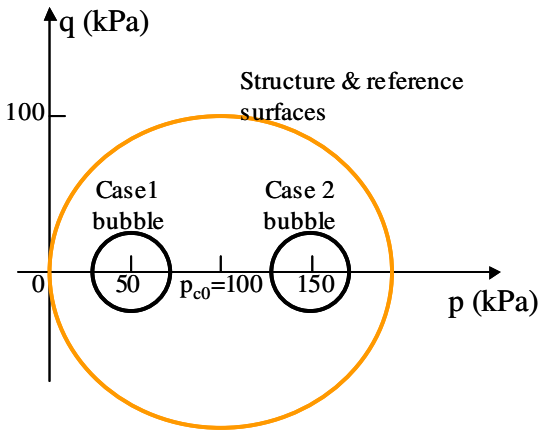

Figure 6.36 Initial stress conditions

For both drained and undrained conditions steady state responses are reached and they stay stable within 200 cycles (see Figures 6.37 to 6.45). For clarity only Figure 6.43 shows the response up to 200 cycles while all other figures only show responses up to 40 cycles.

Figures 6.37 and 6.38 show the drained stress-volume-strain response for Case 1 (σ_3'= 50 kPa). Dilative behaviour is obtained, which results in a cyclic increase in volume before a constant magnitude and amplitude of volume are reached. The amplitude of deviator stress and stiffness of soil decrease cyclically due to dilation before the steady state is reached.

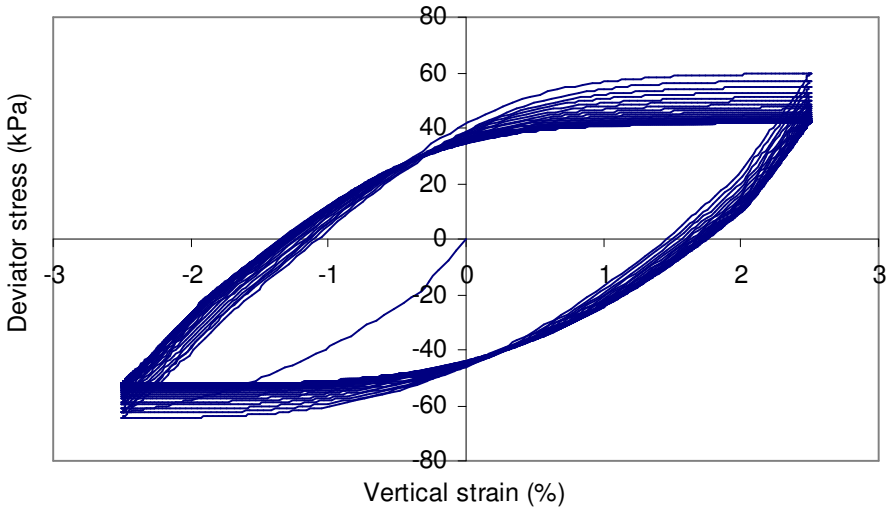

Figure 6.37 Drained dynamic stress-strain behaviour of Case 1 soil

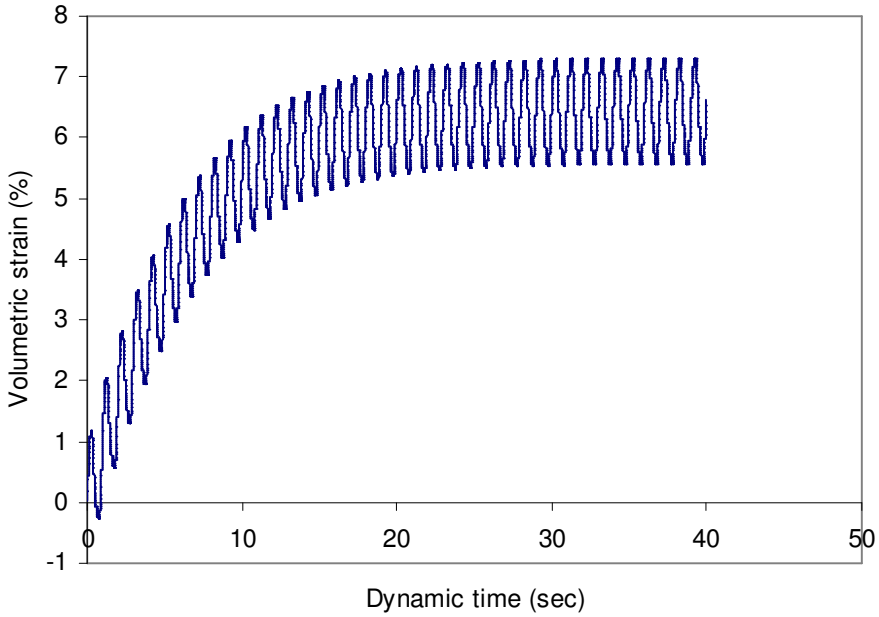

Figure 6.38 Dynamic volumetric response of Case 1 soil

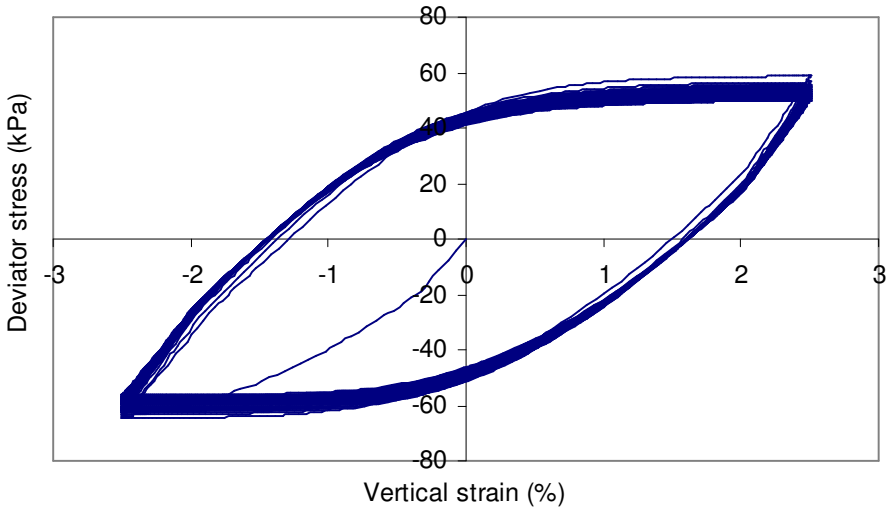

Figure 6.39 Undrained dynamic stress-strain response of Case 1 soil

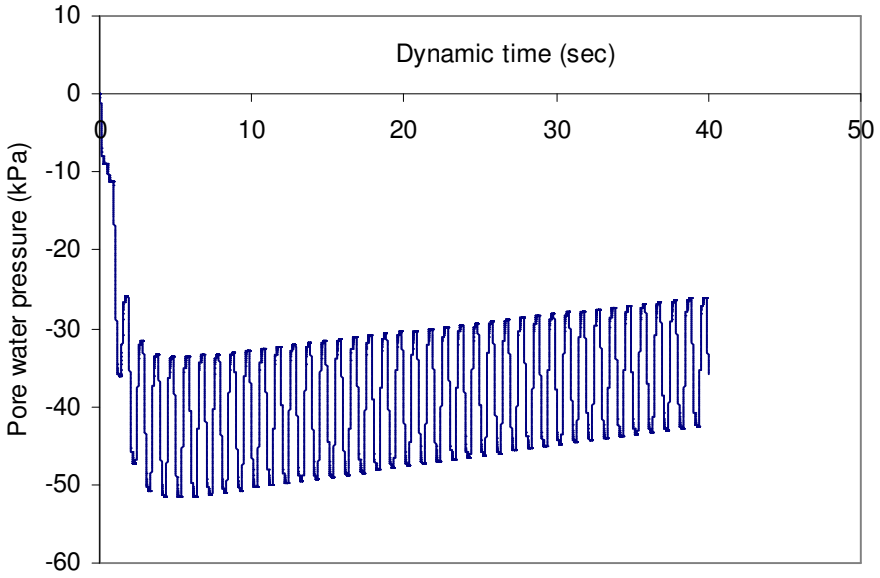

Figure 6.40 Dynamic pore water pressure of Case 1 soil

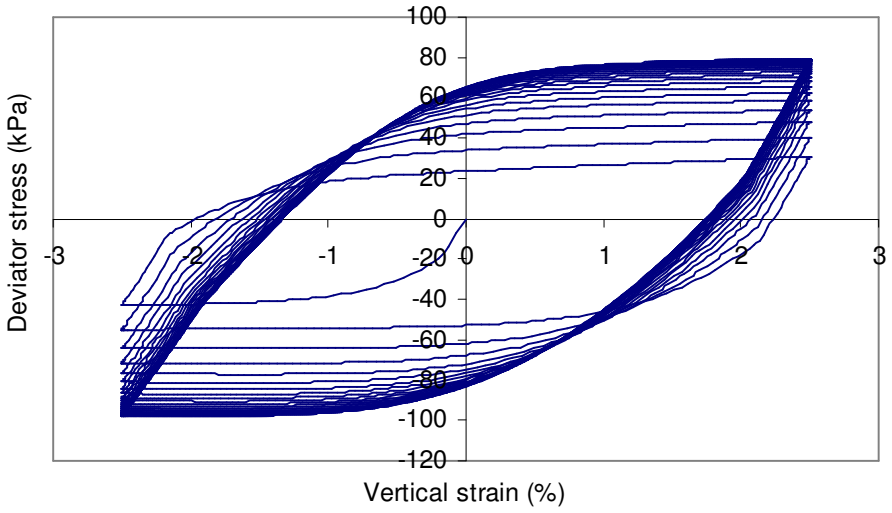

Figure 6.41 Drained dynamic stress-strain behaviour of Case 2 soil

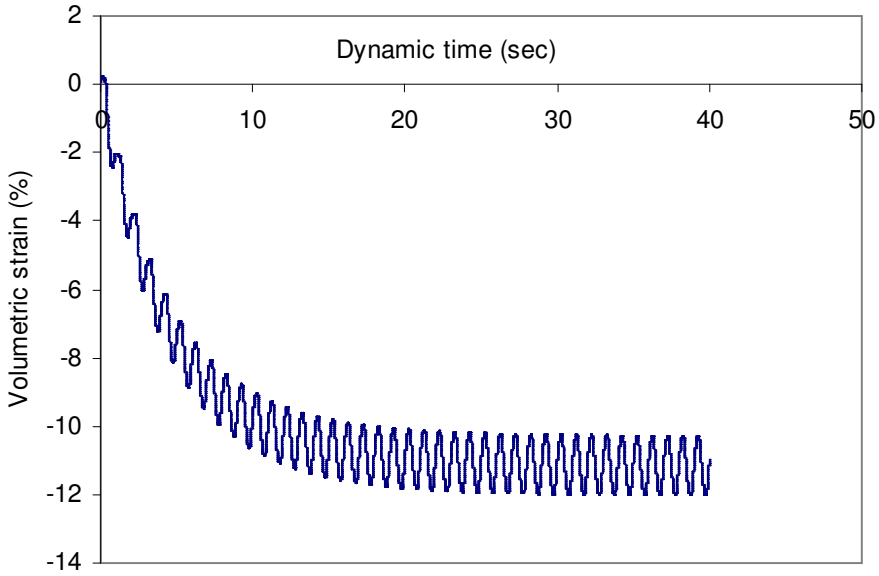

Figure 6.42 Dynamic volumetric response of Case 2 soil (40 cycles)

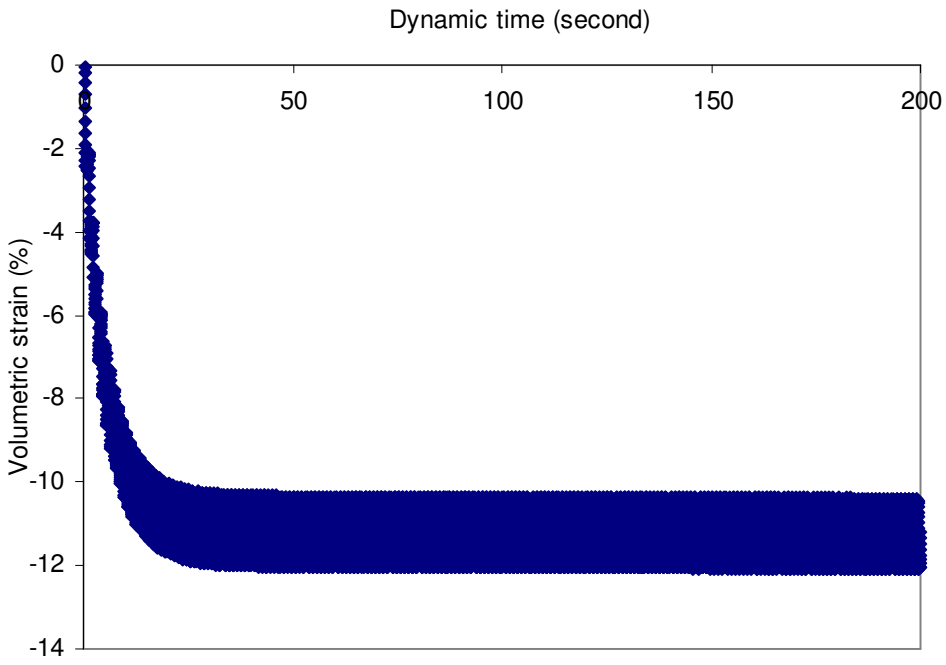

Figure 6.43 Dynamic volumetric response of Case 2 soil (200 cycles)

Figure 6.40 shows that negative pore water pressure is generated, which reach its maximum magnitude in only a few cycles and decreases gently with approximately a constant amplitude. This corresponds to a stable stress-strain response and the cyclic change in stiffness is insignificant (see Figure 6.39)

Drained stress-strain-volume responses of Case 2 soil (σ_3' = 150 kPa) are shown in Figures 6.41 and 42. It can be seen that there is a cyclic densification in volume and hence a cyclic increase in stiffness of soil before the steady state is reached. The steady state response stays stable for the whole duration of vibration (See Figure 6.43).

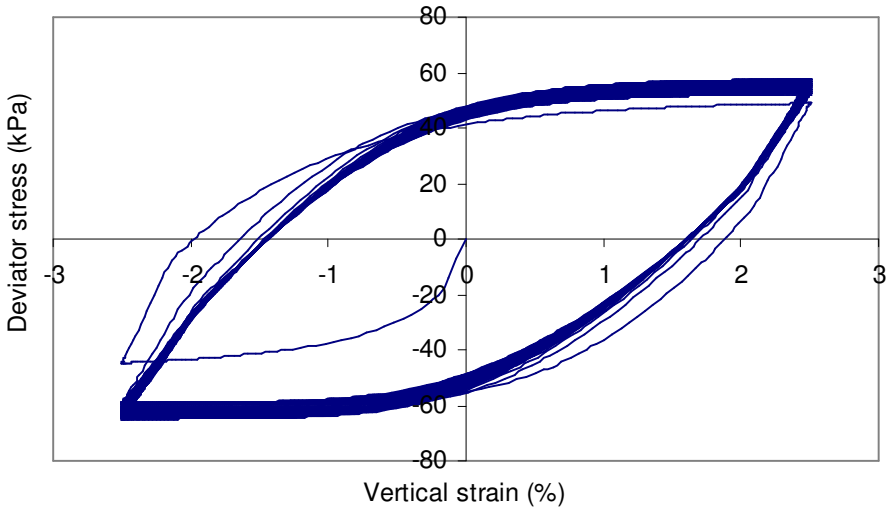

Figure 6.44 Undrained dynamic stress-strain response of Case 2 soil

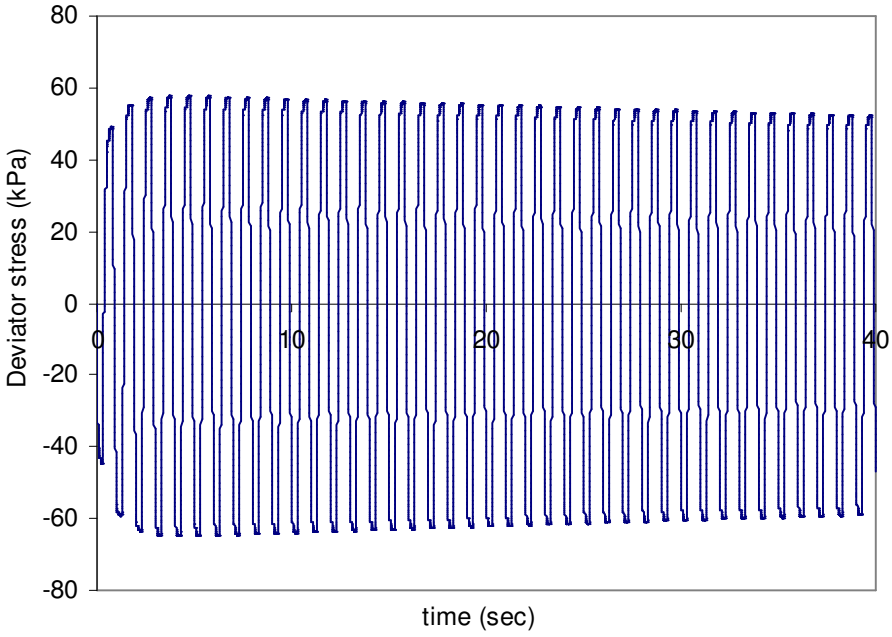

Figure 6.44a Cyclic response of undrained deviator stress of Case 2 soil

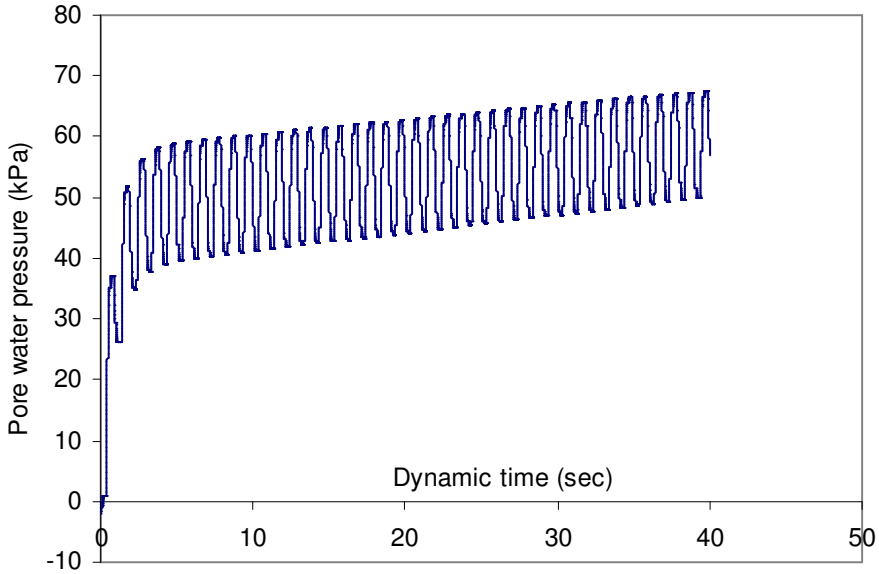

Figure 6.45 Dynamic pore water pressure of Case 2 soil

Undrained responses are similar to those of Case 1 soil except that the pore water pressure is positive (see Figure 6.45). However, the model predicts a stiffness increase in the first three cycles (see Figures 6.44 and 6.44a). This is inconsistent with cyclic behaviours of soils normally observed in laboratory, *i.e.* the stiffness should decreases with the development of a positive pore water pressure. The causes of this disparity remain to be investigated in the future research.

6.5.2 A multizone *FLAC* triaxial model

A multizone numerical model is utilized to represent a triaxial specimen which is 0.2 m in diameter and 0.4 m in height. The model consists of 16 square zones. The size of each zone is 0.05 m.

The same parameters as those for the single-zone model are used except the initial confining pressure is increased to 300 kPa (see Figure 6.46). This is to avoid generation of tensile mean stresses during vibration as the Bubble model does not allow tensile mean stress. Accordingly the initial centre of the structure surface is increased to 200 kPa. The

amplitude of strain is reduced to 1% for the same purpose. The frequency is increased to 10 Hz to further investigate dynamic performance of the model as the higher the frequency is, the more severe the numerical distortion could be.

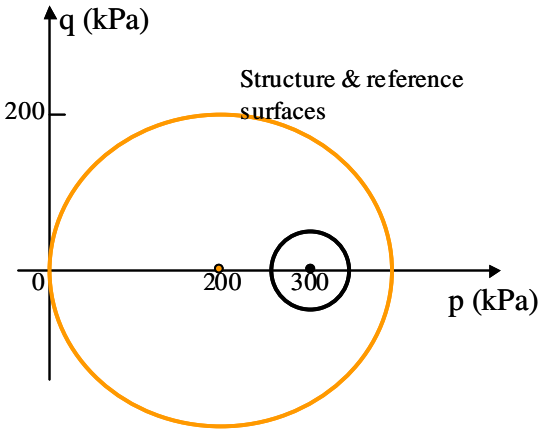

Figure 6.46 Initial stress state of the multizone FLAC model

Undrained dynamic responses of the multizone model are shown in Figures 6.47, 6.47a and 6.48. Results are similar to those of the single-zone model for Case 2 soil. A stable stress-strain response is obtained without using any additional damping.

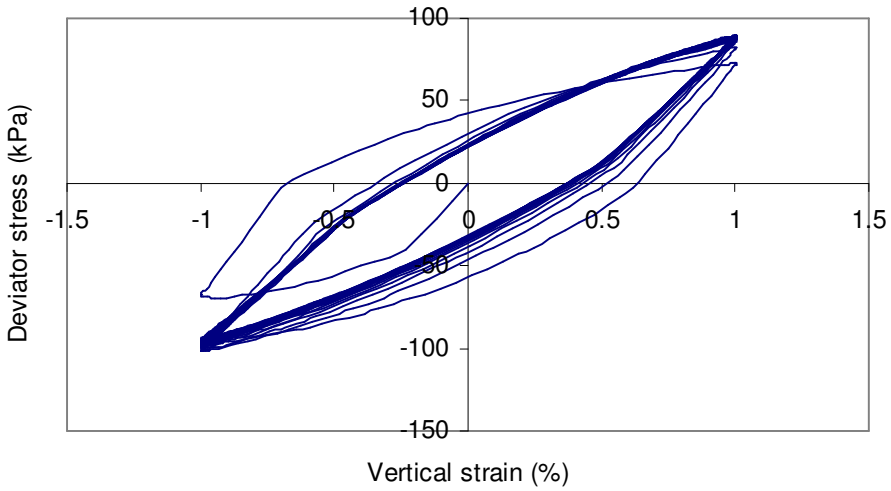

Figure 6.47 Undrained dynamic stress-strain response of a multizone triaxial model

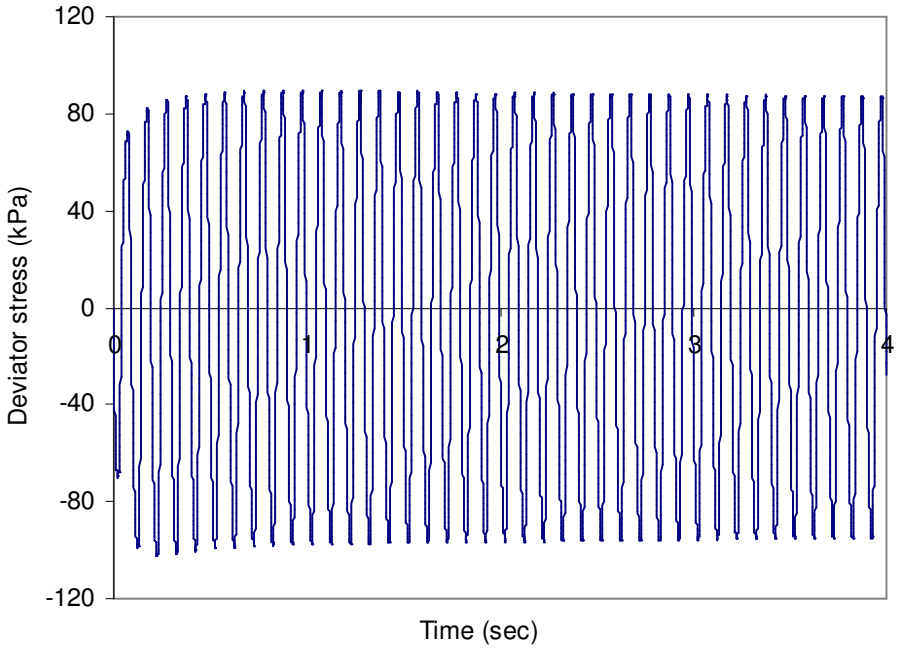

Figure 6.47a Cyclic response of undrained deviator stress of a multizone triaxal model

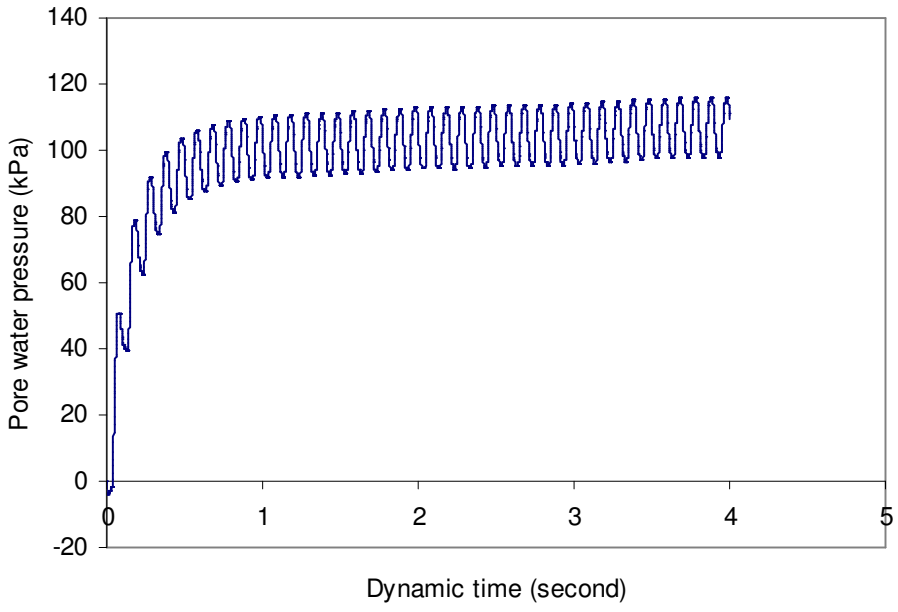

Figure 6.48 Dynamic pore water pressure (40 cycles)

6.6 Summary

The Bubble model has been implemented in *FLAC* with the 'plastic correction' approach. In this chapter fundamental features of the Bubble model have been demonstrated with the *FLAC* programme. The Bubble model has been found to be able to simulate essential behaviours of both remoulded and structured soils. The non-intersection condition between the bubble and the structure surface has been verified. Destructuration process for structured soil has also been illustrated.

The Bubble model has been further verified by its comparison with the modified Cam-clay model and published experimental data (*Lee* and *Seed* 1967). Good agreement has been obtained.

Dynamic performance of the Bubble model has been investigated for both single-zone and multi-zone *FLAC* models. It has been found that a stable response can be obtained without using any additional damping. This verifies that numerical distortion problem in nonlinear dynamic analysis can be eliminated or minimised by means of the implementation methodologies used in this thesis.

The data file for the triaxial model is attached to Chapter 7.

7 PARAMETRIC STUDY OF THE BUBBLE MODEL

The bubble model requires ten soil parameters and some initial conditions. Five of the parameters are similar to those of the Cam-clay model, *i.e.* $\lambda^*, \kappa^*, M, m$ and μ and they can be obtained directly from laboratory tests while the other five are non-standard parameters, *i.e.* R, B, ψ, k, A. Initial conditions include $r_0, \eta_0, p_{c0}, \sigma_{30}$. The non-standard parameters and most of the initial conditions can not be obtained directly from laboratory tests. For a specific type of soil, determinations of these parameters and the initial conditions rely on curve-fitting between numerical modelling and experimental results (Also see discussions in Section 5.3).

The objective of this chapter is to investigate influence of the above parameters and initial conditions on behaviour of the bubble model and importance of each parameter. Particularly qualitative study is carried out to investigate influence of bubble size *R* and plastic modulus parameter *B*. Results obtained from this chapter provide a general guidance in choosing parameters for application of the bubble model in Chapter 8.

The parametric a study is carried out by using a set of selected parameters and varying one parameter while assuming other parameters unchanged although, in reality, some of the parameters are inter-related. This may result in unrealistic behaviours of the model. However, the assumption is considered to be necessary and appropriate for the purpose of parametric study.

7.1 Typical values of parameters

Typical values of parameters are given as below, which are utilised as reference parameters for parametric study.

Table 7.1 Typical soil parameters for parametric study

λ^*	κ^*	M	m	μ	R	B	ψ	k	A	K_0 (MPa)
0.3	0.02	1.0	1.0	0.25	0.2	600	0.5	4	0.5	0

Note: all parameters are dimensionless except K_0 which is elastic bulk modulus associated with zero confining pressure (see Eq.5.22)

Initial conditions are specified as follows:

$r_0 = 1.0,\ \eta_0 = 0$

$p_{c0} = 200\ kPa,\ \sigma'_3 = 200\ kPa$

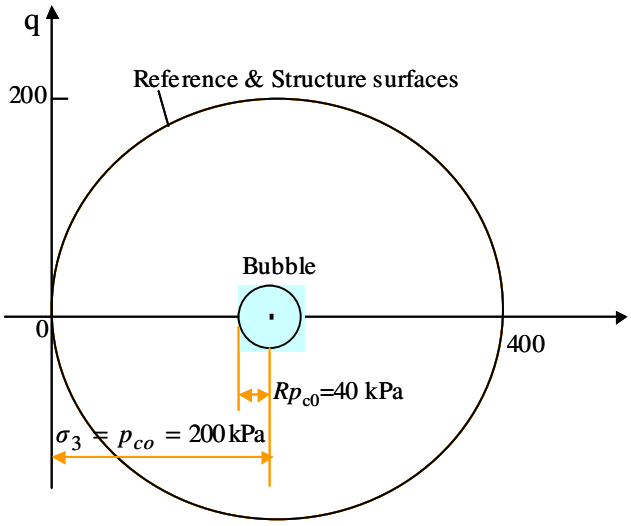

Figure 7.1 Initial locations of surfaces associated with reference parameters

The above parameters are chosen to represent non-structured soil (r_0= 1.0 and $\eta_0 = 0$, *i.e* structure surface coincides with reference surface as shown in Figure 7.1). The initial conditions correspond approximately to cohesive soil with an undrained shear strength of 100 kPa. An initial elastic bulk modulus of 10 MPa is calculated form Eq.5.22 and this corresponds to a shear modulus of 6 MPa and a Young's modulus of 15 MPa.

Plastic modulus parameters (B and ψ) control degradation of stiffness when plastic deformation occurs and affect performance of the model significantly. Little past experience can be based upon for determination of the two parameters. Preliminary study indicates that a value of 600 for B and 0.5 for ψ are suitable in this case.

In order to model nonlinear behaviours of soil at very small strain, a very small bubble size is required, *i.e*. parameter R should be close to zero. However, this will require a very small timestep in analysis (*e.g*. less than 10^{-8} m displacement or 10^{-5} % strain per step for a single element model) while a timestep of 10^{-6} m displacement per step is found to be suitable for most cases. Therefore use of a very small bubble will cause significant computational burden. A value of 0.2 for parameter R is considered to be appropriate for the parametric study. The value is similar to those used by Rouainia & Wood (2000) and Gajo & Wood (2001). They suggested that R has a minor role in affecting overall behaviours of the model compared to parameter B.

Parameters A and k do not affect behaviours of non-structured soils. For structured soils, A can be varied in a range between 0 and 1. Herein A is given a value of 0.5, which means that volumetric and distortional strains are equally taken into account in destructuration law. This is a special case of the bubble model, which is equivalent to S3-SKH model (Baudet and Stallebrass, 2004). k is an arbitrary parameter that controls the rate of destructuration. A value of 4.16 was used for Norrköping clay by Rouainia & Wood (2000) and 0.5 for Bothkennar clay by Baudet and Stallebrass (2004). Herein k is taken to be 4 as a reference value.

Standard parameters λ^*, κ^*, M, m and μ are selected in normal ranges for clay. It needs to be pointed out that Poisson's ratio, μ, is taken to be 0.25 for both undrained analyses (i.e. same as the drained analyses) because effective stresses are utilized in the bubble model. Gajo & Wood (2001) found that Poisson's ratio has a less important role than other parameters. m is a ratio between radii of sections through structure surface for axisymmetrical extension and compression in deviatoric plane, which should be between

0.7 and 1.0 to ensure convexity. Herein *m* is taken to be 1.0 by assuming behaviour of soil in extension is identical to that in compression.

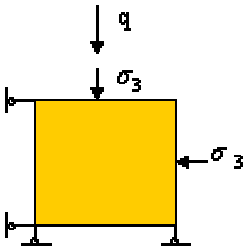

Figure 7.2 Single-element triaxial model

An axisymmetric numerical model comprising a single square element is utilized to model the conventional triaxial test. A square element is considered to be better than a non-square one in reducing numerical errors. Although the single-element model does not match the shape of a real triaxial specimen, it is considered to be suitable for the qualitative study herein.

7.2 Size of bubble

Introduction of a smaller yield surface into the bubble model is to reduce elastic range of soil. The size of elastic range (*i.e*. bubble) is represented by parameter *R* in the bubble model. Figure 7.3 shows stress-strain curves for a range of values of *R*. To show the elastic range clearly, *B* is given a smaller value of 300 rather than the reference value of 600 as the larger the value of B, the smoother the transition of stiffness when the bubble is engaged(see Section 7.3).

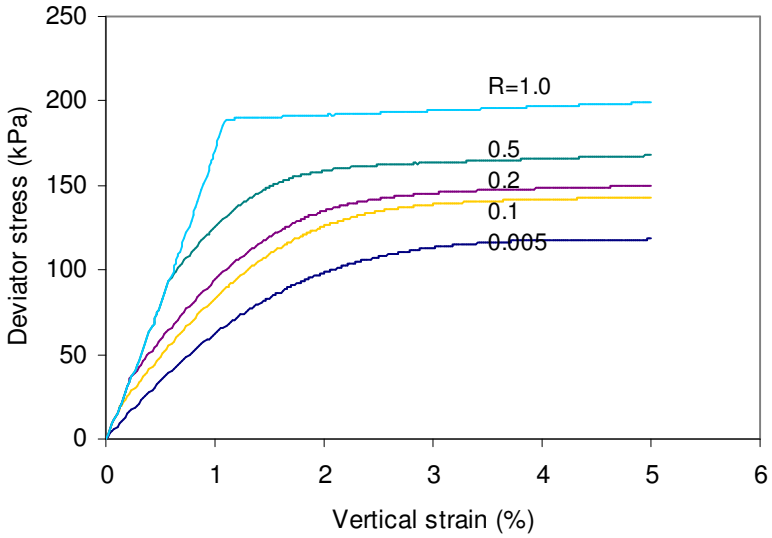

Figure 7.3 Elastic range vs bubble size (B = 300, drained)

The curve for R =1.0 is equivalent to the result of the modified Cam-clay, indicating an apparent elastic range up to a vertical strain of 1% in this case while the curve for R = 0.005 shows a nonlinear behaviour from the beginning of loading.

For most natural soils elastic range is very small. Hence a small value of R should be used so that a smooth transition in modulus can be obtained. However this increases computational time significantly as a much smaller timestep must be used to avoid errors during elastic trial. Otherwise, stress may drift from the bubble. When larger values of R have to be used one has to find a suitable value of B to get a smooth transition in stiffness (See Section 7.7).

Although R affects small strain behaviour, it has little effect on ultimate stress of soil and the stress-strain behaviour at large strains as long as a suitable value of B is selected. This can be seen from Figures 7.4 and 7.5.

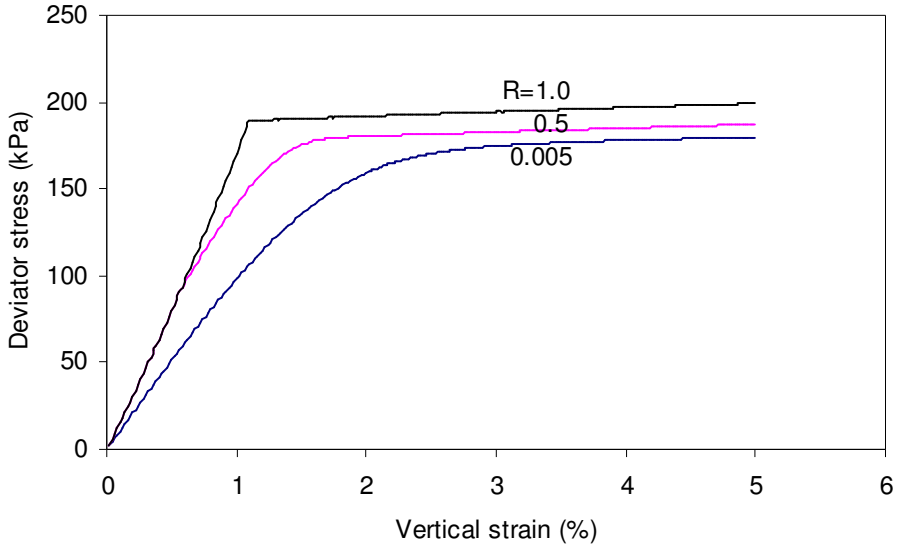

Figure 7.4 Stress-strain behaviour (B =500, drained)

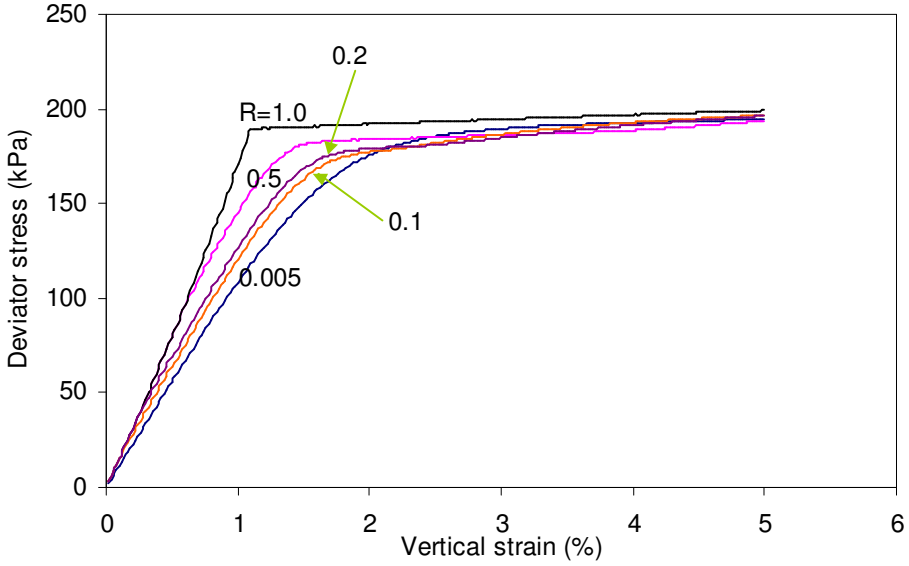

Figure 7.5 Stress-strain behaviour (B=600, drained)

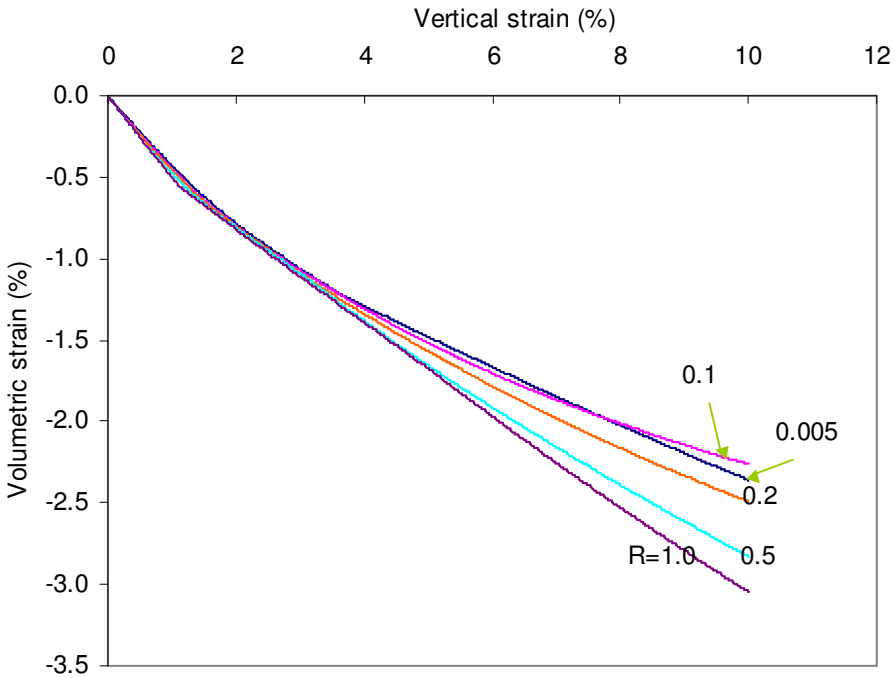

Figure 7.6 Influence of R on volumetric behaviour (B=600, ψ =0.5, drained)

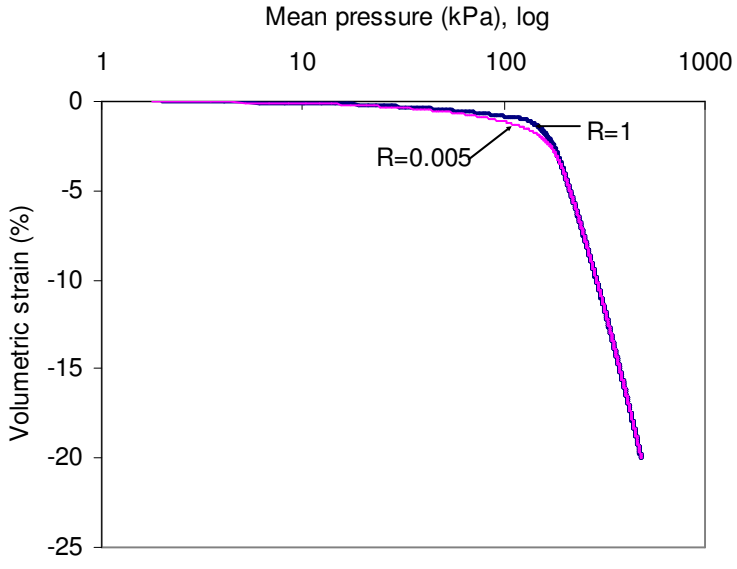

Figure 7.7 Volumetric strain vs mean pressure (B = 600)

It can also be seen from Figure 7.6 that R has only minor influence on volumetric strain. Figure 7.7 shows that R has little influence on relationship between volumetric strain and mean pressure. An oedometer test is simulated by allowing only vertical deformation for the single element model. An initial all-round pressure of 200 kPa is applied to the model so that the model has an initial stiffness prior to loading (Note: bulk modulus is given by $K = \frac{p'}{\kappa^*} + K_0$ and K_0 is zero herein). The mean effective pressure for the plot is the total mean effective pressure acting on the model less the initial all-round pressure.

The results so far suggest that R has little effect on the overall stress-strain response of the bubble model when R is less than 0.2. The following analyses are carried out to check if this is still true when other parameters are changed. To ensure realistic results, B is varied accordingly as B is found to be inter-related to these parameters (see Section 7.3). Figures 7.8 to 7.11 show similar results even when parameters $\psi, \mu, \lambda^\bullet, \kappa^\bullet$ are varied significantly.

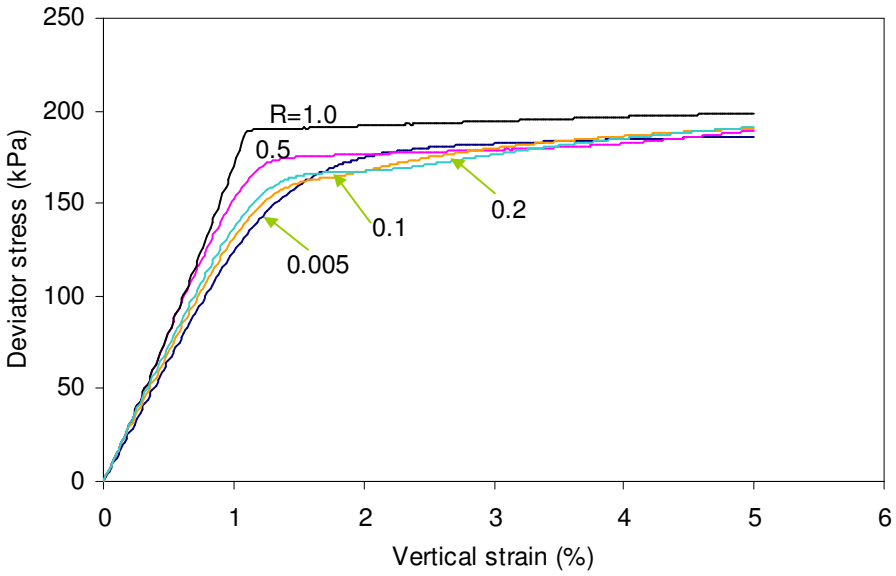

Figure 7.8 Stress-strain behaviour (ψ=1.0, B=1500, drained)

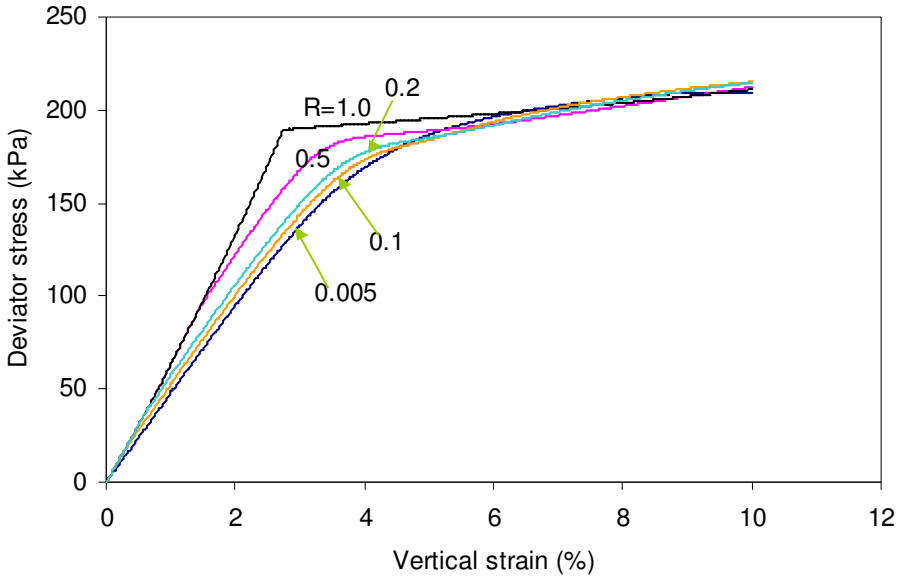

Figure 7.9 Stress-strain behaviour ($\mu = 0.35$, B =250, drained)

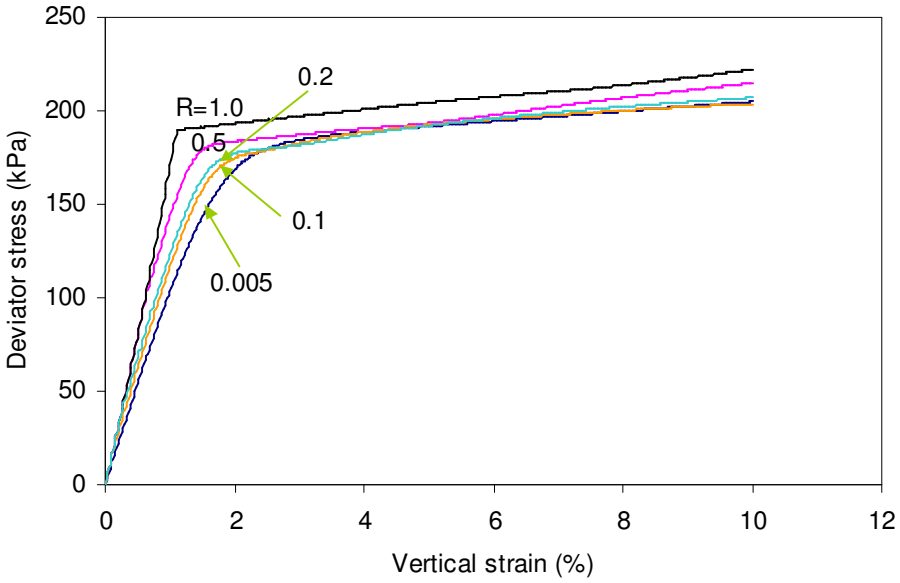

Figure 7.10 Stress-strain behaviour ($\lambda^* = 0.2$, B = 350, drained)

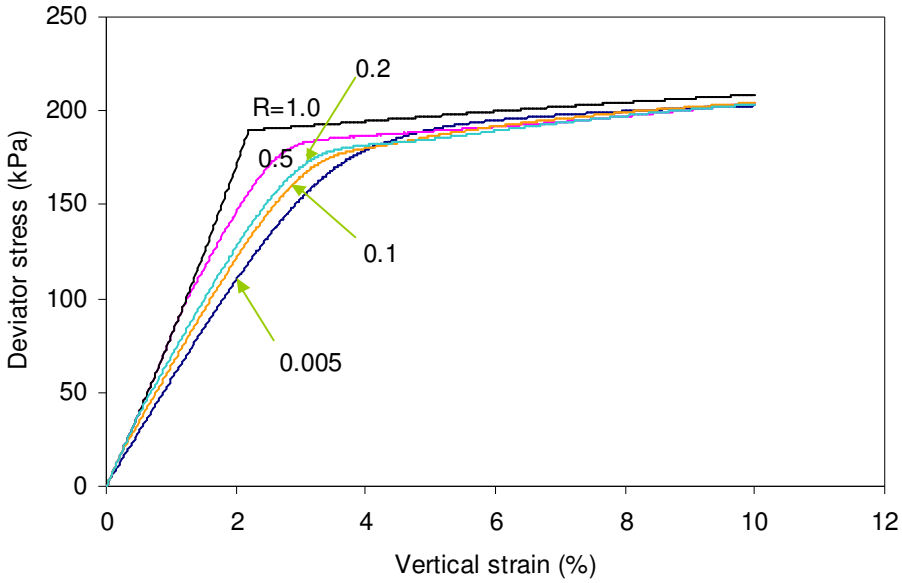

Figure 7.11 Stress-strain behaviour ($\kappa^* = 0.04$, B = 280, drained)

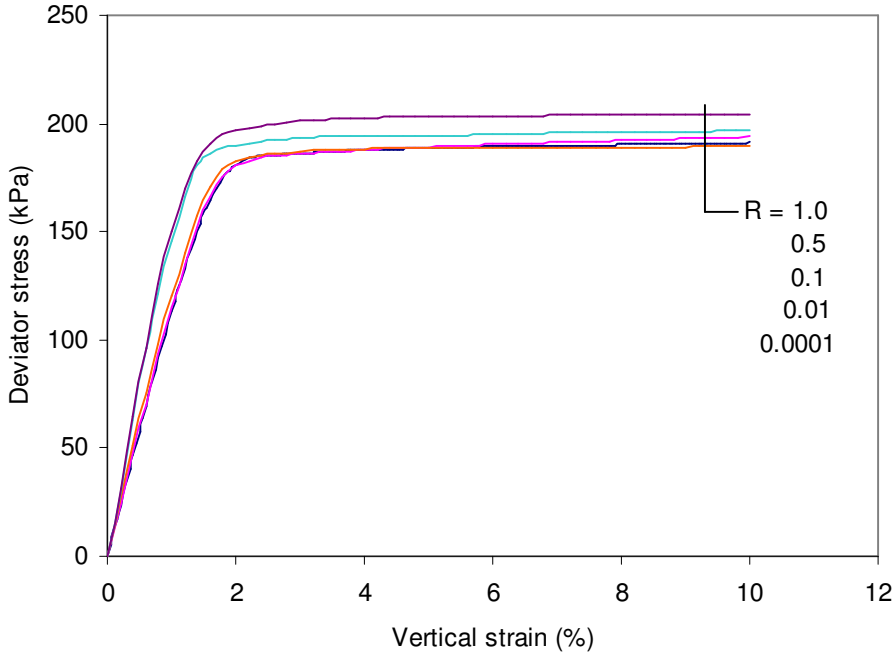

Figure 7.12 Undrained stress-strain behaviour

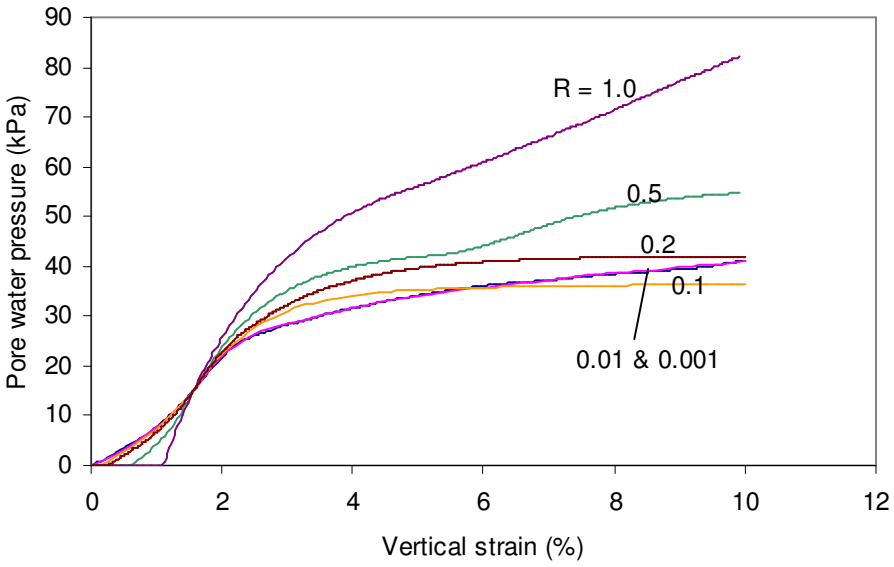

Figure 7.13 Pore water pressure

Figure 7.12 shows that the undrained stress-strain behaviour is also insensitive to the parameter *R* although pore water pressure may increase sharply at high strain levels when *R* is greater than 0.2 (see Figure 7.13). It is also noticed that the same pore water pressure is generated by the model at a particular strain level regardless of the value of *R*.

It can be concluded from the above study that if one is not particularly interested in small strain behaviour of the model, *e.g* G – γ relationship (see Section 7.7), *R* can be selected within a range of 0.1 to 0.2. Unless specified, *R* is 0.2 in the following analyses.

7.3 Plastic modulus parameters '*B* and ψ '

B and ψ are two plastic modulus parameters, which significantly affect stress-strain behaviour of the bubble model after yielding takes place. *B* controls magnitude of stiffness and ψ controls rate of degradation in stiffness.

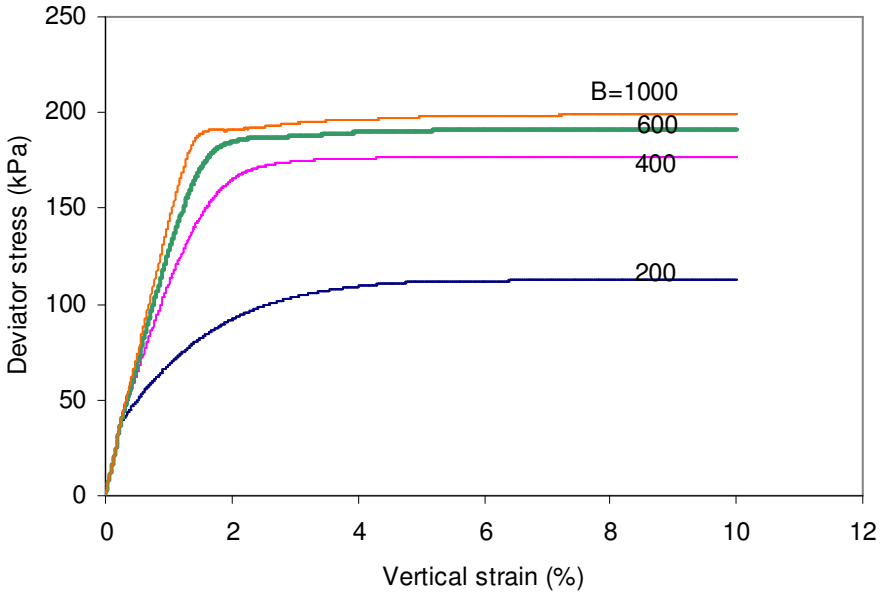

Figure 7.14 Influence of 'B' on stress-strain behaviour (ψ =0.5, R = 0.2)

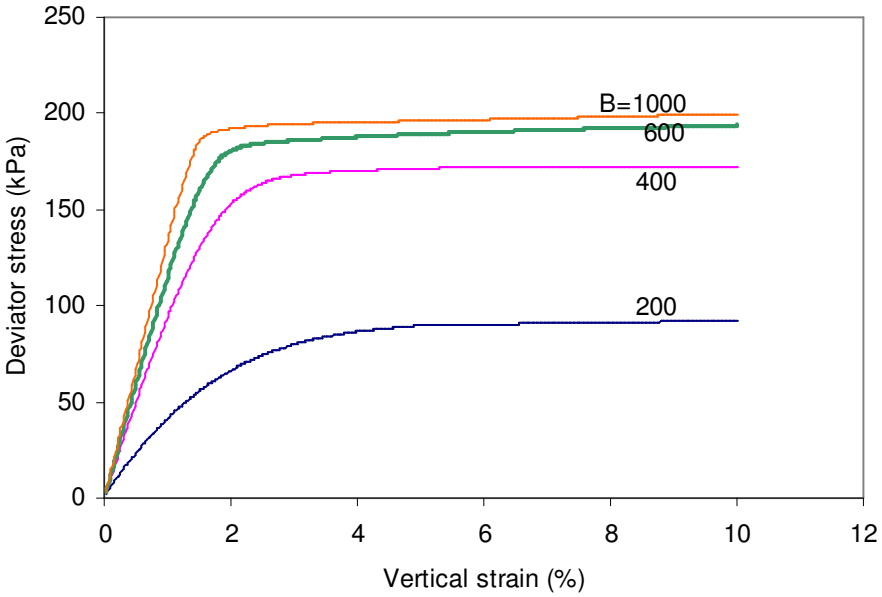

Figure 7.15 Influence of parameter B (ψ = 0.5,R=0.01)

Figure 7.14 shows that post-yielding stiffness of soil increases with B and the larger the value of B, the smoother the transition in stiffness. However the relationship is less sensitive to B when B is greater than a certain value (e.g. 600 in this case). At this value of B a realistic response is obtained with the ultimate deviator stress being approximately 180 kPa ($q_{ult} = p'M \approx p_{c0}M = 200kPa$) .

B only affects the stiffness when plastic deformation occurs. In Figure 7.14 an elastic range up to a maximum vertical strain of about 0.25% can be clearly seen when B is 200. Figure 7.15 shows that B starts to affect stiffness from a much lower level of strain as the elastic range is 20 times smaller, *i.e.* $R = 0.01$.

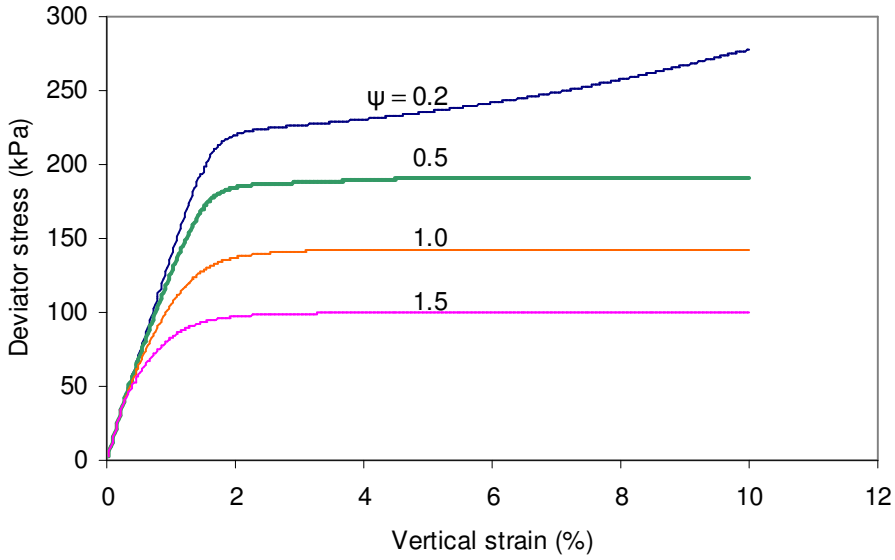

Figure 7.16 Influence of parameter ψ (B=600)

Figure 7.16 shows that stiffness and strength of soil decreases as ψ increases and the realistic response corresponds to a value of 0.5. Therefore if ψ is increased, B must also be increased to get realistic results.

For non-structured soil initial size of bounding surface (p_{c0}) is considered to be the main factor affecting the parameter B. Relationships between p_{c0} and B are explored with a

criterion that ultimate deviator stress approximately equals $p_{c0}M$. The calculated relationships are shown in Figures 7.17 to 7.19 for different values of ψ.

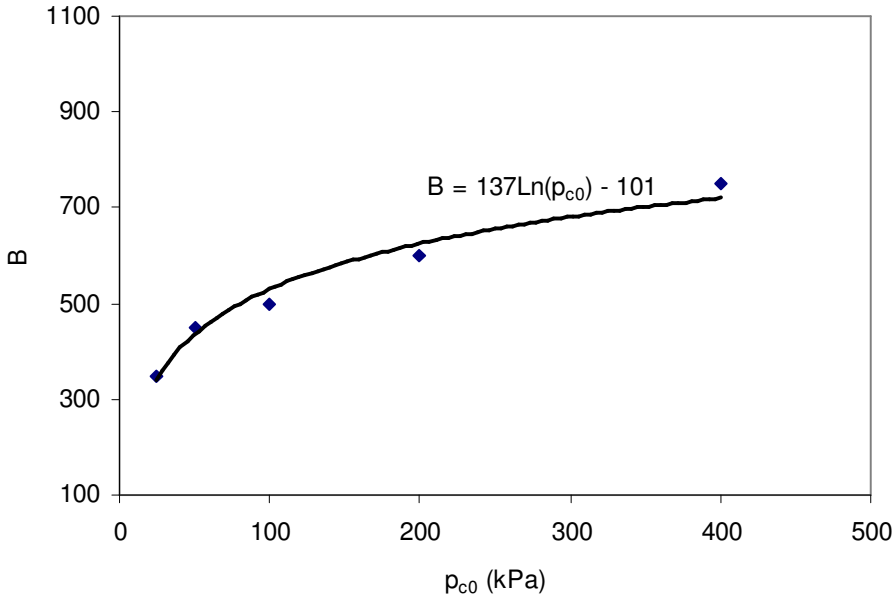

Figure 7.17 Relationship between B and p_{c0} (ψ = 0.5)

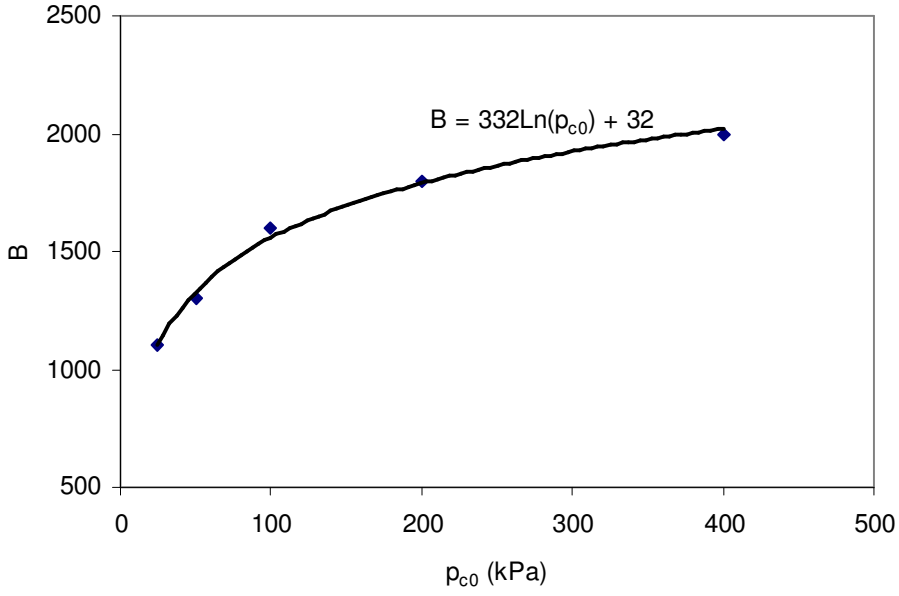

Figure 7.18 Relationship between B and p_{c0} (ψ = 1.0)

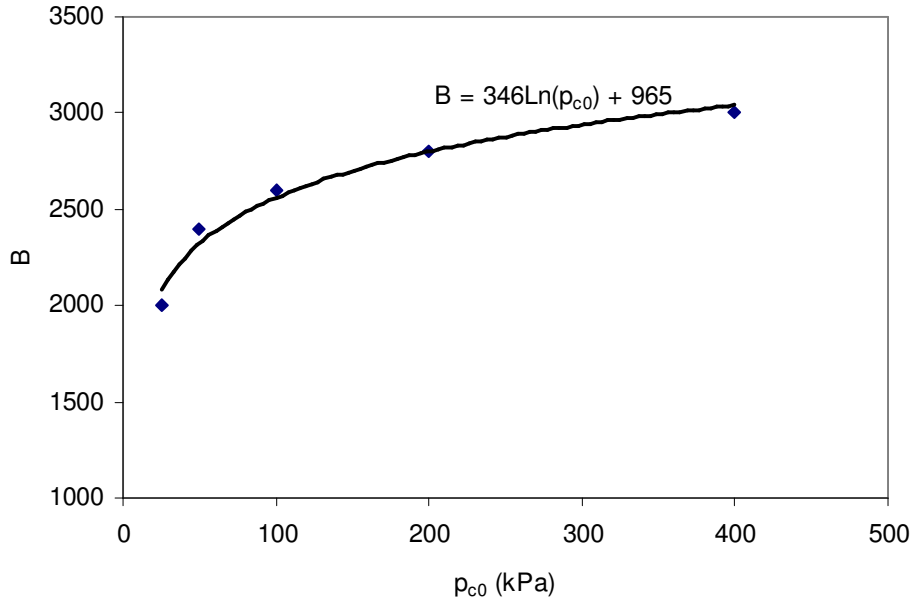

Figure 7.19 Relationship between B and p_{c0} (ψ = 1.5)

The above relationships have been obtained with the parameters $\mu, \lambda^{\bullet}$, $\kappa^{\bullet}$ given in Section 7.1 and are expected to vary as these parameters change. However, these relationships can be used as the first trial for selecting values of parameters *B* and ψ in an analysis.

7.4 Standard parameters

Poisson's ratio 'μ'

The influence of *Poisson*'s ratio is minor compared to that of parameters *B* and ψ. Figures 7.20 and 7.21 show that there is no significant difference in small strain stiffness and undrained shear strength if *Poisson*'s ratio increases from 0.1 to 0.3. This is consistent with the work by Gajo & Wood (2001). However, Possion's ratio affects the drained shear strength significantly.

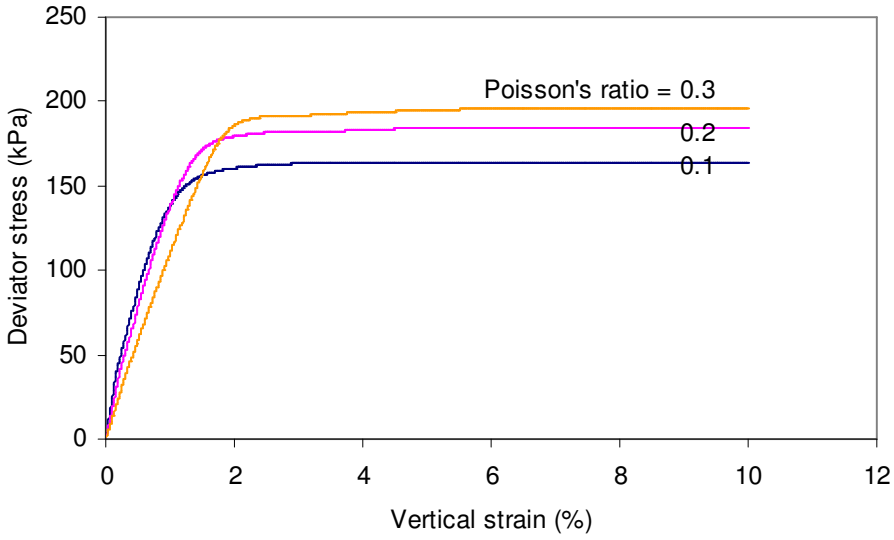

Figure 7.20 Influence of Poisson's ratio on stiffness (undrained)

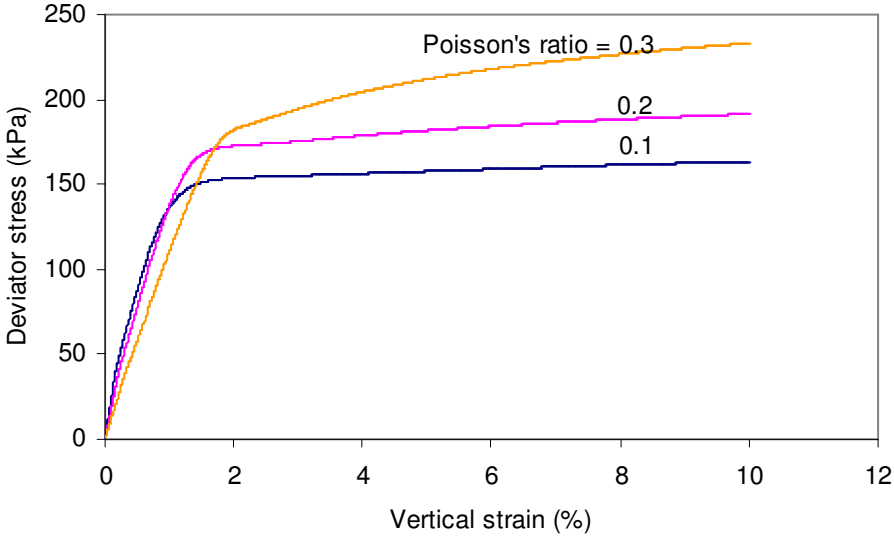

Figure 7.21 Influence of Poisson's ratio on stiffness (drained)

Parameters 'λ^*, κ^*'

λ^*, κ^* are interrelated, *i.e.* variation in one of them should be accompanied by variation of the other. To investigate significance of them, however, influence of each of the two

parameters is explored with the other being kept unchanged although this may result in unrealistic results. Figures 7.22 to 7.23 show that soil stiffness decreases as λ^* increases. Figures 7.24 & 7.25 show that the stiffness also decreases as κ^* increases.

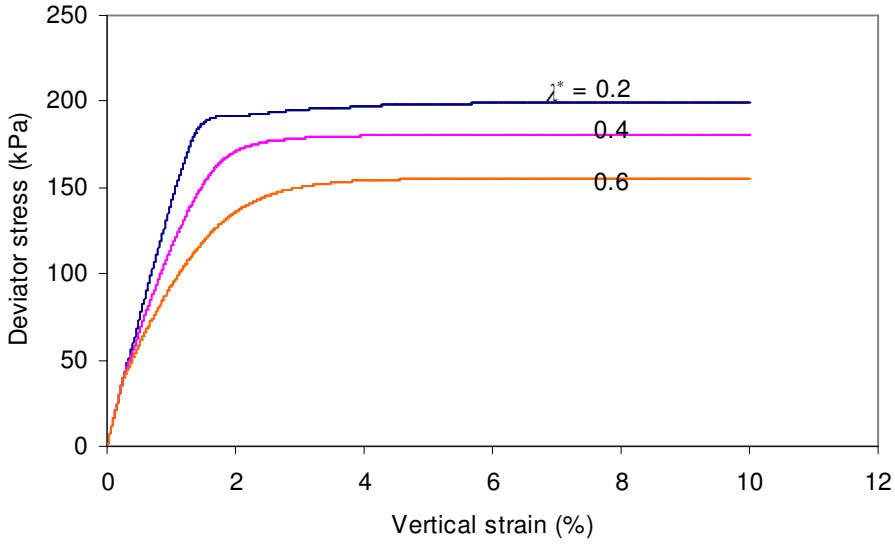

Figure 7.22 Influence of λ^* on stiffness and strength (undrained, κ^*=0.02)

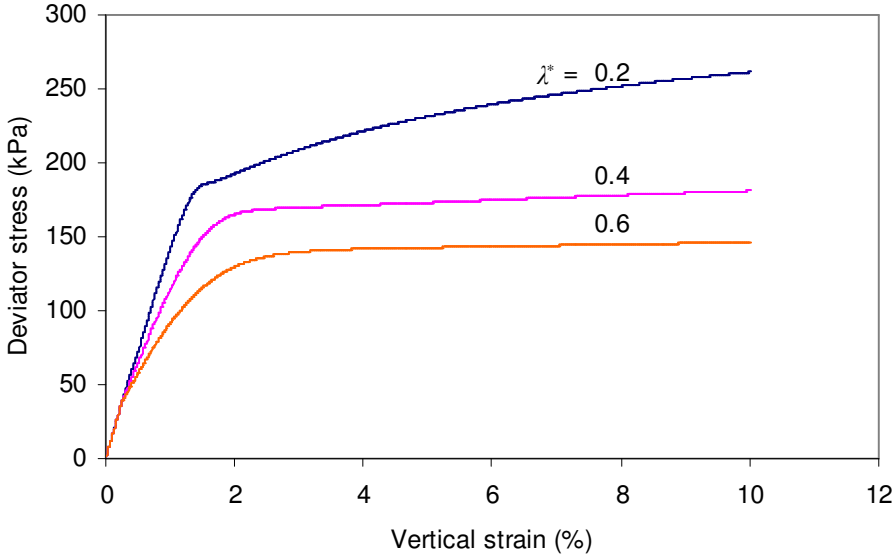

Figure 7.23 Influence of λ^* on stiffness and strength (drained, κ^*=0.02)

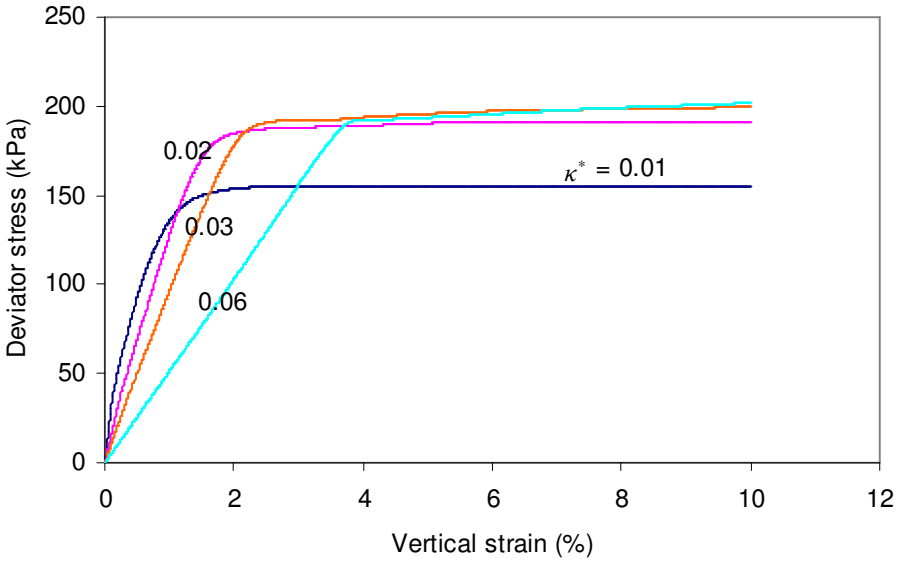

Figure 7.24 Influence of κ^* on stiffness and strength (undrained, $\lambda^* = 0.3$)

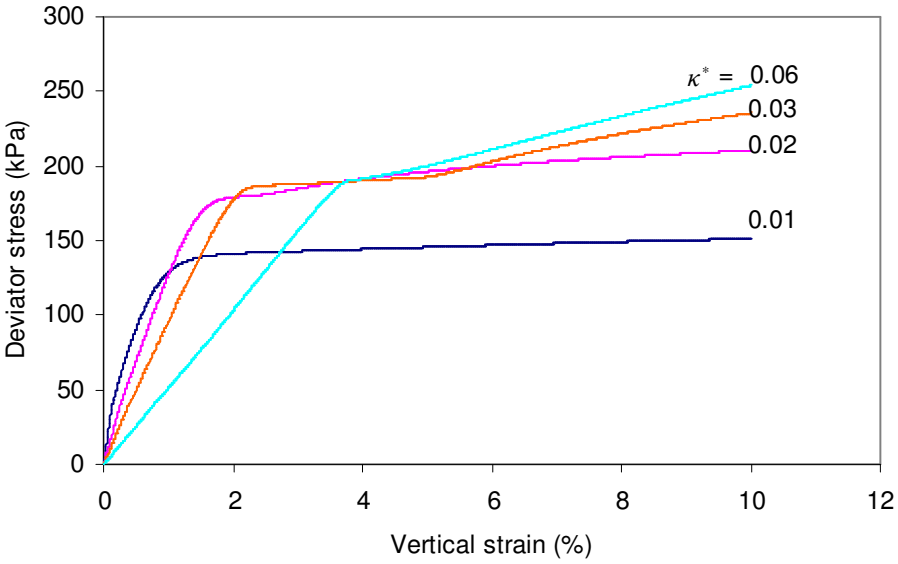

Figure 7.25 Influence of κ^* on stiffness (drained, $\lambda^* = 0.3$)

Parameter ' m'

In the bubble model, dimensionless scaling function, M_θ is given as follows (*i.e.* Eq.5.6),

$$M_\theta = \frac{2mM}{(1+m)-(1-m)\sin(3\theta)}$$

Where M is the critical state stress ratio for axisymmetrical compression. m is the ratio between radii of sections through the structure surface for axisymmetrical extension and compression. Rouainia and Wood (2000) recommended that m should be in the range between 0.7 and 1.0 to ensure convexity. The above equation is illustrated in Figure 7.26.

For axisymmetrical compression (Lode's angle θ=30°), $M_\theta \equiv M$, hence m has no effect on the response of the model (see Figure 7.27). For axisymmetrical extension (Lode's angle θ = -30°), $M_\theta = mM$. Figure 7.28 shows the influence of m on stress-strain response under axisymmetrical extension. It can be seen that ultimate deviator stress decreases linearly with m, *i.e.* $q_{ult} \approx p_{c0} M_\theta = p_{c0} mM = 200m$.

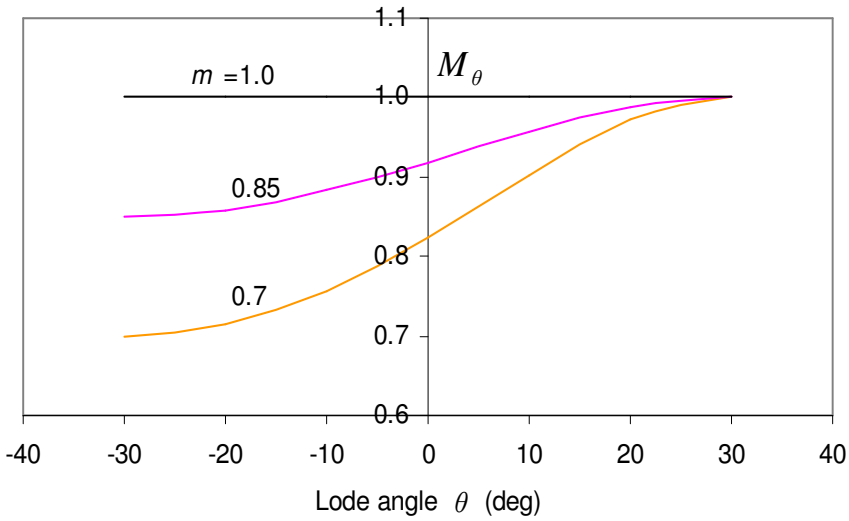

Figure 7.26 Dimensionless scaling function, M_θ (M = 1.0)

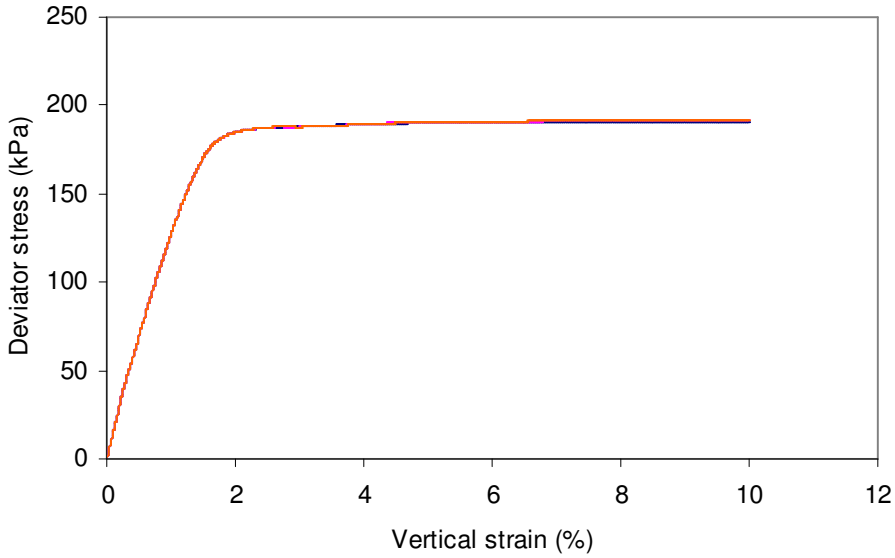

Figure 7.27 Influence of parameter 'm'(undrained axisymmetrical compression, m = 0.7~1.0)

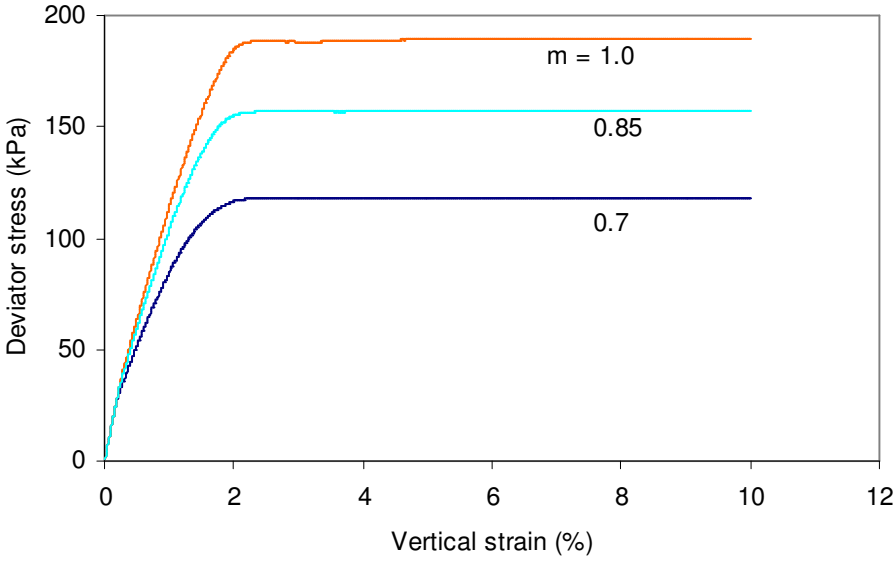

Figure 7.28 Influence of parameter 'm' (undrained axisymmetrical extension)

7.5 Destructuration parameters

Parameter 'A'

'A' is a dimensionless scaling parameter. Destructuration is entirely volumetric if $A = 0$ and is entirely distortional if $A = 1.0$ (refer Eq. 5.12). Influence of parameter A is illustrated in Figures 7.29 and 7.30. Two cases for structured soil are considered, *i.e* r_0 is 2 and 4 respectively. It can be seen that parameter A only affects residual strength of soil and has little effect on peak strength. The more contribution to destructuration of soil from plastic distortional strain, the lower the residual strength. If $A = 0$, post-peak stress-strain curves flat off as plastic volumetric strain rate $\dot{\varepsilon}_v^p = 0$, hence there is no further destructuration. If $A > 0$, destructuration continues beyond the peak as plastic distortional strain rate $\dot{\varepsilon}_q^p \neq 0$. Therefore for structured soil, parameter A should be chosen to be greater than 0, otherwise, destructuration would be incomplete. $A = 0.5$ should be used for the first trial in a modeling.

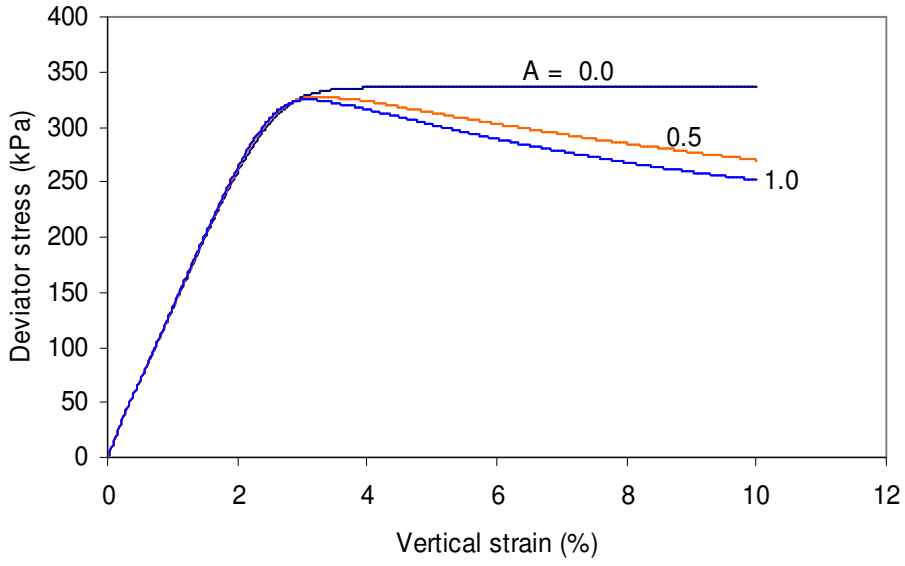

Figure 7.29 Influence of parameter 'A' (r_0=2.0, undrained)

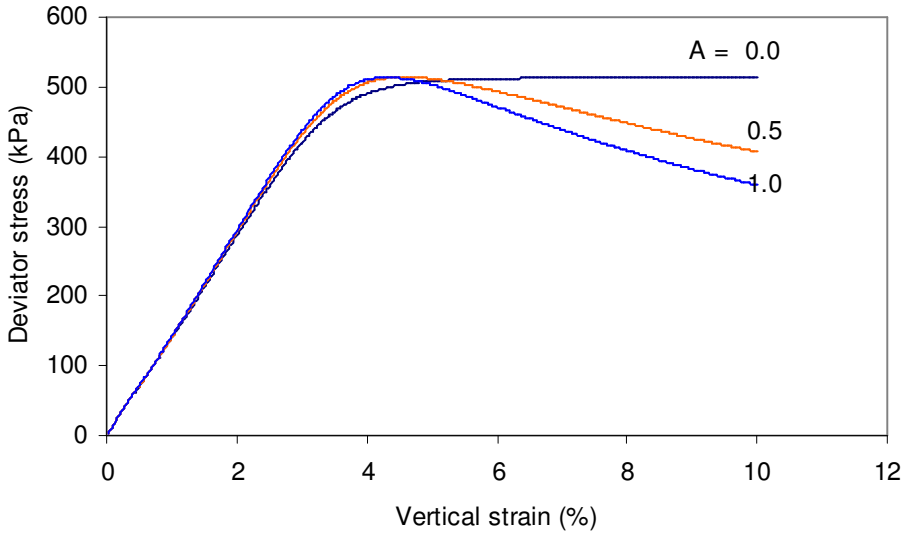

Figure 7.30 Influence of parameter 'A' (r_0 = 4.0, undrained)

Parameter 'k'

k is a parameter controlling rate of destructuration. A destructuration process is completed when the size ratio of the structure surface '*r*' is 1. Figure 7.31 shows *r* always decreases with strain and the larger the parameter *k*, the faster the destructration. However the ultimate size of the structure surface (rp_c) is independent of the parameter *k* (see Figure 7.32).

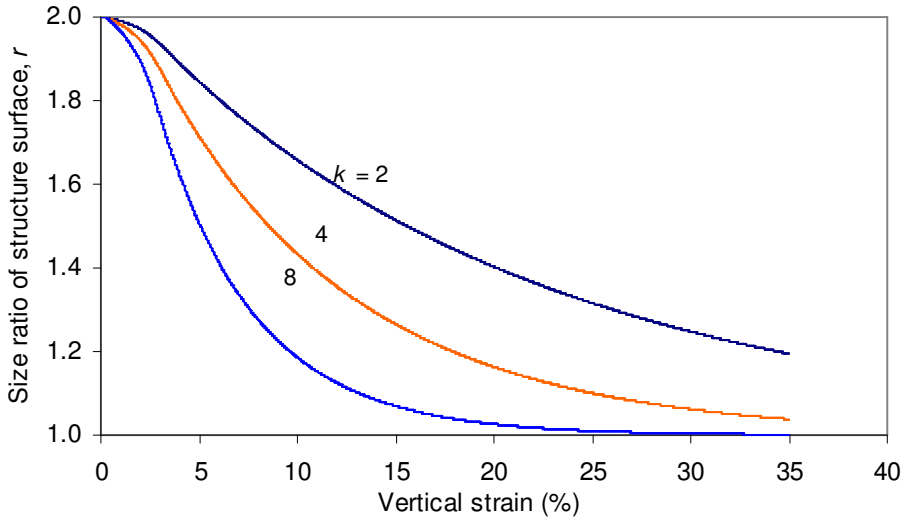

Figure 7.31 Influence of parameter 'k' on destructuration (r_0 =2.0, drained)

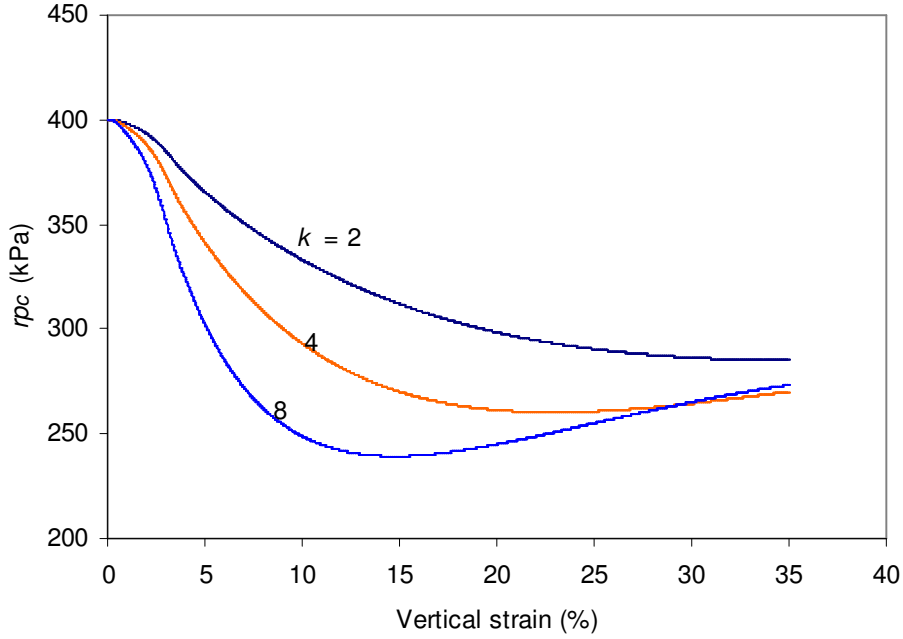

Figure 7.32 Size of structure surface, rp_c (r_0 =2.0, drained)

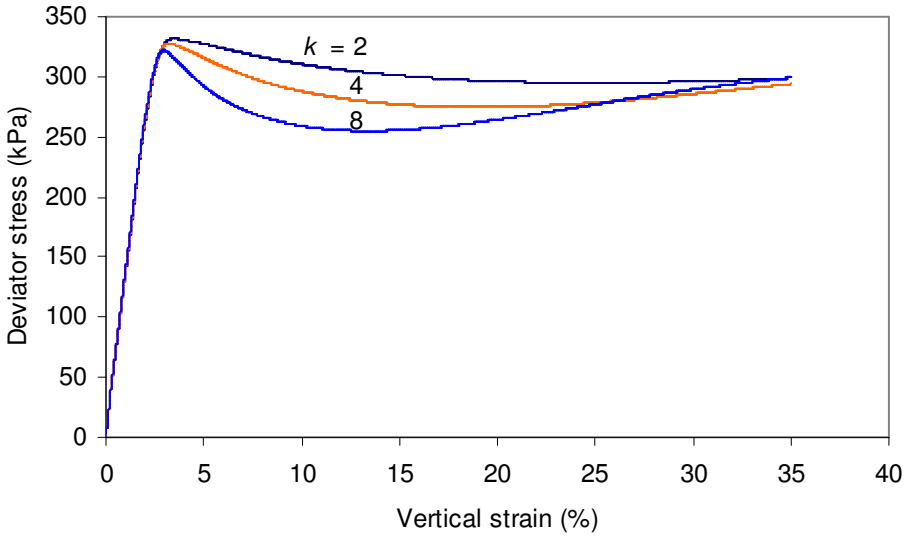

Figure 7.33 Influence of parameter 'k' on stress-strain behaviour (r_0 =2.0, drained)

Figure 7.33 shows that stress-strain curves converge to the same ultimate stress at large strain regardless of k. In addition, k has little influence on peak strength and no effect on the pre-peak behaviour. It only affects the post-peak behaviours.

7.6 Initial conditions

σ_3 *and* p_{co}

σ_3 is equal to the initial mean effective stress (*i.e.* p), which determines initial elastic bulk modulus (Note: $K = \frac{p}{\kappa^*}$ if K_0 = 0). Figure 7.34 shows that initial stiffness of soil increases with σ_3 while ultimate stress is independent of σ_3 as p_{co} is constant (*i.e.* 200 kPa) for the three cases. This corresponds to overconsolidated soil with a preconsolidation pressure $p_{\max} \approx 400kPa$ and the overconsolidation ratio is about 4, 2 and 1.3 respectively. The behaviour is qualitatively consistent with experimental results (Ishihara, 1996).

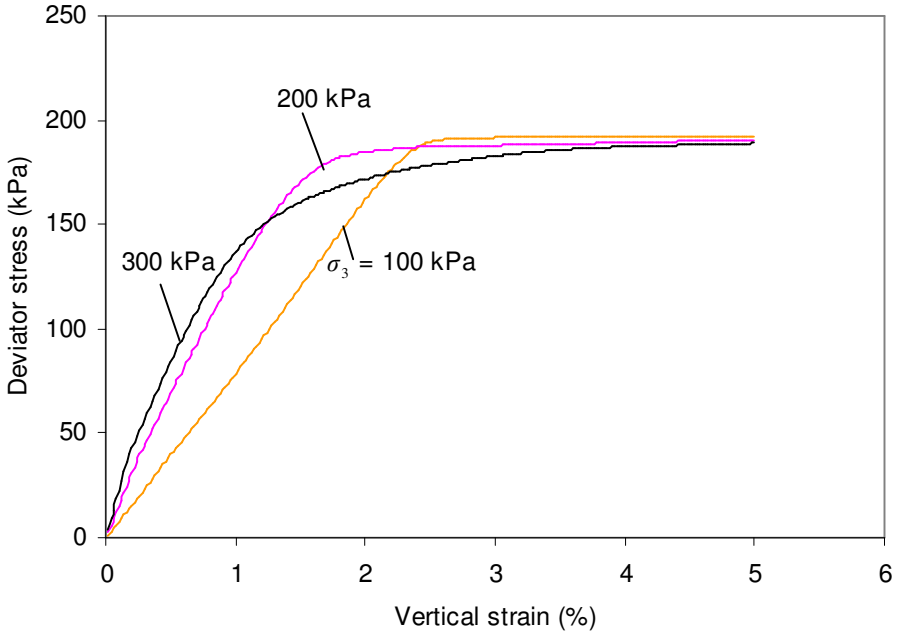

Figure 7.34 Influence of initial stress (undrained, p_{c0} =200 kPa)

p_{co} is a quantity defining the initial size of reference surface and controls the strength of soil (see Figure 7.35). p_{co} is related to the initial void ratio and stress history. For normally consolidated non-structured soil, $p_{co} \approx \sigma_3 / 2$ while for overconsolidated non-structured soil, $p_{co} \approx p_{\max} / 2$. $p_{\max}$ is the maximum preconsolidation pressure. If undrained shear strength 's_u' is available, $p_{co} \approx 2s_u / M$.

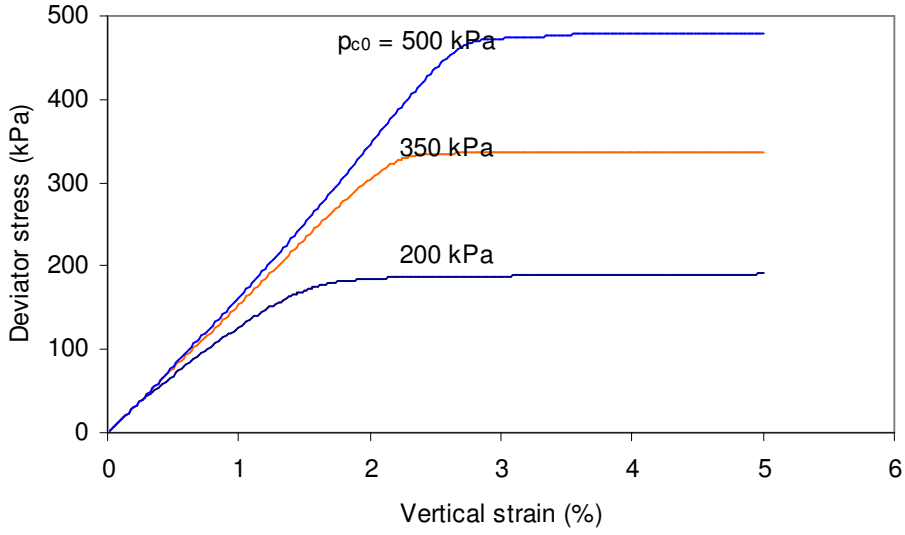

Figure 7.35 Influence of initial size of reference surface (undrained, σ_3 = 200 kPa)

r_0 *and* η_0

r_0 *and* η_0 describe the initial state of structure surface. r_0 is initial size ratio of structure surface to reference surface and η_0 is a measure of the initial anisotropy of the structure surface. r_0 can be interpreted as a measure of sensitivity of the structured soil.

It can be seen from Figure 7.36 that the peak stress increases with r_0 while the residual stress converges to the same stress level close to p_{co} as p_{co} represents strength of

remoulded soil. In this case, r_0 is approximately 1.5 to 2.0 times larger than the ratio between peak and residual stresses.

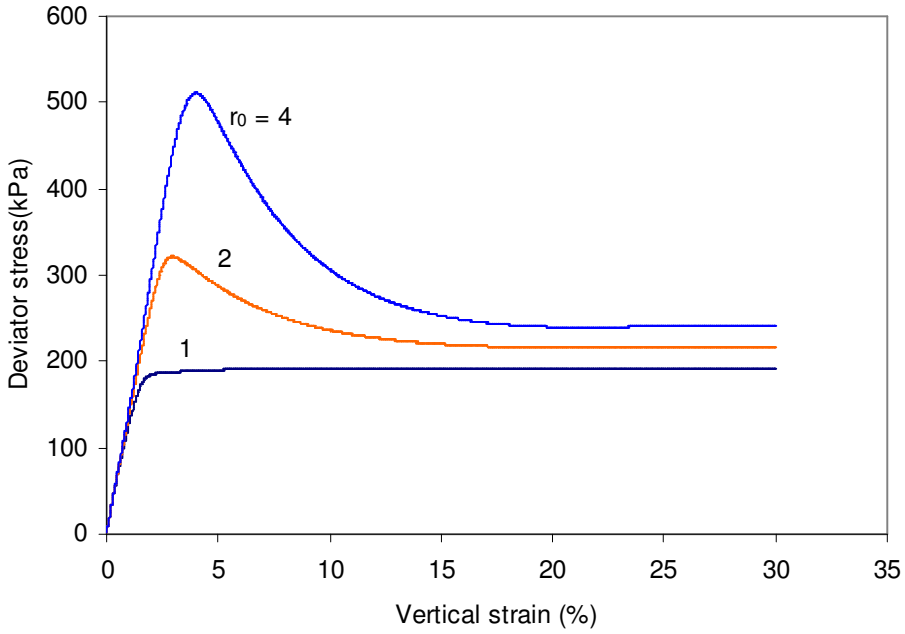

Figure 7.36 Influence of initial size of structure surface (p_{co} =200 kPa, k=8, undrained)

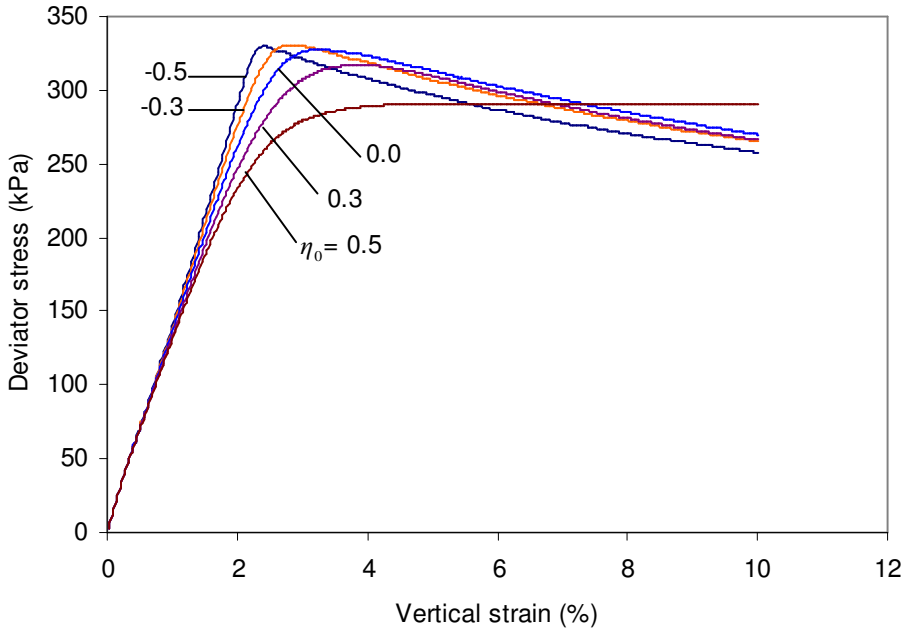

Figure 7.37 Influence of initial anisotropy (r_0 =2.0, p_{co} =200 kPa, k=4, undrained)

Anisotropy means deviation of the initial structure surface from the p axis in p, q space, *i.e.* $q_0 = (r_0 - 1)\eta_0 p_{c0}$. $\eta_0 > 0$ means deviation to above the p axis and $\eta_0 < 0$ to below the p axis. Figure 7.37 shows that the pre-peak behaviour is approximately symmetric about the curve for $\eta_0 = 0$ (*i.e.* isotropic structure surface). However influence of anisotropy on stress-strain behaviour is generally minor given the levels of anisotropy in the case.

Maximum bulk modulus 'K_{max}'

K_{max} is not a parameter of the bubble model but is required by *FLAC* to determine a critical timestep for an analysis. (Note: *FLAC* automatically calculates a critical timestep according to stiffness, zone size and Rayleigh damping ratio. The critical timestep decreases with stiffness and Rayleigh damping ratio but increases with zone size). K_{max} should be greater than the maximum bulk modulus calculated from the formula, $K = \frac{p}{\kappa^*} + K_0$, otherwise, instability may occur for a dynamic analysis. However, K_{max} does not affect a static problem as long as it is greater than a certain value which is not necessarily the maximum bulk modulus calculated from the above function. The maximum bulk modulus is about 12 MPa for the problem as shown in Figure 7.38. It is found that the minimum K_{max} required to ensure stability of the static analysis is only 2 MPa as shown in Figure 7.39 while for dynamic analysis using the single-zone triaxial model $K_{max} = 200\ MPa$ is required for a satisfactory result (see Figure 7.40).

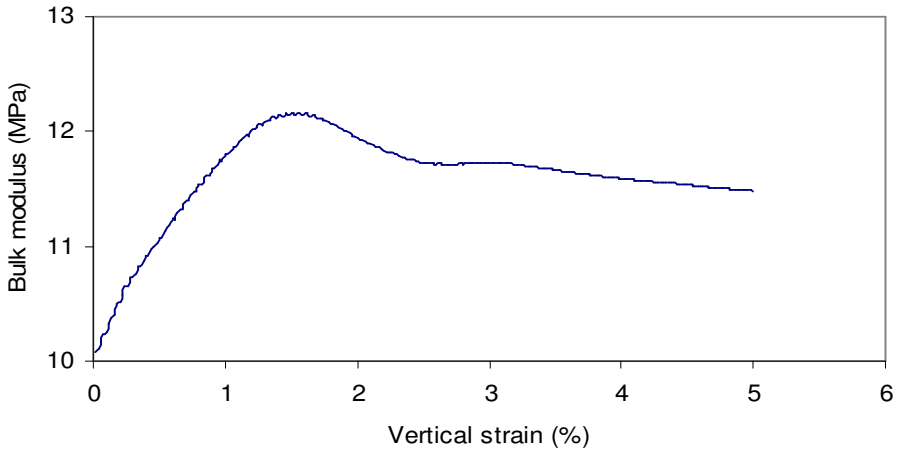

Figure 7.38 Calculated bulk modulus during undrained triaxial compression (With reference parameters given in Section 7.1)

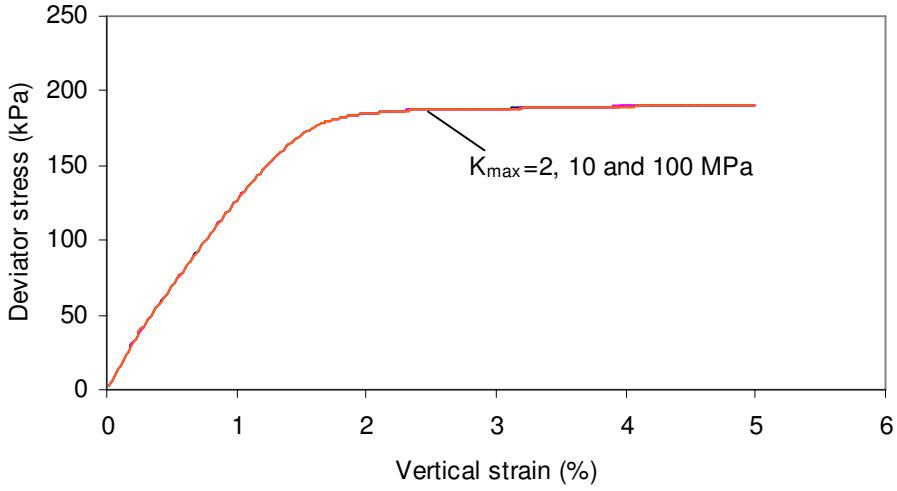

Figure 7.39 Influence of K_{max} on static analysis

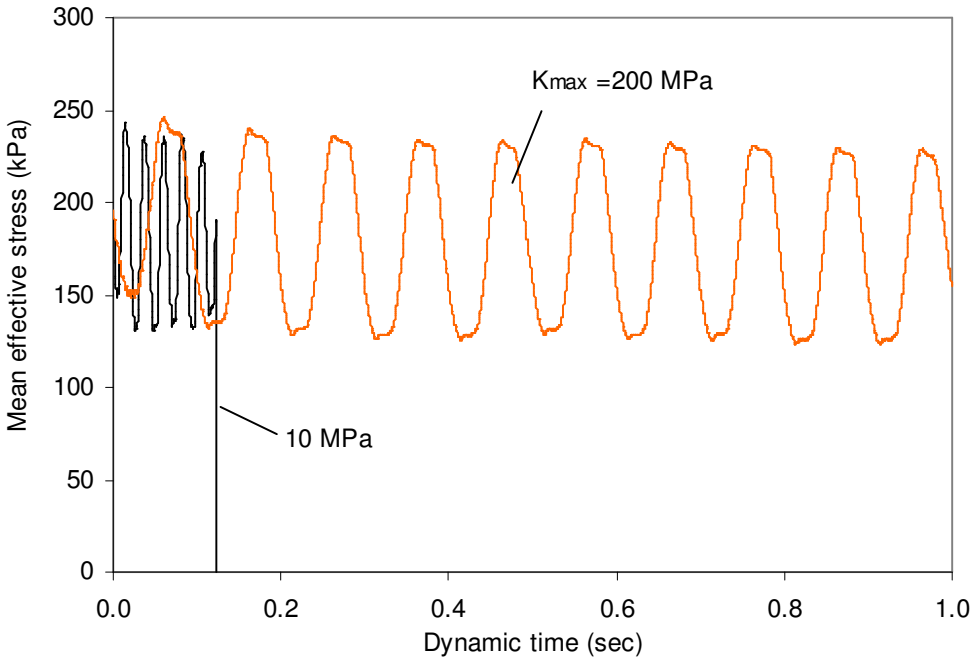

Figure 7.40 Dynamic response of a single-zone triaxial model (10 Hz, 20 cycles, vertical strain amplitude = 2%)

7.7 $G-\gamma$ curves

Three key parameters, R, κ^* and B are considered to have the most influence on the $G-\gamma$ curves, especially in the small strain range. This section presents a general picture of how these parameters affect $G-\gamma$ curves. The abrupt transition in stiffness from elastic region to yielding is discussed. An alternative hardening function is also proposed based on the concept of the model by Kavvadas and Amorosi (2000) in order to smoothen the $G-\gamma$ curves.

7.7.1 Laboratory $G-\gamma$ curves

Reduction in shear modulus (G) with shear strain has been historically expressed as a function of confining pressure and plasticity index (PI) for clays, which is idealised on basis of laboratory testing. Normalised shear modulus (*i.e.* the shear modulus ratio G/G_{max}) is used to express the nonlinear behaviour of strain-dependent modulus of soil. Experimental $G-\gamma$ curves have been presented by many researchers (*e.g.* Ishihara, 1996). A typical laboratory $G-\gamma$ curve is shown in Figure 7.41.

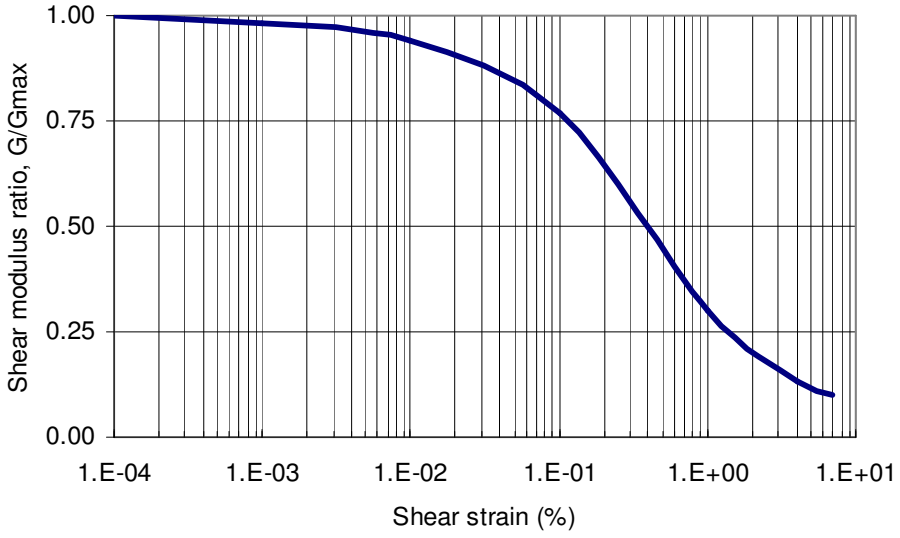

Figure 7.41 A typical laboratory $G-\gamma$ curve for cohesive soils (Based on data from Kokusho et al. 1982)

7.7.2 $G-\gamma$ curves of the Bubble model

The study in this section is to focus on stiffness degradation within small strain range and to explore the transition in stiffness from elastic region to yielding. Al Tabbaa and Wood noted in 1989 that there is an abrupt transition in stiffness from elastic region to yielding. However, there has been no published information on $G-\gamma$ curves of the Bubble model. Stallebrass and Taylor (1997) presented data of tangent shear modulus versus deviator stress but there is no sufficient small strain stiffness data. Their data also indicates there is an abrupt transition in shear modulus. Kavvadas and Amorosi (2000) proposed an alternative hardening function to smoothen the stiffness transition. Although they did not show $G-\gamma$ data, it seems to be obvious that the solution should work. Therefore, their concept is adopted in Section 7.7.3 for the bubble model.

The secant shear modulus is considered for the study. The effective confining pressure p is taken to be 600 kPa herein. Accordingly, the initial reference surface is sized with p_{c0} being 350 kPa. A small bubble is utilised with R equal to 0.001 to explore $G-\gamma$ behaviour at small strain levels. All other parameters and initial conditions are the same as the reference date given in Section 7.1 except parameters κ^* and B which have been found to play main roles in affecting $G-\gamma$ curves.

The same single-element triaxial model is utilised to model undrained response up to 2% vertical strain. A small strain increment of 10^{-6} % per step is used and results of analyses are recorded every other 100 steps to reduce burden in data processing.

Figure 7.42a presents three curves with κ^* equal to 0.02, 0.005 and 0.001 respectively. As bulk modulus is given by $K=\frac{p}{\kappa^{\bullet}}+K_0$ and K_0 is zero in this case, G_{max} for the three curves is 18 MPa, 72 MPa and 360 MPa respectively (Note: the effective Poisson's ratio is 0.25 herein). However, due to data filtering (*i.e.* record and output *FLAC* calculations at a regular period, *e.g.* every 10 to 1000 timesteps in order to reduce data processing burden in Excel and Mathcad), G_{max} obtained from *FLAC* modeling is smaller than that

calculated from the above elastic formula. For convenience, G_{max} is taken to be the shear modulus corresponding to 10^{-4} % shear strain. This is also consistent with published laboratory data (See Figure 7.41). Note: The shear strain herein is so called 'triaxial shear strain' (Schofield and Wroth, 1968), which equals to the vertical strain for undrained triaxial stress conditions.

It can be seen that shear modulus degrades faster with shear strain if κ^* is smaller. Due to presence of the elastic range (*i.e.* the bubble), there is a flat portion of curve at the beginning. This flat portion of curve decreases in length as G_{max} increases on the condition that the bubble size is constant (*i.e.* $R = 0.001$). This means that the bubble with a constant R is engaged at smaller strain if the soil is stiffer.

In Figure 7.42, plastic modulus parameter B is increased proportionally as the elastic modulus κ^* is deceased. It has been found that influence of κ^* has the similar pattern even if B is constant. Analyses have also been carried out by varying other parameters and initial conditions, which suggest the same findings stated above (results are not presented herein).

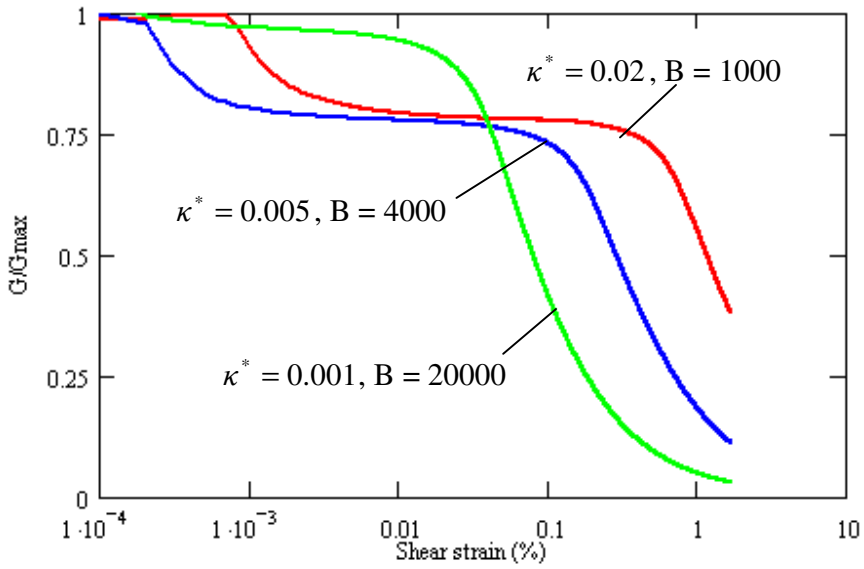

Figure 7.42*(a)* $G - \gamma$ *curves*

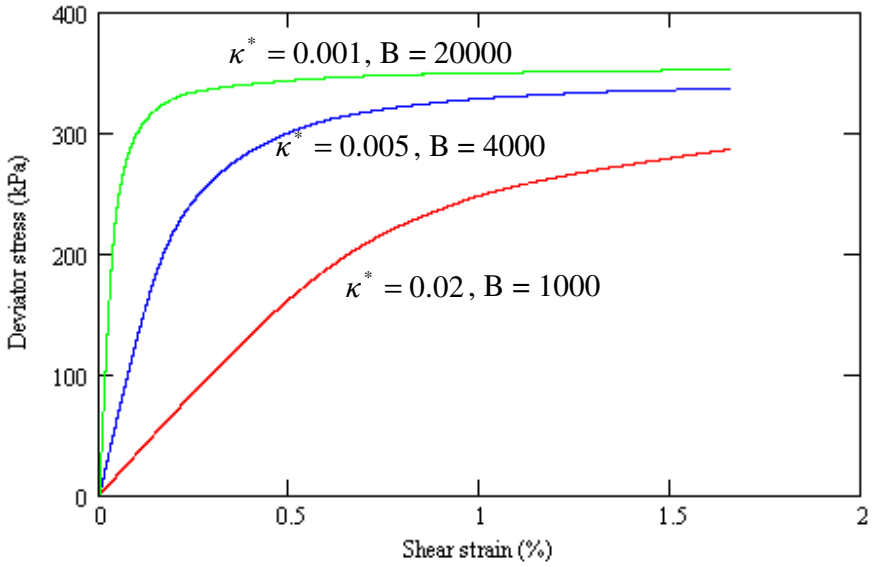

Figure 7.42*(b) Stress-strain curves*

Figure 7.42 Influence of κ^* on small strain behaviour ($K_0 = 0$)

However, the influence of κ^* on $G-\gamma$ curves is secondary when K_0 dominates the bulk modulus. This is illustrated in Figure 7.43a, where the doted curve is associated with $K_0 =$ 90 MPa and $\kappa^* =$0.02 while the solid curve is for $K_0 =$ 0 MPa and $\kappa^* =$ 0.005(*i.e.* the blue curve in Figure 7.42a), hence G_{max} is 72 MPa for both of the two cases. As B is the same, the two $G-\gamma$ curves are almost identical.

Figure 7.43b shows the influence of parameter B on $G-\gamma$ curves. It can be seen that B affects the reduction rate in shear modulus significantly at very small strain levels but has less influence at high strain levels. Parameters λ^* and ψ have similar influence (results are not presented herein).

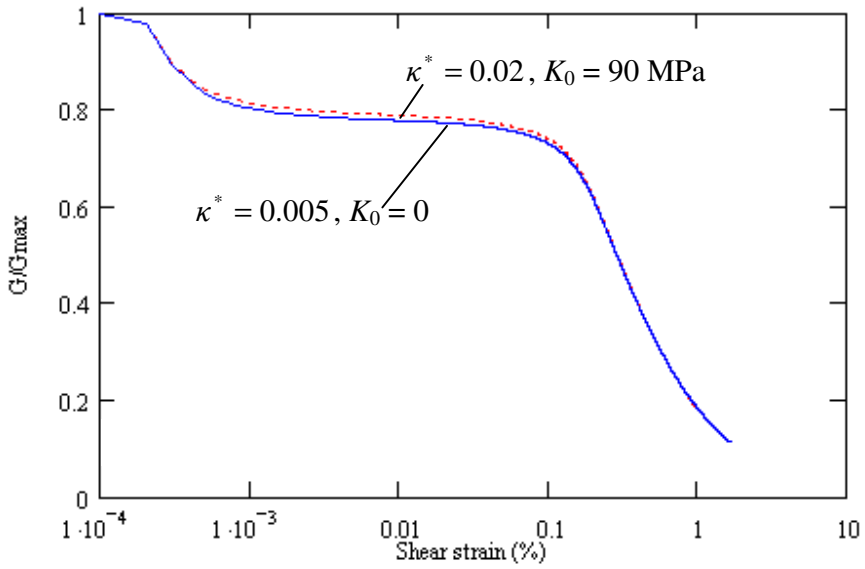

(a) B = 4000 (G_{max} =72 MPa)

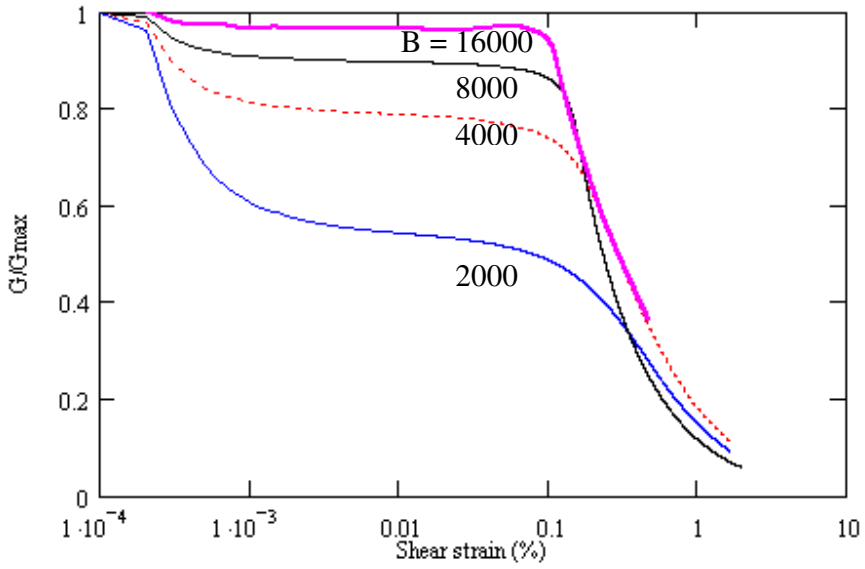

(b) $\kappa^* = 0.02$, $K_0 = 90$ MPa (G_{max} =72 MPa)

Figure 7.43 $G - \gamma$ behaviour when $K_0 \neq 0$

7.7.3 Smooth transition in shear modulus

Although a very large value can be selected for the parameter B to smoothen the transition in stiffness, there is always a drop in stiffness when the yielding starts as B can not be infinity. It has also been found that one penalty to use a large value of B is that the model becomes too stiff after yielding takes place. This can be seen from Figure 7.43b, that is, as B increases, there is less and less reduction in shear modulus between 10^{-3} % and 0.1 % shear strain.

Instead of using a large value of B, a multiplier is applied to the second term of the hardening function (Eq. 5.21), which is infinity at yielding and continuously decreases after yielding. The multiplier is given as follows:

$$\chi = \frac{1}{\left|\gamma - \gamma_0\right|^{\psi}} \tag{7.1}$$

$$H = H_c + \frac{1}{\left\|\boldsymbol{n}\right\|^2} \frac{BR^2 p_c^3}{(\lambda^* - \kappa^*)} \left(\frac{b}{b_{\max}}\right)^{\psi} \chi \tag{7.2}$$

Where γ is shear strain and γ_0 is the shear strain corresponding to the onset of yielding (*i.e.* the point when the bubble is first touched by the stress point). If the stress point moves back into the bubble (unloading) and re-touches the bubble, γ_0 needs to be reset. At yielding, $\gamma = \gamma_0$, hence, $\chi = \infty$ (*i.e.* the hardening modulus is infinity) and it continuously decreases after yielding. As a quantity is not allowed to be divided by zero in *FLAC*, at the yielding point, the plastic strain rate is set to be zero with a 'if…then' logic statement. Figure 7.44 shows three curves using the new hardening function 7.2. Parameters are the same as in Section 7.7.2 except the parameters R, B and κ^*.

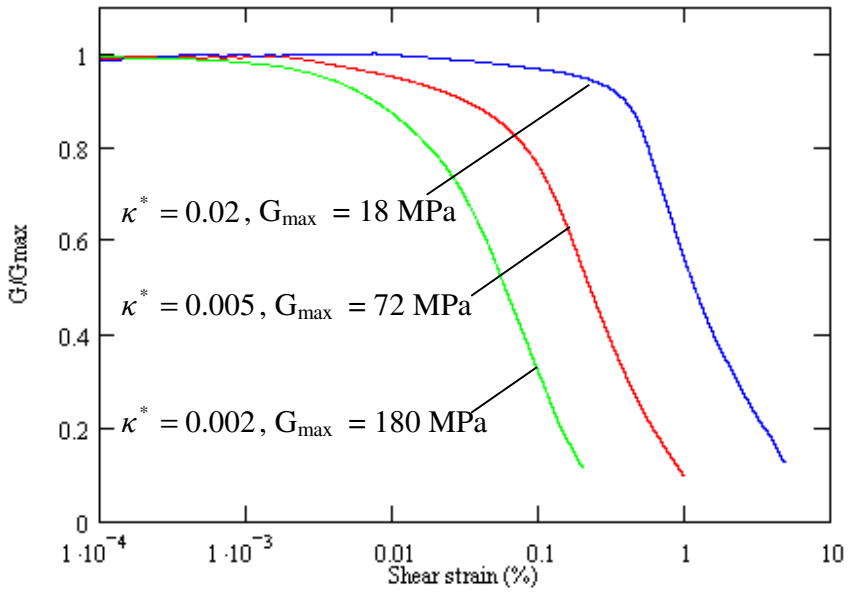

Figure 7.44 $G-\gamma$ curves with smooth transition in shear modulus (R=0.01, B=1000)

It can be seen that there is no abrupt transition in shear modulus when the stress crosses the bubble from the elastic region. The size of the elastic region decreases as κ^* decreases. The shear strain at yielding for the curve in the middle in Figure 7.44 is $1.84e^{-3}$ %. Compared to the typical curve in Figure 7.41, the above curves are satisfactory in terms of the shape and smooth transition. To model a particular soil, one has to optimize the parameters by trial and error.

The hardening function 7.2 is only used in this section to demonstrate an alternative option to eliminate abrupt transition in stiffness. The hardening function 5.21 is used in Chapter 8

7.8 Summary

The study in this chapter indicates that the most important parameters of the bubble model are plastic modulus parameters B, ψ and the Cam-clay parameters λ^*, κ^*. Poisson's ratio (μ) generally has less important role in the bubble model.

Bubble size R affects stiffness at small strains but has no effects on strength of soil. A practical range between 0.1 and 0.2 can be used unless one is to model nonlinear behaviour of soil at very small strains.

B and ψ control degradation in stiffness of soil due to plastic deformation. Stiffness increases with B and decreases with ψ. To smoothen transition in stiffness from elastic region to yielding, one needs to increase B or decreases ψ. However, the two parameters are found to be interrelated. The main factor affecting B is p_{c0}. For normal ranges of λ^* and κ^*, relationships between B, ψ and p_{c0} have been explored and can be used for the first trial in selection of the two parameters to model a problem.

An alternative hardening function based on the concept by Kavvadas is proposed to smoothen transition in stiffness when the stress point crosses the bubble. $G-\gamma$ curves obtained with the function are satisfactory compared to typical laboratory curves.

λ^* and κ^* affect the behaviour of the Bubble model significantly. Stiffness decreases with κ^* and λ^*. κ^* has the most significant role in affecting $G-\gamma$ curves. The small strain shear modulus of soil degrades faster as κ^* decreases.

Parameter m should be in the range of 0.7~1.0 to ensure convexity (Rouania and Wood, 2000). If m =1, behaviour of soil in extension is identical to that in compression. If $m \neq 1$ it only affects the behaviour of soil in extension. The behaviour of soil in compression is not affected by the parameter m.

For structured soils, parameter *A* controls the ratio of contribution between plastic volumetric and distortional strain. Use of lower values of *A* (*i.e.* less contribution from plastic distortional strain) tends to result in higher residual strength. Hence a value of 0.5 is recommended for parameter *A* so that volumetric and distortional strains are equally accounted for.

Parameter *k* controls rate of destructuration of structured soil but only affects the immediate post-peak response. The larger the parameter, the faster the destructuration. However, it has little influence on peak and residual stresses and no effect on the pre-peak behaviour of soil.

Initial size (r_0) of structure surface can be generally interpreted as sensitivity of soil. In the study, r_0 has been found to be 1.5~2 times of sensitivity index, which only affects peak stress. Residual stress is controlled by intrinsic conditions (e.g. p_{c0}) and has been found to be insensitive to r_0.

Anisotropy parameter η_0 has no important effect on stress-strain behaviour of structured soil if it is in the range between –0.5 and 0.5.

Initial mean effective stress (p_0 or σ_3') only affects initial elastic modulus of soil in the bubble model while strength of the soil is only controlled by initial size of the bounding surface, *i.e.* p_{c0} for non-structured soil. For normally consolidated non-structured soil, $p_{co} \approx \sigma_3' / 2$ while for over-consolidated non-structured soil, $p_{co} \approx p_{\max} / 2$. $p_{\max}$ is the maximum preconsolidation pressure. It is also found that $p_{co} \approx 2s_u / M$ for non-structured soil. It can be inferred from this relationship that for structured soils, $p_{co} \approx 2s_u /(M.r_0)$ (s_u is undrained shear strength).

Appendix 7.1 Data file for modelling triaxial/oedometer tests

```
; triaxial/oedometer model(static and dynamic)
; units: m, kPa, t/m3
;
;============== data setup ======================
def setup
;==== given data ======
   ;<grid>
    numXzones       =1 ;2
    numYzones       =1 ;8
    Width           =0.1
    Height          =0.1 ;0.4
   ;<analysis type>
    dynamic         =0; 1---dynamic; 0---static
    axiSym          =1; 1---axis symmetric;0---plane strain
   ;<Loading type>
    LoadType        =1; 1-Velocity loading;2-Stress loading
   ;<Drained condition>
    Drainage=0 ; 1--drained, 0--undrained
   ;<History record frequency>
    HisStepNum      =1
   ;<insitu stress>
    sigma3 =600
    sigma3_=-sigma3
   ;<dynamic setup>
    Frequency       =10
    Cycles          =10
    StrainAmplitude =1e-2
    StressAmplitude =-100.0
    DampingType=0;1-Local damping;2-Rayleigh damping;0-No damping
    DampingRatio=0.01
    DampingFrequency=50
    DydtType=1;1-Auto timestep calculated by FLAC;2-User timestep
    dt_user         =1.0e-5
   ;<static setup>
    MaxStrain =2e-2
    VelocityStatic=-1e-9;1e-8
    DeviatorStress=-50
    StaticPressure=sigma3_+DeviatorStress
    StaticCyc=0;0--monotonic;>1---cyclic
    apparent=0; 1-to calculate apparent shear modulus;0-not calculate
   ;<soil constitutive model>
  ;==== Derived data ==============
    figp  = numXzones + 1
    fjgp  = numYzones + 1
   ;<dynamic>
    period          = 1.0/frequency
    L_damping       =DampingRatio/100.0*pi
    omega = 2.0 * pi / period
    VelocityAmplitude = Height * StrainAmplitude * omega
    Duration = period * Cycles
   ;<static>
    HalfStepNum=int(Height*MaxStrain/abs(VelocityStatic))
    FullStepNum=HalfStepNum*2
```

```
    UnloadStepNum=int(FullStepNum/1.0)
    ReloadStepNum=int(FullStepNum/1.0)
 end
setup
;=========================================
def analysisType
 if axiSym =1 then
  command
  config axi dyn ;gw
  end_command
 end_if
if axiSym =0 then
  command
  config dyn ;gw
  end_command
end_if
if dynamic =0 then
  command
   set dyn off
  end_command
 end_if
end
analysisType
;=======================================
grid numXzones, numYzones
gen 0.0 0.0 0.0,Height Width,Height Width,0.0
fix y j 1
fix x I 1
;fix x ;for oedometer test
;fix x  figp
;set flow off
;water dens 1 bulk 2e6 tens 1e10
Def insitu ;initial stress condition
 command
  m e
  prop sh 4.0e4 bulk 2.0e5 den 1.7
  ini sxx sigma3_ syy sigma3_ szz sigma3_
  app pressure sigma3 I=figp
  app pressure sigma3 j=fjgp
 end_command
 if dynamic=0 then
   command
    solve
   end_command
 end_if
 if dynamic=1.0 then
   command
    set dyn off
    solve
    set dyn on
   end_command
 end_if
end
insitu
his reset
ini xd 0 yd 0
ini xv 0 yv 0
```

```
;===========================================
call bubble.fis
   model bubble
   prop b_kmax 2e5 b_poiss 0.25 b_mod0 9e4
   prop b_lambda 0.3 b_kappa 0.02 b_M 1.0 b_mm 1.0
   prop r_bub 0.001 aa 0.5 bb 4000 k 8 psigh 0.5
   prop nambda0 0.0 r_str0 1.0 pc0 350
   prop density 1.7 psr 3.0
def stress_ratio
  sum = 0.0
  loop i (1,izones)
    loop j (1,jzones)
      sum =sum  + syy(i,j)/sxx(i,j);drained
    endLoop
  endLoop
  stress_ratio= sum/(izones*jzones)
 end
def qq
  sum = 0.0
  loop i (1,izones)
    loop j (1,jzones)
      sum =sum  + syy(i,j)-sxx(i,j)
    endLoop
  endLoop
  qq= sum/(izones*jzones)
 end
def effp
 effp=(sxx+syy+szz)/3.0+pp
end
def totp
 totp=(sxx+syy+szz)/3.0
end

Def hisrecord
   if Dynamic = 1.0 then
     command
       his dytime
     end_command
   end_if
   command
    his nstep HisStepNum
    his qq;1
    his ydis i 1 j fjgp;2
    his vertical_s;3
    his stress_ratio
    his volumetric_s;4
    his pv;5
    his pc;6
    his r_str;7
    his $p;8
    his $q;9
    ;his effp
    his s_p;10
    his s_q;11
    his b_p;12
    his b_q;13
    his q_strain ;14 plastic shear strain
```

```
    his qt_strain ;15 total shear strain
    his b_mod;16
    his $app_g;17
    his pwp;18
  end_command
 end
hisrecord
his dytime
;=========================================
set ncw=100
set step 1000000000
def wave
 if LoadType=1
   wave = VelocityAmplitude * cos(omega * dytime)
 else
   wave = StressAmplitude * sin(omega * dytime)
 endif
end
def ssolve
 if dynamic = 1 then
  if DampingType=1 then
    command
     set dy_damp local L_damping
     end_command
  end_if
  if DampingType=2 then
    command
     set dy_damp rayl DampingRatio Frequency
    end_command
  end_if
  if LoadType = 1
     command
     fix y j fjgp
     app yvel 1.0 his wave j=fjgp
     end_command
  end_if
  if LoadType =2 then
    command
    app nstress -1.0 his wave j fjgp
    end_command
   endif
  if DydtType=2 then
     command
     set dydt dt_user
     end_command
   endif
  command
    solve dytime Duration
  end_command
 end_if
 if dynamic =0 then
   if LoadType =1 then
      command
      fix y j fjgp
      ini yv VelocityStatic j=fjgp
      step HalfStepNum
      end_command
```

```
    if StaticCyc>0 then
     loop n (1,staticCyc)
       VelocityStatic=-VelocityStatic
       command
       ini yv VelocityStatic j=fjgp
        step UnloadStepNum
        end_command
       VelocityStatic=-VelocityStatic
       command
       ini yv VelocityStatic j=fjgp
        step ReloadStepNum
        end_command
     end_loop
    end_if
  end_if
  if LoadType =2 then
   command
    app nstress StaticPressure j fjgp
    ;app nstress StaticPressure i figp
    solve
    ;step 80
   end_command
  end_if
 end_if
end
ssolve
;==============================
plot his -1 vs -2 hold
set hisfile B2000 ;name of file to save data
his write -1 vs -2 skip 100
```

Appendix 7.2 MathCad programme for processing $G-\gamma$ curves

Programme to process G-γ curves (Undrained triaxial test)

Ho := 0.1 Height of triaxial specimen (m)

d1 := D:\..\run1.xls d2 := D:\..\run2.xls d3 := D:\..\run3.xls

Input data of deviator stress (kPa) vs vertical displacement (m).The first column of each matrix(d1, d2 and d3) is displacement and the second is deviator stress.

Gmax1 := 18000 Gmax2 := 72000 Gmax3 := 360000

Process(x) := for $i \in 1..rows(x)$

$\varepsilon_i \leftarrow \frac{(x^{\langle 1 \rangle})_i 100}{Ho}$

$G_i \leftarrow \frac{(x^{\langle 2 \rangle})_i 100}{3\varepsilon_i}$ Secant shear modulus

augment(ε, G)

$G\_ratio1 := \frac{Process(d1)^{\langle 2 \rangle}}{Gmax1}$ $\gamma 1 := Process(d1)^{\langle 1 \rangle}$ $G1 := Process(d1)^{\langle 2 \rangle}$ $q1 := (d1)^{\langle 2 \rangle}$

$G\_ratio2 := \frac{Process(d2)^{\langle 2 \rangle}}{Gmax2}$ $\gamma 2 := Process(d2)^{\langle 1 \rangle}$ $G2 := Process(d2)^{\langle 2 \rangle}$ $q2 := (d2)^{\langle 2 \rangle}$

$G\_ratio3 := \frac{Process(d3)^{\langle 2 \rangle}}{Gmax3}$ $\gamma 3 := Process(d3)^{\langle 1 \rangle}$ $G3 := Process(d3)^{\langle 2 \rangle}$ $q3 := (d3)^{\langle 2 \rangle}$

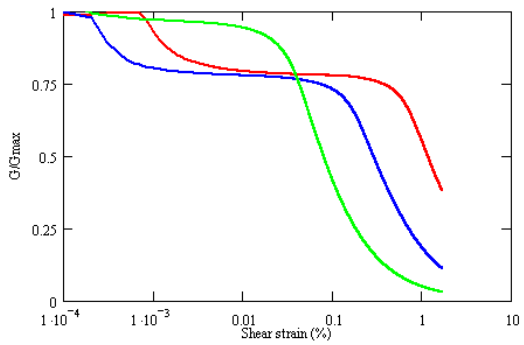

8 APPLICATION OF THE BUBBLE MODEL

In this chapter the Bubble model is applied to the modeling of vertical vibration of a rigid strip foundation. The infinite rigidity of the foundation is modeled using the '*slave y*' feature in *FLAC* so that the dynamic timestep is not affected by the stiffness of the foundation. The foundation is directly subjected to a sinusoidal vertical excitation. Effects of nonlinearity of soil on vertical dynamic compliance of the rigid foundation are investigated. Several factors are considered, which include initial stress condition in the soil, level of excitation and mass ratio of foundation.

8.1 Parameters of the Bubble model

Parameters of the Bubble model have been chosen on the basis of Chapters 5 and 7 and are considered to be associated with homogeneous, over-consolidated and non-structured soil. The modified function for elastic bulk modulus of soil (Eq.5.22, $K = \frac{p}{\kappa^*} + K_0$) is used herein. This gives a virtually constant bulk modulus of soil in the soil-foundation model as the bulk modulus is dominated by the initial modulus (K_0) while influence of change in effective mean pressure (p) is relatively small and negligible under undrained condition. The parameters are given in Table 8.1.

Table 8.1 Soil parameters in modeling foundation vibration

λ^*	κ^*	M	m	μ	R	B	ψ	r_0	η_0
0.15	0.02	1.0	1.0	0.25	0.05	1800	0.5	1.0	0.0

The parameters A and k do not affect results herein as non-structured soil is considered. In addition to the above parameters, other initial conditions are given as follows:

Unit weight of soil, $\rho = 1.8\ t/m^3$

Centre of initial bounding surface, $p_{c0} = 210\ kPa$

Bulk modulus of soil under zero confining pressure, $K_0 = 60\ MPa$

The chosen parameters and initial conditions correspond approximately to soil with an undrained shear strength of 100 kPa and an elastic shear modulus of 40 MPa.

To investigate nonlinear dynamic behaviours of soil under relatively small strains, a small bubble size is utilized, *i.e* R = 0.05 (4 times smaller than the normally used). This will ensure that plastic deformation takes place in the soil immediately beneath the foundation prior to dynamic loading. Therefore, effects of soil nonlinearity on compliance of the foundation are effectively reflected in the modeling. Figure 8.1 shows the static stress-strain behaviours of the soil with the chosen parameters and initial conditions.

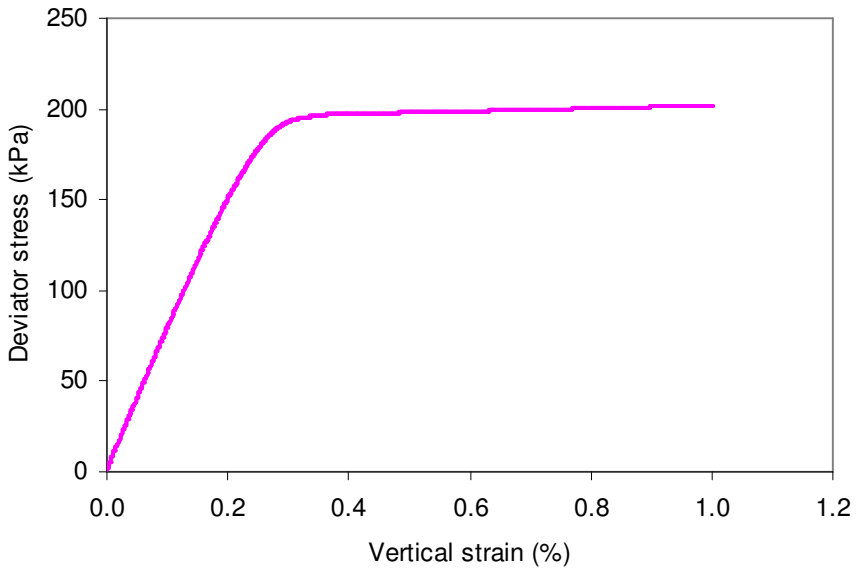

Figure 8.1 Undrained stress-strain response of soil (σ_3=100 kPa)

8.2 *FLAC* model

Due to symmetry in both geometry and loading, the left boundary of the *FLAC* model is set to coincide with the central line of the foundation. The model is 10 m in height and 10 m in width. 400 square elements with the same size are utilised, *i.e*. each element is 0.5 m by 0.5 m.

Initial stresses are generated in the model by switching on 'gravity' and applying an additional surcharge of 20 kPa on the surface. The soil is considered to be elastic at this stage. Then the elastic soil is changed into nonlinear soil characterized by the Bubble model and static vertical loads are applied incrementally to the foundation. Figure 8.2 shows the relationship between settlement and bearing pressure of the foundation. The ultimate bearing capacity of the foundation is considered to be approximately between 400 kPa and 450 kPa.

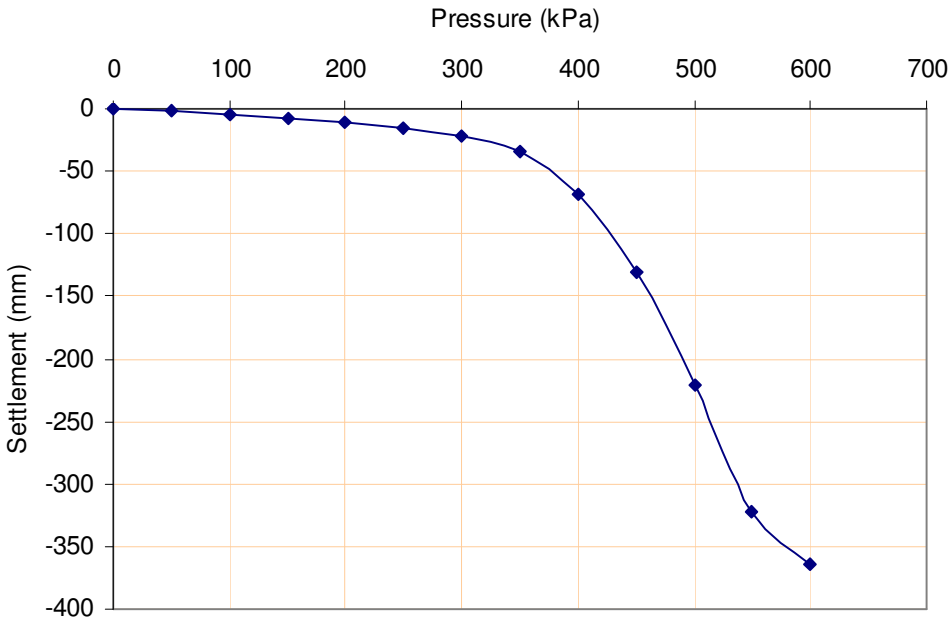

Figure 8.2 Pressure-settlement curve

Static loading prior to dynamic loading is applied in such a way that static bearing pressure of the foundation corresponds to a particular factor of safety with respect to an assumed ultimate bearing capacity of 450 kPa. When the dynamic loading is applied to the foundation the right and lower boundaries are changed to quiet boundaries. The *FLAC* model in the dynamic loading stage is shown as Figure 8.3. For clarity the static pressure on the top boundary is not shown in the figure.

The soil-foundation model has a natural frequency of about 6 *Hz* as shown in Figure 8.4, which has been obtained by letting the model to vibrate under gravity.

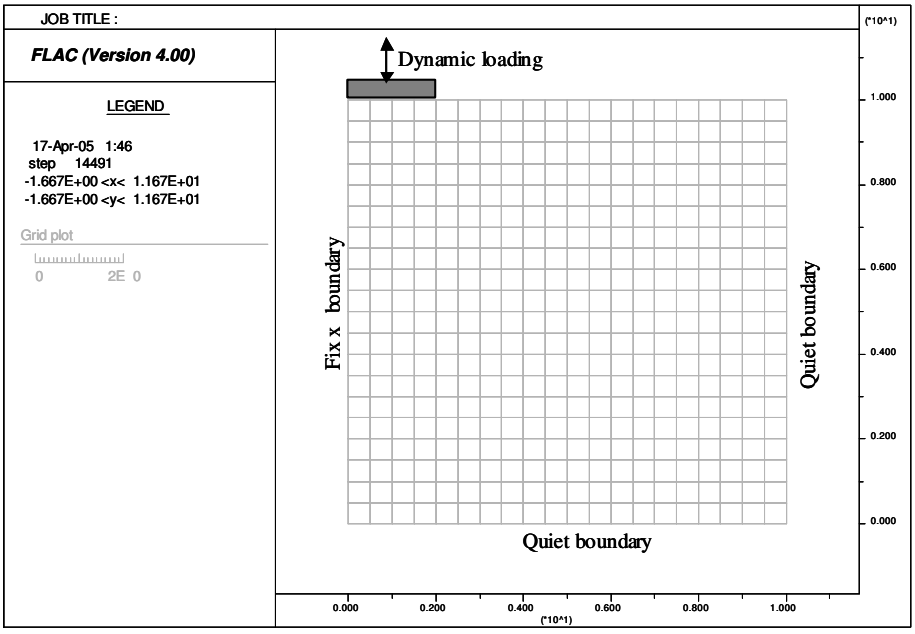

Figure 8.3 FLAC model in dynamic loading stage

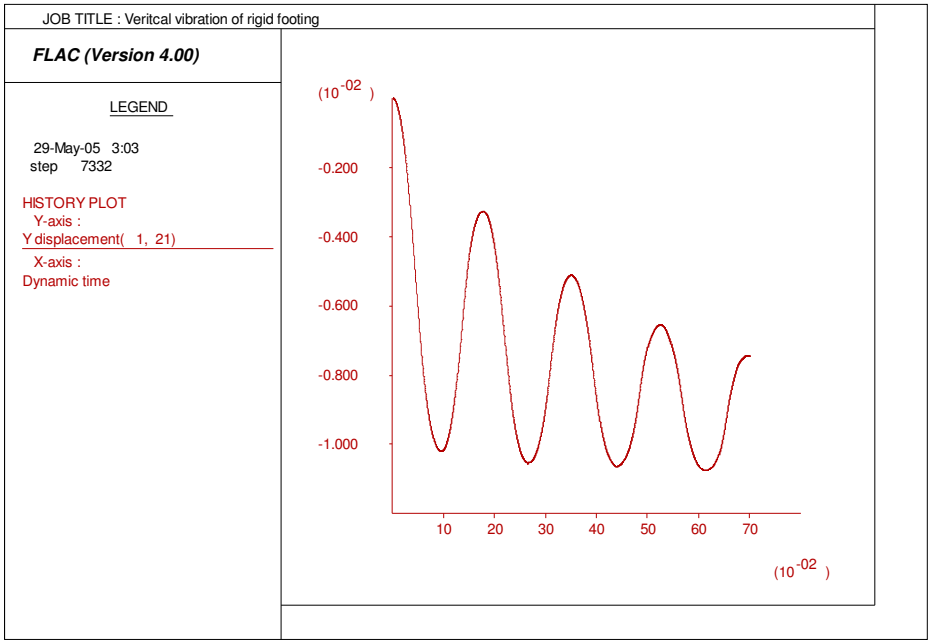

Figure 8.4 Vibration of the soil-foundation model under gravity
(Displacement is in metre and dynamic time in second)

8.3 Typical response

The following dynamic responses of the rigid foundation have been obtained with the initial stress conditions corresponding to a static factor of safety of 3. The foundation is massless.

Figure 8.5 shows that permanent displacement of the foundation increases progressively until a steady state response is reached. This is typical of a machine foundation.

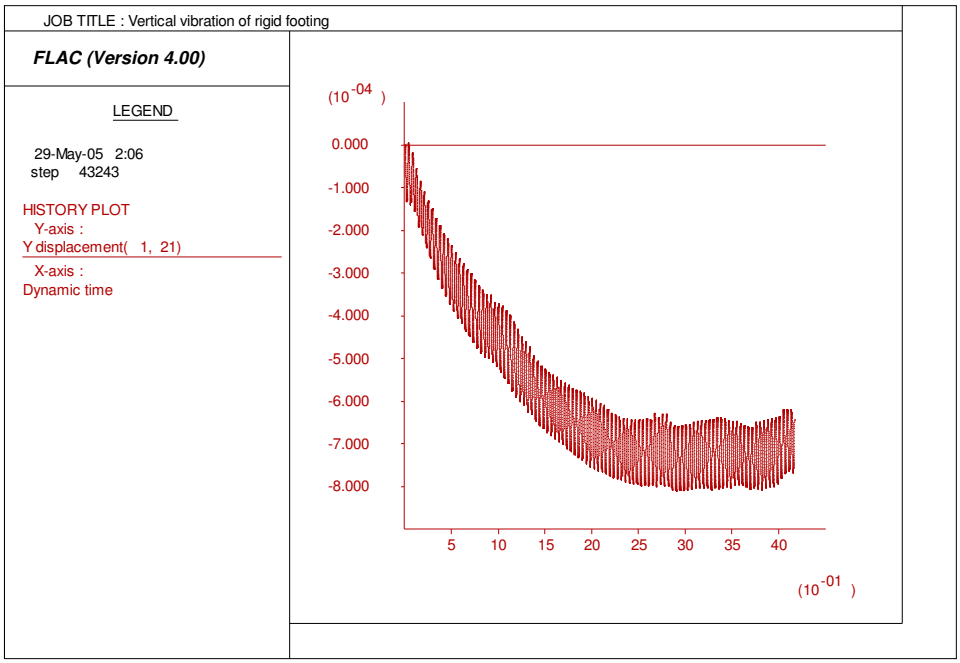

Figure 8.5 Dynamic displacements (24 Hz, 5 kPa stress amplitude, 100 cycles)

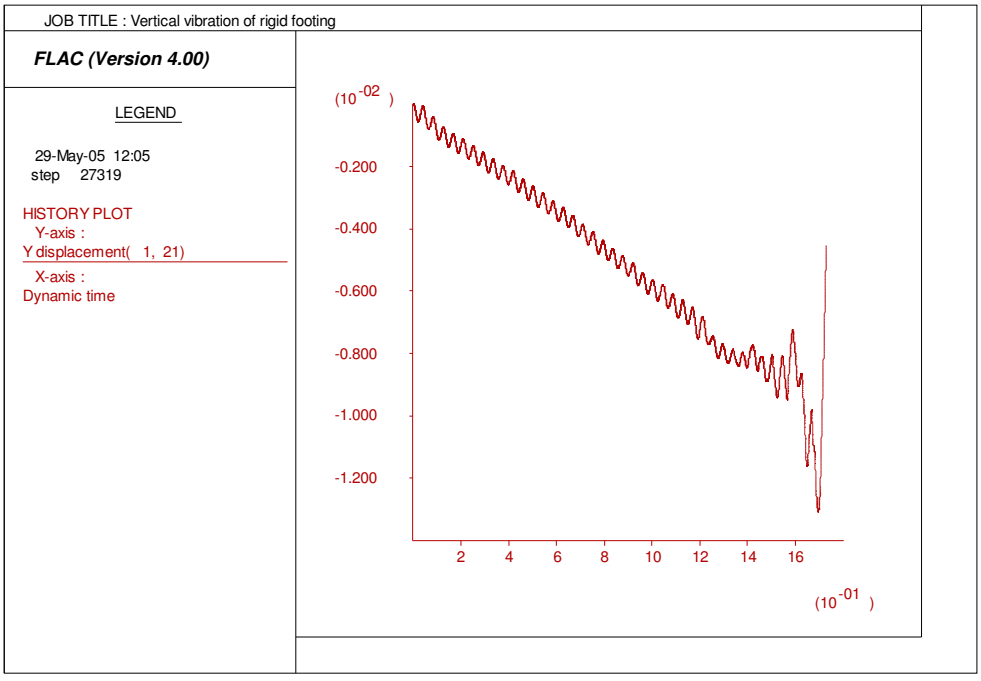

Figure 8.6 Dynamic displacements (24 Hz, 20 kPa stress amplitude, 48 cycles)

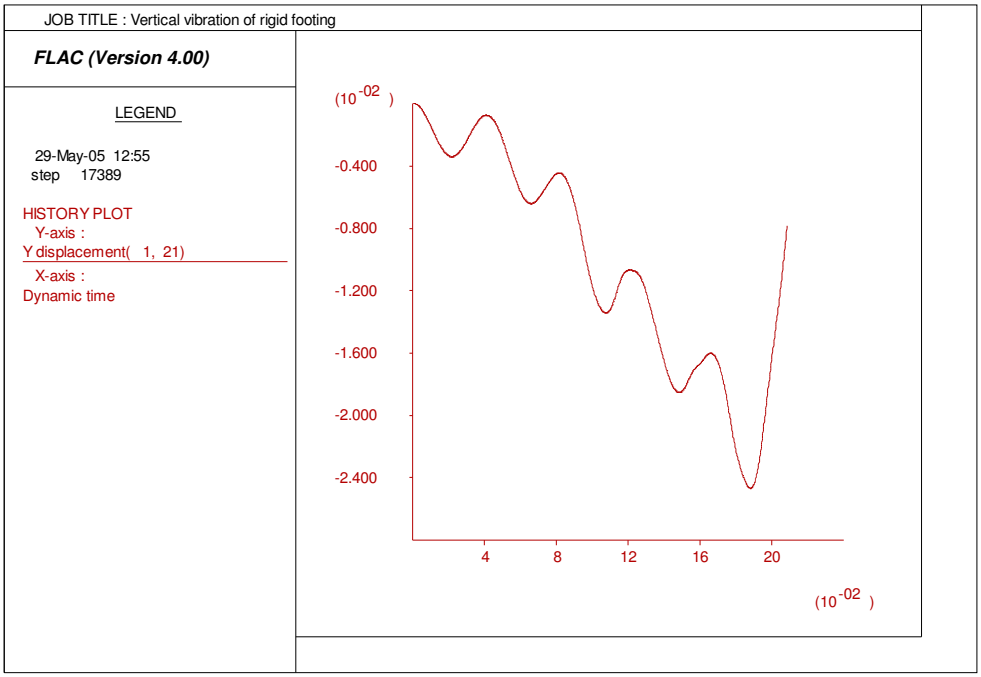

Figure 8.7 Dynamic displacements (24 Hz, 100 kPa stress amplitude, 5 cycles)

When the dynamic stress level increases, large plastic deformation first occurs around the corner of the foundation after some cycles of vibration and develops cyclically to other areas in the soil until failure of the foundation occurs (See discussions in Section 9.2). Figure 8.6 shows that excessive displacement occurs at around 48 cycles when the stress amplitude is increased to 20 kPa. It has been found that the larger the stress amplitude is, the earlier the excessive displacement occurs. Figure 8.7 presents the response when the stress amplitude is 100 kPa.

To investigate effects of nonlinearity of soil on dynamic compliance of the rigid foundation, a minimum of 10 cycles of vibration is considered to be necessary. To ensure that the excessive displacement will not occur within 10 cycles of vibration when the stress amplitude is large, an upper bound of plastic strain rate is specified for plastic correction, which is represented by a plastic strain ratio (*psr*), *i.e.* a ratio of maximum plastic strain rate to total strain rate. The influence on displacement response has been assessed and shown in Figure 8.8 where the stress amplitude is 60 kPa and the plastic

strain ratio (*psr*) ranges from 0.7 to 1.0. Both permanent displacement and amplitude of displacement are affected. The percentage of reduction in the average displacement amplitude due to the use of '*psr*'is calculated and given in Table 8.2.

Table 8.2 Average amplitude of displacement in 10 cycles

Ratio of maximum plastic strain rate to total strain rate (denoted by '*psr*')	1.0	0.9	0.8	0.7
Average amplitude of displacement in 10 cycles (mm)	2.032	1.574	1.433	1.252
Percentage of reduction in displacement amplitude w.r.t. *psr* = 1	-	25%	30%	40%

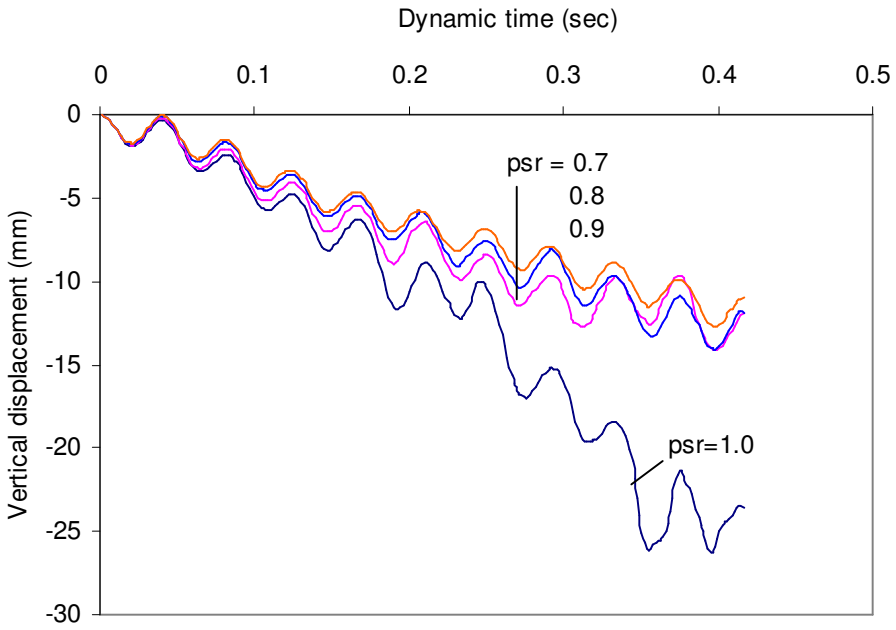

Figure 8.8 Influence of plastic strain ratio on displacement response (24 Hz, 60 kPa stress amplitude, 10 cycles)

As an approximation, *psr* = 0.9 is used in the following analyses for a few cases when stress amplitudes are large and the average displacement amplitudes are amended according to the percentages shown in the above table. Indication will be given when a *psr* smaller than 1.0 is utilised.

The above responses are associated with forced vibration under a continuous sinusoidal loading. Figure 8.9 shows response of the foundation to a half cycle of sinusoidal loading. No additional damping is applied. It can be seen that the transient vibration decays quickly due to hysteretic damping.

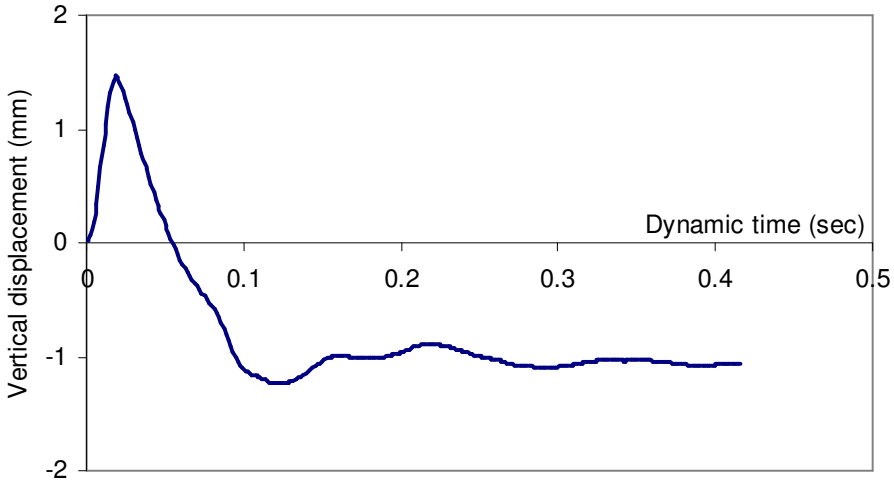

Figure 8.9 Transient vibration (0.5 cycle, 24 Hz, 60 kPa, no additional damping)

8.4 Vertical compliance of the rigid foundation

To investigate influence of soil nonlinearity on vertical compliance (*i.e.* displacement) of the rigid foundation, average amplitudes of displacement in 10 cycles of vibration are calculated for variable conditions which include initial stress (*i.e.* factor of safety), excitation level (*i.e.* stress amplitude and frequency) and mass ratio of foundation.

Dimensionless frequency parameter, a_0, is introduced as it is used traditionally and is given as follows:

$$a_0 = \frac{2\pi fb}{v_s} \tag{8.1}$$

Where f is the excitation frequency in cycles per second, b is the half width of the foundation in meter and v_s is shear wave velocity of soil, which is approximately 150 m/sec for the given soil parameters.

8.4.1 Comparison between nonlinear and elastic models

Average amplitudes of displacement in 10 cycles are plotted against the dimensionless frequency, a_0. Figure 8.10 shows a comparison between the Bubble model and the elastic model, where cyclic stress amplitude is 20 kPa. The initial stress condition corresponds to a static factor of safety of 3. For the Bubble model 0.5% Rayleigh damping is applied and for the elastic model the damping ratio is 5%. Amplitudes of displacement are normalized with respect to the static displacement under a pressure of 20 kPa (see Figure 8.11), where the magnification ratio is the ratio of dynamic displacement amplitude to static displacement amplitude. It can be seen that influence of nonlinearity is important in the low frequency range, especially around the natural frequency of the foundation while this influence is secondary in the high frequency range. The influence can also be seen from the resonant responses. Multiple resonant responses can be obtained with the Bubble model while the elastic model shows that the displacement amplitude decreases monotonically with the exciting frequency.

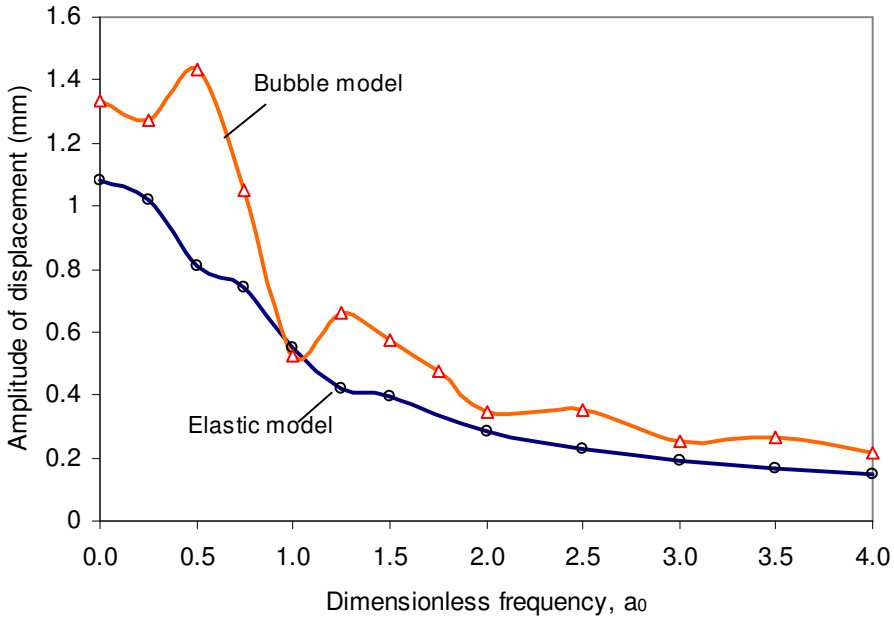

Figure 8.10 Amplitude of displacement (Stress amplitude = 20 kPa)

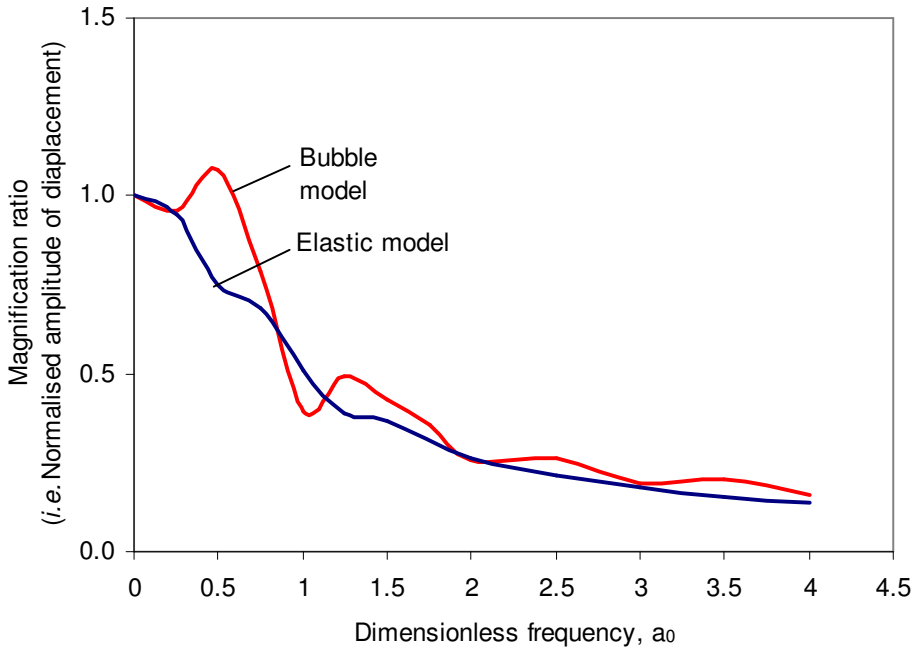

Figure 8.11 Normalised amplitude of displacement (Stress amplitude = 20 kPa)

8.4.2 Effects of dynamic stress level

Calculations have also been carried out to investigate the influence of nonlinear behaviour of soil under different levels of dynamic stress. The results are presented in Figure 8.12, which indicate that the influence of soil nonlinearity increases with the stress amplitude.

Effects of stress amplitude on displacement of foundation have been further investigated at two specific frequencies, *i.e.* a_0 = 0.5 and 2.0 respectively. For stress amplitudes greater than 60 kPa, a plastic strain ratio (*psr*) of 0.9 is applied in nonlinear analyses and accordingly the results are increased by 25% (see Table 8.2 in Section 8.3). These results are shown in Figures 8.13 and 14. It can be seen that nonlinearity of soil corresponds to a significant increase in the amplitude of displacement at certain stress levels. At low levels of dynamic stress, there is insignificant difference between nonlinear and elastic models and this difference becomes negligible if the excitation frequency is high.

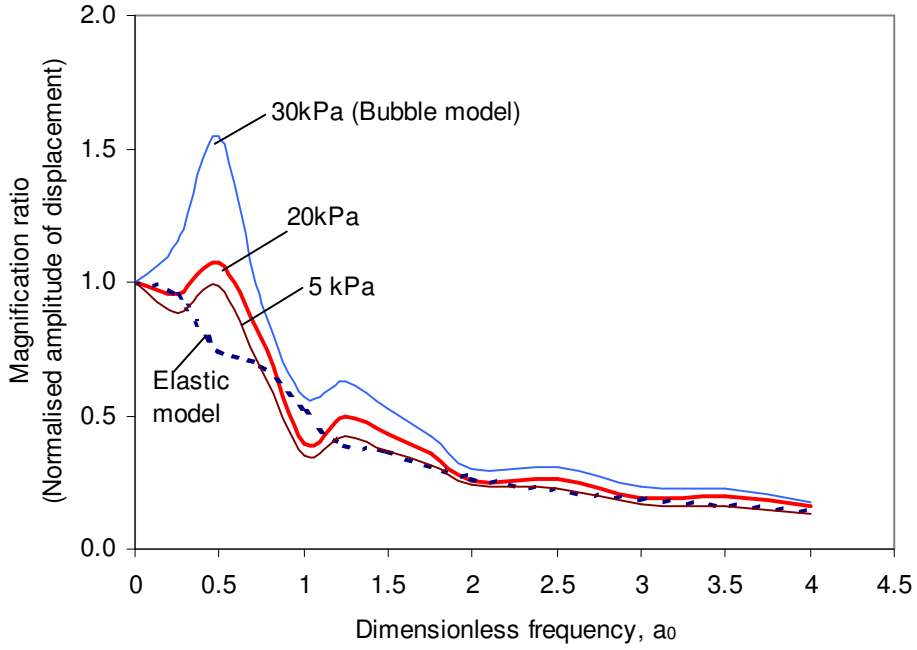

Figure 8.12 Influence of dynamic stress

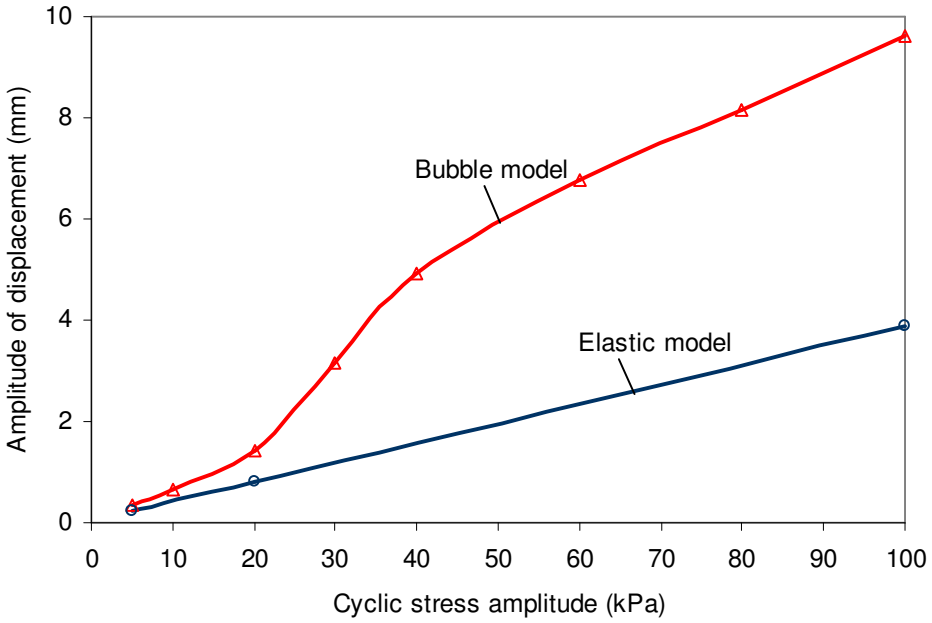

Figure 8.13 Influence of dynamic stress ($a_0 = 0.5$)

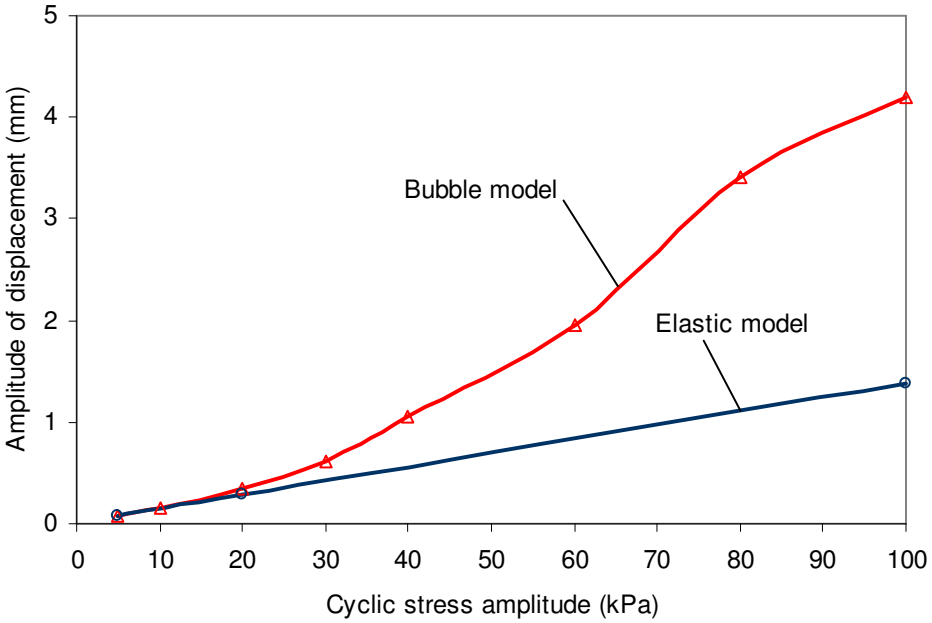

Figure 8.14 Influence of dynamic stress ($a_0 = 2$)

8.4.3 Effects of initial static stress (*i.e*. factor of safety)

Previous analyses are associated with an initial static stress condition having a factor of safety of 3. Higher levels of initial static stresses, *i.e*. lower factors of safety, are expected to induce more plastic deformation during vibration. In this section, the static factor of safety is varied from 1.5 to 9 to investigate its influence on the dynamic displacement of the rigid foundation.

Figure 8.15 shows that there is little change in the amplitude of displacement if the factor of safety is larger than 4 but it increases sharply when the factor of safety is lower than 3. The results have been obtained with a dynamic stress amplitude of 20 kPa and a dimensionless frequency of 0.5.

Figure 8.16 shows the influence of factor of safety at different levels of frequency for the same stress amplitude. As expected, the influence is amplified at resonant frequencies and is minor at high frequencies.

Figure 8.17 shows the time history of displacement. It indicates that permanent displacement is also affected by the factor of safety, *i.e*. the lower the factor of safety the larger the permanent displacement.

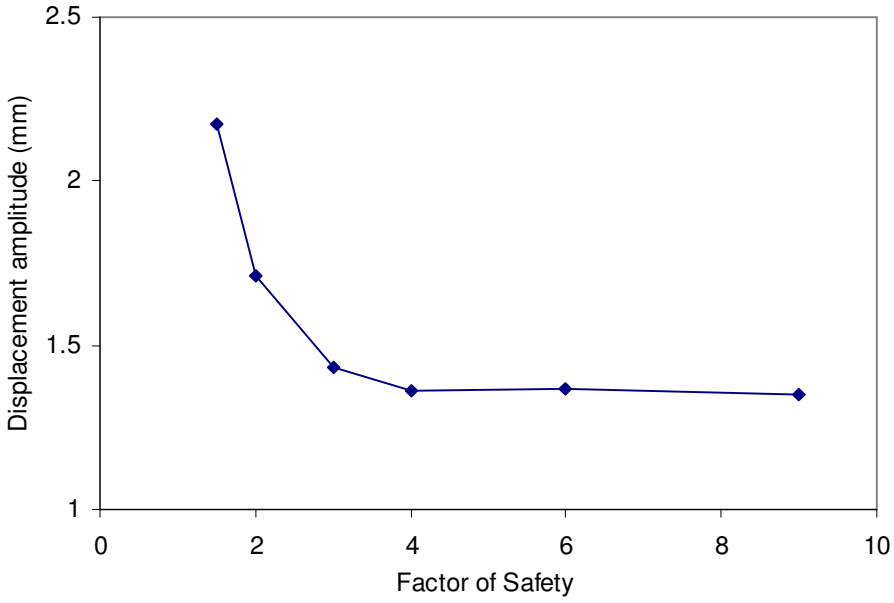

Figure 8.15 Influence of factor of safety (a_0 = 0.5, stress amplitude = 20 kPa)

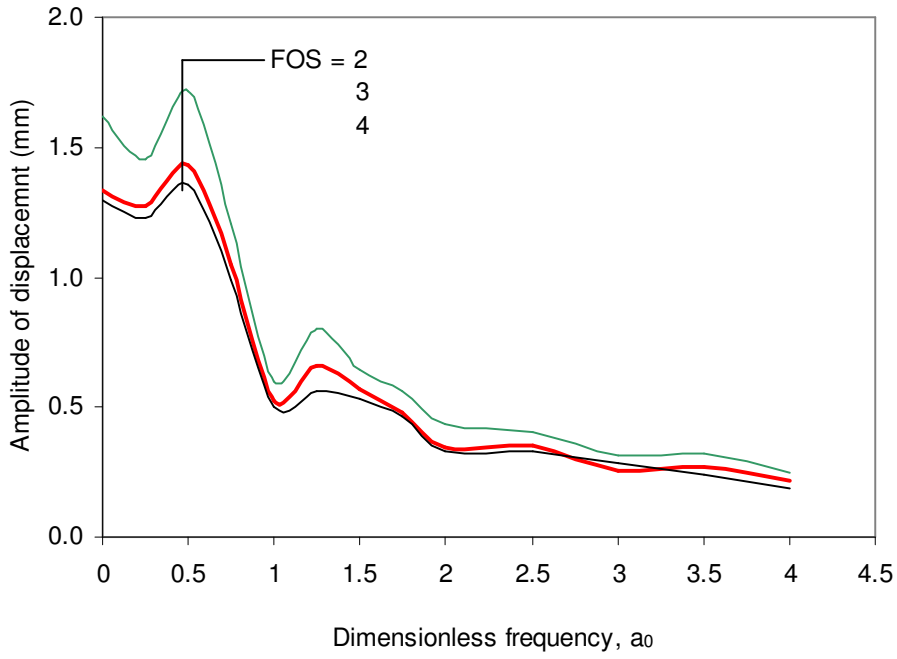

Figure 8.16 Influence of factor of safety (stress amplitude = 20 kPa)

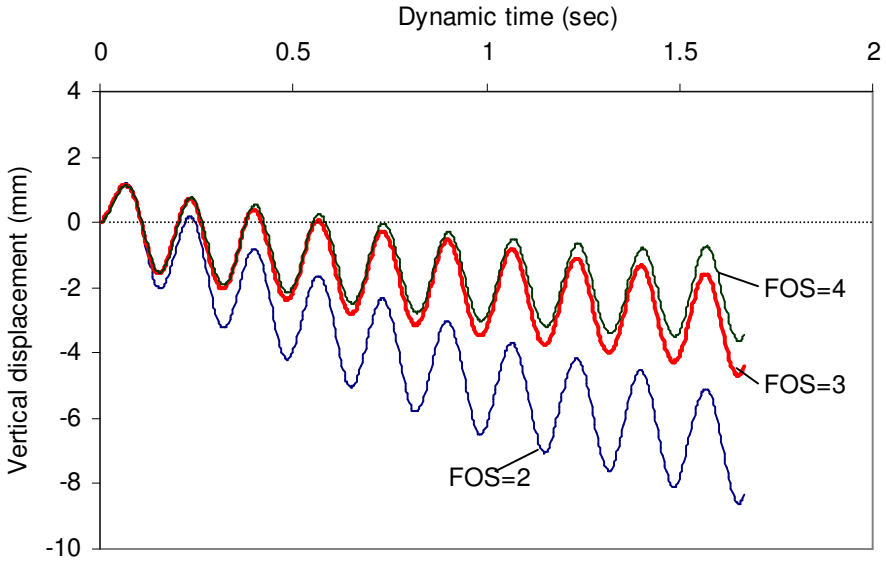

Figure 8.17 Time history of displacement (a_0 = 0.5, stress amplitude = 20kPa)

8.4.4 Effects of mass ratio

A massless foundation has been considered in the previous analyses. Influence of foundation mass is investigated in this section. For a strip foundation the mass ratio is given by

$$m_r = \frac{m}{\rho b^2} \tag{8.2}$$

Where m is the weight of foundation per meter length (kN/m); ρ is the unit weight of soil (kN/m^3); b is the half width of the foundation. It has been found that the mass ratio has a significant influence on the amplitude of displacement if the ratio is greater than 1.0 (see Figure 8.18). However, unlike the results obtained from a damped single-degree-of-freedom system (*Richart & Woods, 1970*), nonlinear analyses show that mass ratio has little influence on resonant frequencies of the vibrating system. This is consistent with the findings by Gazetas & Roesset (1979). Using a semi-analytical procedure in their study on a strip foundation on layered halfspace, they found that the resonant frequency is

almost independent of the mass ratio of the foundation when the mass ratio is less than 2. Further study is required in this area.

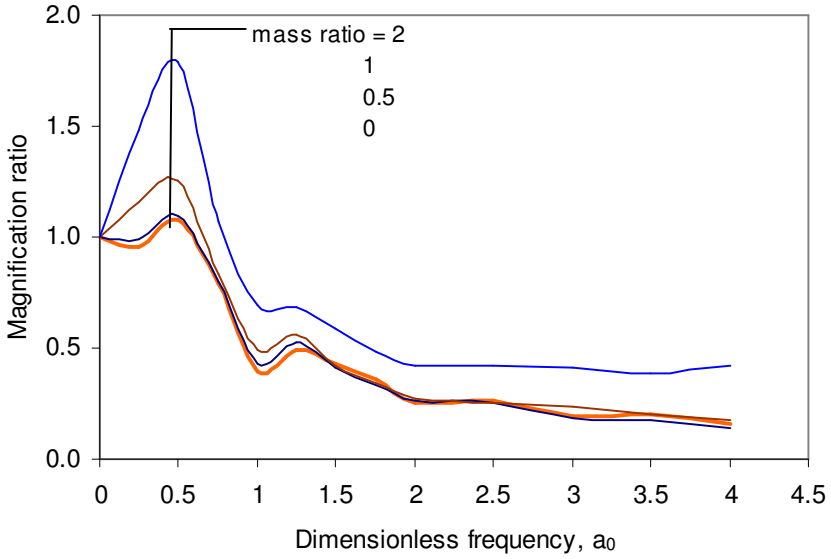

Figure 8.18 Influence of mass ratio (stress amplitude = 20 kPa, FOS = 3)

8.5 Compliance and impedance functions

Figure 8.19 shows comparisons of the real and imaginary parts of the compliance functions between *FLAC* modelling and the semi-analytical solution (Gazetas & Roesset, 1979). The *FLAC* results have been obtained using the method described in *FLAC* manuals for a machine foundation (see Figures 3.58 and 3.60, *Dynamic Analysis, FLAC 4.0*). If a_0 is greater than 0.5, there is a good agreement. When a_0 is below 0.5, however, there is a significant difference in imaginary part (*i.e.* $f_{2,v}$). Figure 8.20 shows comparison of the real and imaginary parts of the impedance functions between the two methods. It can be seen that there is a general agreement in the real part of the impedance function, *i.e.* $f_{1,v}/(f_{1,v}^2 + f_{2,v}^2)$, in the frequency range of 0.5 to 1.5. However the difference is significant beyond this frequency range. There is a good agreement in the imaginary part of the impedance function, *i.e.* $f_{2,v}/(f_{1,v}^2 + f_{2,v}^2)$, for the frequency range of 0.25 to 2.5.

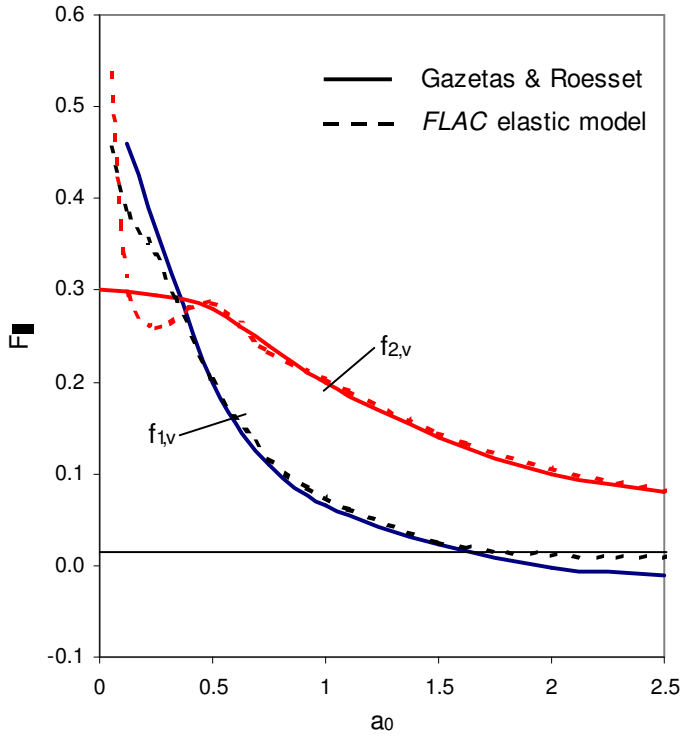

Figure 8.19 Comparison of compliance functions of a rigid foundation between FLAC modeling and the semi-analytical solution by Gazetas & Roesset, 1979

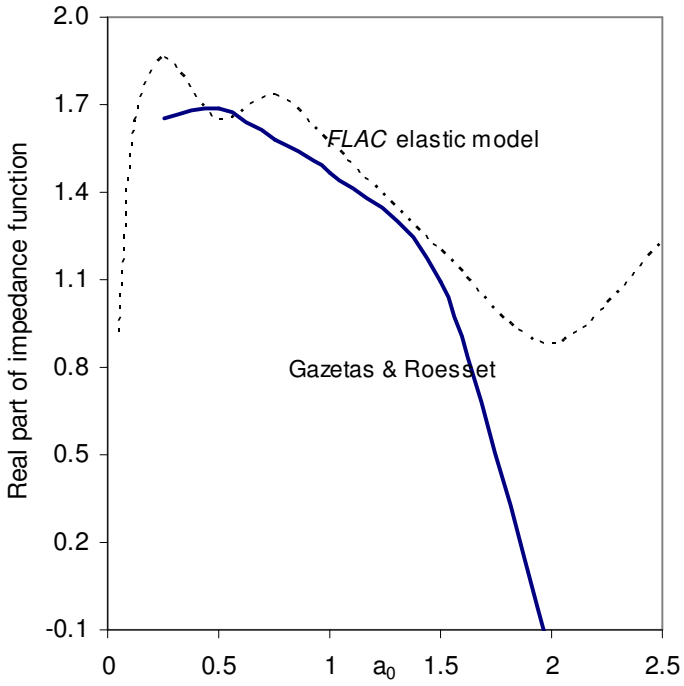

(a) Real part

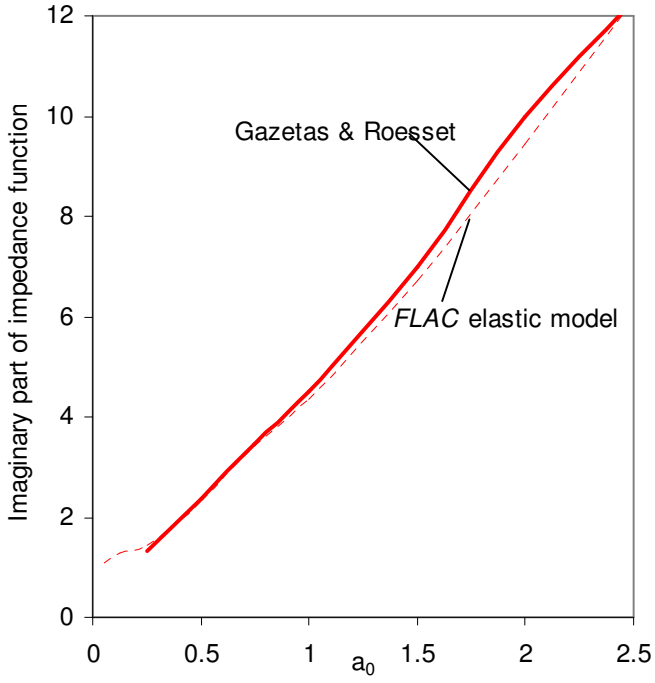

(b) Imaginary part

Figure 8.20 Comparison of impedance functions of a rigid foundation between FLAC modeling and the semi-analytical solution by Gazetas & Roesset, 1979

8.6 Summary

The Bubble model has been applied to numerical modeling of a 2D soil-foundation boundary problem to investigate influence of soil nonlinearity on dynamic compliance of a rigid strip foundation subject to vertical vibration.

Static analyses were carried out prior to dynamic modeling, which indicated that the ultimate bearing capacity of a 4 m wide strip shallow foundation is about 450 kPa for homogeneous soil with an undrained shear strength of 100 kPa.

Typical dynamic responses have been obtained with the model, which shows that a steady state response is expected to be obtained if excitation stress is small while excessive displacement is expected to occur within limited cycles when the dynamic stress is large.

Amplitude of displacement is averaged over 10 cycles to assess dynamic compliance of the foundation. Comparative study indicates that there is no significant difference in the dynamic compliance between nonlinear and elastic soil at low stress levels. For a given excitation frequency, amplitude of displacement increases linearly with dynamic stress for elastic soil while it increases sharply at a certain stress level for nonlinear soil. For a given dynamic stress, amplitude of displacement decreases monotonically with frequency for elastic soil while it peaks at multiple frequencies for nonlinear soil. Significant differences between nonlinear and elastic results occur at the fundamental natural frequency of the vibratory system.

Dynamic has been found to be affected by initial stress, *i.e* static factor of safety. Amplitude of displacement decreases with factor of safety but becomes virtually constant if the factor of safety is greater than a certain level.

Mass ratio of the foundation has been found to affect the amplitude of displacement significantly. However resonant frequencies are not affected by the mass ratio. This is different from the traditional single-degree-of-freedom solution.

Appendix 8.1 *FLAC* data files for vertical vibration of rigid foundations

```
; Initial stress
; File name:v1.dat
Config dyn
Def setup
  Width   =10.0
  Height  =10.0
  NumXzones =20
  NumYzones =20
  ;derived data
  figp=numXzones+1
  fjgp=numYzones+1
end
setup
Grid numXzones, numYzones
Gen 0.0 0.0 0.0 Height, Width, height, width, 0.0
m e
Prop den 1.8 shear 4e4 bulk 6.0e4
;set large
Fix y j 1
Fix x I 1
Fix x I figp
Set grav 10
Set dyn off
app pressure 20 j fjgp
Solve
pause
Save v1.sav
New

;Rigid footing subject to vertical static loading
;File name:v2.dat
rest v1.sav
ini xd 0.0 yd 0.0
ini xv 0 yv 0
def footing
 drainage=1.0;1.0 for drained,0 for undrained
 B = 4.0 ;total width of footing
 ;derived data
 ZoneXsize=width/numXzones
 Finum=B/2.0/zoneXsize
 Fi=finum+1
 Fjgp_1=fjgp-1
 Fj=numYzones-finum
 End
Footing

;set dyn on
call bubble.fis
model bubble
prop b_kmax 2.0e5 b_poiss 0.25 b_mod0 6e4
prop b_lambda 0.15 b_kappa 0.02 b_M 1.0 b_mm 1.0
prop r_bub 0.05 aa 0.5 bb 1800 k 4 psigh 0.5
prop nambda0 0.0 r_str0 1.0 pc0 210.0
prop density 1.8 psr 1.0
```

```
def beamsetup
  loop I (1, finum)
    j=I+1
    command
     struc beam beg grid i fjgp end grid j fjgp
    end_command
  end_loop
end
beamsetup
stru prop 1 e=1 I=1 a=0.00001 den=2.4 ;massless
def ggg
  loop nn(1,fi)
    command
     struct node nn fix x r
    end_command
    nn1=nn-1
    if nn>1 then
     command
      struct node nn slave y nn1
     end_command
    end_if
  end_loop
end
ggg
His nstep 20
His yd I 1 j fjgp
Set ncw=1
;set gravity 15;check natural frequency
;set dyn on
;solve dytime 0.7
App pressure 50 I 1,fi j fjgp
solve
save v2_50.sav
App pressure 100 I 1,fi j fjgp
solve
save v2_100.sav
App pressure 100 I 1,fi j fjgp
solve
save v2_150.sav
step 3000
save v2_150_FOS3.sav
new

; Rigid footing subject to vertical vibration
;File name:v3.dat
rest v2_150_FOS3.sav
ini xd 0.0 yd 0.0
ini xv 0 yv 0
def dynamicData
  Drainage=0.0 ; undrained during dynamic loading
  a0=0.5
  Frequency =a0*150.6/4.0/pi
  StressAmplitude=20.0
  Cycles=10
  HisStep=20
  ;L_damping=5/100.0*pi
```

```
  Onecycle=1.0/frequency
  Endcycle=1000*onecycle
  Duration=cycles*onecycle
  Count=0.0; for compliance function computation
  Sh_mod=4.0e4
  Period=1.0/frequency
End
DynamicData
stru prop 1 e=1 I=1 a=0.00001 den=2.4;mass ratio=0.0
;stru prop 1 e=1 I=1 a=0.375 den=2.4 ;mass ratio=0.5
;stru prop 1 e=1 I=1 a=0.75 den=2.4 ;mass ratio=1.0
;stru prop 1 e=1 I=1 a=1.5 den=2.4 ;mass ratio=2.0
set dyn on
def wave
  if dytime>endcycle
  wave=0.0
 else
  Wave = stressAmplitude*sin(2*pi*frequency*dytime)
 endif
End
app xquiet yquiet i figp
app xquiet yquiet j 1
app nstress 1.0 his wave I 1,fi j fjgp
def dummy; for computing average amplitude, real/imaginary
  count=count+1.0
end
;set large
his nstep HisStep
his reset
his dytime
His yd I 1 j fjgp
his dummy
his wave
Set ncw=1
Set step=9000000
;set dy_damp Local L_damping
set dy_damp=rayl 0.005 frequency ;mass
solve dytime Duration
save v3.sav
plot his 2 vs 1 hold
call com.dat ;compute compliance function
;Compute static displacement under 20kPa
;File name:v2_20.dat
;rest v2_150_FOS3.sav
ini xd 0.0 yd 0.0
ini xv 0 yv 0
His nstep 20
His yd I 1 j fjgp

App pressure 170 I 1,fi j fjgp
solve
step 4000
print yd
```

9 CONCLUSIONS AND DISCUSSIONS

This thesis presents a study on implementation of nonlinear soil models in *FLAC*, the Bubble model and its application in nonlinear dynamic analysis with *FLAC*. Section 9.1 summaries the main results and conclusions. Discussions on the limitations of the Bubble model are given in Section 9.2.

9.1 Main results and conclusions

9.1.1 Implementation of soil constitutive models in *FLAC*

Some important aspects related to implementation of constitutive models in *FLAC* have been explored. Understanding them is critical to implementation of a soil model.

- In *FLAC* each quadrilateral element comprises two overlaid sets of triangular sub-elements. A user-defined constitutive model (UDM) is called four times per element (once for each sub-element) each timestep. Whether stress or strain is constant or not over the four sub-elements depends on boundary conditions and shape of the element. Stress and strain may need to be averaged over the four sub-elements for more accurate results. If this is not specified in a user defined model (UDM), however, stress and strain of an element are only associated with the last-called sub-element.

- If pore water pressure is generated by the UDM, stresses must be converted into effective stresses before the yield function is called in the UDM. If the pore water pressure is generated by *FLAC (e.g.* in *FLAC's GW* mode analysis), stresses are automatically converted to effective stresses.

9.1.2 Numerical distortion in nonlinear dynamic analysis

Efforts have been made to overcome a specific type of numerical distortion which only occurs in nonlinear dynamic analysis, not in static incrementally nonlinear or linear dynamic analysis.

- The study indicates that severe numerical distortion may occur in dynamic analysis if a nonlinear constitutive soil model is implemented using the 'apparent modulus' approach. In this approach, an apparent tangent modulus is used to account for nonlinear stress-strain behaviour of soil and there is a sudden change in the apparent modulus when a strain reversal takes place.

- It has been found that reducing the timestep does not help to solve the problem of numerical distortion. However the numerical distortion can be minimised by applying additional mechanical damping using the in built mechanisms in *FLAC*.

- Alternatively, the 'plastic correction' approach has been found to be a solution to the problem. Satisfactory dynamic performance of nonlinear soil models implemented with this approach can be obtained without applying any additional damping. This has been verified using different nonlinear soil models (e.g. Bubble, Bilinear, Cam-clay models)

9.1.3 The Bubble model

The Bubble model proposed by Rouania & Wood (2000) has been studied and implemented in *FLAC* with the 'plastic correction' approach.

- An alternative form to the plastic modulus function of the model has been proposed, which is considered to better incorporate size ratio effects of the yield surface.

- A multiplier to the plastic modulus function is also proposed to smoothen transition in stiffness from elastic region to yielding, which is based on the concept of the hardening function proposed by Kavvadas (2000).

- The non-intersection translation rule of the yield surface and monotonic destructuration rule of the structure surface have been verified.

- The Bubble model can be reduced to be equivalent to the modified Cam-clay model. Comparison of the Bubble model with the modified Cam-clay model built in *FLAC* has indicated that virtually identical results can be obtained if equivalent parameters are chosen for the two models.

- There is a general agreement between the Bubble model and the published experimental data (*Lee* and *Seed* 1967) in modelling the stress-strain behaviours of loose sand. However, the agreement is poor in lower range of effective confining stress. The Bubble model predicts less dilatancy than the measured in laboratory. As a result, the predicted small strain behaviours are less stiff than the measured.

- Performance of the Bubble model in dynamic analysis has been found satisfactory in terms of the numerical stability. A steady state response can be obtained and maintained for at least 200 cycles without using any additional damping to cope with numerical instability in modelling a triaxial dynamic test. The drained cyclic behaviours of sands (e.g. cyclic densification and dilation) can be satisfactorily predicted with the model. However, the prediction for undrained behaviours of soil is unsatisfactory. The problem lies in the unrealistic simulation of cyclic responses during the first few cycles although the overall behaviours are consistent with laboratory observations.

9.1.4 Parameters of the Bubble model

The Bubble model requires ten parameters and some initial conditions. Five of the parameters are similar to those of the Cam-clay model, *i.e.* $\lambda^*, \kappa^*, M, m$ and μ, while the other five are non-standard parameters, *i.e.* R, B, ψ, k, A. The initial conditions include $r_0, \eta_0, p_{c0}, \sigma_{30}$.

- The Bubble model is most affected by the plastic modulus parameters B, ψ and the Cam-clay type parameters λ^*, κ^*. The Poisson's ratio generally has less important role in the Bubble model.

- Parameters B and ψ control degradation in stiffness of soil. Stiffness increases with B and decreases with ψ. To smooth the transition in stiffness from elastic to elasto-plastic behaviour, one needs to increase B or decreases ψ. However, the two parameters are found to be interrelated. The main factor affecting B is p_{c0}. For normal ranges of λ^* and κ^*, relationships between B, ψ and p_{c0} have been explored and can be used for the first trial in selection of the two parameters to model a problem.

- Parameter R (size ratio of the yield surface) affects stiffness at small strain levels but has no effects on the shear strength of soil. An effective range between 0.1 and 0.2 can be used unless one is to model nonlinear behaviour of soil at very small strain levels.

- Stiffness decreases with κ^* and λ^*. κ^* has the most significant role in affecting $G - \gamma$ curves. Shear modulus degrades more quickly with shear strain as κ^* decreases.

- Parameter m should be in the range of 0.7~1.0 to ensure convexity (Rouania and Wood, 2000). If $m = 1$, behaviour of the Bubble model in extension is identical to that in compression. If $m \neq 1$, it only affects the model in extension. The behaviour of the model in compression is not affected by the parameter m.

- For structured soils, parameter A controls the ratio of contribution between plastic volumetric and distortional strains. Use of lower values for A (*i.e.* less contribution from plastic distortional strain) tends to result in larger residual strength. A value of 0.5 (*i.e.* volumetric and distortional strains are equally accounted for) is recommended for the parameter A in the first trial of a modelling.

- Parameter k controls rate of destructuration of structured soil but has little influence on peak and residual stresses.

- Initial size (r_0) of structure surface can be generally interpreted as sensitivity of soil. In the study, r_0 has been found to be 1.5~2 times of sensitivity index, which only affects peak stress. Residual stress is controlled by intrinsic conditions (*e.g.* p_{c0}) and has been found to be insensitive to r_0.

- Anisotropy parameter η_0 has no important effects on stress-strain behaviours of structured soil if it is in the range between –0.5 and 0.5.

9.1.5 Application of the Bubble model

The Bubble model has been used in modeling with *FLAC* of the vertical vibration of rigid strip foundations to investigate influence of soil nonlinearity on dynamic compliance of the foundations.

- For an elastic soil-foundation system, a steady state dynamic response can always be reached regardless of excitation levels. However, for a foundation rested on a highly nonlinear soil, the steady state response can only be obtained when the excitation level is low. Excessive displacement of the foundation is expected to occur within limited cycles if the dynamic stress is large. Due to the limitation of the Bubble model that it does not allow tensile mean principal stress, the steady state response can not be demonstrated numerically under high levels of excitation (see the discussion in Section 9.2).

- There is no significant difference in the dynamic compliance between nonlinear and elastic soil if the excitation stress level is low.

- For a given excitation frequency, amplitude of displacement increases linearly with dynamic stress for elastic soil while it increases sharply at a certain magnitude of stress for nonlinear soil.

- For a given dynamic stress, amplitude of displacement decreases monotonically with frequency for elastic soil while it peaks at multiple frequencies for nonlinear soil. Significant differences between nonlinear and elastic results occur at the fundamental natural frequency of the vibratory system.

- Dynamic compliance has been found to be affected by initial stress, *i.e* static factor of safety. Amplitude of displacement decreases with factor of safety but becomes virtually constant if the factor of safety is greater than a certain level.

- Mass ratio of the foundation has been found to affect the amplitude of displacement significantly. However resonant frequencies are not affected by the mass ratio. This is different from the results of the traditional single-degree-of-freedom solution.

9.2 Discussion

The Bubble model can not sustain tension, *i.e.* the effective mean stress must be always compressive ($p' < 0$) in an analysis. If a positive mean stress occurs even in a single element, the model will stop functioning and as a result the analysis will not be able to continue. This is the same as in the modified Cam-clay model.

It is easy to prevent a positive mean stress from occurring in modeling a triaxial dynamic test. An all-round static confining pressure can be applied to the numerical model to counteract dynamic pore water pressure and tensile stress induced by dynamic loading so that the effective mean stress remains negative.

However, positive mean stress becomes an issue in modeling of the vertical vibration of shallow foundations. It has been found that a positive mean stress normally occurs in

elements immediately adjacent to the two sides of a shallow strip foundation, especially when the dynamic stress is large. This can be explained using the following equation:

$$p' = p'_0 + \Sigma(\Delta p + \Delta u) \qquad (9.1)$$

Where p' is the effective mean stress (negative for compressive and positive for tension). p'_0 is the initial effective mean stress corresponding to overburden pressure (always negative). Δp is the rate of total mean stress induced by dynamic loading, which is either positive or negative depending on the direction of the dynamic loading. Δu is the rate of pore water pressure, which is related to volumetric plastic strain and is always positive or zero unless dilative behaviours occur.

As p'_0 is small in elements near the ground surface while Δu is significantly larger in elements immediately adjacent to the two sides of the foundation than other elements, *p'* becomes zero or positive after some cycles of vibration due to build-up of the pore water pressure. The higher the stress or frequency, the earlier the positive mean stress occurs. It can be seen from Eq. 9.1 that even under drained condition, positive mean stress may still occur.

Similarly to the modeling of a dynamic triaxial test, an overburden surcharge can be applied to the foundation model (*e.g.* for a deep foundation). This will delay or prevent occurrence of the positive mean stress. However, unlike triaxial modeling where plastic strain is virtually uniform in all the elements, plastic strain develops unevenly in a foundation model (*i.e.* significantly higher in elements adjacent to corners of the foundation). Although the effective mean stress may be maintained negative by applying an overburden surcharge, excessive plastic deformation or even plastic flow may be generated in those elements and this consequently results in severe damage to the geometry of the elements (See Figure 9.1). Even if this occurs to one single element, *FLAC* stepping will stop automatically.

More work is needed to understand the problems described above although it seems quite clear that they may be common when a highly nonlinear plasticity soil constitutive is used. The Bubble model has a small yield surface. The smaller the yield surface, the more nonlinear the behaviours of the model. In Chapter 8, the size ratio of the yield surface is only 0.05 (4 times smaller than that used in the available published references). Hence high nonlinearity is considered to have significant effects on the problem. It has been found that if a larger size ratio is used for the yield surface, a larger dynamic stress can be applied to the foundation without inducing the above problem. In Chapter 8, the plastic strain is reduced by a factor (*psr*) of 0.7~0.9 to ensure 10 cycles of vibration are achieved for cases when the dynamic stress is large.

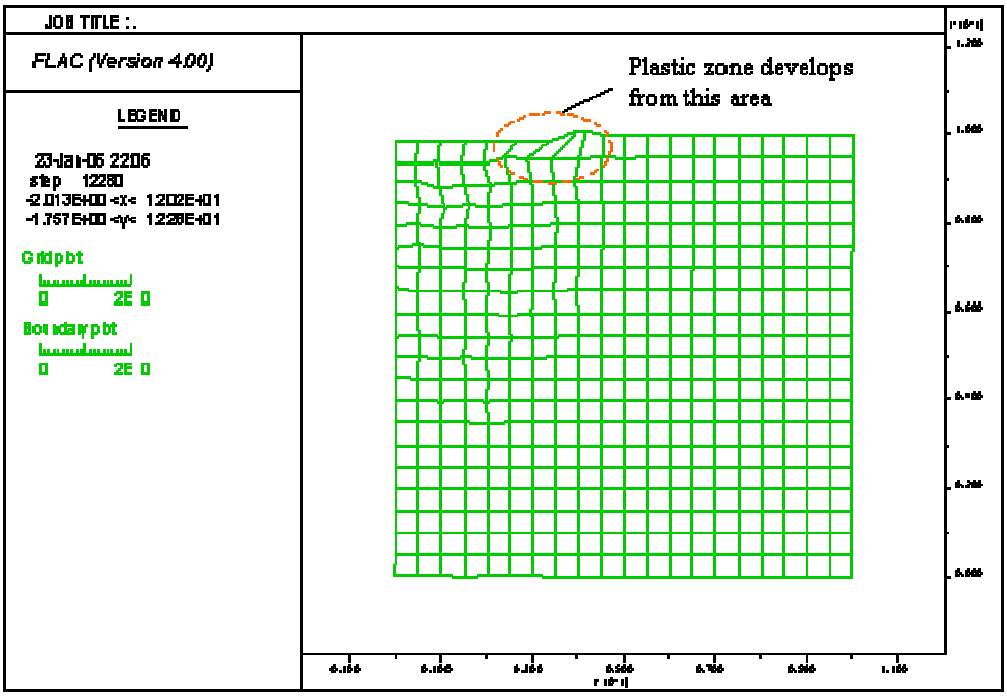

Figure 9.1 Badly deformed elements

9.3 Suggestions for further research

The following areas are recommended for further research:

- Determination of parameters

Parameters (A, B, k, R, r_0, ψ) can not be obtained directly by laboratory testing. Their correlations with well-defined and measurable parameters need to be investigated by numerical simulations of laboratory testing results.

- Model tests

The Bubble model has been used by other researchers to simulate different types of clay. The current study has also found that the model can capture general behaviors of natural soils. However, much more numerical simulations of experimental results need to be carried out in order to better understand the capabilities and limitations of the Bubble model. The outcome of further verifications can then be used to identify rules and to define scope for application of the model in the engineering practice and research studies.

- Implementation of the Bubble model for non-plane strain problems

The Bubble model has been implemented for 2D plane strain problems and the *FISH* code of the model can be readily extended for use in general 3D problems without changing its framework and procedure set out in the thesis.

LIST OF REFERENCES

Al-Tabbaa, A. and Wood, D. M. (1989). An experimentally based 'bubble' model for clay. *Numerical models in geomechanics - NUMOG 3* (eds S. Pietruszczak & G. N Pande). Elsevier Applied Science, London, 91 - 99.

Bardet, J. P. (1986). Bounding surface plasticity model for sands. *J. of Engineering Mechanics*, Vol. 112, No.11, 1198 - 1217.

Bardet, J. P. (1990). Hypoplastic model for sands. *J. of Engineering Mechanics*, Vol. 116, No.9, 1973 - 1995.

Baudet, B. and Stallebrass, S. (2004). A constitutive model for structured soils. *Géotechnique,* 54, 269 - 278.

Bolton, M. D., Dasari, G. R. and Britto, A. M. (1994). Putting small strain non-linearity into modified Cam-Clay model. *Computer methods and advance in Geomechanics*, *Siriwardane & Zaman (eds), Balkema, Rotterdam, 537 - 541.*

Borja, R. I., Wu, W. H. and Smith, H. A. (1993). Nonlinear response of vertically oscillating rigid foundations. *J. of Geotechnical Engineering*, Vol. 119, No. 5, 893 - 911.

Botts, M. E. (1998). Effects of slaking on the strength of clay shales: A critical state approach. *Proc. of 2nd Int. Sym. on the Geotechnics of Hard Soils / Soft Rocks*, Naples, 447 - 458

Britto, A. M. and Gunn, M. J. (1987). *Critical state soil mechanics via finite elements*. Ellis - Horwood, Chichester / Halsted Press , New York, 1 - 488.

Burland, J. B. (1965). The yielding and dilation of clay. *Géotechnique,* 15, 211 - 214.

Burland, J. B. (1990). On the compressibility and shear strength of natural clays. *Géotechnique,* 40, 329 - 378.

Butterfield, R. (1979). A natural compression law for soils (an advance on $e - \log p'$). *Géotechnique,* 29, 469 - 480.

Celep, Z. , et al. (1983). Spurious reflection of elastic waves due to gradually changing finite element size, Intern, *J. for Numerical Methods In Engineering, 19, 631 - 646.*

Cotecchia, F. and Chandler, R. J. (2000). A general framework for the mechanical behaviour of clays. *Géotechnique,* 50, 431 - 447.

Cundall, P. A. (2000). Dynamic analysis. *FLAC 4.0 manual*.

Dafalias, Y. F. and Popov, E. P. (1976). Plastic internal variables formalism of cyclic plasticity. *J. of Applied Mechanics*, Vol. 98, 645 - 651.

Dafalias, Y. F. (1986). Bounding surface plasticity. I: Mathematical foundation and hypoplasticity. *J. of Engineering Mechanics*, Vol. 116, No. 9, 966 - 987.

Drucker, D. C., Gibson, R. E. and Henkel, D. J. (1957). Soil mechanics and work hardening theories of plasticity. *Trans ASCE*, Vol. 122, 101 - 106.

Duncan, J. M., and Chang, C. Y. (1970). Nonlinear Analysis of Stress and Strain in Soils. *Soil Mechanic*s, *9*6(SM5), 1629 - 1653.

Dunne, F. and Petrinic, N. (2005) Implicit and explicit integration of von Mises plasticity. *Introduction to Computational Plasticity*. Oxford University Press, Oxford / New York, 143 - 150.

Gajo, A. and Wood, D. M. (1999). A kinematic hardening constitutive model for sands: the multiaxial formulation. *Int. J. Num. Analy. Methods in Geomech*., 23, 925 - 965.

Gajo, A. and Wood, D. M. (1999). Severn-Trent sand: a kinematic hardening constitutive model: the q-p formulation. *Géotechnique,* 49, 595 - 614.

Gajo, A. and Wood, D. M. (2001). A new approach to anisotropic bounding surface plasticity: general formulation and simulations of natural and reconstituted clays. *Int. J. Num. Analy. Methods in Geomech*., 25, 207 - 242.

Gazetas, G. and Roesset, J. M. (1979). Vertical vibration of Machine Foundations. *J. Geotech*., Div. ASCE, 105 (GT12), 1435 - 1454.

Houlsby, G. T. (1999). A model for the variable stiffness of undrained clay. Pre-failure Deformatoin characteristics of geomaterials, Jamiolkowski, Lancellotta & Lo Presti (eds). Balkema, Rotterdam, 443 - 452.

Ishihara, K. (1996). Strain dependency of modulus and damping. *Soil Behaviour in Earthquake Geotechnics*. Clarendon Press, Oxford; Oxford University Press, New York , 127 - 143.

Ishihara, K. (1996). Sand behaviour under monotonic loading. *Soil Behaviour in Earthquake Geotechnics*. Clarendon Press, Oxford; Oxford University Press, New York , 247 - 269.

Hashiguchi, K. (1981). Constitutive equations of elastoplastic materials with anisotropic hardening and elastic-plastic translation. *J. Appl. Mech*., 48, 297 - 301.

Hashiguchi, K. (1983). Constitutive equations of granular materials. In J. T. Jenkins & M. Satake (eds), *Mechanics of Granular Meterials*, 127 – 136. Amsterdam, Elsevier.

Hashiguchi, K. (1985). Two-and three-surface models of plasticity. *Proc. of 5th int. conf. On numerical methods in geomechanics, Nagoy*a, 285 - 292.

Hashiguchi, K. (2002). A proposal of the simplest convex-conical surface for soils. *Soils and foundations*, Vol. 42, No. 3, 107 - 113.

Kavvadas, M. and Amorsoi, A. (2000). A constitutive model for structured soil. *Géotechnique,* 50, 263 - 273.

Lee, K. L. and Seed, H. B. (1967). Drained strength characteristics of sands. J. *SMFD,* Vol. 93, No. 6, 117 - 141.

Luco, J.E. and Westmann, R.A. (1968). Dynamic response of a rigid footing bonded to an elastic halfspace. *J. Appl. Mech.,* 35, 697-705.

McDowell, G. R. and Hau, K. W. (2003). A simple non-associated three surface kinematic hardening model. *Géotechnique,* 53, 433 - 437.

Mitchell, J.K. (1976). Foundations of soil behaviour. New York: Wiley.

Mroz, Z., Norris, V. A. and Zienkiewicz, O. C. (1978). An anisotropic hardening model for soils and its application to cyclic loading. *Int. J. Numer. Anal. Meth. Geomech.,* 2, 203 - 221.

Mroz, Z., Norris, V. A. and Zienkiewicz, O. C. (1979). Application of an anisotropic hardening model in the analysis of elasto-plastic deformation of soils. *Géotechnique*, 29, 1 - 34.

Mroz, Z., Norris, V. A. and Zienkiewicz, O. C. (1981). An anisotropic, critical state model for soils subject to cyclic loading. *Géotechnique*, 3, 451 - 469.

Mroz, Z. and Norris, V. A. (1982). Elastoplastic and viscoplastic constitutive models for soils with application to cyclic loading. *Soil Mechanics-Transient Cyclic Loads*, G. N. Pande & O. C. Zienkiewicz (eds), 173 - 215.

Ni, B. (2001). Nonlinear dynamic soil - structure interaction analysis with *FLAC*. M. E. thesis, University of Auckland, 1-121.

Ni, B. and Pender, M. J. (2004). Nonlinear rocking compliance of a rigid footing. *Proc.* of *9th Australian and New Zealand Conference on Geomechanics, Auckland,* 562 - 568.

Pender, M. J. (1978). A model for behaviour of overconsolidated soil. *Géotechnique,* 28, 1-25.

Pender, M. J. (1989). *Constitutive modelling of geotechnical materials*. CE 298, University of Auckland.

Pender, M. J. (1999). Implementing a soil stress-strain model with hysteretic damping in FLAC. *Proc. of Int. FLAC Sym. on Numerical Modelling in Geomechanics, Minnesota, 475 - 482.*

Pender, M. J. (2000). Dynamic compliance of shallow footings on nonlinear soil. *Proc. of 12th WCEE,* Vol.7, 2739 - 2743.

Pender, M. J. and Ni, B. (2004). Nonlinear vertical vibration characteristics of rigid foundations. *Proc. of 11th Int. Conference on Soil Dynamics & Earthquake Engineering*, *Berkley*, 719 - 725.

Richart, F. E, Woods, R. D and Hall, J. R. (1970). Theories for vibration of foundations on elastic media. *Vibration of soils and foundations*. Prentice-Hall, New Jersey, 191 - 243.

Roscoe, K. H. and Schofield, A .N. and Wroth, C. P. (1958). On the yielding of soils. *Géotechnique,* 8, 22 - 53

Roscoe, K. H. and Schofield, A. N. (1963). Mechanical behaviour of an idealized 'Wet Clay'. *Proc. of 2nd European Conference on Soil Mechanics*, Wiesbaden, 1, 47 - 54.

Roscoe, K. H. and Burland, J. B. (1968). On the generalized stress-strain behaviour of wet clay. *Engineering Plasticity*, edited by J. Heyman and F. A. Leckie, Cambridge University Press, Cambridge, 535 - 609.

Rouainia, M. and Wood, D. M. (1998) A kinematic hardening model for structured clays. *The Geotechnics of Hard Soils-Soft Rocks*, Evangelista & Picarelli (eds), Rotterdam, 817 - 824.

Rouainia, M. and Wood, D. M. (2000). *Géotechnique,* 50, 153 - 164

Seed, H. B., Wong, R. T., Idriss, I. M., and Tokimatsu, K. (1986). Moduli and damping factors for dynamic analysis of cohesionless soils. *J. of Geotechnical Engineering*, ASCE, Vol. 112, 1016 - 1031.

Shao, C. and Desai, C. S. (2000). Implementation of DSC model and application for analysis of field pile tests under cyclic loading. *Int. J. of Numerical and Analytical Methods in Geomechanics*, Vol.24, No 6, 601 - 624.

Schofield, A. N. and Wroth, C. P. (1968). Undrained tests on Cam-clay. *Critical state soil mechanics.* McGraw-Hill, London , New York, 146 - 149.

Schofield, A. N. and Wroth, C. P. (1968). Models and soil mechanics. *Critical state soil mechanics.* McGraw-Hill, London , New York, 20 - 21.

Simo, J. C. and Hughes, J. J. R. (1998) *Computational Inelasticity.* Springer, New York, 1 - 412.

Skempton, A. W and Sowa, V. A. (1963). The behaviour of saturated clays during sampling and testing. *Géotechnique,* 13, 269 - 290.

Smith, P. R., Jardine R. J. High, P. W. (1992). The yielding of Bothkanna clay. *Géotechnique,* 42, 257 - 274.

Stallebrass, S.E. (1991). Modelling the deformation of overconsolidated soils using finite element analysis. *Experimental characterization and modeling of soils and soft rocks*, A workshop in Napoli, 29 - 31.

Stallebrass, S. E. and Taylor, R. N. (1997). The development of a constitutive model for the prediction of ground movements in overconsolidated clay. *Géotechnique,* 47, 235 - 253.

Zhang, J., Stewart, D. P. and Randolph, M.F. (2002). Kinematic hardening model for pipeline-soil interaction under various loading conditions. *Int. J. of Geomechanics*, Vol. 2, No. 4, 419 - 446.

Wang, Z. L. and Makdisi, F. I. (1999). Implementing a boundary surface hypoplasticity model for sand into FLAC program. *FLAC and Numerical Modeling in Geomechanics,* Detoumay & Hart (eds) Balkema, Rotterdam, 483 - 490.

Wood, D. M. (1990). *Soil Behaviour and critical state soil mechanics*. Cambridge University Press, England / New York, 1 - 462.

Wood, D. M. (1995). Kinematic hardening model for structured soil. *Numerical Modles in Geomechanics - NUMOG V*, Pande & Pietruszczak (eds), Bakema, Rotterdam, 83 - 88.

Wood, D. M. and Graham, J. (1995). State boundary surface and anisotropy. *Numerical models in Geomechanics - NUMOG V*, Pande & Pietruszczak (eds), Bakema, Rotterdam, 77 - 82.

THE UNIVERSITY OF AUCKLAND
SCHOOL OF GRADUATE STUDIES

DECLARATION TO ACCOMPANY A DOCTORAL THESIS ON SUBMISSION

DOC 7

Graduate Centre
Building 119, East Wing, ClockTower
Phone: 373 7599 ext. 86899
Fax: 373 7610
postgraduate@auckland.ac.nz

Name: BING NI

Address: 10 Paradise Place
Pakuranga
Auckland

Degree: PhD

Thesis title: Implementation of a Bubble model in FLAC and its application in dynamic analysis

1. I do solemnly declare that I am currently registered as a candidate for the above degree at The University of Auckland.
2. I am making a submission to The University of Auckland to be examined for the degree of Doctor of Philosophy
3. I have attached to this declaration three bound copies of a thesis and the necessary documentation for examination (e.g. CV, portfolios if appropriate).
4. The thesis/work in substantially its present form has not been submitted or accepted previously for the award of a degree or diploma in this or any other tertiary institution, and is not being submitted for a degree or diploma in any other tertiary institution or for another degree or diploma at this institution.*
5. ***Higher Degree candidates only** should state if any portion of the work submitted has been previously presented for a degree or diploma in this or any other tertiary institution:
6. The thesis/work submitted for examination is made up of the following components:
   a. The research in the chapters of the thesis/work, (the development of methodologies, experimentation, interpretation of results, and preparation of the manuscript) were my own *(please tick one)* ✓ in full in part.
   b. I have attached additional material in the form of: *(tick, as appropriate)*
      CD ROM audio cassette map other *(please specify)*
      Provide a description of the content of this additional material and explain how it is related to the thesis:

      This material does not contain any direct appeal to the examiners. Where additional material is included, this part of the declaration (6b) must be endorsed by the Main Supervisor and the Head of Department.

      Signature of Main Supervisor *Signature of Head of Department*
   c. i Where research was jointly authored please state the chapters, authors and extent to their contribution. In addition, where work has been previously presented in some other form, please state what portion:

      ii Please supply evidence *(in the form of a signed letter)* that all co-authors have approved the inclusion of the joint work.

I, BING NI of AUCKLAND declare that the above information is complete and accurate, that no relevant information has been withheld that I am aware of, and believe that I have complied with all of the University's requirements in the regulations associated with my degree.

Signed ..... Date 27 September 2006

Before me John Rofe (Justice of the Peace) Auckland.

Signed ..... Date 27 September 2006

J.P.